

***An investigation of the physio-chemical  
transformations and moisture migration  
processes occurring in concrete during  
spalling***

**A.M. U Thathsarani Kannangara**

BSc, MSc

Thesis submitted for the fulfilment of the requirement for the degree of Doctor of  
Philosophy (PhD)

Victoria University, Australia

Institute for Sustainable Industries and Liveable Cities (ISILC)

December 2024

## **Abstract**

Concrete spalling, which is the flaking, or exploding of concrete layers during fire, can be catastrophic, resulting in collapsing of the structures in some situations. While several theories have been put forward with a view to explaining this undesirable phenomenon, none of these have been able to explain the phenomenological evolution of spalling with an acceptable level of certainty. However, the migration and pooling of considerable amounts of water from the unexposed surface during fire has been established to be key contributor of spalling. Although numerous studies are available, due to the complex physio-chemical transformations occurring to concrete structures under heat/fire, it has proved to be difficult to experimentally analyse the phenomenon of moisture migration. Therefore, it is evidently an area that requires investigation on a much deeper level. Consequently, there is a knowledge gap in the available literature, which warrants a systematic and quantitative approach to investigating, especially, the theories behind the transportation of moisture during spalling.

The current project was primarily aimed to examine the mass loss, migration of moisture through the micro flow-channels and the associated transportation processes. For this purpose, three types of mix designs that were based on ordinary Portland cement (OPC), and one based on geopolymer paste, were chosen. The latter was primarily selected for comparison purpose as geopolymer-based concrete elements are relatively resistant to the phenomenon of spalling. Here, in order to address the physio-chemical mechanism(s) of spalling of concrete structures in actual fire scenarios using an appropriate testing regime, both small- and medium- and large-scale investigations were carried out. Furthermore, during the course of the investigation, several synthetic polymeric components, such as, polypropylene, polyester and cotton fibres, were employed as ‘sacrificial’ agents in mitigating the spalling behaviour of test samples. These agents were subjected routine analyses, which included, morphological (Scanning Electron Microscope with Energy Dispersive provision: SEM/EDS), spectroscopic (Fourier transform Infrared: FT-IR), thermal (Thermo-gravimetric Analysis: TGA) and calorimetric tests (Differential Scanning Calorimetry: DSC and Pyrolysis Combustion Flow Calorimetry: PCFC), etc.

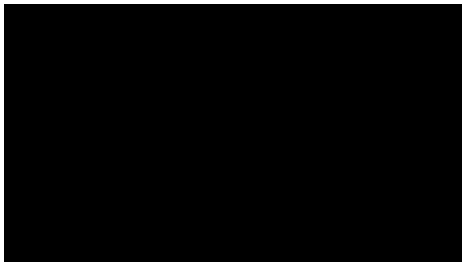
To realize the above goals, an appropriate methodological approach to the problem was carefully employed. This included bespoke analyses, both at the small- and medium-scale, and the former primarily included: TGA, X-ray diffraction technique (XRD), solid-state Nuclear Magnetic Resonance spectroscopy (NMR), SEM imaging. Furthermore, porosity measurements (based on Rapid Chloride Penetration test and BET theory) were carried out, with a view to identifying the pores/micro-channels within the test samples. Here, measurements relating to the moisture content of the mixtures, cured specimens, and the test samples during the various analyses, were conducted. In addition, with a view to gaining insights into the chemical environments of hydrated calcium centres, before and after spalling, in some cubical test specimens, small-angle neutron scattering studies (SANS) were utilized. Furthermore, a high-resolution optical microscopy was used to scan the surfaces of the cured and heat-treated samples. Finally, appropriate mechanical testings on samples were carried out, primarily, to measure the compressive strengths. Here, a short analysis on the difference in compressive strength using different types of specimens, namely cubical and cylindrical, was also investigated. Finally, the set of empirical data, collated through the above experiments, was systematically analysed with a view to elucidating the various physio-chemical transformations that lead to spalling.

The current investigation clearly demonstrated that the incorporation of polymeric components, as sacrificial agents, resulted in a lesser degree of spalling in OPC-based cubical specimens. The fundamental physio-chemical process(es) responsible for this effect can be attributed to the preferential melting/degradation of the polymeric elements within the concrete matrix, thus relieving the built-up pore pressure owing to the generation of water within the samples upon exposure to heat/fire. The same effect was also observed in the case of large-scale test specimens. In the case of cubical samples, the exposure to heat and/or carbon dioxide (through accelerated carbonation tests) had an effect on their mechanical properties albeit to different degrees. On a comparative scale, the geopolymer-based cubical specimens, as expected, only suffered a nominal degree of spalling, if at all, and in general the effect of carbonation/heat treatment on the mechanical properties were minimal.

## Declaration of Authenticity

I, Alahakoon Mudiyanse Uppalawanna Thathsarani Kannangara, declare that the PhD thesis entitled, '*An investigation of the physio-chemical transformations and moisture migration processes occurring in concrete during spalling*', is no more than 80,000 words in length including quotes and exclusive of tables, figures, appendices, bibliography, references and footnotes. This thesis contains no material that has been submitted previously, in whole or in part, for the award of any other academic degree or diploma. Except where otherwise indicated, this thesis is my own work.

I have conducted my research in alignment with the [Australian Code for the Responsible Conduct of Research](#) and [Victoria University's Higher Degree by Research Policy and Procedures](#).



Signature

02 December 2024

## Acknowledgements

Firstly, I greatly acknowledge my principal supervisor, Dr Paul Joseph, for accepting me as his student and for his enduring guidance and constant encouragement, without which this thesis would not have been possible. I am also grateful to my associate supervisors, Professors Maurice Gurrieri and Sam Fragomeni, for their help and support throughout my PhD programme. I also greatly acknowledge the technical support from various people at Victoria University: Donald Ermel; Miroslav Radev; Lyndon Mcindoe; Philip Dunn; Khanh Ho; Rhann Chenery; Stacey Lloyd; Nishantha Illangatilaka; Larruceo Bautista; and Dr Suneela Pyreddy. In addition, I am greatly indebted to Victoria University for the provision of a Research Scholarship for my doctoral study.

I also register my deep sense of gratitude to Dr Luke O'Dell, Deakin University, for recording the solid- state NMR spectra; Dr Hemayet Uddin, Melbourne Centre for Nanofabrication for surface imaging using high-resolution optical microscopy; Dr Janitha Migunthanna Kariyakaranage, Swinburne University, for accelerated carbonation tests; Dr Joseph Bevitt, Australian Centre for Neutron Scattering for recording the SANS data; and Dr Anthony De Girolamo, Monash University, for his support in obtaining the porosity data through the Brunauer-Emmett-Teller method.

My family has always been my pillars of support, and I am forever indebted and deeply register my heartfelt gratitude towards my parents, Upali and Indrani, and especially my sister, Suwani, for their unfailing love and support from the very beginning. I am who I am because I am apart of you, and no words could ever express how blessed I am to have you all in my life.

I also express my profound gratefulness to my teachers, past and present and all my friends and close relatives who helped me.

Last but never the least, I thank my truly amazing husband, Ferdison, who is my soulmate and my best friend. Thank you, my love, for supporting me in every way possible and for keeping me sane during this doctoral journey!

*'While my father gave me wings to dream,  
my mother shaped them into reality'*

To my *Amma* and *Thaththa* for never letting me stray away from this journey

## Research outputs relating to the PhD programme

### I. Manuscripts in preparation:

1. Thathsarani Kannangara, Paul Joseph, Sam Fragomeni, Maurice Guerrieri, *Physio-chemical characterization of some polymeric components used as mitigating agents against spalling in concrete structures when exposed to fire* (to be submitted to a Special Issue of *Applied Sciences: New Challenges in Civil Structure for Fire Response Volume II*)
2. Paul Joseph, Thathsarani Kannangara, Maurice Gurrieri, Sam Fragomeni, *A study of the effects of incorporating polymeric components on the spalling behaviour of concrete*, 5<sup>th</sup> International Fire Safety Symposium, Ulster University, Belfast, United Kingdom, June 25-27, 2025 (*accepted*)

### II. Published papers (directly emanating from the current project)

1. Thathsarani Kannangara, Paul Joseph, Sam Fragomeni, Maurice Guerrieri. Existing theories of concrete spalling and test methods relating to moisture migration patterns upon exposure to elevated temperatures – A review. Case Studies in Construction Materials, (2022), <https://doi.org/10.1016/j.cscm.2022.e01111> (Chapter 2: Literature Review)
2. Thathsarani Kannangara, Maurice Guerrieri, Sam Fragomeni, Paul Joseph. Effects of Initial Surface Evaporation on the Performance of Fly Ash-Based Geopolymer Paste at Elevated Temperatures. *Applied Sciences*. (2022), <https://doi.org/10.3390/app12010364> (Chapters: 3, 4 and 5)
3. Thathsarani Kannangara, Maurice Guerrieri, Sam Fragomeni, Paul Joseph. A Study of the Residual Strength of Reactive Powder-Based Geopolymer Concrete under Elevated Temperatures. *Applied Sciences*, (2021), <https://doi.org/10.3390/app112411834> (Chapters: 3, 4 and 5)

## **List of abbreviations**

With a view to simplifying the main text, the following abbreviations are used:

HSC – High strength concrete

SCM – Supplementary cementitious materials

SF – Silica fumes

FA – Fly ash

GGBFS – Ground granulated blast furnace slag

MK – Metakaolin

RHA – Rice husk ash

GP – Geopolymer

FRC – Fibre reinforced concrete

PP – Polypropylene

OPC – Ordinary Portland cement

NMR – Nuclear magnetic resonance

ICP/OES – Inductively coupled plasma/optical emission spectrometry

SANS – Small angle neutron scattering

XRD – X-Ray diffraction

SEM/EDS – Scanning electron microscope with energy dispersive provision

FT-IR – Fourier-transform infrared

TGA – Thermogravimetric analysis

DSC – Differential scanning calorimetry

PCFC – Pyrolysis combustion flow calorimetry

BET – Brunauer-Emmett-Teller

RCPT – Rapid chloride penetration test

NSC – Normal strength concrete

W/C ratio – Water: Cement ratio

BLEVE – Boiling liquid expanding vapour explosion

SSD – Saturate surface dry

EM – Electromagnetic

GPR – Ground-Penetrating Radar ITZ – Interfacial transition zone



## Contents

Abstract.....	II
Declaration of Authenticity .....	IV
Acknowledgements.....	V
Research outputs relating to the PhD programme .....	VII
List of abbreviations .....	VIII
Contents .....	IX
List of Figures.....	XIII
List of Tables .....	XVIII
CHAPTER 1 .....	1
INTRODUCTION .....	1
1.1. General background.....	2
1.2. Rationale behind the current programme.....	6
1.3. Significance of research.....	7
1.4. Overall aim of the project .....	9
1.5. Individual objectives.....	9
1.6. Thesis outline.....	10
CHAPTER 2 .....	13
LITERATURE REVIEW .....	13
2.1. Chapter overview .....	14
2.2. Concrete in construction .....	14
2.3. Concretes in fire.....	16
2.4. Theories in concrete spalling .....	21
2.4.1. Thermal stress theory.....	22
2.4.2. Moisture clog theory.....	23
2.4.3. Pore pressure theory .....	24
2.4.4. BLEVE and the frictional flow from vapour flow theories.....	25
2.5. Geopolymer-based concrete .....	26
2.6. The fire performance of GP-based concretes.....	29
2.7. Fibre reinforced concretes .....	30

2.7.1.	Polypropylene fibres.....	31
2.7.2.	Non-absorbent cotton fibres .....	34
2.7.3.	Polyester fibres .....	36
2.8.	Test methods and strategies to gauge spalling.....	37
2.9.	Summary of literature review .....	42
CHAPTER 3 .....		45
EXPERIMENTAL.....		45
(MATERIAL AND METHODS) .....		45
3.1.	Introduction.....	46
3.2.	Raw materials .....	46
3.2.1.	Cementitious materials .....	46
3.2.2.	Aggregates .....	48
3.2.3.	Liquid components .....	48
3.2.4.	Essential laboratory reagents and solvents .....	50
3.2.5.	Fibrous materials (Sacrificial agents) .....	50
3.3.	Mix designs.....	51
3.4.	Preparation of specimens and subsequent treatment .....	52
3.5.	Heating regime of concrete specimens .....	55
3.6.	Analytical instrumentation and test methods.....	58
3.6.1.	Scanning electron microscope .....	58
3.6.2.	X-Ray diffraction.....	59
3.6.3.	Fourier-transform infrared spectroscopy .....	59
3.6.4.	Solid-state nuclear magnetic resonance spectroscopy .....	60
3.6.5.	Differential scanning calorimetry .....	60
3.6.6.	Thermogravimetric analysis .....	60
3.6.7.	Pyrolysis combustion flow calorimetry .....	61
3.6.8.	Inductively coupled plasma/optical emission spectrometry .....	62

3.6.9.	Flow table test.....	65
3.6.10.	Compression tests .....	66
3.6.11.	Accelerated carbonation tests .....	67
3.6.12.	Small angle neutron scattering.....	68
3.6.13.	Surface imaging using 3-D optical profilometry .....	68
3.6.14.	Rapid chloride penetration test .....	69
3.6.15.	Measurements using the Brunauer-Emmett-Teller (BET) theory .....	70
CHAPTER 4 .....		72
RESULTS AND DISCUSSION .....		72
4.1.	Introduction.....	73
4.2.	Characterization of the raw materials .....	74
4.3.	Workability .....	91
4.4	Characterization of cured and heat-treated samples .....	93
4.5.	Physical appearance .....	114
4.6.	Density studies .....	119
4.7.	Porosity assessment using rapid chloride penetration test and BET approach...	122
4.8.	Compressive and residual performance .....	126
4.9.	Mass loss after thermal exposure .....	134
4.10.	Carbonation studies on spalled specimens .....	138
4.11	. Imaging of the cubical specimens using SANS and high-resolution optical microscopy .....	140
4.12.	Spalling behaviour of large-scale specimens.....	149
4.13.	Water analysis test results .....	152
4.14.	Post – test spalling assessment of large-scale panels .....	154
4.15.	Summary of the main findings .....	156
CHAPTER 5 .....		159
CONCLUSIONS AND SUGGESTIONS FOR FUTURE WORK .....		159
5.1.	Main Conclusions .....	160

5.2. Some suggestions for future work .....	164
REFERENCES .....	165

## List of Figures

Figure 2.1: Microstructural changes of OPC- based concrete at high temperatures	16
Figure 2.2: Time of occurrence for the types of spalling	19
Figure 2.3: A schematic description of the thermo-mechanical spalling of concrete	23
Figure 2.4: A cross-sectional view of the concrete element showing the moisture clog region	24
Figure 2.5: Sequence of moisture movement	24
Figure 2.6: A schematic diagram of thermo-hygral spalling	25
Figure 2.7: Chemical structure of Polysialates	28
Figure 2.8: An image of a void formed through the melting of PP fibres in concrete	32
Figure 2.9: Specimens encased in a special casing to ensure unilateral heating	39
Figure 2.10: Movement of the moisture front as temperature levels increased	39
Figure 2.11: Concrete specimen with a 70 mm cut on the unexposed surface	40
Figure 2.12: Test specimens 15 minutes after fire exposure	40
Figure 2.13: Test specimens 20 minutes after fire exposure	40
Figure 2.14: Schematic diagram of the principle of the electromagnetic wave reflecting at the waterfront	41
Figure 3.1: Cement and fly ash used in the study	45
Figure 3.2: Aggregate used in the study	46
Figure 3.3: Fibrous materials used in the study	48

Figure 3.4: <i>Breville</i> mixer used in the study	53
Figure 3.5: Small- and medium- scale test specimens	54
Figure 3.6: Location of thermocouples	55
Figure 3.7: Test setup	57
Figure 3.8: Temperature vs. time fire curves for the test panels 1, 2 and 3	58
Figure 3.9: Calibration curve of the Beer-Lambert law for $\text{Ca}^{2+}$	63
Figure 3.10: Calibration curve of the Beer-Lambert law for $\text{Fe}^{3+}$	63
Figure 3.11: Calibration curve of the Beer-Lambert law for $\text{Al}^{3+}$	64
Figure 3.12: Calibration curve of the Beer-Lambert law for Si	64
Figure 3.13: Schematic diagram of diameter ( $d_1$ and $d_2$ ) measurement	65
Figure 3.14: Flow table apparatus	66
Figure 3.15: Test setup for the RCPT	70
Figure 4.1: SEM/EDS of cement	74
Figure 4.2: SEM/EDS of fly ash	75
Figure 4.3: SEM/EDS of fine aggregate	76
Figure 4.4: SEM/EDS of coarse aggregate	77
Figure 4.5: XRD pattern of cement	79
Figure 4.6: XRD pattern of fly ash	79
Figure 4.7: XRD pattern of fine aggregate	79
Figure 4.8: XRD pattern of coarse aggregate	79
Figure 4.9: FT-IR spectrum of cement	80
Figure 4.10: FT-IR spectrum of fly ash	80
Figure 4.11: FT-IR spectrum of fine aggregate	80

Figure 4.12: FT-IR spectrum of coarse aggregate	80
Figure 4.13: Solid-state $^{27}\text{Al}$ spectrum of cement	82
Figure 4.14: Solid-state $^{29}\text{Si}$ spectrum of cement	82
Figure 4.15: Solid-state $^{27}\text{Al}$ spectrum of fine aggregate	83
Figure 4.16: Solid-state $^{29}\text{Si}$ spectrum of fine aggregate	83
Figure 4.17: DSC thermogram of 12mm polypropylene fibres	85
Figure 4.18: DSC thermogram of 48mm polypropylene fibres	85
Figure 4.19: DSC thermogram of cotton fibres	86
Figure 4.20: DSC thermogram of polyester fibres	86
Figure 4.21: TGA thermogram of 12 mm PP fibres	88
Figure 4.22: TGA thermogram of 48 mm PP fibres	88
Figure 4.23: TGA thermogram of cotton fibres	89
Figure 4.24: TGA thermogram of polyester fibres	89
Figure 4.25: Images from the flow table tests of control samples	91
Figure 4.26: SEM/EDS of MD01 cured samples	95
Figure 4.27: SEM/EDS of MD01 samples heat-treated at 400°C	96
Figure 4.28: SEM/EDS of MD01 samples heat-treated at 800°C	97
Figure 4.29: SEM/EDS of MD02 cured samples	98
Figure 4.30: SEM/EDS of MD02 samples heat-treated at 400°C	99
Figure 4.31: SEM/EDS of MD02 samples heat-treated at 800°C	100
Figure 4.32: SEM/EDS of MD03 cured samples	101
Figure 4.33: SEM/EDS of GP01 cured samples	102
Figure 4.34: SEM/EDS of GP01 samples heat-treated at 400°C	103

Figure 4.35: SEM/EDS of GP01 samples heat-treated at 800°C	104
Figure 4.36: XRD pattern of MD01 cured	106
Figure 4.37: XRD pattern of MD01 heat-treated at 400°C	106
Figure 4.38: XRD pattern of MD01 heat-treated at 800°C	106
Figure 4.39: XRD pattern of MD02 cured	107
Figure 4.40: XRD pattern of MD02 heat-treated at 400°C	107
Figure 4.41: XRD pattern of MD02 heat-treated at 800°C	107
Figure 4.42: XRD pattern of GP01 cured	108
Figure 4.43: XRD pattern of GP01 heat-treated at 400°C	108
Figure 4.44: XRD pattern of GP01 heat-treated at 800°C	108
Figure 4.45: XRD pattern of MD03 cured	109
Figure 4.46: Physical appearances of MD01 a-h specimens at room temperature, and after exposure to 400°C and 800°C	114
Figure 4.47: Physical appearances of M02 a-h specimens at room temperature, and after exposure to 400°C and 800°C	115
Figure 4.48: Physical appearances of M03 a-h specimens at room temperature, and after exposure to 400°C and 800°C	115
Figure 4.49: Physical appearances of GP01 a-h specimens at room temperature, and after exposure to 400°C and 800°C	116
Figure 4.50: Comparison of the physical appearance of MD01, MD02 and GP01 specimens	119
Figure 4.51: Density patterns for MD01, MD02, MD03 and GP01 mixes a – h	121
Figure 4.52: Graphical representation of the chloride ion penetration test for control mixes	123



Figure 4.53: Pore size distribution of each mix as obtained from the BET approach	125
Figure 4.54: Graphical representation of the average initial compressive strength readings of specimens	128
Figure 4.55: Average strength loss of specimens (%) after exposure to 400°C	132
Figure 4.56: Average strength loss of specimens (%) after exposure to 800°C	133
Figure 4.57: A comparison of the average mass loss (%) after 400°C	138
Figure 4.58: A comparison of the average mass loss (%) after 800°C	138
Figure 4.59: SANS processed images for MD01	141
Figure 4.60: SANS processed images for MD02	142
Figure 4.61: SANS processed images for MD03	142
Figure 4.62: SANS processed images for GP01	143
Figure 4.63: Colour gradation contour map of MD01 specimens	145
Figure 4.64: Colour gradation contour map of MD02 specimens	146
Figure 4.65: Colour gradation contour map of MD03 specimens	147
Figure 4.66: Colour gradation contour map of GP01 specimens	148
Figure 4.67: Water and steam being expelled from the unexposed surface of the panels (time ca. 60 mins)	153
Figure 4.68: Images of the fire exposed surface of the panels after test	154
Figure 4.69: A contour plot of Panel 1 after the fire test	155

## List of Tables

Table 2.1: Production of cement in year 2020	15
Table 2.2: Some key findings on concrete spalling	17
Table 2.3: Characteristics of the different forms of spalling	18
Table 2.4: Main categories of fly ash	27
Table 2.5: Information on the pressure and spalling behaviour	33
Table 3.1: Chemical composition of cementitious materials as provided by the supplier	47
Table 3.2: Chemical compositions of Grade D sodium silicate.	49
Table 3.3: Quantities of sodium hydroxide (NaOH) and water to produce sodium hydroxide solution of given molarity	49
Table 3.4: Details of the mix designs	51
Table 3.5: Mix design terminology incorporating polymeric additives	52
Table 3.6: Details of large-scale fibre mix designs	54
Table 3.7: Details regarding chloride ion penetrability (based on charge passed) as per C1202-09	70
Table 4.1: DSC data of the sacrificial agents	84
Table 4.2: PCFC data for sacrificial agents	90
Table 4.3: Average slump flow readings	92
Table 4.4: Essential NMR data of the cured samples of concrete and geopolymer before and after exposure to 400°C and 800°C	110
Table 4.5: Visual observations of the physical appearance of cubical specimens after exposure to 800°C	117
Table 4.6: Average density measurements for cubical specimens	120
Table 4.7: Average charge passed and classification of chloride ion penetration	122
Table 4.8: Summary of surface area results obtained by the nitrogen adsorption method	124

Table 4.9: Summary of pore volume results obtained by the nitrogen adsorption method	124
Table 4.10: Summary of pore size results obtained by the nitrogen adsorption method	124
Table 4.11: Tabulated readings of the average initial compressive of specimens	127
Table 4.12: Tabulated readings of the residual strength of specimens	129
Table 4.13: Compressive strength readings (MPa) obtained from cubical and cylindrical specimens	133
Table 4.14: Correlation between cubical and cylindrical specimens	134
Table 4.15: Average mass loss of MD01 cubical specimens (%)	135
Table 4.16: Average mass loss of MD02 cubical specimens (%)	135
Table 4.17: Average mass loss of MD03 cubical specimens (%)	136
Table 4.18: Average mass loss of GP01 cubical specimens (%)	136
Table 4.19: Strength and mass loss results of non-carbonated and carbonated specimens	139
Table 4.20: Spalling depths (mm) at every 100 mm from the fire exposed surface	150
Table 4.21: Summary of the spalling and mass loss results	151
Table 4.22: Spalling results as per the above-mentioned criteria	151
Table 4.23: Some qualitative visual observations during the tests	152
Table 4.24: Calcium contents, determined through ICP/OES measurement	154
Table 4.25: Aluminium contents, determined through ICP/OES measurement	154

# **CHAPTER 1**

## **INTRODUCTION**

## **1.1. General background**

Concrete can be identified as one of the most commonly used materials within the construction industry for several reasons, such as durability, high compressive strengths, stability, and high resistance to fire. Whilst concrete is generally regarded as having superior properties at elevated temperatures compared to other building materials, such as timber or steel, some concretes, mainly high strength concretes (HSC), undergo a phenomenon referred to as ‘spalling’, which is associated with the flaking, breaking off, or in severe cases, exploding of concrete layers. This can subsequently reduce the load bearing capacity of the structure, or in some cases, impede firefighting efforts if concrete spalling is explosive in nature (Guerrieri and Fragomeni, 2010, Kannangara et al., 2022, Amran et al., 2022). The first recorded observation of concrete spalling was made by Barret (1854) which was reported by Jansson (2013a) in 1854. It was reported that the concrete was seen to split and yield when exposed to high temperatures when the aggregate used in the concrete is flint (Jansson and Boström, 2014, Jansson, 2013a). From then on, there have been uncountable efforts to reason and understand this phenomenon, and hence, mitigate the high levels of damage caused on the stability and structural integrity of concrete structures after heat/fire exposure (Jansson, 2013a, Jansson and Boström, 2014, Barret, 1854, Hertz and Sorensen, 2005). While there have been several theories brought forth by numerous researchers as contributory factors towards spalling, due to concrete being a heterogenous material with complex physical and chemical processes occurring simultaneously during heating, it has proven to being a difficult task to agree to a consensus hypothesis (Jansson, 2013a).

As mentioned above, concrete undergoes several physical and chemical changes when exposed to elevated temperatures. These changes have been mainly categorised as being thermo-hydral, or thermo-mechanical. Thermo-hydral refers to the changes in the microstructure associated with the changes in moisture within the concrete, such as, moisture movement, water build-up, dehydration, etc., whereas, thermo-mechanical focuses on the changes in the microstructure of concrete with respect to the stresses formed as temperature increases, such as, thermal stresses, residual stresses, tensile stresses, etc. (Hedayati et al., 2015, McCormack and Postma, 1977, Chen et al., 2009b, Hertz, 2003, Hertz and Sorensen, 2005, Kannangara et al., 2022).

Another interesting observation relating to concrete spalling was made in 1905 by Woolson (1905), who reported an egress or accumulation of water from the unexposed

surface of heated concrete, which is referred to as ‘water pooling’. This is now a common observation in concrete fire tests, where water can be seen to flow out from the unexposed surface while the opposite face is being exposed to high heat/fire (Guerrieri et al., 2020, Lee et al., 2023). In a study conducted by Jansson (2013a), it was reported that water was seen to egress from the unexposed surface, just 40 minutes after a 30 cm thick concrete slab began exposure to a single-sided fire. It was also reported that the reason for such an occurrence could be due to the presence of a continuous crack-system within the concrete, which would have allowed the water molecules within the concrete to flow through the concrete and pour out of the cool surface. Moreover, it was also stated that the formation of these cracks is unclear, and could be a collection of old cracks, together with newly formed cracks before and after exposure to high temperature levels (Jansson, 2013a). The interesting recognition of this condition of water pouring out from the unexposed surface with the gradual rise in internal temperature is that it has now been classified as a major contributor in concrete spalling, which could dictate the type and time of spalling (McNamee, 2019, Chapman and England, 1977, Choe et al., 2019). In a study conducted by Ye et al. (2020), a major cause for concrete spalling was acknowledged as being the entrapment of water vapour pressure within the concrete as the internal temperature rises. In addition to this, the accumulation of internal pore pressure together with flexural cracking have also been identified as key contributors towards concrete spalling (Guerrieri and Fragomeni, 2010, Amran et al., 2022). It was reported that pathways would have been created by the flexural cracking within the concrete which would have facilitated considerable amounts of water molecules to move through the concrete microstructure and egress from the cool surface during exposure to high heat/fire.

During a study conducted by Hedayati et al. (2015), it was mentioned that the compressive strength reduces when the exposed temperature is below 100°C, mainly because of the movement of free water and an increase in energy. Furthermore, during the heating process, the development and spread of cracks are seen as significant events that can result in serious spalling issues. In addition to this, as the temperature increases, the thermal gradients which occur within the concrete due to the very hot external face and the comparatively cooler internal core, were reported to have created a crack network within the concrete as water molecules were forced out of the cement paste (Van der Heijden et al., 2007, England and Khoylou, 1995). However, while this phenomenon of moisture movement and egress is reported as being a major contributor for concrete spalling which,

in turn has several adverse effects on the structural stability of the concrete, the factors that influence the movement of moisture and its patterns within the concrete are difficult to identify and define using experimentation. Moreover, modelling of the flow of water as it moves through the cold regions during exposure to high heat/fire also presents significant challenges. Therefore, new and advanced experimentation which can look through the dense microstructure of this complexly behaving concrete is crucial in understanding the level of influence moisture migration has on spalling (Jansson, 2013a, McNamee, 2019, Hedayati et al., 2015, Kannangara et al., 2022).

In contrast to the phenomenon of concrete spalling, concrete also possess a major threat on the environment due to its binding ingredient, cement. With the global carbon dioxide (CO<sub>2</sub>) emission generated through the production of cement, projected to reach 2.34 Gt/year in 2050 (Khongprom et al., 2020), concrete is a material which has a high carbon footprint and researchers are striving to find new and alternative replacements to concrete binders. Cement replacement materials are being tested on in large scales, with hope of reducing the cement consumption in partial or in full replacement to cement during concrete production. Supplementary cementitious materials (SCM) have become a popular option, where materials which are high in pozzolanic properties such as silica fumes (SF), fly ash (FA), ground granulated blast furnace slag (GGBFS), metakaolin (MK), rice husk ash (RHA), etc., are being tested on with a view to reducing the overall cement consumption in concrete (Swamy, 1986, Ramezaniapour, 2014, Thomas et al., 2019).

Amongst these supplementary cementitious concretes, geopolymer (GP) concretes were first developed in the 1970s, by Joseph Davidovits, which is free from traditional cement (Davidovits, 2002b). Fly ash, which is a by-product of coal power stations, is a material which is very commonly used as the cement replacement material in the production of geopolymer concretes (Li and Wu, 2005). In addition to this, pozzolanic materials such as GGBFS, or MK, which are rich in silicon-dioxide and aluminium oxide are also used as the source material (Swanepoel and Strydom, 2002, Hardjito et al., 2004a, Rovnaník, 2010). While a key advantage in using SCM in full replacement to conventional cement reduces the overall carbon emission of concrete, another benefit can be identified as the high early strength (within 24 hours of casting) these SCM can achieve using optimal curing conditions. In addition to this, the reduced levels of spalling reported by the use of such SCM- based

concretes have also proven to being a valuable advantage in the realm of building fire-safe infrastructures (Ryu et al., 2013, Lloyd and Rangan, 2010).

In addition to this, while concrete performs exceptionally well under compression, the flexure-tensile properties are comparatively low (Xiao et al., 2024). Which is why structures cannot be built using concrete alone as there needs to be a material high in tensile performance to take in these tensile or flexural loads. While using steel rebars during placement of concrete is the popular option, the extreme energy consumption which creates a high carbon footprint on the environment during the manufacturing of steel has driven researchers to investigate new and innovative materials to cope with this matter. Hence, fibre-reinforced concretes (FRC), which incorporate fibrous materials during the mixing of concrete in its wet state, has become a popular option. Materials such as glass, polypropylene (PP), nylon, carbon, steel, etc. can be used to improve the tensile strength of concrete. In addition to this, research also shows that these FRC have excellent permeability, a higher resistance to spitting, better resistance to frost damage and higher impact resistance (Rai and Joshi, 2014, Löfgren, 2005, Nili et al., 2018, Kannangara, 2018). Furthermore, studies also show a reduction in the spalling behaviour of FRC, i.e. with the addition of fibrous materials such as steel, polypropylene (PP), glass, etc., compared to conventional concretes (Gong et al., 2023, Sanchayan and Foster, 2016, Eidan et al., 2019, Canbaz, 2014).

By taking into consideration all the above factors, this project focused on a quantitative approach to acquiring a systematic and reliable compilation of data and new information on the transformations occurring in concrete during fire. Through a series of small-, medium- and large- scale experimentation, several factors such as the compressive strength, flow properties, residual strength, mass loss, etc. were assessed. Here, three types of ordinary Portland cement (OPC)- based concretes having varying levels of strength, and one FA-based GP concrete were tested on. In addition, synthetic fibrous materials, namely PP, cotton and polyester were incorporated to investigate the effects/microstructural changes of using such fibres when concrete is exposed to fire/heat. It was expected that the empirical data obtained through the above investigations will lead into possible analytical correlations amongst test data, thus aiding in deciphering the fundamental physio-chemical processes underpinning the spalling phenomenon of spalling of concrete.



## **1.2. Rationale behind the current programme**

The topic of concrete spalling has been a prominent subject of discussion and research in the field of concrete construction worldwide. During the phenomenon of spalling, a significant flow of considerable amounts of water is seen to egress from the concrete's unexposed surface during fire. This pooling of water assumed to be occurring due to the microstructural changes occurring within concrete during temperature rise, and was highlighted in 1905 as being a prominent cause of spalling (Woolson, 1905, Weber, 2022, Chen et al., 2009a). However, while various studies have been undertaken to understand moisture pooling, due to several complex physio-chemical changes occurring simultaneously within concrete during fire, a quantitatively-structured experimental approach which can interpret test results into spalling predications based on moisture migration and water pooling is yet to be found. Moreover, post fire studies of spalling show that the highest form of devastation occurs when the concrete layers break away and leave the reinforcement bars directly exposed to fire and vulnerable to failure. Conventional steel generally shows a significant loss in yield strength over a temperature of 400°C (Franssen and Real, 2012). Although the embedded steel in the concrete would not instantly reach the external temperature of the concrete structure during a fire (which could reach over 1000°C within a few minutes, if in the case of a tunnel fire), spalling of the concrete cover would make the steel vulnerable to external fire exposure. This then leaves the entire structure at risk of sudden collapse due to the significant loss of strength of the steel reinforcement. Therefore, the time and type of concrete spalling is important and is still an area which consists of undetermined parameters. While various studies have been undertaken to understand this phenomenon, spalling is one of the most inadequately understood processes occurring inside concrete in reaction to fire (Choe et al., 2019, Jansson, 2015, Stelzner et al., 2019a, Kannangara et al., 2022).

The contribution to the existing knowledge from the present work falls under the realm of better understanding the mechanism(s) responsible for the spalling of concrete elements through a direct experimental approach. While the project was built on the existing knowledge of concrete spalling, it also explored the provisions of the routine analytical techniques in elucidating the fundamental physio-chemical processes underlying the phenomenon of spalling of concrete. Results obtained from the relevant tests also contributed to understanding the spalling of the test specimens at a molecular level. Therefore, the

novelty of this research lies in gathering relevant data through the deployment of a host of analytical techniques, such as, solid-state nuclear magnetic resonance (NMR), inductively coupled plasma/optical emission spectrometry (ICP/OES), small angle neutron scattering (SANS), X-ray diffraction (XRD), scanning electron microscopy with energy dispersive provision (SEM/EDS), etc. In addition, a variety of polymeric materials, referred to as sacrificial agents, with varying physio-chemical properties were employed in concrete production with a view to mitigating spalling in test specimens.

### **1.3. Significance of research**

This research will mainly help address two of Australia's National Research Priorities: Safeguarding Australia and Reducing the Carbon Footprint.

Firstly, the prediction of concrete behaviour in fire will provide security against bushfires, acts of terrorism and hydrocarbon fuel accidents for high fire risk infrastructures such as tunnel fires. Especially in countries like Australia where there is high risk of bushfires occurring, structures need to be protected against spalling conditions. Recent studies show that the 2019–2020 bushfires which took place in New South Wales, Australia burnt more than 17 million hectares of land, claiming lives and destroying houses (Deb et al., 2020), and the demand for housing and infrastructures in rural and suburban areas around Australia have increased, (Stewart et al., 2007, McLennan et al., 2015). Moreover, these areas, being in close proximity to bush areas or forests, having a high probability of reaching high temperature levels in conjunction with high wind speeds and low humidity, entertain the formation and spread of bushfires at a higher degree. Studies also show a major increment in the duration of the fire seasons, which can only be expected to intensify in the future (Jolly et al., 2015) and bushfires can reach temperatures of over 1000°C. Papalou and Baros (2019) provided information of the damage on reinforced concrete structures after exposure to bushfire, where it was reported that cracks in beams and columns, sagging of slab sections, and spalling of elements, to a degree where the cover of concrete had deteriorated and the structural steel members was visible, had been observed. Schulze et al. (2020) also provided a case study of schools and hospitals which were built with concrete that underwent extreme spalling due to bushfire, with significant structural damage. Therefore, it is vital to understand the spalling risks that elevated temperature levels pose on concrete elements, as

the understanding of how concretes will behave when exposed to fire will help in the construction of more fire-resilient buildings, especially, in bush-fire prone areas. This will in turn provide enhanced security and safety for the occupants.

Secondly, global warming is a major contributor of climate change around the world. Significant increments have been recorded in the rise in global temperature, which, in one way augment to the fire risks, and in another, reflect on the impacts caused on the environment. Additionally, studies show that the greenhouse gas emissions would double over the next 20 years (Initiative, 2009); hence, it is crucial to reduce the carbon footprint and build using a more innovatively sustainable framework within the construction industry. This project will contribute to areas of sustainability and innovation by increasing the lifespan of structures. To elaborate on this point, it is evident that spalling is indeed a hazardous condition which degrades the structural integrity, and mechanical properties of concrete structures once exposed to fire. So, if structure were built to withstand extreme heat and maintain the structural integrity, rehabilitation, or demolition and rebuilding would not be necessary. Hence, this would reduce the overall concrete consumption for such reconstructions or renovations. Moreover, understanding the possibilities of using a cementitious material (s), which are generally a by-product (s) (residue) of other industries (such as FA), in replacement to cement, or sacrificial agents, such as polyester, which is now gathering more attention as having high negative impacts on the environment owing to its poor recyclability (Slater, 2008, Zuo et al., 2024), will further help in reducing the carbon footprint of concrete.

Therefore, the potential benefits and significance of this research can be given as: reducing the risks caused by aggressive spalling conditions; increasing the structural integrity of concrete elements; prolonging the lifetime of concrete structures; requiring lesser remedial measures in the case of fire; and improving the sustainability of concrete materials, through the use of environmentally friendly replacements, thus reducing the overall carbon footprint.

#### **1.4. Overall aim of the project**

The overall aim of the project is to systematically investigate the physio-chemical transformations occurring in selected OPC- based concrete and FA- based GP concrete mixes during spalling, when test specimens are exposed to heat/fire. Subsequently, to investigate the beneficial effects of some selected polymeric materials in mitigating the extents of spalling of the test specimens.

#### **1.5. Individual objectives**

1. Evaluate the morphology, chemical natures, and thermal and calorimetric properties of the various raw materials and polymeric fibres, by using appropriate techniques such as high-resolution optical microscopy-SEM/EDS, XRD, Fourier-transform infrared (FT-IR), solid-state NMR, thermogravimetric analysis (TGA), differential scanning calorimetry (DSC) and pyrolysis combustion flow calorimetry (PCFC).
2. Formulate the mix designs and undertake casting and curing of test specimens (both cubical and cylindrical) based on OPC and FA.
3. Determine the relevant morphological, spectroscopic, thermal and calorimetric properties of powdered samples obtained from control and heat-exposed specimens using SEM/EDS, XRD and solid-state NMR techniques.
4. Assess the mechanical properties of OPC- based concretes and FA- based GP concretes, such as flow properties of fresh concrete, density and compressive strength of hardened specimens with and without the incorporation of polymeric fibres, and the residual, and mass loss properties of these specimens, after exposure to high temperature levels.
5. Measure the porosity of control samples by employing Brunauer–Emmett–Teller (BET) theory and rapid chloride penetration test (RCPT).
6. Estimate the levels of carbonation of control and heat-exposed specimens that underwent accelerated carbonation reactions with a view to gauging the build-up of carbonate in the specimens using TGA.

7. Gauge the changes in the surface profiles and chemical natures of the hydration shell around the calcium oxide centres using SANS and 3-D optical profilometry studies for control and heat-exposed specimens.
8. Conduct atomic absorption spectroscopic analyses using ICP/OES for determining the amounts of  $\text{Ca}^{2+}$ ,  $\text{Fe}^{3+}$ ,  $\text{Al}^{3+}$  and Si in the pooled water obtained through large-scale furnace tests.
9. Correlate of relevant empirical data with view to deciphering the basic physio-chemical processes underpinning spalling.

## **1.6. Thesis outline**

This thesis is organized into five chapters. Chapter one presents a background to the study which has led to identifying some research gaps, which also resulted in the research questions and their respective rationale. Moreover, the overall aim and the individual objectives of the research programme are described towards the end of this chapter, including an outline to the thesis.

Chapter two, predominantly, discusses the relevant literature precedents in the subject area in detail. Here, concrete as a construction material, including the performance of it in fire-based scenarios and theories associated with concrete spalling are adequately covered. In addition, GP concretes, focusing mainly on FA being used as the base material, is also covered in this chapter, with a view to understanding the spalling attributes of these GP concretes, when used as the binding material, in comparison to OPC-based concretes. Furthermore, current studies on the effects of adding various synthetic polymeric materials, namely PP, cotton and polyester (also referred to as ‘sacrificial agents’ in this study), into concrete in order to mitigate the spalling behaviour of test samples were also investigated. Towards the latter parts of this chapter the main test methods focused on concrete spalling and moisture migration techniques at small-, medium- and large-scale are also covered.

Chapter three presents the materials and experimental procedures which were employed in this study. Here, the physio-chemical properties, as per supplier information, of the different raw materials which were used to cast the specimens in the study (such as, dry

ingredients, liquid components, and reinforcing materials) are given. In addition, the various methods which were employed to cast and cure the specimens are also explained thoroughly. In the latter parts of the chapter, the test equipment, instrumentation and experimental parameters, including typical operating conditions are discussed in detail.

Chapter four reflects the main emphasis of the PhD programme, where the information from the various test methods is collated, and correlations are drawn. First, the morphology, chemical natures, and thermal and calorimetric properties of the raw materials and sacrificial agents (polymeric materials), were analysed using SEM/EDS, XRD, solid-state NMR, FT-IR, TGA, DSC and PCFC tests. Following on from this, the flow properties of each mix designs were tested and assessed. Once the concrete specimens reached full conditioning, the relevant morphological, spectroscopic, thermal, and calorimetric properties of powdered samples obtained from both cured and heat exposed concrete specimens were conducted using techniques of SEM/EDS, XRD and solid-state NMR. Next the densities and the initial compressive strengths were assessed for the concrete specimens with and without the addition of sacrificial agents (polymeric materials). Subsequently, residual strength and mass loss properties were analysed with a view to understanding the spalling behaviour of the each of the mix designs after exposing the specimens to elevated temperature levels of both 400°C and 800°C. Moreover, cubical and cylindrical samples were tested and correlations between the two sizes were drawn in regard to the initial compressive strength. In addition, to understanding the porosity of the different mixes, which could be used to draw up correlations between the spalling behaviour and the permeability, the control specimens were subjected to porosity testing thorough the RCPT and BET techniques.

Towards the latter stages of the study, TGA thermograms were primarily utilized to gauge the extents of chemical transformation of the hydration shell around  $\text{Ca}^{2+}$  centres on concrete specimens which underwent accelerated carbonation. Furthermore, the morphology from the cured to the heated samples were studied using optical profilometer and SANS investigations. In addition to this, the pooled water samples obtained from the large-scale furnace tests specimens were analysed for dissolved chemical species ( $\text{Ca}^{2+}$ ,  $\text{Fe}^{3+}$ ,  $\text{Al}^{3+}$  and Si) by using the ICP/OES. Moreover, this chapter presents the results obtained from the large-scale tests. The important aspect of these experiments in this category was to investigate the micro-elemental composition of the pooled water, based on the levels of

spalling the specimens underwent when exposed to high temperatures, with a view to gaining a better understanding the physio-chemical processes underpinning spalling.

Chapter five presents the main conclusions (i.e., the summary of the research outcomes) which highlights the key findings. It also forms the part of the thesis where a brief account of the future perspectives, including some suggestions for further work is discussed. This will be also followed by a list of relevant references.

## **CHAPTER 2**

### **LITERATURE REVIEW**



## **2.1. Chapter overview**

This chapter presents a comprehensive literature review on the subject matter, where the background and overview of the concrete spalling phenomenon, existing theories and moisture migration processes are given. Studies on the use of synthetic polymers materials, such as PP, cotton and polyester (sacrificial agents) in the manufacturing of structural concretes are also presented. A brief introduction on the use, mechanical properties and spalling behaviour of GP concretes is also covered in this chapter. In the latter parts of this chapter, information on small-, medium- and large-scale testing after exposure to elevated temperatures is presented, where, materials, test methods, loading conditions, temperature curves, results obtained, and main conclusions are given. Here, the focus is to understand the test methods which can be used to gauge the spalling behaviour by focusing on techniques used for measuring the moisture migration processes when concretes undergo heat/fire exposure.

## **2.2. Concrete in construction**

Concrete can be identified as one of the oldest and traditional building materials used in the realm of construction. A few of the main properties which make concrete such a vital material are its versatility, high compressive strengths, durability, ease in moulding and shaping, and comparatively high fire performance (Gan, 1997). In addition to this, while concrete does not perform well under tensile properties, being a comparatively brittle material, its ability to perform in unisons with steel to share the tensile and flexural loads, has made it an even more valuable material in construction (Neville, 1995).

The basic constituents which make up concrete are cement, aggregate (fine and coarse) and water. In addition, mineral and chemical admixtures are also optionally incorporated to enhance the performance of concrete under different environmental and exposure conditions (Neville, 1995). Amongst these raw materials, the production of cement, which is the primary binder in concrete that gives concrete its cohesive nature, comes with noticeable environmental implications. The production of cement is considered as a very energy intensive process, emitting high levels of greenhouse gases into the atmosphere (Mehta, 2001, Durastanti and Moretti, 2020). Reports also show that for every ton of cement produced, one and quarter tonnes of CO<sub>2</sub> is emitted into the environment, where 60% of this

CO<sub>2</sub> is a result of the energy required for the production of cement (Griffin, 1987, Mohamad et al., 2022, Dunuweera and Rajapakse, 2018). **Table 2.1** gives information on the global cement production in the year 2020 (Mohamad et al., 2022).

**Table 2.1:** Production of cement in year 2020 (Mohamad et al., 2022).

Country	Production (Thousands of Tonnes)
China	22,489
India	20,850
Russia	6,060.0
Japan	4,917.0
Pakistan	4,100.0
Thailand	3,243.0
Malaysia	1,866.0
Poland	1,718.0
Taiwan	987.00

Previously published data also shows that the cement production in Australia accounted for approximately 1.3% of the GHG emissions in 2008 (McLellan et al., 2011). A study also reported that the concrete and cement industry is accountable for the production of 7% carbon dioxide of the total world CO<sub>2</sub> emission (Ramezaniapour, 2014). Flower and Sanjayan (2007) conducted a study regarding the levels of CO<sub>2</sub> which is released through the manufacturing of OPC which revealed that about 81% of CO<sub>2</sub> emission in concrete was a result of the burning of fossil fuels, calcination of limestone, mixing and transportation during cement making. In a very recent review article by Singh et al. (2023), it was highlighted that the increase in the use of cement will have unpredictable implications on the environment and the high levels of CO<sub>2</sub> in the atmosphere will cause an unavoidable reality in anthropogenic climate changes. Here, data were also presented which stated that in 2010, the cement industry produced 136 tonnes of nitrogen oxides, 4833 tonnes of sulphur dioxide and 183 tonnes of volatile organic compounds (including harmful dioxins and furans) which can cause damage to the liver, kidney, and the central nervous system (Xing et al., 2016, Grey and Canter, 2011, Singh et al., 2023). Hence, while concrete has several advantageous factors, the environmental implications brought about through the production of cement, has driven researchers to test and find innovative materials which can be used in the place of cement (Cook, 2009, Anand et al., 2006).

### 2.3. Concretes in fire

The fire performance of concrete is known to be of a higher standard when compared with other building materials such as steel and timber. While timber burns in layers and steel melts in fire -based scenarios, concrete can withstand fire by preventing the movement of heat in through the concrete element. **Figure 2.1** presents the microstructural changes which occur within concrete as the temperature increases (Khoury, 2000).

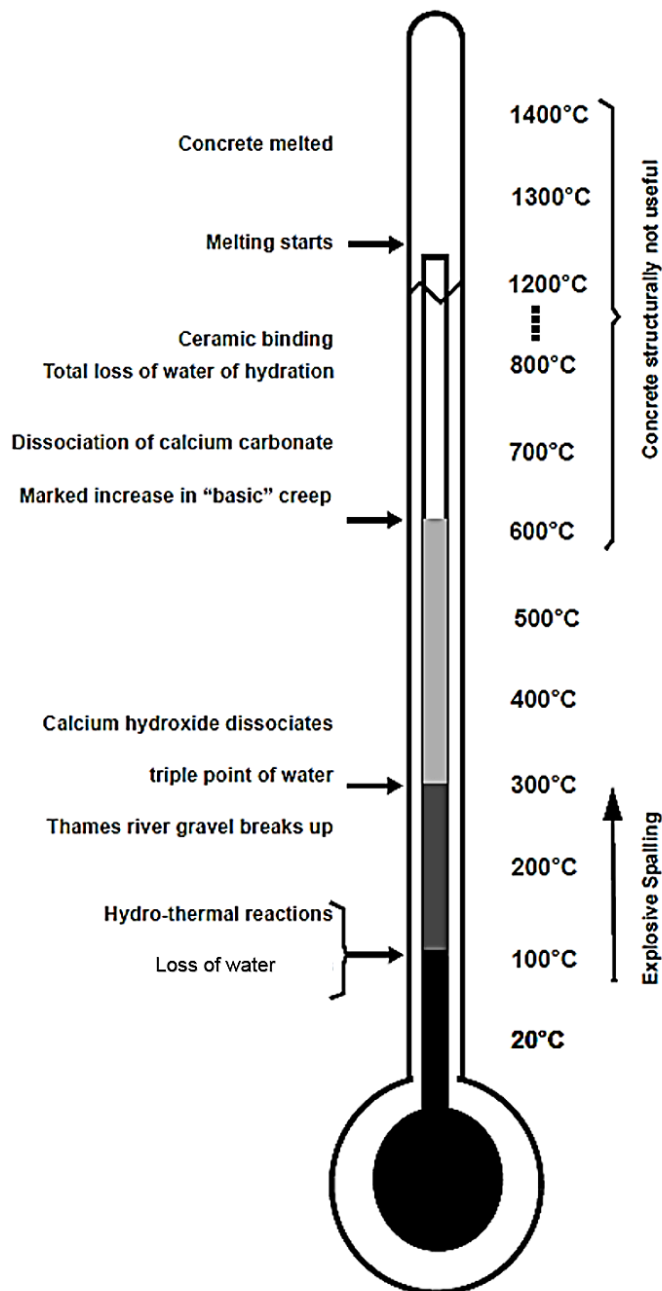


**Figure 2.1:** Microstructural changes of OPC- based concrete at high temperatures (Khoury, 2000)

However, in extreme fires, concrete does undergo a phenomenon referred to as spalling, where layers of the concrete can be seen to break away or, in severe cases, explode, leading to the damages including the disintegration of concrete particles, element failure and loss of structural integrity, which can, in turn, lead to the collapse of entire structures (Deeny et al., 2008). But it is extremely difficult to pinpoint the key initiator of the spalling process and consequently mitigate its effects, due to the heterogenous nature of concretes. The most prominent parameters contributing to concrete spalling has been identified as the permeability, strength, aggregate type, curing regime and moisture content of concrete, the rate of heating, the restraint to thermal expansion and extent of reinforcement (Lalu et al., 2021). During a presentation by Barret (1854), it was discussed that the concrete had a tendency to split and yield during fire if the type of aggregate used in the concrete were of flint stones. In 1905, Woolson was the first person to provide a record of liquid water being expelled from the surface which was unexposed to the fire (Woolson, 1905). In this study, it was reported that about  $\frac{1}{2}$ - $\frac{3}{4}$  inch of water was observed on the unexposed surface of 15 feet span concrete floor specimens in a two-hour fire exposure test. Afterwards, several milestones in the realm of concrete spalling have been identified and recorded over the years. **Table 2.2** provides information on some of these key findings in concrete spalling.

**Table 2.2:** Some key findings on concrete spalling (Jansson, 2013a)

<b>Year</b>	<b>Ref</b>	<b>Finding</b>
1854	(Barret, 1854)	First record of spalling
1905	(Woolson, 1905)	First observation of water being expelled from unexposed surface of concrete during fire
1911	(Meyer-Ottens, 1975)	Early characterization of the types of spalling
1935	(Hasenjäger, 1935)	Main factors which govern spalling was updated
1961	(Harmathy, 1965)	Moisture Clog Theory was brought to light
1966	(McNamee, 2019)	Frictional flow theory
1997	(Khoylou, 1997)	Hydraulic Spalling Theory
2000	(Ichikawa, 2000)	BLEVE theory

Spalling is commonly grouped into four categories; aggregate, corner, surface and explosive spalling (Guerrieri, 2008, Gerasimidis et al., 2021, Meyer-Ottens, 1975, Jansson, 2013a). Aggregate spalling is the splitting off or breaking away of the aggregate particles which is generally recorded to occur within the first 20 minutes of a fire. Corner spalling

occurs 30 minutes after fire exposure and is identified as the breaking-off of the corner sections of the structural element. Surface and explosive spalling are considered more violent forms of spalling. Surface spalling is associated with the degradation of the surface layers which can occur as a progressive form of spalling, which can start within the first 20 minutes of fire exposure. One of the main concerns of this type of spalling is that it leaves the reinforcement exposed and vulnerable to fire exposure. Similarly, explosive spalling, which causes parts of the concrete to explode can be catastrophic. Occurring during the first 30 minutes of a fire and reported to be dependent on high heating rates ( $>30^{\circ}\text{C}/\text{min}$ ), explosive spalling can be loud, fast and occur in a random, unplanned pattern (Connolly, 1995, Shah and Sharma, 2017, Guerrieri, 2009, Phan, 2008, Hertz, 2003, Kannangara et al., 2022). **Table 2.3** gives information on the characteristics of these different forms of spalling, including the factors which are assumed to cause them (Khoury, 2000), and a graphical representation is provided in **Figure 2.2** (So, 2016).

**Table 2.3:** Characteristics of the different forms of spalling (Khoury, 2000)

Spalling	Time of occurrence (min)	Nature	Sound	Influence	Main Influences
Aggregate	7 – 30	Splitting	Popping	Superficial	H, A, S, D, W
Corner	30 – 90	Non-violent	None	Can be serious	T, A, F <sub>s</sub> , R
Surface	7 – 30	Violent	Cracking	Can be serious	H, W, P, F <sub>t</sub>
Explosive	7 – 30	Violent	Loud Bang	Serious	H, A, S, F <sub>s</sub> , G, L, O, P, Q, R, S, W, Z

A-aggregate thermal expansion, D-aggregate thermal diffusivity, F<sub>s</sub>-shear strength of concrete, F<sub>t</sub>-tensile strength of concrete, G-age of concrete, H-heating rate, L-loading/restraint, O-heating profile, P-permeability, Q-section shape, R-reinforcement, S-aggregate size, T-maximum temperature, W-moisture content, Z-section size

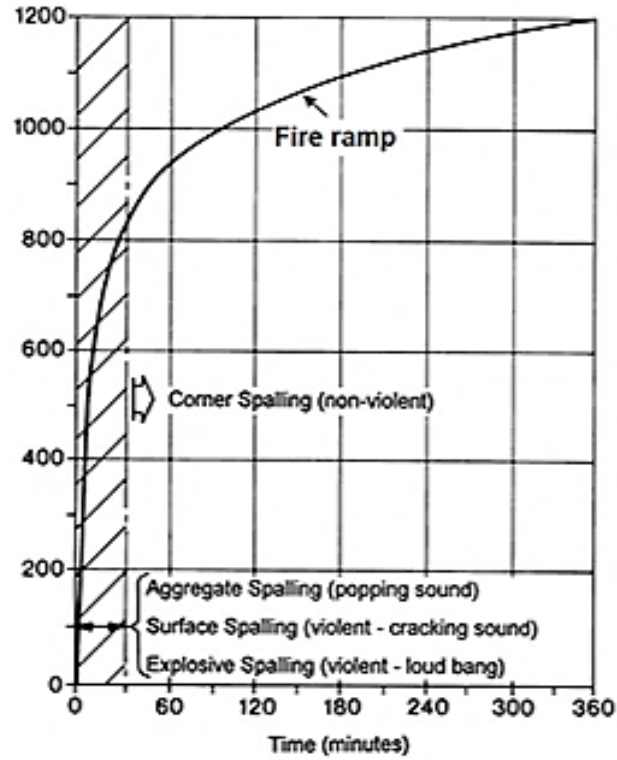


**Figure 2.2:** Time of occurrence for the types of spalling (So, 2016)

The strength of concrete is also known to have a major impact on the spalling behaviour during a fire, with normal strength concretes (NSC) behaving exceptionally well and high strength concrete (HSC), achieved through the modification of conventional concretes, being more susceptible to concrete spalling (Sanjayan and Stocks, 1993, Li et al., 2004a, Shah et al., 2019). While NSC can reach strengths of up to around 40 MPa, HSC, can reach strengths up to 100 MPa, with concrete having strengths of above 100 MPa classified as ultra-HSC (Amran et al., 2022). While the strength improvements, are achieved through enhancement techniques of the microstructural matrix, such as reducing the particle size, increasing the compaction, improving the density, etc. (Hertz, 1984, Kodur and Sultan, 1998, Kodur, 2000, Hertz, 2003, Kodur and Phan, 2007, Kushnir et al., 2021, Menefy, 2007, Chan and Chu, 2004), the water: cement (w/c) ratio has been proven to being a critical factor which governs the compressive strength. The review article published by Amran et al. (2022) summarised the range of w/c ratios appropriate in producing different concretes as being; 0.41–0.70 for NSC; 0.25–0.40 for HSC and; 0.15–0.28 for ultra-HSC. Other related research also showed that the strength of concrete increased with the incorporation of smaller/finer aggregate particles and a lower w/c ratio compared to medium strength concretes (Ali et al., 2001, Yan et al., 2007, Han et al., 2009).

Studies conducted on the fire performance of HSC by Peng et al. (2012) reported that samples having a lower w/c ratio, which achieve high strength readings at the beginning suffered considerable levels of spalling. Furthermore, the residual strength decreased significantly after exposure to 400°C. Rossino et al. (2015) studied the correlation between mechanical properties and the microstructure of concrete after exposure to high temperatures and found that heating to 500°C affects the total porosity of the concrete mixes. Ali (2002) also studied the susceptibility of concrete columns of 127 mm × 127 mm × 1800 mm made using NSC, which displayed a compressive strength of 43 N/mm<sup>2</sup> at 28 days, and HSC, which displayed a compressive strength of 106 N/mm<sup>2</sup> at 28 days, to their spalling behaviours. It was found that the HSC columns suffered explosive spalling conditions with some explosion being very violent. In a study where the spalling behaviour of ultra HSC were assessed, explosive spalling conditions had been observed at temperatures as low as 350°C – 400°C, while NSC withstood temperatures of above 400°C easily (Kannangara et al., 2021b).

The effects of the type and size of aggregate is also known to have an effect on the level of spalling which was studied by Mohd Ali et al. (2018), where three aggregate sizes (7 mm, 14 mm and 20 mm) of granite and basalt were used in the concrete mixes. It was found that specimens which were casted using small size aggregate spalled more severely compared to the bigger aggregate concretes. However, when considering the type of aggregate, basalt had been observed to perform better in fire when compared to the granite mixes.

Dwaikat and Kodur (2010) conducted an experimental analysis of the levels of spalling at various stages of the phenomenon. Testing was carried out on OPC- based NSC and HSC which was achieved by varying the proportions of the mix design while the type of cement, aggregate, casting and curing processes were kept the same. The results revealed that a higher extent of spalling was observed in HSC specimens, which could be attributed to the higher compactness or low permeability within the microstructure. This was further explained through the low permeability within the concrete which would result in an enhancement of pore pressure, and once this exceeds the tensile strength, spalling can occur (Dwaikat and Kodur, 2010).

While the overall durability of HSC and ultra-HSC are found to being higher than that of NSC, thus making them popular in the construction of complex constructions, the extremely poor fire performance of these HSC and ultra-HSC has made them a critical area requiring thorough understanding. The establishment of suitable fire-safety measures have become a fundamental necessity when using HSC and ultra-HSC within the construction industry to ensure fire-safe infrastructures, where more detailed analyses of the causes of spalling is crucial now more than ever, in order to achieve concretes which are both of high strengths and high fire performance.

## 2.4. Theories in concrete spalling

Amongst the several theories brought forth by various researchers for the causes of spalling, thermo-mechanical and thermo-hydral are classified as the most common ones. Concrete, being a heterogeneous material, consisting of cement paste and aggregate particles, responds differently when exposed to heat/ fire. The rate of contraction and expansion varies among these two materials which, in conjunction with the dense microstructure and low thermal diffusivity within concrete, can cause high thermal gradients, leading to an increase in thermal stress within the concrete, thus resulting in micro-cracking (McNamee, 2019). In a relevant publication, Ali (2002) used the concept of *Spalling Degree* to quantify the severity of spalling as given in **Equation 1**

$$\text{Spalling Degree} = \frac{\text{Mass of concrete lost due to spalling}}{\text{Mass of specimen before spalling}} \quad [1]$$

Reports suggest that one reason denser concretes behave poorly in fires is due to the restrictions in the expansions of the materials and moisture which in-turn builds up a greater stress and pressure within the concrete, thus increasing the level of spalling (McNamee, 2019, Zhang et al., 2021). The rate of heating is also reported to influence spalling (Mindeguia et al., 2011). Amran et al. (2022) summarised a set of factors which result in concrete spalling, some of which are; different thermal expansions between cement paste and aggregate which causes an internal crack network; thermal distortion differences between the concrete and the reinforcement bars which causes cracking; opposing thermal expansions of the aggregates and strength loss caused by the chemical changes which causes internal cracking; differential temperatures across the concrete member causing varying compression levels which can cause cracking; increase in the pore pressure as water expands



and vaporises at increasing temperatures; etc. While McNamee (2019) stated that the stresses caused by expanding concrete layers and the stress caused by restrained moisture are in the forefront as being responsible for spalling. The moisture clog theory which was brought to light by Harmathy (1965) is also a popular theory. Some other theories include the frictional flow theory (McNamee, 2019), hydraulic spalling theory (Khoylou, 1997) and the BLEVE theory (Ichikawa, 2000). The following sections discuss these main theories presented on the causes of spalling.

#### **2.4.1. Thermal stress theory**

Regardless of heat exposure, stress can be identified as a key factor for the reduction in strength and the performance of concrete. As the stresses within the element increases, cracks can form within the concrete which can be visible on the external surface as well. Thermal stress can be brought about by the rapidly increasing temperature causing a very high differential gradient between the hot outside and the cool inner core, thus giving rise to stresses. In addition, local strain incompatibilities between the behaviour of the concrete materials (cement and aggregates) can also occur simultaneously, with the aggregates having a tendency to expand until they are chemically degraded, and the cement paste shrinking with the escaping of both physically and chemically bound water as temperature increases. These differential movements can form cracks within the microstructure, thus create spalling (Kalifa et al., 2000). Research also shows that this non-uniform temperature can then cause brittle fractures and delamination buckling (Hedayati et al., 2015, McNamee, 2019). Furthermore, prestressed loading and surface compression may be augmented which can superimpose upon the thermal stresses (Fu and Li, 2011). Hedayati et al. (2015) defined spalling being a result of the thermal instability of concrete elements when exposed to elevated temperatures. However, different processes can occur concurrently, with the spalling mechanism occurring due to the thermal stresses or the vapour pressure build up, or due to a combination of both (Choe et al., 2019). However, predicting concrete spalling based solely on thermal stresses would have the merit of simplicity in this vastly changing concrete. **Figure 2.3** shows a schematic description of thermo-mechanical spalling (Liu et al., 2018).

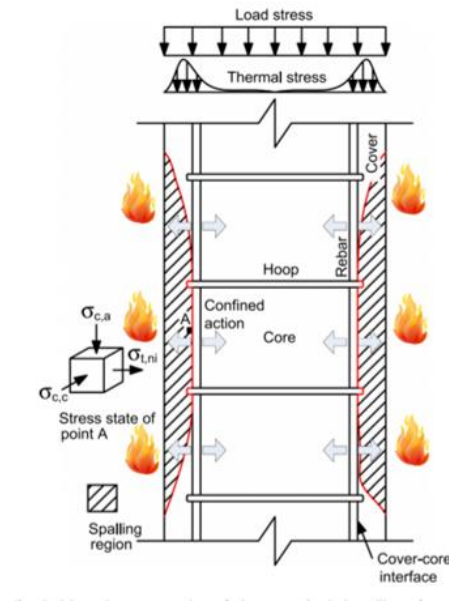


**Figure 2.3:** A schematic description of the thermo-mechanical spalling of concrete (Liu et al., 2018)

#### 2.4.2. Moisture clog theory

Ever since Woolson (1905) noticed water egressing from the non-fire exposed surface during heating, the contribution of moisture and its movement through the concrete towards spalling has been an interesting area of research. The moisture clog theory was described in detail by Harmathy (1965) which stated that as the temperature increases the water molecules found in the pores close to the heat exposed surface would increase in pore pressure and drive the steam not only outside but in to the concrete as well. Subsequently, as this steam reaches the cooler regions within the concrete, it would undergo condensation and become liquid once more. This then would create a fully saturated layer within the concrete of considerable thickness and this layer would create a moisture clogged region restricting the movement of additional moisture, hence, giving rise to pore pressure. Once this pore pressure exceeds the tensile strength of the concrete, spalling would occur (McNamee, 2019, Chapman and England, 1977, Harmathy, 1965, Van Der Heijden et al., 2012). This moisture clog region can be very clearly observed in a study conducted Jansson (2013b) where a 600 mm × 500 mm × 200 mm slab section was split immediately after fire exposure, thus revealing this layer (**Figure 2.4**). However, according to McNamee (2019), no quantitative support has been presented in support of this theory and its effect towards spalling. It was stated that the migration of water entertains the occurrence of a moisture filled region, but

this layer would move through the concrete and cause the pouring out or accumulation of water on the unexposed surface of heated concrete, referred to as ‘water pooling’ (McNamee, 2019, Powierza et al., 2018). **Figure 2.5** shows the moisture movement and formation of the moisture clogged region (Kang et al., 2016).

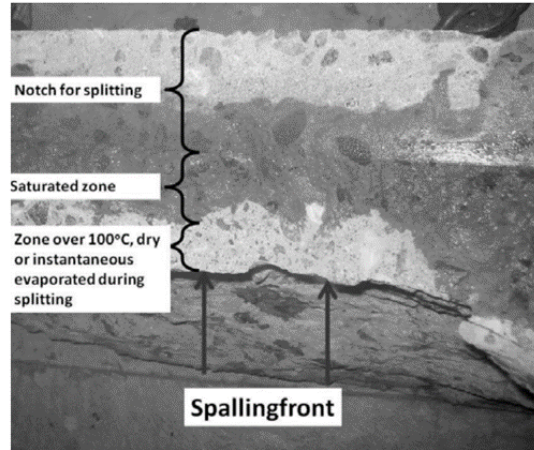


**Figure 2.4:** A cross-sectional view of the concrete element showing the moisture clog region (Jansson, 2013b)

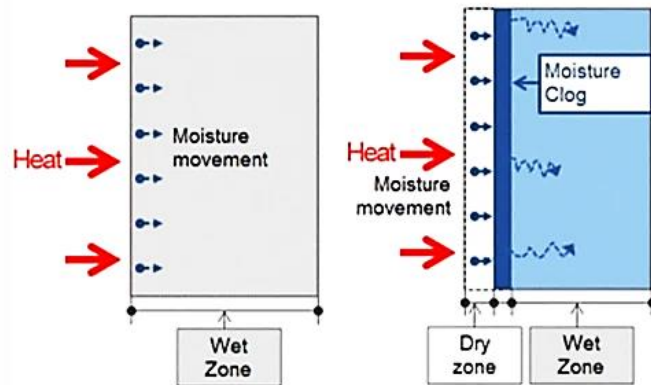


**Figure 2.5:** Sequence of moisture movement (Kang et al., 2016)

### 2.4.3. Pore pressure theory

Pore pressure spalling, also known as thermo-hydral spalling, has been considered a primary factor which can cause spalling by several researchers (McNamee, 2019, Debicki et al., 2012, Zeiml et al., 2006, Liu et al., 2018, Li et al., 2021), though others may disagree (Bažant and Cusatis, 2005). In this theory, it is assumed that if the pore system is partially filled with water at the beginning of heat exposure, water will expand and force the air into

the solid regions within the concrete as temperature increases. This can build up a very high hydraulic pressure within the concrete matrix where the fracture properties will vary, causing cracks to form and eventually leading to spalling (Jansson, 2008, Jansson, 2013b, McNamee, 2019, Van der Heijden et al., 2007, Hedayati et al., 2015, Hertz, 2003). In a recent state-of-the-art review by Li et al. (2021) it was reported that a standard method to quantitatively measure the pore pressure during concrete heating is still unavailable, despite many attempts having been made. Liu et al. (2018) presents a schematic description of the thermo-hygral spalling process in concrete (**Figure 2.6**)

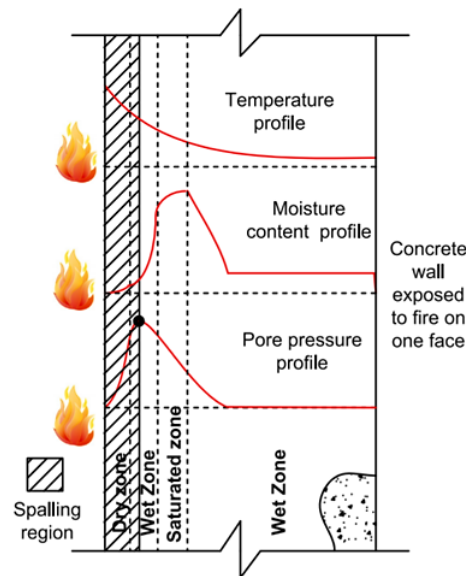


**Figure 2.6:** A schematic diagram of thermo-hygral spalling (Liu et al., 2018)

#### 2.4.4. BLEVE and the frictional flow from vapour flow theories

The boiling liquid expanding vapour explosion (BLEVE) theory states that as the concrete specimen heats up, beyond 100°C the rapid conversion of the water molecules into steam/vapour would create an instantaneous release of accumulate energy. This would then create cracking within the concrete matrix and cause concrete spalling to occur (Ichikawa, 2000).

Another interesting theory according to Shorter and Harmathy (1961) is that as the pressure gradients within the concrete starts driving some of the moisture into the cooler regions of the concrete, frictional forces will be created in its flow path, which can in turn create tensile stress in the concrete. This will cause the concrete which has already suffered

a reduction in strength to break away and spall. This is referred to as the frictional flow from vapour flow theory (McNamee, 2019, Jansson, 2013a).

While it has certainly proven to being a difficult task, with the introduction of new and innovative techniques to understand concrete spalling ground-breaking theories can emerge. Along with theories, changes in concrete compositions have also proven to help combat spalling. Variations of concrete with superior resistance to heat/fire has been studied and one such alternative to concrete which has proven to have a higher resistance to heat/fire are Geopolymer (GP) concretes. The following sections will discuss the properties GP concretes, its main constituent and the performance of these concretes in extreme fire-based scenarios.

## **2.5. Geopolymer-based concrete**

Geopolymer (GP) concretes were first introduced in 1978 by a French scientist, Joseph Davidovits, where a source material, rich in silicon and aluminium, was treated with alkaline solutions, most commonly a mixture consisting of sodium hydroxide or potassium hydroxide and sodium silicate or potassium silicate, to produce an adhesive binder through the process of geopolymerization (Davidovits, 2002b, Lloyd and Rangan, 2010). One of the main reasons for GP binders to have gained increasing attention, as a valuable sustainable material, is because of the inherent reduction in the carbon footprint during its production. For instance, statistics show that about one tonne of CO<sub>2</sub> is released during the production of one tonne of cement, in comparison to only 0.184 tonnes of CO<sub>2</sub> released during the production of GP binders (Davidovits, 2015, Davidovits, 2002a). Hence, a considerable reduction in the global carbon footprint can be achieved through the course of using geopolymer binders (Kannangara, 2018).

When considering the source material used in GP concretes, the most commonly used industrial materials can be identified as fly ash (FA), ground granulated blast furnace slag (GGBFS), also referred to as ‘slag’, silica fumes (SF) and metakaolin (MK). FA, which is a residue generated during the combustion of coal, is identified as the fine part of the ash, which is mostly spherical in shape, having a diameter ranging from 1µm–150µm (Brahmajji and Muthyalu, 2015, Siddique, 2008). During the manufacturing of GP concretes, FA has been rapidly attracting attention due to high levels of silicon and

aluminium contents which greatly enhances the polymerization process (Davidovits, 2008b).

Based on the level of calcium, FA can be classified into two categories, as class C or class F. Class C fly ash consists of a calcium oxide (CaO) content of greater than 10%, whereas, class F FA consists of a CaO content of less than 10% (Hardjito and Rangan, 2005). **Table 2.4** presents the two main categories of FA. Literature shows several studies utilize class F FA over class C FA, due to the high levels of calcium reported to affect the polymerization process, altering the microstructure, thus affecting the strength of GPs (Kong and Sanjayan, 2010, Mane and Jadhav, 2012b, Brahammaji and Muthyalu, 2015, Bakharev, 2006, Hardjito et al., 2005, Gourley and Johnson, 2005). In a study conducted by Duxson et al. (2007a) it was reported that FA based GPs were stronger and more durable compared to slags.

**Table 2.4** – Main categories of FA (Davidovits, 2008a)

Low-calcium FA Class F	High-calcium FA Class C
CaO content is less than 10%	CaO content is greater than 10%
Generally produced from anthracite and bituminous coals.	Generally produced from sub-bituminous and lignite coals.
Roughly corresponds to American (ASTM 618) Class F	Roughly corresponds to American (ASTM 618) Class C

In addition to the source material, geopolymers require a chemical activator which is generally sodium- or potassium-based (Aleem and Arumairaj, 2012); however, due to the better performance in compressive strength, achieved by the sodium- based activators, sodium silicate ( $\text{Na}_2\text{SiO}_3$ ) and sodium hydroxide (NaOH) activators are found to be more commonly used (Zhang et al., 2014, Palomo et al., 1999, Verma and Dev, 2021, Kannangara et al., 2021a).

When considering the chemistry behind GP concretes, during the geopolymerization process, a chain of chemical reactions of alumina-silicate oxides with alkali polysilicates are formed through which these GP binders are created. Aluminium and silicate monomers are formed through these initial chemical reactions which produce Si-O-Al-O bonds. These monomers then change into oligomers and afterward change into silicate polymers (**Figure 2.7**). These three formulas can be used to express these three-dimensional silico-aluminate GP structures; (1) Poly(sialate) type (-SiO-Al-O-); (2) Poly(sialate-siloxo) type (-Si-O-Al-

O-Si-O-) and (3) Poly(sialate-disiloxo) type (-Si-O-Al-O-Si-O-Si-O-). Finally, these GP reactions produce a three-dimensional tecto-aluminosilicate network product (Davidovits, 1994).

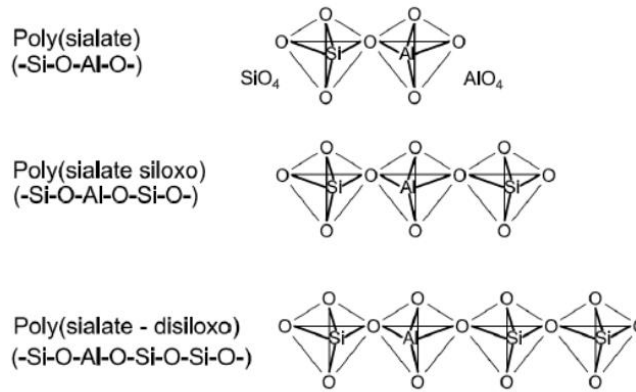


**Figure 2.7:** Chemical structure of Polysialates (Davidovits, 1994)

Unlike conventional concretes, which are cured using water, the curing of GP concretes is achieved through heat. While water curing has been conducted, studies show that the highest mechanical properties such as the durability, strength, permeability, etc. can be achieved when GP concretes are cured at temperatures of  $\geq 60^{\circ}\text{C}$  for a period of 24 hours (Shuaibu, 1950, Sindhunata et al., 2004, Duxson et al., 2007a). While conventional OPC-based concretes require a minimum of 28 days to achieve its full strength, GP concretes are reported to reach its full strength within 24 hours of heat curing (Hardjito et al., 2004b, Rangan et al., 2006, Kannangara et al., 2021a). In another study it was reported that GP concrete specimens resulted in rapid increments in compressive strength up to 24 hours of heat curing at  $60^{\circ}\text{C}$ , after which only very slight increments were observed (Hardjito, 2005). Moreover, in a study which compared heat and steam curing of GP concrete specimens over a period of 24 hours, an increase in compressive strength had been observed in heat cured specimens compared to the steam cured specimens (Hardjito and Rangan, 2005). In addition, Kannangara et al. (2021a) reported that the initial surface evaporation during heat curing of FA- based GP concrete samples has a major effect on both the compressive as well as the residual strength. In this study when the specimens were sealed and protected against initial surface evaporation during the first 24 hours of heat curing, the compressive strength was seen to improve by about 25MPa compared to the non-sealed specimens.

Apart from the high early strength and reduced carbon footprint of GP concretes, several studies have showed that GP concretes have excellent resistance to fire attacks when compared to conventional concretes (Li et al., 2004b, Duxson et al., 2007b, Davidovits, 2013, Wallah and Rangan, 2006, Kannangara et al., 2021a). This serves to be highly beneficial in the case of spalling because HSC have been reported to undergo explosive spalling conditions even at low temperatures. Hence, a concrete which can withstand high temperature levels for a considerable period of time is highly advantageous within the building industry.

## **2.6. The fire performance of GP-based concretes**

The fire performance of GP-based concretes being superior to OPC-based concretes have been proven time and time again. These high levels of fire resistance properties have been reported to be closely associated with the ductility within the mix matrix when exposed to fire/heat (Guerrieri and Sanjayan, 2010, Abdulkareem et al., 2014, Pan et al., 2009). In a recent study where FA was utilized in full replacement to cement, drastic improvements in the resistance to explosive spalling conditions were observed (Kannangara et al., 2021b). In this study, high strength concrete produced with the OPC displayed explosive spalling conditions at around 360°C, whereas the same mix design made using class F FA and sodium-based alkaline solutions, exhibited minimum levels of spalling, even at a temperature as high as 800°C. Mane and Jadhav (2012a) conducted studies on the residual properties of class F FA-based concretes and found that after exposed to 500°C, GP concretes retained 84% more strength, compared to cement-based concretes.

In a study conducted by Zhao and Sanjayan (2011) the fire resistance of OPC- based concretes and GP concretes were tested using the rapid surface temperature rise exposure test and the standard curve fire test. Results had revealed that severe spalling conditions were observed in the high strength OPC concretes, while no spalling was evident in the GP concrete specimens. Furthermore, a sorptivity test showed that the internal structure of the GP concretes was more porous compared the concrete specimens which would have facilitated the release of internal steam during heating, thus reducing spalling. Another similar investigation tested the fire performance of sodium-based GP concrete specimens using two types of fire tests; the standard ISO 834 fire load curve and the Rijkswaterstaat



(RWS) fire load curve, and found, under thermal loading, good mechanical properties with high thermal resistance (Sakkas et al., 2015). Large-scale fire testing was conducted on wall panels made using FA-based GP concretes and reinforced with a single layered steel mesh. The specimens were subjected to single face heating for a period of two hours. The failure loads were calculated and found to be within a range of 61%-71% of the initial strength compared to 50%-53% of the initial strength in OPC- based specimens, thus proving that FA- based GP concretes do indeed possess superior fire performance compared to cement-based concretes (Sarker and McBeath, 2011). In a recent study presented by Abd Razak et al. (2022), the residual strength of 100 mm<sup>3</sup> OPC- and FA- based concrete specimens were compared over a temperature range of 500°C – 1200°C. Results showed that while all OPC-based concrete specimens rapidly lost their strength, the GP concrete specimens were seen to gain strengths of approximately 145% and 113% compared to their original compressive strength. Hence, proving that GP concretes have a higher thermal stability compared to OPC-based concrete specimens (Sarker et al., 2014, Kodur and Phan, 2007).

In addition to the high fire performance of GP concretes, the addition of various fibrous materials such as glass fibres, PP fibres, carbon fibres, steel fibres, polymeric fibres, natural fibres, etc. has been found to improve the fire resistance of concretes. The following section will discuss some of the various fibrous materials which can be used in FRC constructions.

## **2.7. Fibre reinforced concretes**

Reinforcing concrete with randomly oriented fibrous materials, also referred to as fibre reinforced concretes (FRC) was first introduced in the early 1960s (Romualdi and Mandel, 1964, Romualdi and Batson, 1963), after which a large number of researchers have contributed into the development of FRC. As mentioned before, concrete alone cannot bear the tensile loads due to its brittle nature; hence, a ductile material, such a steel reinforcement bars, is required to carry these tensile or flexural loads. In general construction, steel bars are built in, then enclosed in formwork, after which fresh concrete is poured in and allowed to harden. However, in FRC, fibres are incorporated into concrete during mixing of the raw materials and several factors, such as the type of fibre, distribution, geometry and orientation of fibres and concentration of fibres were reported to govern the performance of FRC (Zollo, 1997).

While FRC was introduced as a method to improve the fracture mechanics on concretes by aiding in strength development of brittle OPC- based concretes (Romualdi and Batson, 1963), as research developed it was found that FRC perform exceptionally well in the case of elevated temperature exposure (Tai et al., 2011, Poon et al., 2004, Agra et al., 2021). Thus, the demand for FRC has rapidly increased as a material which can be used for the development of high-performance concretes, i.e., concretes which perform well overall, including in fire- based scenarios. It is reported that the melting and formation of small voids/ cavities of these fibrous materials as the temperature increases, allows the release of internal stresses, thus improving the fire resistance (Varghese et al., 2021).

The several fibrous materials which can be incorporated into concrete can be classified into mainly four categories; SFRC – steel fibre reinforced concrete; GFRC – glass fibre reinforced concrete; SNFRC – synthetic fibre reinforced concrete, which include PP fibres, nylon fibres, polyester fibres, carbon fibres, and polyethylene fibres; and NFRC – natural fibre reinforced concrete, which include wood fibres, coconut fibres, bamboo fibres, etc. (Kaur and Talwar, 2017). Most of these fibrous materials have been used extensively in the production of FRC in construction due to the several superior properties they possess. For example, steel fibres are known to improve the crack and fire resistances, with better residual mechanical properties (Lau and Anson, 2006, Zhang et al., 2020b). In a study conducted by Reis et al. (2001), it was found that none of the SFRC specimens had undergone explosive conditions during heating, which provided strong evidence that steel fibres may be a way of reducing the spalling behaviour. Several other researchers have reported that steel fibres can indeed reduce spalling by bridging the cracks inside concrete and by aiding in reducing the water vapor pressure in the pores of concrete (Poon et al., 2004, Purkiss, 1984, Faiyadh and Al-Ausi, 1989). Amongst the different fibres which can be used in concrete production, this research is focused on using synthetic fibres such as PP fibres, non-absorbent cotton fibres and polyester fibres as the sacrificial agents to mitigate concrete spalling.

### **2.7.1. Polypropylene fibres**

As the concrete industry evolved and the demand for high performance concretes increased, PP fibres became famous as being used as a reinforcement material in FRC to enhance its properties. PP fibres are typically added to the concrete mix to improve its

durability, strength, and resistance to cracking. When used in concrete, PP has also been found to improve several properties (Debicki et al., 2012), some of which are: (1) crack control: which helps control plastic shrinkage cracking in concrete, where these fibres create a three-dimensional matrix within the concrete, reducing the formation and propagation of cracks. This is particularly useful in situations where concrete is exposed to drying conditions or temperature fluctuations; (2) impact resistance: PP fibres improve the impact resistance of concrete. By dispersing energy and enhancing the ductility of the material, they help prevent cracking and spalling caused by impact or heavy loads; (3) durability enhancement: concrete reinforced with PP fibres exhibits improved resistance to freeze-thaw cycles, chemical attack, and abrasion; (4) the fibres generally enhance the overall durability of the concrete, making it suitable for applications that require high durability and fire resistance. Several reports state that the incorporation of polypropylene (PP) fibres can assist in mitigating the levels of spalling (Du et al., 2020, Kalifa et al., 2000, Bentz, 2000, Kalifa et al., 2001, Sultangaliyeva et al., 2019). So (2016) reported that, when exposed to high temperatures, the fibres are reported to melt and create voids within the concrete, thus creating channels for the escape of vapour, thus enhancing the fire resistance properties. **Figure 2.8** gives an image of a concrete specimen after exposure to high temperature levels which clearly shows the void formed after the melting of PP fibres (Hun et al., 2005).

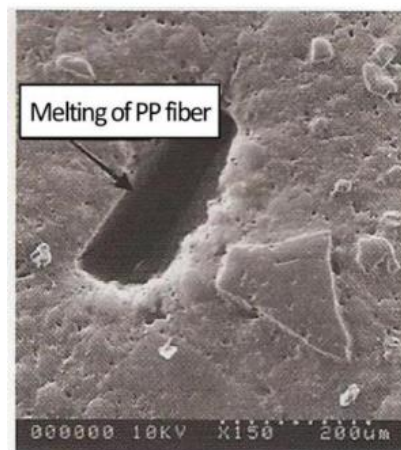


**Figure 2.8:** An image of a void formed through the melting of PP fibres in concrete (Hun et al., 2005)

Previous studies also show that the incorporation of monofilament PP fibres is currently one of the most useful methods in reducing the explosive spalling nature of concretes (Pistol et al., 2014). The investigation proved that as the temperature increases, capillary channels,

which are created as a result of the thermal decomposition of the fibres, connect together to form a net-like micro-crack formation which aids in releasing the internal stress and allows the transportation of vapour. Another study showed that the use of PP fibres help reduce the pore pressure through: (1) reservoirs, which relieves the expanding steam and; (2) continuous channels, which provide pathways for the vapour to migrate (Khoury, 2008). The spalling behaviour was also studied by Zeiml et al. (2006) who reported that the addition of PP fibres resulted in a rise in the permeability of the concrete specimens at elevated temperatures. Li et al. (2019) tested the effects of various aggregate sizes and the inclusion of polypropylene (PP) fibres on the level of spalling and found that the addition of PP fibres was seen to fully prevent spalling for a set strength and are much more effective in increasing permeability than steel fibres and larger aggregates.

When considering the fibre content which can be incorporated in to concrete to achieve optimum conditions, it was reported that  $1 \text{ kg/m}^3$  was sufficient to prevent spalling in high performance concretes (Debicki et al., 2012). However, Kalifa et al. (2001) stated that a dosage of  $2 \text{ kg/m}^3$  was needed to prevent spalling of concretes up to 100 MPa in compression strength, under ISO 834 conditions. In addition, their study reported a fibre length of 10–20 mm and diameter of 50–200  $\mu\text{m}$  produced optimal results. However, these values are not optimized and a dosage of as low as  $0.9 \text{ kg/m}^3$  can be effective in reducing spalling. Another study followed the spalling behaviour of self-settling and tunnel concrete with the incorporation of PP fibres and reported that no spalling was witnessed on specimens having a PP fibre addition of  $1 \text{ kg/m}^3$ . A research conducted by Jansson and Boström (2010) reported that while pressure assists in the redistribution of moisture during heating of concretes, the pressure in the capillary system does not serve as the driving force in concrete spalling. The authors stated that a simple correlation between spalling and the degree of pressure cannot be easily made. Moreover, in the discussion based on the use of PP fibres, the authors deduced that the melting of PP fibres during heating helps in reducing the moisture content in the critical zone on the fire exposed surface, which has a positive effect on the mechanical properties.

The size or length of PP fibres used in concrete can have an impact on their effectiveness and the resulting properties of the concrete (Bentz, 2000). The length of PP fibres affects their distribution within the concrete mix. Longer fibres may have a tendency to clump together, leading to an uneven dispersion. This can potentially result in areas with a higher

concentration of fibres and areas with fewer fibres, thus affecting the overall reinforcement effectiveness. Longer PP fibres have a greater potential for bridging cracks in concrete. They can also span across cracks and help distribute stress, and hence, reducing the crack width and preventing their propagation. Overall, these aid to improve the crack control capabilities of the fibres, and hence contribute to enhanced durability and reduced spalling. The length of PP fibres can also influence their orientation within the concrete. Generally, longer fibres have a greater likelihood of aligning in the direction of casting, or the flow of concrete during placement. This alignment can also enhance the reinforcement properties along specific directions, such as improving tensile strength or controlling cracking in a particular plane (Du et al., 2020).

According to Kalifa et al. (2000) the size of PP fibres can affect the workability and mixing characteristics of the concrete. Longer fibres may require additional mixing effort, or specialized equipment, to ensure proper dispersion and homogeneity in the mix. It is also essential to consider the fibre length and its compatibility with the specific concrete mix design and construction methods being employed. Pistol et al. (2014) stated that shorter fibres are often used for applications where the primary purpose is crack control, while longer fibres are employed in scenarios where additional reinforcement and crack bridging capabilities are desired. However, the selection of the appropriate fibre size should be based on comprehensive testing.

### **2.7.2. Non-absorbent cotton fibres**

The use of cotton fibres in concrete manufacturing is a direction which has not been studied extensively in literature. Cotton fibres can be used as a reinforcement material in concrete, offering certain advantages and characteristics. However, it is worth noting that cotton fibres are less commonly used compared to other types of fibres such as steel or glass or PP fibres. Non-absorbent cotton fibres are typically derived from natural cotton plant sources, made by combing through the natural cotton to extract the shorter fibres then processing through dilution in soda ash/bleach. These fibres are shorter in length, ranging from 15 – 56 mm, with a diameter of about 10 – 45  $\mu$ m (Elfaleh et al., 2023). The use of cotton fibres in concrete aligns with sustainable practices, as they are derived from a renewable natural resource, and incorporating such fibres in concretes can be

environmentally friendly.

When considering the use of these non-absorbent cotton fibres in concrete manufacturing, proper dispersion and mixing of fibres within the concrete mix are crucial for achieving effective reinforcement, as they can clump together. Hence, care must be taken to make sure a uniform distribution of the fibres throughout the concrete matrix during the mixing process and saturate surface dry (SSD) conditions must be ensured (Bartulović et al., 2021)

According to Peña-Pichardo et al. (2018), cotton fibres can provide several benefits when added to concrete, such as, improving the tensile strength and ductility of the material, thereby enhancing its crack resistance and resistance to plastic shrinkage. Moreover, cotton fibres can also improve impact resistance and reduce the occurrence of spalling in concrete. However, it was reported that the compressive strength was seen to reduce as the cotton fibre content increased. Additionally, the dosage of cotton fibres in concrete should be determined through testing, considering factors such as desired reinforcement properties, concrete mix design, and project requirements (Hamada et al., 2023). Peña-Pichardo et al. (2018) recommended a loading of 1 wt.% of cotton fibres in order to obtain the highest mechanical performance in terms of improved tensile strain and young's modules. Here, the cotton fibres were subjected to a novel-type of gamma irradiation treatment when using in concrete manufacturing which helped to increase the flexural strength by 7%.

Adhering to industry guidelines and consulting with concrete experts is recommended when using cotton fibres in concrete applications. While cotton fibres can offer reinforcement benefits in concrete, it is essential to carefully evaluate their suitability for a particular project, specific performance requirements and compatibility with the concrete mix. Albeit, cotton FRC has been used in various applications, including non-structural elements like countertops, decorative concrete, and in some cases, as a replacement for traditional fibres in low-stress applications. However, it important to note that the use of cotton fibres in concrete has certain limitations and considerations. They can be more susceptible to degradation when exposed to moisture and alkaline conditions in the concrete mix. Therefore, it is essential to employ appropriate measures to protect the fibres during mixing, curing, and service life (Wei and Meyer, 2014).

When considering the spalling behaviour of cotton FRC, it is expected that the fibres

would char and create pathways within the internal microstructure at relatively low temperature levels, given that the ignition temperature of cotton is approximately 255°C to 280°C (YAZI, 1956, Li et al., 2023, Hagen et al., 2011), thus, relieving the internal pressure. However, it must be noted that due to the comparatively low number of studies in the area of cotton FRC, mainly in the residual and spalling properties, it is difficult to compare and predict its behaviour.

### **2.7.3. Polyester fibres**

Unlike cotton fibres, the use of polyester fibres in FRC production has evolved into a more common approach in recent years. This has come about through the environmental impacts developed by the textile industry (Peña-Pichardo et al., 2018). At present, the demand for textile products is experiencing an exponential growth, due to the rapidly changing fashion trends and the significant decrease in the life cycle of current clothing products. According to Sandin and Peters (2018), the annual demand for textile increased from 3 kg/person to 31 kg/person, from 2010 to 2020, in developed countries. Moreover, with the increase in world population, which is estimated to exceed 8.5 billion by 2030, the demand for clothing products is expected to increase by more than 60%, from 92 million tons in 2018, to approximately 150 million tons by 2030, thus, creating significant impacts on the environment (Exchange, 2018). During the disposal of textile waste, several adverse effects such as water pollution, soil contamination through landfills, canal obstructions, stagnation in drainage systems, etc., have been reported. Out of these impacts, the pollution of water is reported to be greatly affected mainly through the leeching out of various substances such as sulphur, naphthol, and dyes from clothing (Kant, 2011). Moreover, it was reported that the contaminated water from the textile industry had severely affected the soil by causing changes in the salinity and alkalinity of the soil, which was observed to cause long-term effects on crop yields (Kanan et al., 2014, Kant, 2011).

The use of textile waste in construction, has been reported as being one of the most long-lasting methods in extending the life cycle of textiles and various studies have been published which investigate the use of textile waste materials in the production of composite building materials (Nistorac and Loghin, 2023). The striking benefits were identified as: lowering the carbon footprint, reducing the overall manufacturing costs and improving some

properties in the base material. In a study conducted by Aspiras and Manalo (1995), textiles cuttings were incorporated into the production of OPC-based concrete blocks, at ratios of 1:3, 1:4 and 1:5 by weight (cement: textile waste) and was found that the samples tested under compression loading did not display a sudden brittle fracture even beyond the failure load, unlike conventional concretes. Moreover, while textile waste strips are flammable on its own, as a polymeric additive in the production of these experimental blocks, no evidence of burning was observed even after being subjected to an open fire for 30 minutes. The authors stated that a more lightweight block can be produced for the application of ceilings, walls or even as a substitute for wooden boards. Another study investigated the behaviour of FRC with a 1% and 2% (wt.%) addition of polyester fibres and found that the flexural strength readings of these FRC were higher than that of the control mixes, however, a decrease was observed in the readings with increasing fibre concentration (Reis, 2009).

Another study conducted by Ucar and Wang (2011) reported carpet fibres being utilized in the production of lightweight cementitious composites. Recycled carpet fibres were added up to 20% (fibre: cement wt.% ratio), and the toughness, flexure properties and impact properties were assessed. It was found that the ductile behaviour and bending strength, tested using the three-point bending test, increased. The use of carpet fibres as an polymeric additive in the production of building materials was found to provide a great benefit, because carpet fibres had exhibited the highest levels of leaching out of heavy metals among eight tested polyester textiles, namely: carpet, blackout fabric, curtain, acoustic foam, sweater, short sleeve, scarf and plush toy (Zuo et al., 2024).

The following section discusses the various testing strategies based on small-, medium- and large-scale specimens focusing on the difference in the spalling behaviour and the moisture migration processes.

## **2.8. Test methods and strategies to gauge spalling**

Unlike parameters such as compressive strength, density or tensile strength, there is no direct approach in quantitatively analysing spalling. Generally, spalling is assessed through the loss in mass after exposure to elevated temperature levels. In cases where the concrete is exposed to situations where a rapid increase in temperature is experienced, such as in tunnel fires, spalling can be fast and random, and the degree of spalling can be very difficult to



assess in such cases. Assessment is generally conducted using fire testing, preferably at large scale, which can be extremely expensive and time consuming (Lee et al., 2023). Hence, testing at a smaller scale to medium scale is being conducted by various researchers in order to obtain a collation of information through the measurement of other parameters such as internal pressure, temperature, moisture movement, etc. which could help in quantifying spalling. Discussed below are some test method and techniques at small-, medium- and large-scales.

The pore network of cement paste specimens was studied using mercury intrusion porosimetry by Farage et al. (2003) on specimens that were exposed to temperature levels between 80 °C and 300 °C and found that the total mercury porosity varied up to a temperature of 150 °C. Researchers indicated that it may be a result of the loss of water from the concrete matrix. Nilsson et al. (2018) reported that NMR spectroscopy can be a very useful tool in understanding the moisture content and changes in moisture within concretes during heating, where semi-quantitative results can be obtained using NMR imaging through non-destructive approaches (Pel et al., 2012, Van der Heijden et al., 2011). In a study conducted by Pel et al. (2012) the first quantitative proof of the build-up of a moisture peak/clog in heated concrete specimens was presented. Experimentation was carried out using the NMR test setup where the temperature and moisture profiles were measured more accurately and it was found that the temperatures of the boiling front increased from around 160 °C to 195 °C, thus proving the formation of the moisture clog within the concrete.

The movement of moisture within concrete during heating was studied in cylindrical samples (Stelzner et al., 2019b). The specimens were subjected to unilateral heating, which was obtained by encasing the specimens in a special insulation casing (**Figure 2.9**) while heating to temperatures of up to 300 °C and 500 °C. Results on the moisture distribution analysis had showed that the position of the drying front accommodated explosive spalling. In addition to this, images and measurements from the X-ray CT scan showed that the build-up of moisture occurred in the more internal/deeper sections of the cylinders as the temperature increased. **Figure 2.10** shows the movement of the drying front within the concrete at different depth at varying times of 30, 60 and 135 minutes.

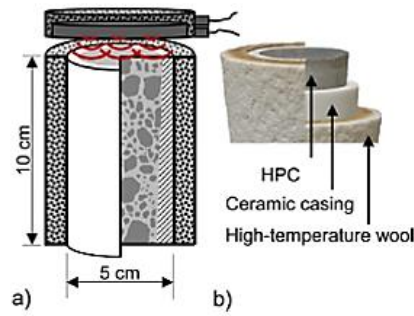


**Figure 2.9:** Specimens encased in a special casing to ensure unilateral heating (Stelzner et al., 2019b)

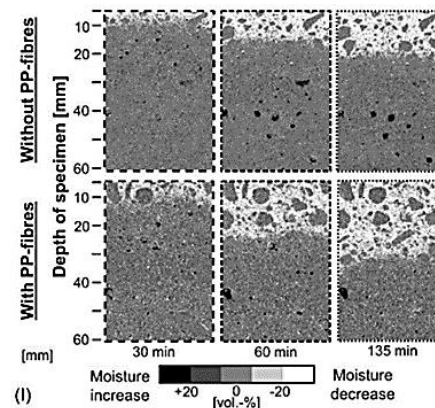


**Figure 2.10:** Movement of the moisture front as temperature levels increased (Stelzner et al., 2019b)

The influence of the moisture clog and movement on the level of spalling was studied by using medium to ultra HSC specimens subjected to two different heating rates:  $1^{\circ}\text{C}/\text{min}$  and  $18^{\circ}\text{C}/\text{min}$ . Results showed that a moisture clog had not occurred at the slower heating rate, however, a supersaturated region (moisture clog) was formed during the fast heating rate, which had caused an increase in the vapour pressure which had in turn caused the specimens to spall vigorously (Choe et al., 2019). Chapman and England (1977) studied the pressure gradients and the permeability of heated concrete specimens and found that the movement of moisture had caused a shrinkage in the dry areas with the mass loss of about 50% compared to the original reading. Moreover, SEM images had shown hydrated products break up and reduce in size causing cracking or flaking of the concrete (spalling).

With the moisture clog theory being a popular one, Jansson and Boström (2009) studied the development of the moisture clog by examining the location of the saturation layer with increasing temperature levels. They achieved this by initially making a 70 mm cut on the side of the cube (**Figure 2.11**), then exposing the bottom section of cube to fire, and then immediately after heating, splitting the cubes to visually identify the location of the saturated

region. Through this method, they were able to provide the first ever visual confirmation of the occurrence of a moisture clog region and the movement of this moisture layer. **Figure 2.12** and **figure 2.13** shows the saturation after 15 and 20 minutes respectively in different concretes.

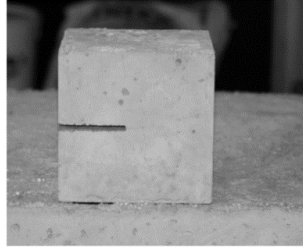


**Figure 2.11:** Concrete specimen with a 70 mm cut on the unexposed surface (Jansson and Boström, 2009)

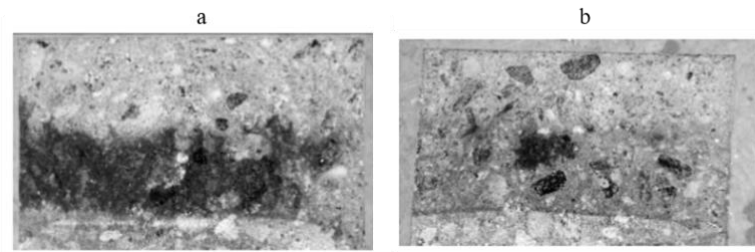


**Figure 2.12:** Test specimens 15 minutes after fire exposure (Jansson and Boström, 2009)  
a. No PP fibres                      b. 1 kg/m<sup>3</sup> PP fibres

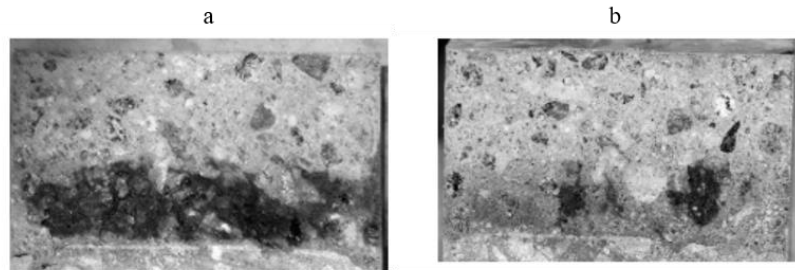


**Figure 2.13:** Test specimens 20 minutes after fire exposure (Jansson and Boström, 2009)  
a. No PP fibres                      b. 1 kg/m<sup>3</sup> PP fibres

Electromagnetic (EM) waves using a Ground-Penetrating Radar (GPR) was employed. by Monte et al. (2017), to assess and follow the movement of the waterfront within concrete specimens during heating. Here, the EM waves, moving at a constant velocity, were directed into the concrete using a handheld geo-radar. Once the waves encounter the waterfront, where the saturation levels are different (between dry and moist regions), they reflected back. The period between the sent and received waves were recorded at different intervals and using this principle the position, and mainly the movement, of the saturation layer was identified. Both temperature and pressure measurements were also taken at depths of 10 mm,

20 mm, 30 mm, 40 mm, 50 mm and 60 mm. **Figure 2.14** presents a schematic diagram of the GPR principle. Results of this study revealed that the waterfront starts rising at about 10 minutes after heating, and around 100 minutes of heating the waterfront is about 70 mm from the heat exposed surface.

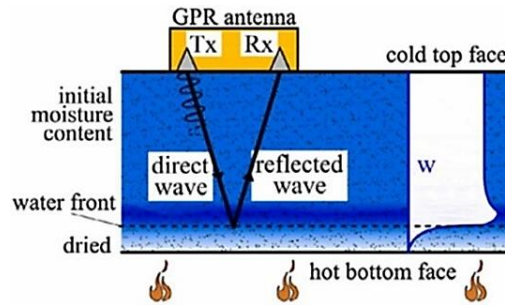


**Figure 2.14:** Schematic diagram of the principle of the electromagnetic wave reflecting at the waterfront

Large-scale concrete wall specimens were investigated after exposure to hydrocarbon fire in a study conducted by Guerrieri and Fragomeni (2019), where the formation of a moisture clog region was reported by studying the pore pressure profiles. The authors reported that as the temperature rose, the pore pressure, which was seen to increase in the moisture clog region, exceeded the tensile strength of the member and caused spalling to occur. Similar conclusions were drawn in another study conducted by Šelih et al. (1994) where 0.2 m thick concrete walls were tested for pressure, temperature and moisture distributions across the member upon exposed to elevated temperature levels. It was stated that the higher temperature gradients had caused an increase in the thermal stresses which was reported as being a possible cause of spalling and early collapse. In addition, an increase in the pore pressure had been witnessed, which could be a result of the increased rate of evaporation of the water molecules with the rise in temperature. The authors reported that once this pore pressure had exceeded the tensile strength, spalling was observed.

Guerrieri et al. (2020) explored the spalling behaviour of unloaded flat concrete panels ( $1550 \times 1550 \times 300$  mm) after being exposed to the RABT ZTV (train) fire curve for 1 hour. Water pooling, at a height of between 5 and 11 mm had been observed on the unexposed surface of all specimens after 30 minutes of heating, and the spalling behaviour was found to be mitigated in the tested specimens made with the addition of PP fibres. In another study, cylindrical samples of 150 mm (diameter)  $\times$  100 mm (height) were studied for spalling behaviour by counting the number of steel grid squares ( $10 \times 10$  mm), placed over the

concrete surface, which were damaged by more than 50%, which allowed the measurement of spalling to be expressed as a percentage of the total surface area (Connolly, 1995).

In addition to this, the spalling behaviour was reported to being evaluated by two other methods: through an acoustic emission method and real-time visual observation (Krzemień and Hager, 2015). Huismann et al. (2011) used the innovative technique of assessing spalling through an acoustic emission analysis, where a commercial acoustic emission system, connected to the unexposed surface of the concrete specimens, was used to measure the number of acoustic events occurring during heating. Carré et al. (2013) used concrete slab specimens to gauge the spalling behaviour after exposure to an ISO 834-1 fire test for a period of 2 hours by measuring the temperature and pressure changes within the concrete, and through visual observations. In addition, the noise generated through explosive spalling was also recorded and used when measuring the extent of spalling.

Unloaded large scale flat panels were used to examine the spalling performance by exposing the panels to a hydrocarbon fire curve in a vertical configuration. Panels were made to different dimensions with three different thicknesses, i.e. 50, 100 and 200 mm. To assess spalling, measurements were made on the loss of water and the total mass loss of the specimen in terms of solid material mass loss (spalled material) **Equation 2** (Guerrieri and Fragomeni, 2016)

$$sw = mb - ma - ss \quad [2]$$

Where, **sw** is the spalled water mass loss; **mb** is the mass of specimen before heating; **ma** is the mass of the specimen after heating; and **ss** is the spalled solid mass loss

## 2.9. Summary of literature review

In summary, the current chapter presents a comprehensive literature review pertaining to the research topic. Subject areas on OPC- based concretes and FA- based GP concretes have been comprehensively covered by focusing mainly on the fire performance of each material. In addition, an insight into the different polymeric materials used in this study are also given with a detailed analysis on different test methods used to gauge the spalling behaviour scale at different specimen sizes. This chapter has re-iterated some research gaps, and hence the rationale for following the experimental protocol of the programme, as given

in chapter 1. A summary from the literature review chapter can be given as follows:

1. While concrete has several advantageous factors, the production of cement, which is the binding ingredient in concrete, is greatly impacting the environment, with cement production being accountable for about 81% of the total CO<sub>2</sub> emissions. Thus, driving researchers to find sustainable alternative materials for construction.
2. Although normal strength concretes have superior fire resistance properties compared to many other building materials, high strength concretes have been reported to explode at temperatures as low as about 350°C. This condition, which can be identified as explosive spalling, can be devastating, and is a phenomenon which have been extensively studied in literature. However, due to the heterogenous nature of concretes, only theories regarding this behaviour are available, with limited quantifiable methods to measure the full spalling behaviour of concrete elements.
3. Amongst the various theories brought forward regarding concrete spalling, such as thermal stress theory, pore pressure theory, frictional flow theory, etc., it has been suggested that the movement of water plays a key role in governing the type and time of spalling
4. Geopolymer concretes, which are made using supplementary cementitious materials, such as fly ash, slag, silica fumes, etc., and a sodium- or potassium-based activator, has been reported to mitigate the negative effects on the environment and also improve the spalling behaviour of concrete.
5. Fly ash, which is a by-product from coal powerplants, has been found to be a high performing, sustainable material, which can be used in full replacement to cement to achieve similar compressive strengths and, more importantly, higher residual strengths.
6. High early strengths from GP concretes can be achieved within 24 hours after casting by subjecting GP specimens to sealed oven curing techniques at 60°C.
7. Polymeric fibres have been reported to improve the tensile and flexural strength of concrete and also the spalling behaviour during fire exposure. It is suggested that when these polymeric materials are exposed to high temperature levels, the polymers would melt or char and create void spaces inside the concrete matrix. This then would provide openings which would help relieve the thermal stresses and pore pressures formed

through heating.

8. Numerous test methods to gauge the spalling behaviour are available at small-, medium- and large-scale. However, small- and medium-scale testing alone cannot comprehensively explain the changes occurring when concrete heats up, and assessing spalling on a large-scale platform is crucial. However, due to time, money and repeatability constraints, conducting large- scale testing is restricted and correlating between different specimen sizes and geometries require detailed investigation.

By considering the overall findings from past literature, it is quite evident that several relevant gaps in the knowledge in this research area need to be appropriately addressed. In particular, the role of polymeric components as sacrificial agents in mitigating the spalling of concrete specimens are not systematically investigated to date. In addition, a comparative study of the spalling behaviour of OPC- and FA-based concrete specimens, especially at a molecular level using advanced techniques are very scarce in the reported literature. In the wake of the above, a systematic experimental approach was designed to understand the behaviour of concrete during heat/fire exposure, with a view to deciphering the underlying physio-chemical phenomena responsible for spalling. Therefore, starting from micro- to large-scale, a series of tests, based on analytical and visual approaches, is used to help determine the spalling behaviour of not just plain OPC-based concretes, but also of fly ash based Geopolymer concretes, as well as of fibre reinforced concretes. Both chapters 3 and 4 comprehensively covers the test methods, results and discussion which will address the gap in research of understanding the degree of spalling and how it can be mitigated by changing concrete compositions/ingredients.

**CHAPTER 3**  
**EXPERIMENTAL**  
**(MATERIAL AND METHODS)**



### 3.1. Introduction

This chapter presents a detailed account of the materials and methodologies which were used to elucidate the behaviours of small-, medium- and large-scale concrete specimens under heat/fire. This section is sub-divided, firstly, based on the different classes of raw materials, which include the cementitious materials, the aggregate fillers, sacrificial agents (polymeric materials) and the liquid components. The follow-on section deals with the preparation of the different samples, which also includes the mix proportions, curing and conditioning methods and heating regimes. Finally, the chapter furnishes detailed accounts of the various instrumentation, analytical and the test methods which were used to evaluate the various parameters.

For the small-scale specimens, three control mix designs of OPC- based concrete, based on low, medium and high compressive strengths, and one control mix design of FA- based geopolymer (GP) concrete were developed. Each control mix was then incorporated with varied proportions of fibrous materials, namely polypropylene (PP), or cotton, or polyester, and varying percentages. For the medium scale cylindrical specimens, three mix designs of OPC- based concrete, based on varying levels of compressive strengths were casted. When considering the large-scale tests, slab panels were casted and used to measure the temperature variations and the spalling depths at various points during and after exposure to elevated temperature levels.

### 3.2. Raw materials

#### 3.2.1. Cementitious materials

The main binder which was used in the three conventional concrete mixes was Type 1 Bastion General Purpose Cement, obtained from *DINGO cement Pty Ltd* complying with AS 3972–2010-General purpose and blended cements (Standard, 2010). FA, supplied from *Cement Australia*, which fully complies with the requirements of AS/NZS 3582.3:2002–Supplementary cementitious materials Part 1–Fly Ash (Standard, 2016) was used for making the GP mix. **Figure 3.1** presents an image of the cement and FA materials used in the study. FA was classified under class F (low calcium FA). The fineness percentage passing the 45  $\mu\text{m}$  sieve was recorded to be 80.48% and classified as highly reactive FA that may be

prepared by various processes including milling and centrifugal separation (Standard, 2016). The chemical composition of FA as provided by the supplier, is given in **Table 3.1**.

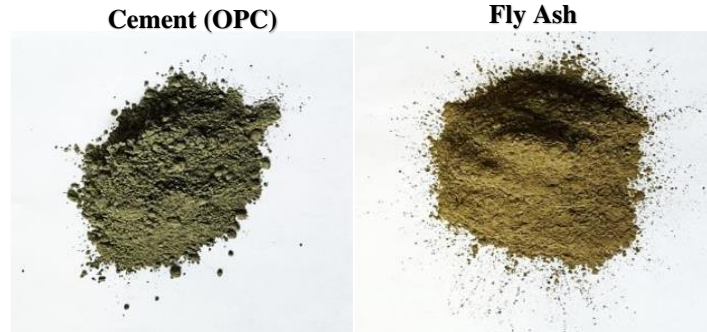


**Figure 3.1:** Cement and fly ash used in the study

**Table 3.1:** Chemical composition of cementitious materials as provided by the supplier

Chemical component (wt. %)	Ordinary Portland cement	Fly ash Class F
Al <sub>2</sub> O <sub>3</sub>	5.840	28.82
SiO <sub>2</sub>	21.47	52.76
CaO	61.44	2.700
Fe <sub>2</sub> O <sub>3</sub>	2.850	9.990
K <sub>2</sub> O	0.590	0.450
MgO	2.440	1.130
Na <sub>2</sub> O	0.320	0.440
TiO <sub>2</sub>	0.320	1.710
SO <sub>4</sub> <sup>2-</sup>	2.420	0.170
Residue	1.780	1.180

### 3.2.2. Aggregates

Natural-river sand as the fine aggregate and basalt rock as the coarse aggregate were locally sourced and used in the present study (**Figure 3.2**). The fine aggregate, primarily made up of silicon dioxide ( $\text{SiO}_2$ ), was sieved through a 600  $\mu\text{m}$  sieve prior to use, whereas the basalt-based coarse aggregate had a maximum aggregate size of 14 mm. Owing to its dense microstructure, thus making it a hard and durable aggregate, basalt aggregate was used in this study. This is an igneous rock, consisting of  $\text{SiO}_2$  (48.70 %),  $\text{Al}_2\text{O}_3$  (16.15 %),  $\text{Fe}_2\text{O}_3$  (11.55 %), and other compounds such as  $\text{CaO}$ ,  $\text{MgO}$ ,  $\text{K}_2\text{O}$ , etc. at lesser percentages. Coarse aggregate was pre-treated in order to obtain saturate surface dry (SSD) condition in order to avoid an effect on the water: cement ratio of the mixes.



**Figure 3.2:** Aggregate used in the study

### 3.2.3. Liquid components

Deionized water (Milli-Q) was used for all mixes during the casting processes. In addition, Glenium 51: high range water reducer (*ca.* 0.3 wt.%) was used as the superplasticiser in the high spalling mix. For the GP mix, a silicate based alkaline activator was used, where a combination of Grade D sodium silicate ( $\text{Na}_2\text{SiO}_3$ ), sourced locally) and 8M sodium hydroxide ( $\text{NaOH}$ ) solution were employed. Sodium silicate, also known as waterglass, or liquid glass, was clear and colourless having a density of  $1.53\text{g/cm}^3$  and a pH of 12.7. **Table 3.2** shows the chemical compositions of sodium silicate.

**Table 3.2:** Chemical compositions of Grade D sodium silicate.

Sodium silicate Grade D	
% SiO <sub>2</sub> per kg	29.40
% Na <sub>2</sub> O per kg	14.70
% H <sub>2</sub> O per kg	55.90
pH	12.70
Wt. Ratio (SiO <sub>2</sub> /Na <sub>2</sub> O)	2.000
Density (g/cm <sup>3</sup> )	1.530

Sodium hydroxide solution was prepared by dissolving sodium hydroxide pellets (obtained from *Aldrich chemical company*) in deionised water approximately 24 hours prior to sample preparation. In reference to Rajamane and Jeyalakshmi (2014), 225 grams of NaOH grains were slowly mixed with 745 grams of water to produce 1litre of 8 M NaOH solution (**Table 3.3**). Dissolution of the NaOH continued until a clear solution was observed.

**Table 3.3:** Quantities of sodium hydroxide (NaOH) and water to produce sodium hydroxide solution of given molarity (Rajamane and Jeyalakshmi, 2014)

Molarity M	For preparation of 1kg of NaOH solution		
	NaOH (g)	Water (g)	NaOH solution (g)
1.00	39	961	1000
2.00	71	926	1000
3.00	108	892	1000
4.00	140	860	1000
5.00	171	829	1000
6.00	200	800	1000
7.00	228	772	1000
8.00	255	745	1000
9.00	281	719	1000
10.00	306	694	1000
11.00	331	669	1000

12.00	354	646	1000
13.00	377	623	1000
14.00	400	600	1000
15.00	422	578	1000
16.00	443	557	1000
17.00	464	536	1000
18.00	485	515	1000
19.00	505	495	1000

---

#### 3.2.4. Essential laboratory reagents and solvents

All other common reagents and solvents used in the present study were obtained from the *Aldrich chemical company* and were used as received. This also included the various standards for the inductively coupled plasma/optical emission spectrometry (ICP/OES) measurements.

#### 3.2.5. Fibrous materials (Sacrificial agents)

Polypropylene (PP) fibres were supplied from *BarChipINC., Australia*. These fibres consisted of virgin PP, classified under class II fibres and made in accordance with ISO 9001:2015 Certification (0044943). Two different fibre lengths were used, namely 12 mm and 48 mm. The 12 mm fibres, having a tensile strength of 680 MPa and young's modulus of 10 GPa, and 48 mm fibres, having a tensile strength of 640 MPa and young's modulus of 12 GPa (as provided by the supplier), were used in the present work. In the mix designs, PP fibres were incorporated at different weight percentages: *ca.* 0.5, 1.0 and 1.5. Cotton fibres were sourced, locally, and consisted of 100% bleached cotton combers treated with a non-absorbent finish. Polyester fibres, which was a lightweight, abrasion resistant synthetic polymer, was extracted from used high-visible vests. This was supplied by *OC Connections, Melbourne, Australia*. All the fillers were used as received. In the mix designs, cotton and polyester fibres were incorporated at weight percentages: *ca.* 1.0. **Figure 3.3** gives images of these fibrous materials.

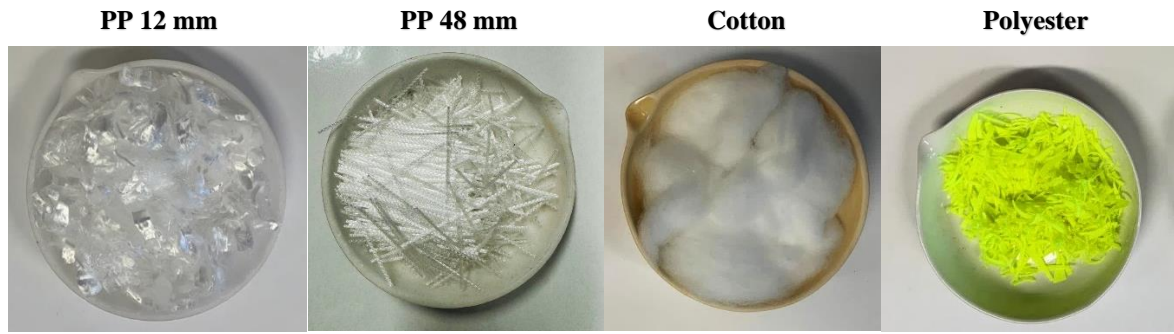


**Figure 3.3** Fibrous materials used in the study

### 3.3. Mix designs

Mix designs for small- and medium- scale OPC- based concrete and FA- based GP mixes are presented in **Table 3.4**, with their relevant mix designs with the incorporation of sacrificial agents (i.e., the polymeric components, such as PP, cotton and polyester) are given in **Table 3.5**.

**Table 3.4:** Details of the mix designs

Material	MD 01	MD 02	MD 03	GP 01
	Control (kg/m <sup>3</sup> )	Control (kg/m <sup>3</sup> )	Control (kg/m <sup>3</sup> )	Control (kg/m <sup>3</sup> )
OPC	375	467	640	-
FA	-	-	-	467.0
Fine aggregate	730	647	615	647.0
Coarse aggregate	1050	1056	930	1056
Water	225	210	167	-
Grade D Sodium silicate	-	-	-	150.0
Sodium hydroxide solution (8M)	-	-	-	60.00
W/C ratio	0.6	0.45	0.26	0.450
Water reducer	-	-	7.90	-

**Table 3.5:** Mix design terminology incorporating polymeric additives

Polymer content	MD 01	MD 02	MD 03	GP 01
0%	MD01	MD02	MD03	GP01
PP 12 mm 0.5%	MD01a	MD02a	MD03a	GP01a
PP 12 mm 0.1%	MD01b	MD02b	MD03b	GP01b
PP 12 mm 1.5%	MD01c	MD02c	MD03c	GP01c
PP 48 mm 0.5%	MD01d	MD02d	MD03d	GP01d
PP 48 mm 0.1 %	MD01e	MD02e	MD03e	GP01e
PP 48 mm 1.5%	MD01f	MD02f	MD03f	GP01f
Cotton 1%	MD01g	MD02g	MD03g	GP01g
Polyester 1%	MD01h	MD02h	MD03h	GP01h

### 3.4. Preparation of specimens and subsequent treatment

For preparation of MD01 and MD02 small- and medium-scale concrete specimens, the dry materials (cement, fine and coarse aggregate) were initially machine-mixed in a *Breville* mixer (**Figure 3.4**) for 2 minutes at a working speed of 50 rpm until they almost reached homogeneity, and once sufficient homogeneity was reached, water was added, and machine mixed for another 2 minutes at 50 rpm and then for 3 minutes at 85 rpm.

For preparing specimens under the high strength category (MD03), after the dry materials (cement, fine and coarse aggregate) reached homogeneity, the required amounts of superplasticizer and water were pre-mixed and added into the dry mix. This mix was then machine-mixed at 85 rpm until a workable mixture was obtained.

Mixing procedures for the GP mix (GP01) followed similar mixing procedures, where the dry materials (FA, fine and coarse aggregate) were machine- mixed until sufficient homogeneity was reached for a period of 2 minutes at 50 rpm, after which the alkaline solution (sodium hydroxide and sodium silicate which were premixed for 1 minute) was added and machine mixed at 50 rpm and then at 85 rpm until a workable mix was obtained.



**Figure 3.4:** *Breville* mixer used in the study

Moulding of samples was conducted in accordance with AS/NZS 1012.8.2. For the preparation of the cubical specimens, the mixtures were casted in  $50 \times 50 \times 50$  mm Teflon coated steel cube moulds, and for preparation of the cylindrical specimens, the mixtures were casted into 200 mm (L) by 100 mm (d) steel moulds. The mixtures were added in three layers, with each layer tamped 25 times, and finally slightly tapped on the sides to remove any air bubbles or voids. To test the repeatability and accuracy of each result, all specimens were measured in triplicates to obtain the compressive and the residual strengths. These included: MD01, MD02, MD03 and GP01 cubical specimens before and after exposure to 400°C and 800°C, and MD01a-h, MD02a-h, MD03a-h and GP 01a-h cubical specimens with the incorporation of sacrificial agents before and after exposure to both 400°C and 800°C. In order to understand the compressive strength relationship between cubical and cylindrical samples, 10 specimens were tested on for each of the data points using the MD01, MD02 and MD03 mix designs. **Figure 3.5** provide photographs of the cubical and cylindrical samples.





**Figure 3.5:** Small- and medium- scale test specimens

When considering the large-scale panels, these were off-site casted using cement, fine aggregate, coarse aggregate and water, and incorporated with PP fibres, to section dimensions of 1800 mm × 1800 mm × 350 mm. Mix information regarding the percentage of fibres is given in **Table 3.6**. During casting they were fitted with 15 K-type thermocouples cast *in situ* in accordance with EFNARC 132F r3:2006, to record the temperature of the specimen during fire exposure. The larger thickness of the slabs allowed for a greater number of data points for the measurement of the temperature and thus, an understanding of the movement of the waterfront within the concrete. Thermocouples were located at depths of 25 mm (4 thermocouples), 50 mm (5 thermocouples), 75 mm (4 thermocouples) and 100 mm (2 thermocouples). **Figure 3.6** shows the general location of the *in-situ* thermocouples.

**Table 3.6:** Details of large-scale fibre mix designs\*

Panel	PP Fibre (kg/m <sup>3</sup> )
1	1.0
2	1.5
3	2.0

*\*only limited information is available given the commercial sensitivity of the test specimens, which were obtained from external stakeholders- it is also relevant to note here that all the test specimens contained PP fibres at different loading. (no control sample was available for testing)*

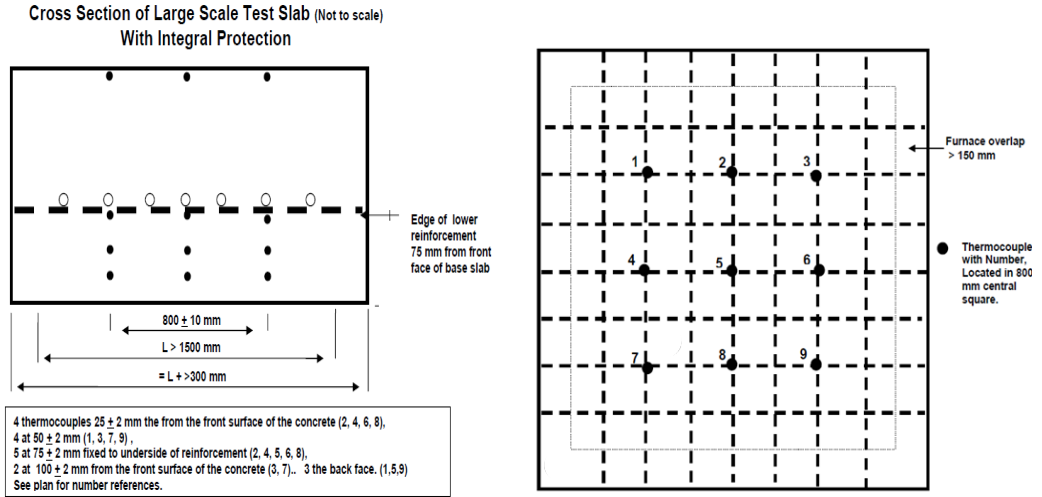


**Figure 3.6:** Location of thermocouples

The OPC- based specimens were cured in water (fully submerged) for a period of 28 days, after which were kept under laboratory conditions used, they were used to testing procedures. The FA- based GP specimens were subjected to sealed curing conditions at 60°C for 24 hours in a temperature-controlled oven (Thermoline- model: RH150MD-706-D). GP specimens were sealed during curing as it has been proven by past research that the initial surface evaporation of FA-based GP specimens during curing has a significant effect on the compressive as well as the residual strength of the specimens (Kannangara et al., 2021a). After curing the specimens were kept under ambient conditions until testing. Once hardened and demoulded at 24 hours, the large-scale panels were covered with wet hessian sacks for 7 days, after which they were kept in at 20°C+/- 2°C and 50% +/- 10% relative humidity until testing.

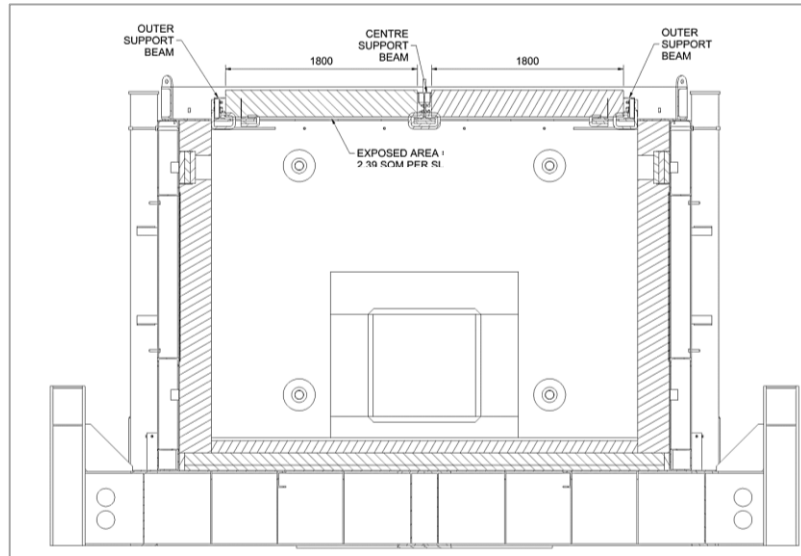
### 3.5. Heating regime of concrete specimens

An important parameter used in analysing and assessing structures which have been exposed to heat/fire is the residual strength. In order to understand the post-heat/fire bearing capacity and/or any repair or rehabilitation procedures which may be necessary, the residual strength profiles can provide a great deal of information (Phan and Peacock, 1999). Two methods in which the residual strength can be assessed are the stressed and the unstressed methods. In the stressed test method, the specimens are preloaded during room temperature and this load is sustained during the heating process. After the required temperature is reached and the concrete specimens remain under a steady state condition, the specimens are

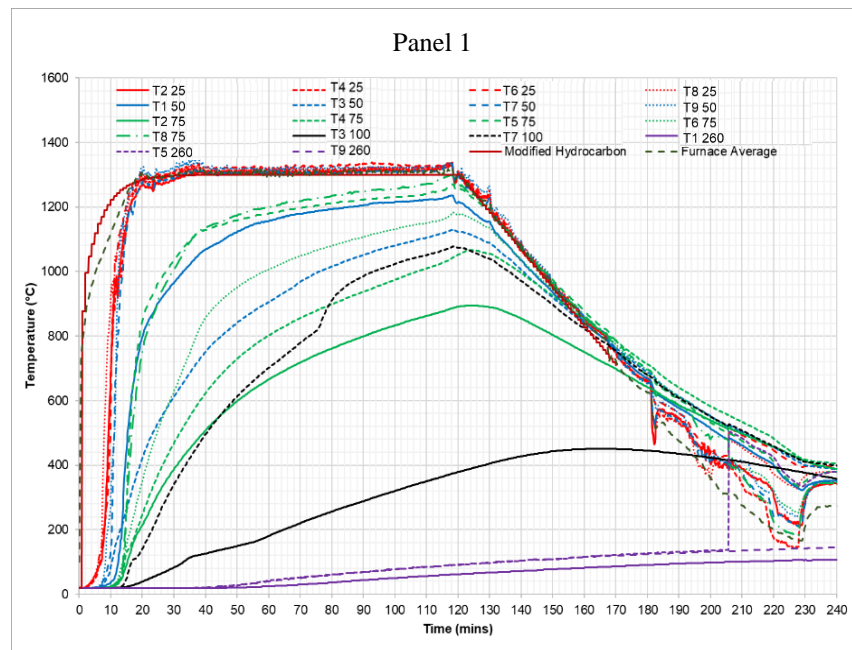
subjected to loading until failure. In the other method, which is the unstressed test method, specimens are not subjected to any such preloading and once the specimens reach a steady state at target temperature, they are subjected to loading until failure. A different method that is employed for obtaining the residual strength profiles is the residual property test method. Here, the specimens are not subjected to any preloading conditions, and they are heated to a target temperature at a steady rate. Upon reaching this target temperature, the temperature is then maintained for a period of time and then the specimens are allowed to cool down at a normal pace until they reach room temperature. Once room temperature is reached, the specimens are subjected to loading until failure.

In the present study, the residual property test was conducted on OPC- based cubical specimens after full-strength gain (i.e., after 28 days of casting) and on FA- based cubical GP specimens 24 hours after casting. In order to measure the residual performance, the specimens were subjected to elevated temperatures of 400°C and 800°C, increasing at a steady rate of 10°C/min using the muffle furnace. Upon reaching the target temperature, the specimens were exposed for a period of 60 minutes and then allowed to cool down to room temperature, after which testing were carried out. Here, temperature points of 400°C and 800°C were selected due to the aim of the fire tests being to follow the phenomenological evolution of the physio-chemical transformation leading spalling, rather than subjecting the test specimens to undergo explosive transformations.

In the large-scale tests, the panels were subjected to heating under the modified hydrocarbon fire curve (120 mins) after which specimens were allowed to cool at 12°C/min. Panels were simply supported and unloaded, and testing was conducted in accordance with AS 1530.4: 2014. The total test duration was approximately 230 min. **Figure 3.7** shows a section view of the test setup and **Figure 3.8** shows the approximate *in situ* temperature vs. time curve for the each of the panels.



**Figure 3.7:** Test setup



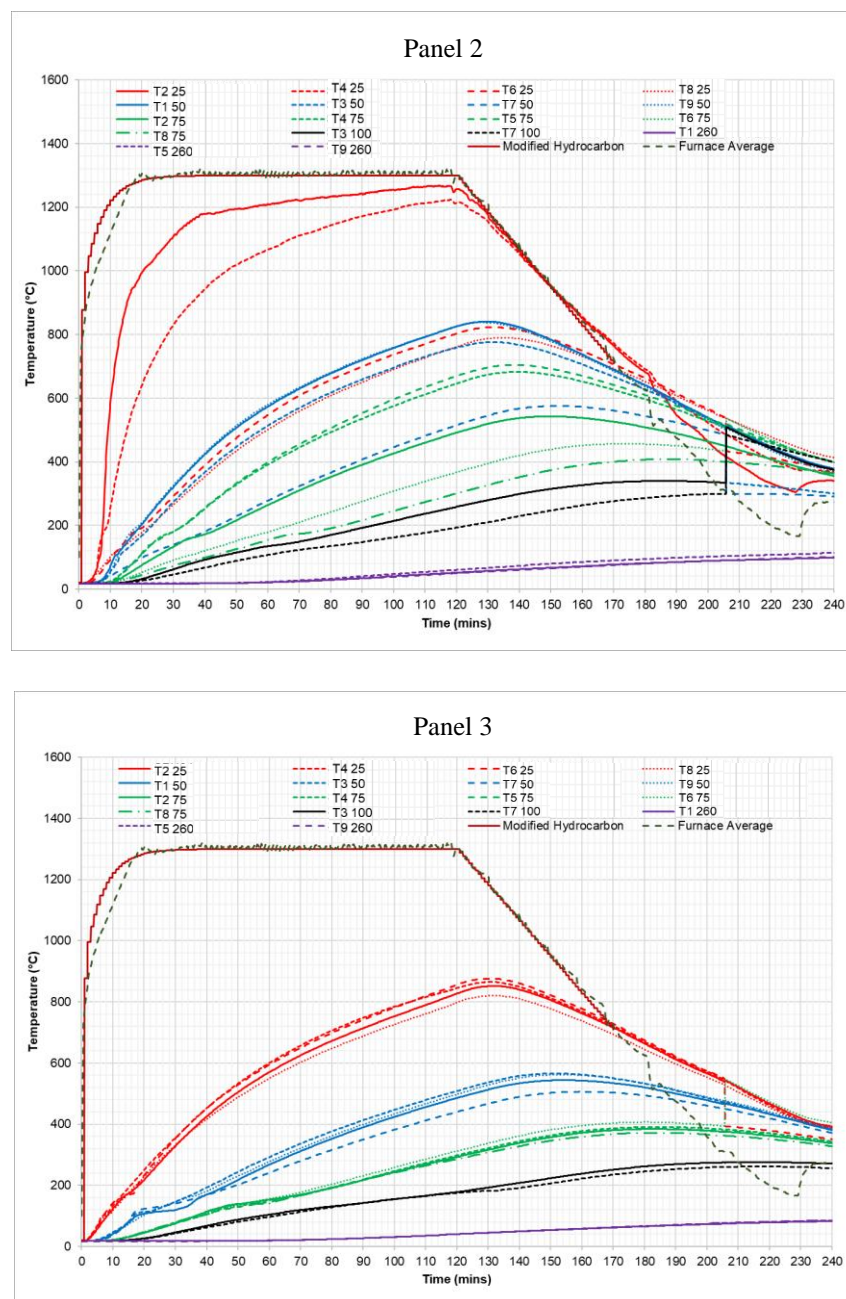


**Figure 3.8:** Temperature vs. time fire curves for the test panels 1, 2 and 3

### 3.6. Analytical instrumentation and test methods

#### 3.6.1. Scanning electron microscope

A Scanning electron microscope with Energy Dispersive (SEM/EDS) provision (ThermoScientific- Phenom XL) was used to obtain the images/and elemental composition of the sample materials. Here, SEM images were obtained first for the raw materials (OPC,

FA, fine aggregate and coarse aggregate), and afterwards for the cured samples (MD01, MD02, MD03 and GP01) and heat-treated samples after exposure to 400°C and 800°C. The samples were sputtered with gold (by using aa Quorum setup) before mounting them onto the instrument.

### **3.6.2. X-Ray diffraction**

X-Ray diffraction (XRD) patterns were collected on using powdered samples obtained by employing a *Rigaku MiniFlex600* instrument that employed Cu ( $K\alpha$ ) source and a D/teX Ultra detector. Scans were performed with a range of  $2\theta$  values from 2 to 70°, and at a step rate of 2° per minute. XRD patterns were obtained for the raw materials (OPC, FA, powdered fine and coarse aggregate), the cured samples (MD01, MD02, MD03 and GP01) and heat-treated samples of MD01, MD02, MD03 and GP01 after exposure to 400°C and 800°C. Both cured and spalled specimens were crushed and powdered for test purposes.

### **3.6.3. Fourier-transform infrared spectroscopy**

Fourier-transform infrared (FT-IR) spectroscopy is a standard method commonly used to identify the main functional groups which can be found in a sample. Both qualitative and quantitative information of the chemical nature of a particular sample can be obtained by using this technique. A *Perkin-Elmer* 1600 model instrument where infrared radiation in the range 4000  $\text{cm}^{-1}$  to 600  $\text{cm}^{-1}$  is absorbed by the sample in the attenuated total reflectance (ATR) mode was used in the current study. The FT-IR spectroscopy was employed for investigating the authenticity/structural features of the raw materials, namely, OPC, FA, fine and coarse aggregate. A few milligrams of powered sample were mounted onto the diamond crystal stage and after appropriate baseline correction for each run, the spectrum of absorbance versus wavenumber was generated for each of the samples which was then used in identifying various functional groups present within their structure. Here the number of scans used was 32 with a resolution of 4  $\text{cm}^{-1}$ .

#### **3.6.4. Solid-state nuclear magnetic resonance spectroscopy**

A 500 MHz *Bruker* nuclear magnetic resonance (NMR) instrument was used to record the spectra of nucleus of interest, namely  $\text{Al}^{3+}$  and Si, under ambient probe conditions (with cross-polarization and magic angle spinning) on finely powdered samples. The central idea was to follow the chemical environments of these nuclei in relation to the transformations relating to the production of water (i.e., through physical desorption and/or dehydration reactions). Here, raw materials, cured and heat-treated samples (after exposure to 400°C and 800°C) were tested on using the NMR instrument. The spectra were processed using the version of the software provided by the supplier (i.e., *TopSpin 4.1.4*)

#### **3.6.5. Differential scanning calorimetry**

The differential scanning calorimetry (DSC) is a thermal analysis technique where the heat flow going in and out of the sample can be measured as a function of time, or the temperature. This can be done while the sample is exposed to a controlled temperature program. Several transition phases, namely crystalline transition, melting, curing, etc., can be identified using the DSC quickly and conveniently (Menczel et al., 2009).

In the current study, the DSC runs were conducted to evaluate the heats of pyrolysis of the polymeric components (i.e., PP, cotton and polyester). Using a *Mettler-Toledo* instrument, at a heating rate of 10°C/min, and a temperature ranging from 30°C to 550°C, the thermograms were recorded in a nitrogen atmosphere. The DSC runs were optionally checked in order to confirm the reproducibility of the results and were found to be satisfactory.

#### **3.6.6. Thermogravimetric analysis**

The thermogravimetric analysis (TGA) technique was initially used to study the thermal behaviour of the polymeric materials (i.e., PP, cotton and polyester), and then later for the cured and heat exposed samples for both OPC-based and FA-based GP concretes before and after they underwent accelerated carbonation.

All samples were in powdered form and the decomposition behaviour that is generally monitored in terms of mass loss (wt.%) over a set range of temperature was tested. Samples were subjected to a pre- set heating regime under a controlled atmosphere (such as air, or nitrogen, or oxygen). In the present study, the TGA runs on powdered samples (ca. 20 mg) were run, in a nitrogen atmosphere, at  $10^{\circ}\text{C min}^{-1}$ , typically from  $30^{\circ}\text{C}$  to  $800^{\circ}\text{C}$  (optionally up to  $1000^{\circ}\text{C}$ ), using a *Mettler-Toledo* instrument with a gas flow rate of  $50\text{ mL min}^{-1}$ . The runs were done in triplicate, and it was found to be highly reproducible in that the associated thermograms were found to be perfectly overlapped on each other.

### **3.6.7. Pyrolysis combustion flow calorimetry**

The pyrolysis combustion flow calorimetry (PCFC), developed several years ago by Lyon and Walters (2004), is a small- scale calorimetric test method which can be used to analyse the fire behaviour of different solid materials when the materials are exposed to a forced non-flaming combustion, under anaerobic, or aerobic, conditions (Janssens, 2024, D7309, 2021). With the most influential work behind this technique being carried out in the late 1990's at the Federal Aviation Administration in USA, this technique is also known as 'microscale combustion calorimetry' (MCC).

Through a controlled pyrolysis of the test sample in a nitrogen atmosphere, the PCFC method can mimic the condensed and gaseous parts of the flaming combustion within a systematic non-flaming regime. This is then followed by combustion of the pyrolyzate in the presence of oxygen. The need for a very small quantity of sample serves as a key advantage in using this method, through which important parameters, such as heat release capacity (HRC), effective heat of combustion (EHC:  $h_c$ ), total heat released (THR), peak heat release rate (pHRR), temperature to pHRR and percentage of char yield can be obtained (Lyon and Walters, 2004, Cogen et al., 2009, Sonnier et al., 2012). In the current scope of work, PCFC runs were carried out on the polymeric materials, i.e., the PP, cotton and polyester, at  $1^{\circ}\text{C/min}$ , using an FTT microscale calorimeter, using method A: i.e., in a nitrogen atmosphere for pyrolysis, followed by 'forced combustion' in air.



### 3.6.8. Inductively coupled plasma/optical emission spectrometry

In the present work, a *Shimadzu* ICPE- 9000 inductively coupled plasma/optical emission spectrometry (ICP/OES) was employed to determine the constitutions found in the water extracted from heated concrete specimens. In an ICP/OES machine, the atoms/ions get excited from the plasma which causes the electrons to jump to a higher energy level from a lower energy level. Once these excited electrons relax and return to their initial ‘ground state’, the energy is dissipated in the form of photons. This dissipated energy possesses different wavelengths at different intensities that are characteristic of their respective elements, which can be quantified by studying these intensities.

The basis for the calibration curve is based on the Beer-Lamberts law which governs the absorption of molecular species in dilute homogeneous media. According to this law, a linear relationship exists between the absorbance and concentration of an absorbing species which is derived in **Equation 3**.

$$A = \varepsilon \times b \times c \quad [3]$$

where **A** is the measured absorbance;  $\varepsilon$  is the molar extinction coefficient; **b** is the path length; and **c** is the concentration of the absorbing species. Initially the Beer- Lambert plots were constructed using standard solutions of elements of interest namely,  $\text{Ca}^{2+}$ ,  $\text{Fe}^{3+}$ ,  $\text{Al}^{3+}$  and Si.

The extracted water samples were first weighed (*ca.* 10-15 mg) in triplicate and boiled in 50 cm<sup>3</sup> beakers to digest them with 5 cm<sup>3</sup> of analytical grade con.  $\text{HNO}_3$ . Upon digestion, the resulting solution was quantitatively transferred into a 25 cm<sup>3</sup> volumetric flask and filled to the mark with deionized water. This solution was then transferred to tubes of volume 15 cm<sup>3</sup> to be tested. Measurements were made in triplicate for accuracy. **Figures 3.9 – 3.12** give the calibration curves of  $\text{Ca}^{2+}$ ,  $\text{Fe}^{3+}$ ,  $\text{Al}^{3+}$  and Si of the Beer-Lambert law which was used to quantitatively measure the amounts of calcium, iron, aluminium, and silicon incorporation of the modified substrates, generated by the inbuilt software of the instrument.

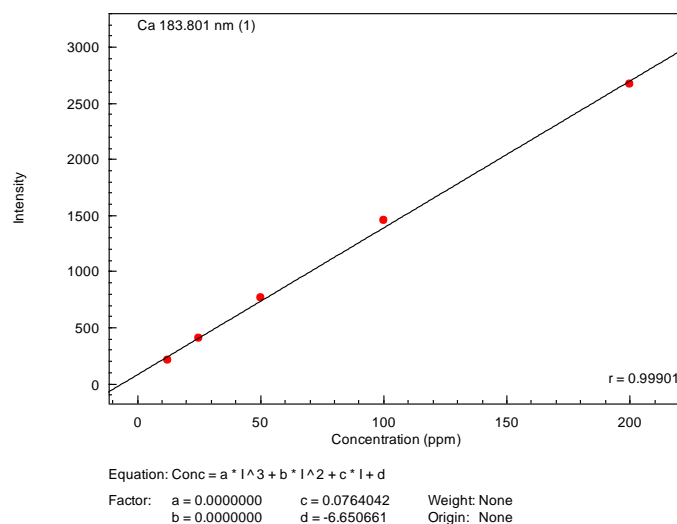


**Figure 3.9:** Calibration curve of the Beer-Lambert law for  $\text{Ca}^{2+}$

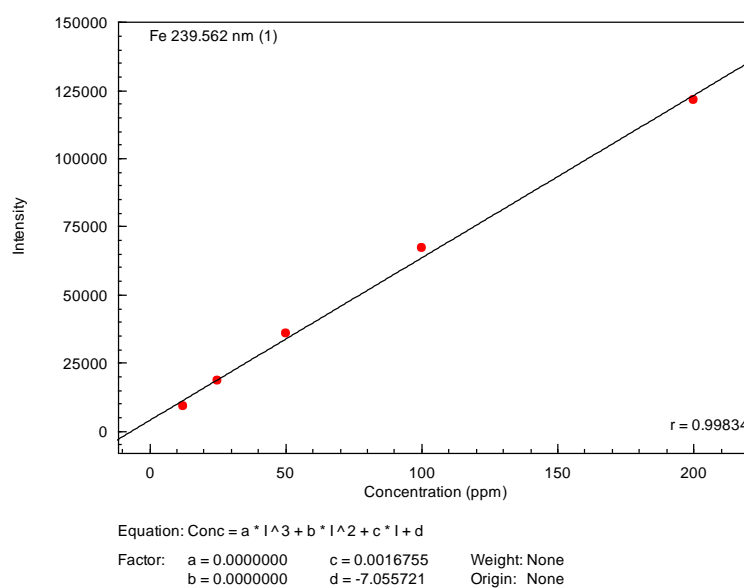


**Figure 3.10:** Calibration curve of the Beer-Lambert law for  $\text{Fe}^{3+}$

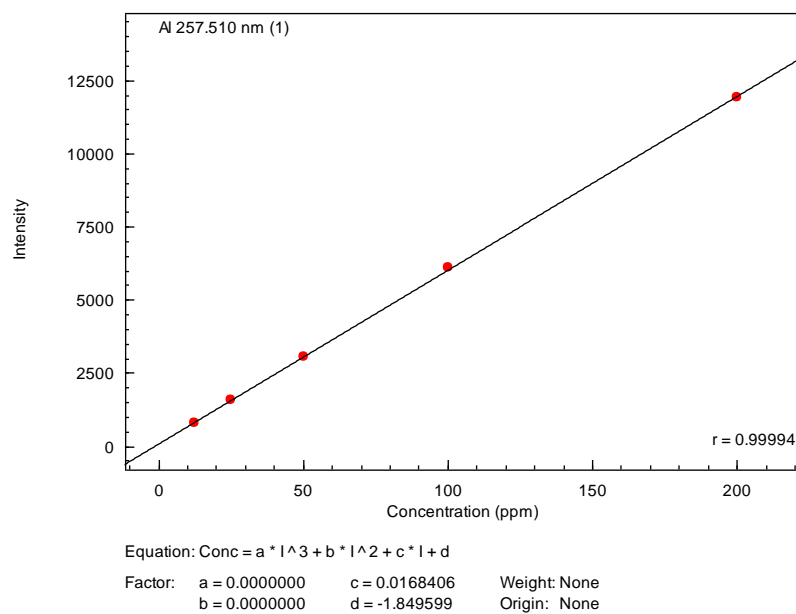


**Figure 3.11:** Calibration curve of the Beer-Lambert law for  $\text{Al}^{3+}$

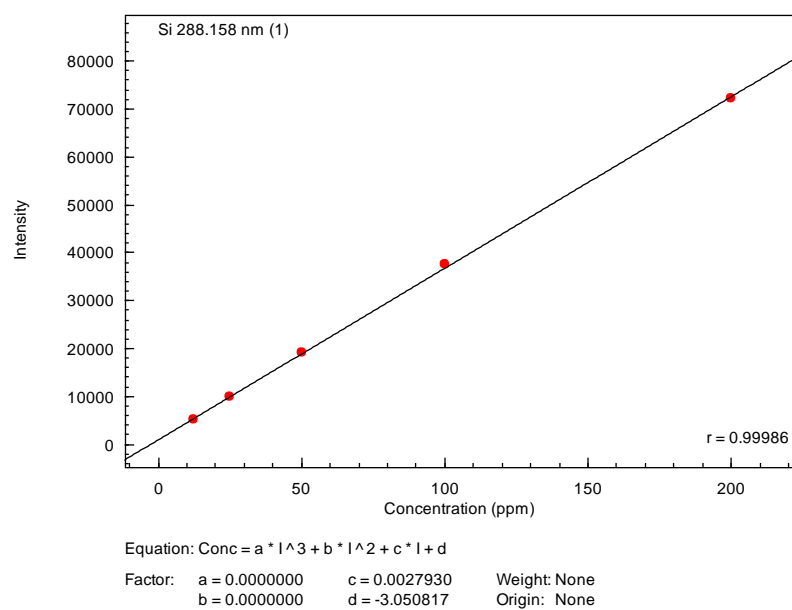


**Figure 3.12:** Calibration curve of the Beer-Lambert law for Si

### 3.6.9. Flow table test

The workability of concrete is an important factor to assess because concrete needs to remain in its liquid state for transportation, pumping, placement, compaction, and to achieve a uniform specimen, or structural component. The flow table test is a quick and easy test method in assessing the ability to work with the concrete in its wet state. In the present study, the flow table test was conducted in accordance with ASTM (2014). Firstly, the flow table apparatus was placed on a level surface and the cone and base plate was damped with a wet cloth. Next, concrete was inserted into the cone in three equal layers with each layer being tamped 25 times each in circular motion. Once the top was levelled and any excess material wiped from the plate, the cone was lifted vertical upwards, by avoiding any sideways movement which could collapse the concrete sample. Immediately after this, the plate was dropped 25 times within a time period of fifteen seconds and two readings on the diameter of concrete flow was recorded as d1 and d2 in millimetres. The slump flow was calculated using **Equation 4** (Topçu and Uygunoğlu, 2010). **Figure 3.13** gives an image of how the diameter readings were taken and **Figure 3.14** show the flow table apparatus.

$$Slump\ flow = \frac{[d1+d2]}{2} \quad [4]$$

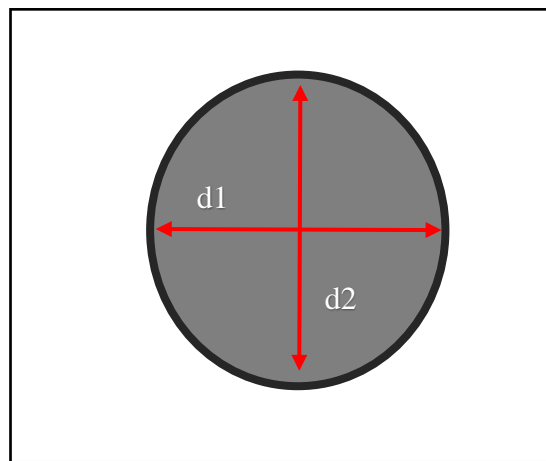


**Figure 3.13:** Schematic diagram of diameter (d1 and d2) measurement



**Figure 3.14:** Flow table apparatus

### 3.6.10. Compression tests

The compressive and residual strengths of specimens were tested in accordance with AS 1012.9.2014 - Methods of testing concrete Method 9: Compressive strength for the determination of the strength tests—Concrete, mortar and grout specimens (Standard, 2014). A 300T *Mori* testing machines at a loading rate of  $20 \pm 2$  MPa/min was used for the testing of the maximum load which can be subjected on the specimens before failure. Testing was conducted on all OPC-based and FA-based GP concretes with and without the incorporation of sacrificial agents. Residual strengths were obtained after the specimens were exposed to elevated temperature levels of 400°C and 800°C. In addition, specimens which underwent accelerated carbonation tests were also tested on for both compressive and residual strength to understand the effects of carbonation on the loading capacity of both OPC and GP concretes. Moreover, cylindrical samples of control mixes MD01, MD02 and MD03 were tested on for initial compressive strength to understand the difference in readings between cubical and cylindrical specimens. **Equation 5** was used to calculate the strength (stress in MPa) of the specimens.

$$\sigma = \frac{F}{A} \quad [5]$$

where:

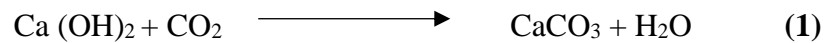
$\sigma$  = stress (MPa)

F = applied force (N)

A = cross sectional area (mm<sup>2</sup>)

### 3.6.11. Accelerated carbonation tests

Carbonation is a condition which can occur in concrete when the carbon dioxide (CO<sub>2</sub>) in the atmosphere enters the concrete through the pores and reacts with the calcium hydroxide found in cement. This reaction produces calcium carbonate which lowers the alkalinity of concrete to around pH 9 (**Scheme 1**). This reduced pH level can be very detrimental in structural elements as the protective passivation layer around the steel reinforcement can be broken down and leave the bars vulnerable to any corrosion. For the present study, the carbonation of concretes was studied as it is greatly associated with the moisture content within concrete, and the results from this test can help understand the extents of hydrated calcium centres that were converted into the corresponding carbonates.



In reality, the natural process of carbonation takes place over a few decades. However, for our purpose, control cubical specimens were subjected to an accelerated carbonation test by placing them in an environmental chamber at a CO<sub>2</sub> concentration of 2%, temperature within 25°C – 35°C and relative humidity between 50 – 70%. Afterwards, some samples were directly tested on for compressive strength and others were exposed to temperature levels of 400°C and 800°C, after which were tested on for residual strength. In addition to this mechanical parameter, powdered samples were also tested on using the TGA in order to gauge the build-up of carbonate in the specimens. This was primarily conducted to help understand the chemical natures of the hydration shell around CaO centres.

### 3.6.12. Small angle neutron scattering

Small angle neutron scattering (SANS) was conducted with a view to understanding the chemical natures of the hydration shell around  $\text{Ca}^{2+}$  centres. The measurements were performed at the *DINGO* thermal-neutron radiography/ tomography/ imaging station at the Australian Nuclear Science and Technology Organisation's (ANSTO) 20 MW OPAL nuclear research reactor, Sydney, Australia (Garbe et al., 2015).

The instrument was equipped with a ZWO ASI2600MM Pro camera and Zeiss Ikon 100 mm f/2.0 Makro Planar lens. The *DINGO* instrument was configured with a 20  $\mu\text{m}$  thick terbium-doped GdO scintillating screen ( $\text{Gd}_2\text{O}_2\text{S}$ : Tb, RC Tritec AG) and  $22.4 \times 22.4 \times 22.4 \mu\text{m}$  voxels for a Field-of-View of  $100 \times 93.6 \text{ mm}$ . To maximise counting statistics, a collimation ratio (L/D) of 500 was used, where L is the neutron aperture-to-sample length and D is the neutron aperture diameter.

For each sample, a total of 1250 equally spaced angle shadow-radiographs were obtained every  $0.144^\circ$  as the sample was rotated  $180^\circ$  about its vertical axis. Both dark (closed shutter) and beam profile (open shutter) images were obtained for calibration before initiating shadow-radiograph acquisition. To reduce anomalous noise, a total of three individual radiographs with an exposure length of 10 s were acquired at each angle (Mays et al., 2017) for a total scan time of 11.8 h. The individual radiographs were summed in post-acquisition processing using the 'Grouped ZProjector' plugin in ImageJ v.1.51h in accordance with our previous measurements (Gee et al., 2019), and tomographic reconstruction of the 16-bit raw data accomplished using Octopus Reconstruction v.8.8.

### 3.6.13. Surface imaging using 3-D optical profilometry

A *Bruker* contour GT-I 3D optical microscope was used in the study to measure the surface profiles of the OPC- based and FA- based GP concrete samples before and after exposure to elevated temperature levels of  $400^\circ\text{C}$  and  $800^\circ\text{C}$ . Samples of  $50 \text{ mm} \times 50 \text{ mm} \times 15 \text{ mm}$  were tested on using the fully automated bench top profiler with tip/tilt head function in order to obtain nanometre-scale resolution on high-contour surfaces. Unlike traditional pitch-an-roll designs, the tip/tilt head design provides optimized image acquisition and efficient data processing. The main aim here was to determine the changes in surface morphology between the non-heat treated and heat-treated specimens using colour gradation

contour mapping. Surface imaging analysis was conducted at the Melbourne Centre for Nanofabrication (MNC) in Victoria, Australia.

#### **3.6.14. Rapid chloride penetration test**

Rapid chloride penetration tests (RCPT) were carried out on cylindrical samples (100 mm diameter and 200 mm in length) in accordance with ATSM C-1202-9 using a Chloride Penetration Meter- CIVIT Test, to measure the amount of chloride ions entering the concrete specimens in Coulombs (C), which can be used to understand the porosity of the different mixes (C1202-09).

Testing was conducted on fully cured OPC- based concrete and FA- based GP concrete samples at 28 days. All samples were cut to a sample size of 50 mm (height)  $\times$  100 mm (diameter) using a diamond cutting saw blade. Once the samples were removed from curing, they were dried in an air oven for 24 hours at  $110 \pm 5^\circ\text{C}$ , after which an epoxy coating was applied ( $\times 3$  times) on the curved surface of the specimens. Once the coating process was complete, samples were fully submerged in distilled water and placed in a vacuum desiccator. Here the distilled water level was kept 50 mm above the samples. The samples were then subjected to reduced pressure (*ca.* 15 mm of Hg) for a period of 18 hours. The samples were then wiped with a cloth and placed in the testing chamber. Rubber seals and silicon grease were used to prevent any possible seepage of the solutions. **Figure 3.15** shows the test setup for the RCPT test apparatus. Solution of NaOH (0.3% w/w) and NaCl (3% w/w) were introduced into each side of the testing chamber, and a 60 V was connected to the solution chamber to measure the electric flux for a period of 6 hours. The resistance against chloride ions, i.e., the amount of charge passed, the porosity of the concrete specimens can be determined using **Table 3.7**.



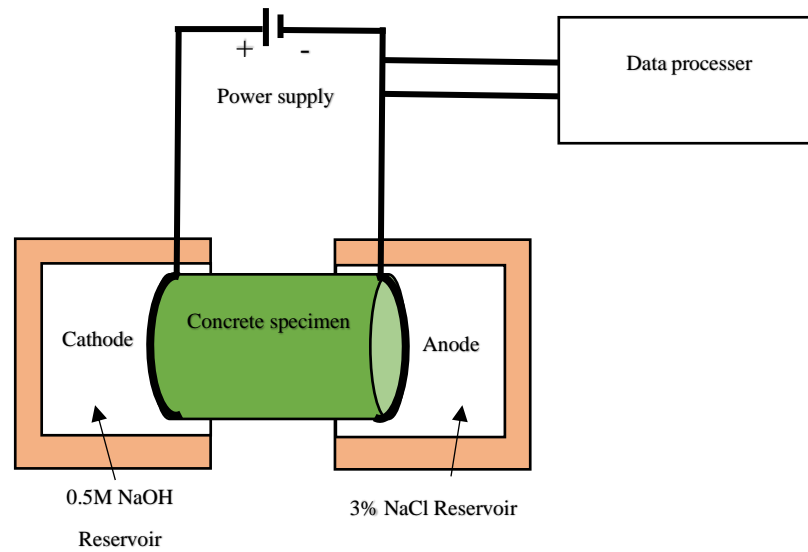


**Figure 3.15:** Test setup for the RCPT

**Table 3.7:** Details regarding chloride ion penetrability (based on charge passed) as per C1202-09

Charge passed (C)	Chloride ion penetrability
>4000	High
2000–4000	Moderate
1000–2000	Low
100–1000	Very low
<100	Negligible

### 3.6.15. Measurements using the Brunauer-Emmett-Teller (BET) theory

The Brunauer-Emmett-Teller (BET) method is a well-established method to establish the specific surface area of materials (Brunauer et al., 1938). This method can be employed in analysing the fineness or the porosity of the microstructure within concretes (Odler, 2003). In this study, the BET approach was used to gain an understanding to the specific surface area, porosity and pore volume of the concrete before and after heat exposure. Any change in the pore structure before and after temperature exposure may help understand spalling at a molecular level. Results obtained through the BET approach are based on adsorption of a suitable gaseous phase. Therefore, as hardened concrete is a material having physically bound or free water molecules in the existing pores or adsorbed on its

surface, this free and adsorbed water first need to be removed to allow the movement of the adsorbate gas into the internal matrix.

In this study the measurements were accomplished by using a *Micromeritics TriStar II 3020 Surface Area and Porosity Analyser*. Both OPC- specimens and FA- based GP specimens were first broken down to small chunks of approximately 5 mm and inserted into the bulb. This was placed under vacuum at 200°C, and were subjected to vacuum pumping, until the pressure went below 100 MTorr. During this process, nitrogen gas was flushed in through the specimen to ensure drying of specimens. The glass tubes containing the samples were detached from the heating/vacuum set-up, quickly stoppered, and assembled onto the measuring rig, and cooled down using liquid nitrogen before purging with nitrogen gas, which was employed as the probe molecule. Nitrogen adsorption/desorption plots for each of the concrete specimens were carried out under continuous adsorption conditions. The total volume of the pores/micropore were then calculated using by t-plot analysis.

## **CHAPTER 4**

### **RESULTS AND DISCUSSION**

#### 4.1. Introduction

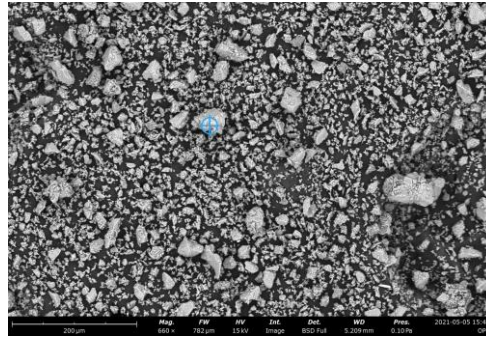
This chapter covers the results, and ensuing discussions and inferences, which were obtained so far through the course of this investigation. Initially, morphology, chemical natures, and thermal and calorimetric properties of the raw materials and fibrous fillers, were analysed using scanning electron microscope (SEM/EDS), X-Ray diffraction (XRD), solid-state nuclear magnetic resonance (NMR), Fourier-transform infrared (FT-IR), thermogravimetric analysis (TGA), differential scanning calorimetry (DSC) and pyrolysis combustion flow calorimetry (PCFC). Subsequently, details regarding the densities, workability and flow properties of each mix combination, that were tested and assessed, are given. Once the concrete specimens reached full conditioning, the relevant morphological, spectroscopic, thermal and calorimetric properties of powdered samples obtained from both cured and heat exposed concrete specimens were assessed using appropriate analytical techniques. Furthermore, the compressive, residual strength and mass loss properties were analysed with a view to understanding the spalling behaviours of the each of the mixes.

In an attempt to understand the porosity of the different mixes, which could be used to draw up correlations between the spalling behaviour and air voids, the specimens were subjected to porosity assessments thorough the rapid chloride penetration tests (RCPT), and measurements based on Brunauer-Emmett-Teller (BET) theory. Towards the latter stages of the study, small angle neutron scattering (SANS) studies were conducted on cured and heat-treated samples and thermogravimetric analyses were conducted on concrete specimens which underwent accelerated carbonation to gauge the changes in the chemical environment of the hydration shell around  $\text{Ca}^{2+}$  centres. The spalling behaviours of cubical samples were gauged through visual examinations, and optionally by employing a high-resolution optical microscope.

In addition, this chapter also covers the results obtained from the large-scale concrete tests that was conducted for the purpose of obtaining and analysing the elemental composition of the pooled water (i.e., to carryout quantitative analyses of the concentrations of the chemical species of interest, such as,  $\text{Ca}^{2+}$ ,  $\text{Al}^{3+}$ ,  $\text{Fe}^{3+}$  and Si, using atomic absorption spectroscopic (i.e., ICP/OES). Moreover, the assessment on the spalling behaviour of these large-scale slab panels is also presented here.

## 4.2. Characterization of the raw materials

The central idea here was to subject the raw materials to some routine morphological/elemental, diffraction and spectroscopic analyses. Firstly, SEM/EDS runs were conducted on cement (ordinary Portland), fly ash (FA), and fine and coarse aggregates, and the outputs from the machine are given below (**Figures 4.1-4.4**).



	Element Number	Element Symbol	Element Name	Atomic Conc.	Weight Conc.
	8	O	Oxygen	27.313	13.200
	12	Mg	Magnesium	0.817	0.600
	13	Al	Aluminum	9.329	7.600
	14	Si	Silicon	5.068	4.300
	16	S	Sulfur	0.929	0.900
	20	Ca	Calcium	50.221	60.800
	26	Fe	Iron	5.928	10.000
	79	Au	Gold	0.235	1.400
	96	Cm	Curium	0.161	1.200

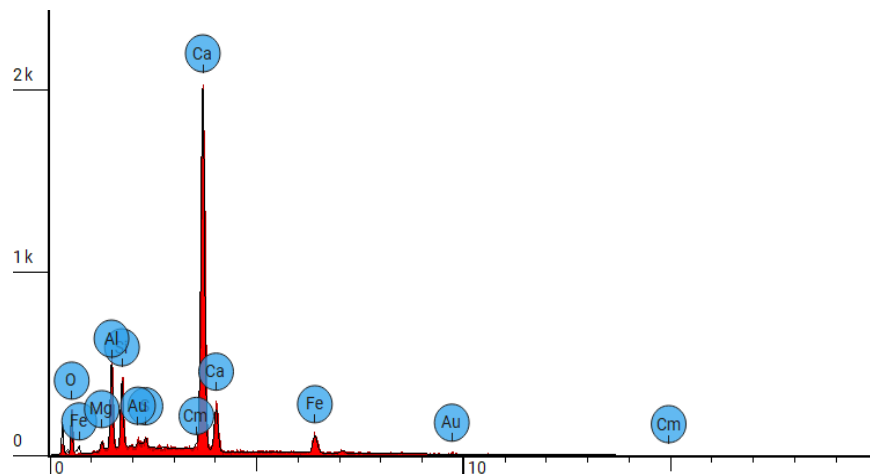
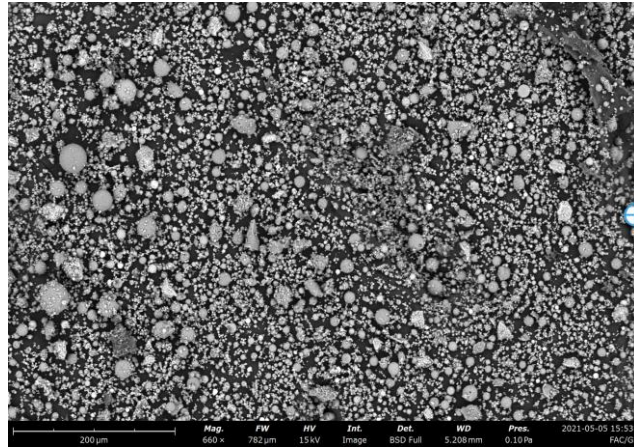


**Figure 4.1: SEM/EDS of cement**



	Element Number	Element Symbol	Element Name	Atomic Conc.	Weight Conc.
	6	C	Carbon	36.304	21.179
	8	O	Oxygen	44.218	34.366
	13	Al	Aluminum	3.432	4.496
	14	Si	Silicon	2.709	3.696
	20	Ca	Calcium	0.308	0.599
	26	Fe	Iron	12.852	34.865
	41	Nb	Niobium	0.177	0.799

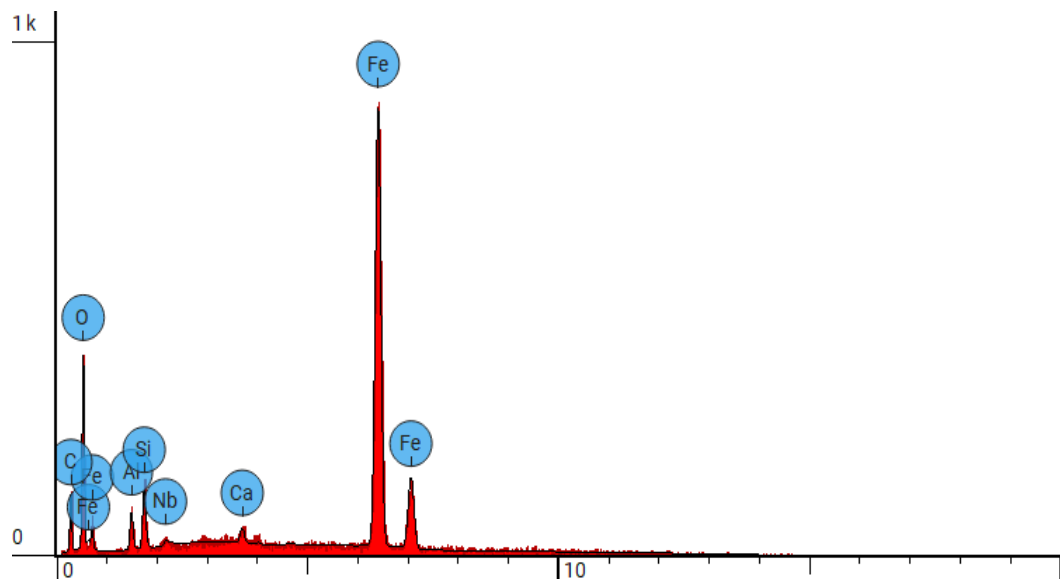
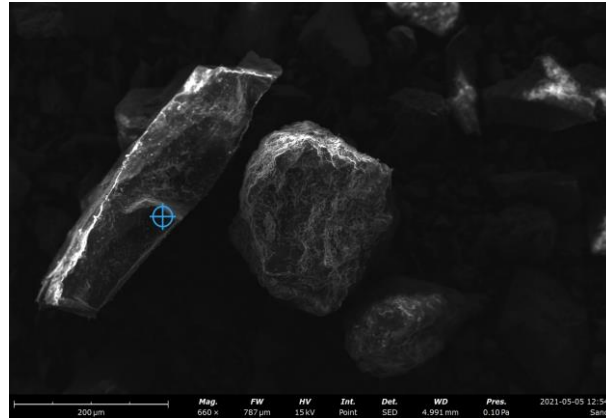


**Figure 4.2:** SEM/EDS of fly ash



	Element Number	Element Symbol	Element Name	Atomic Conc.	Weight Conc.
	6	C	Carbon	7.383	4.700
	8	O	Oxygen	66.263	56.200
	13	Al	Aluminum	2.378	3.400
	14	Si	Silicon	23.976	35.700

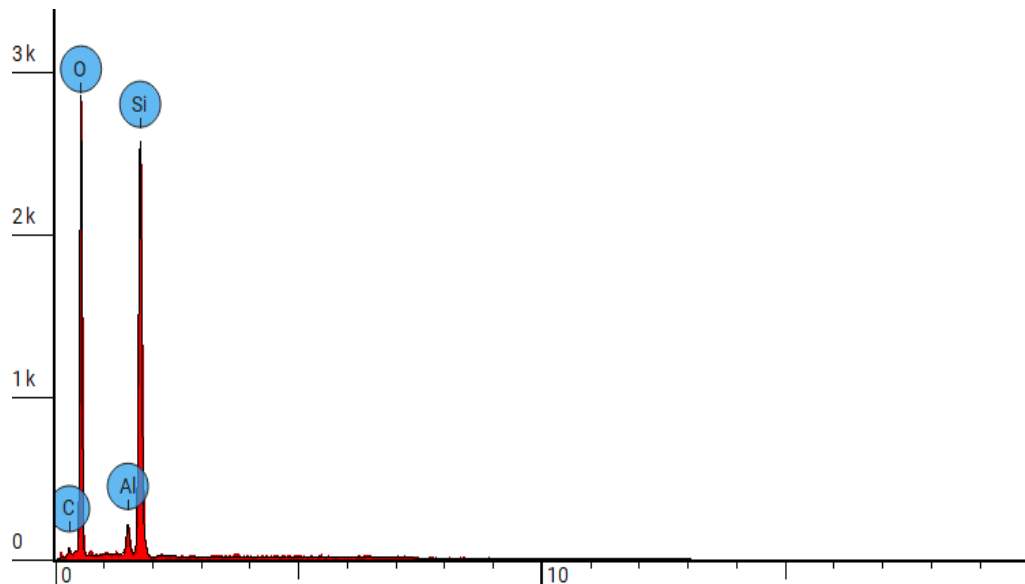
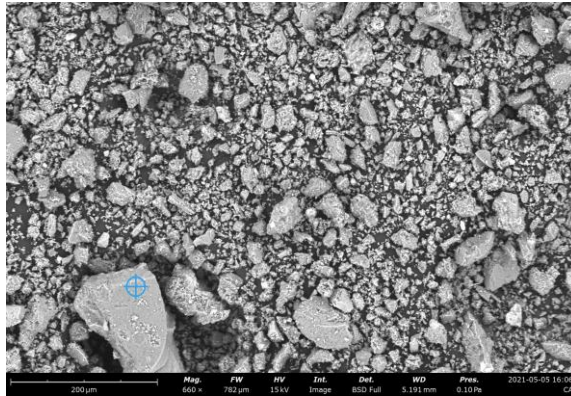


**Figure 4.3:** SEM/EDS of fine aggregate



	Element Number	Element Symbol	Element Name	Atomic Conc.	Weight Conc.
	8	O	Oxygen	39.586	25.200
	12	Mg	Magnesium	0.620	0.600
	13	Al	Aluminum	21.807	23.400
	14	Si	Silicon	31.227	34.900
	19	K	Potassium	1.286	2.000
	22	Ti	Titanium	0.630	1.200
	26	Fe	Iron	4.500	10.000
	79	Au	Gold	0.344	2.700

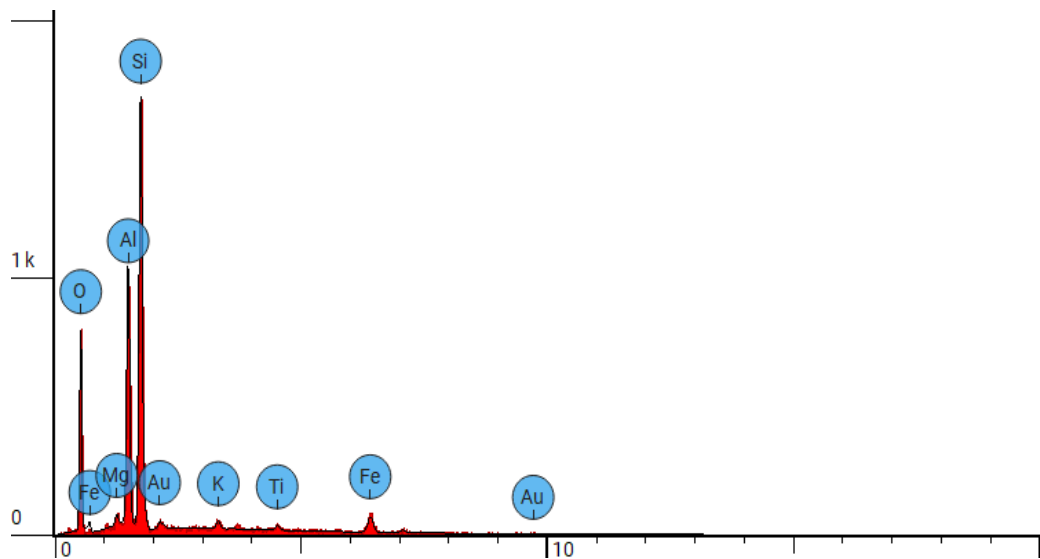


**Figure 4.4:** SEM/EDS of coarse aggregate



The micrographs revealed the particulate structures of the materials in sufficient detail. The elemental analyses results showed that cement had the highest levels of calcium followed by oxygen, aluminium and silicon compared to FA, where the element with the maximum loading was iron followed by oxygen, carbon, aluminium and silicon. When considering the particle shape, it was evident that the FA particles displayed a more spherical shape and was finer as compared to OPC. The main reason for this particle shape and size could be due to the manufacturing process of the FA (Kannangara, 2018, Dodds, 2013, Ismail et al., 2022, Kutchko and Kim, 2006). The mineral matter within the coal, combustion and cooling process governs both the physical and chemical properties of FA. During combustion the inorganic minerals can become fluid and unstable or react with oxygen and during cooling it may form amorphous particles which are spherical in nature and more reactive. Both fine and coarse aggregates showed similar results with high silicon, aluminium and oxygen level and traces of iron. However, here the sizes/distribution of the particles were markedly different as expected.

Powder-XRD can be considered a primary tool for solid state characterization and can be helpful in delivering quantitative and qualitative phase abundance analysis to classify the different materials (Li et al., 2014, Liss et al., 2003). Here, powder XRD was conducted on the four dry raw materials, namely cement (OPC), FA, fine aggregate and coarse aggregate (**Figures 4.5 - 4.8**), and it was found that the diffraction patterns were typical of such materials (Chauhan and Chauhan, 2015, De Matos et al., 2022, Bae et al., 2014). When considering the FT-IR spectroscopy, while there are limitation in the provision of quantified interpretations and in the detection of certain compounds, it has been proven to being a convenient tool in studying cementitious materials (Horgnies et al., 2013). The corresponding vibrational spectra were also revealed typical vibration patterns of cementitious and aluminosilicate materials (Mollah et al., 1998), as the case may be. **Figures 4.9-4.12** shows the FT-IR spectra.

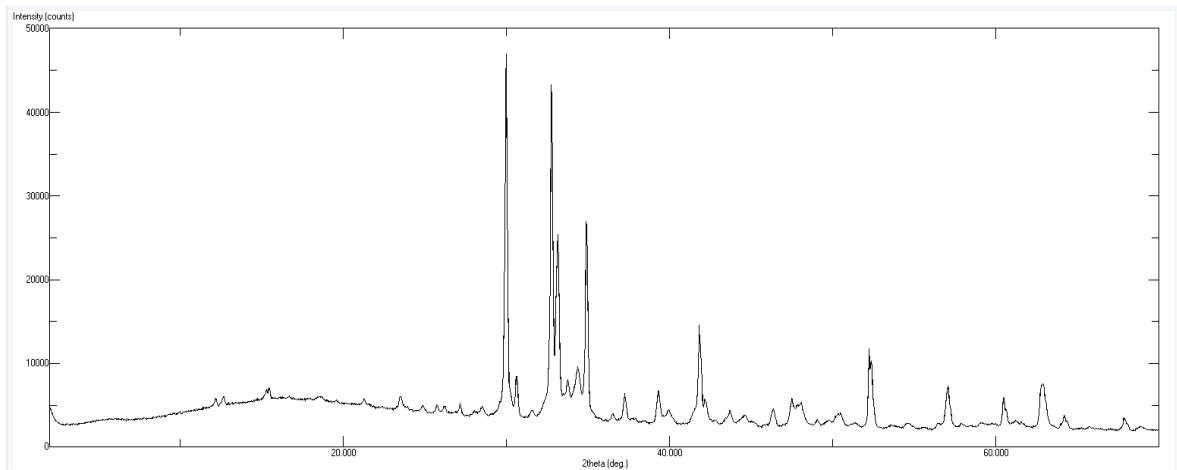


**Figure 4.5:** XRD pattern of cement

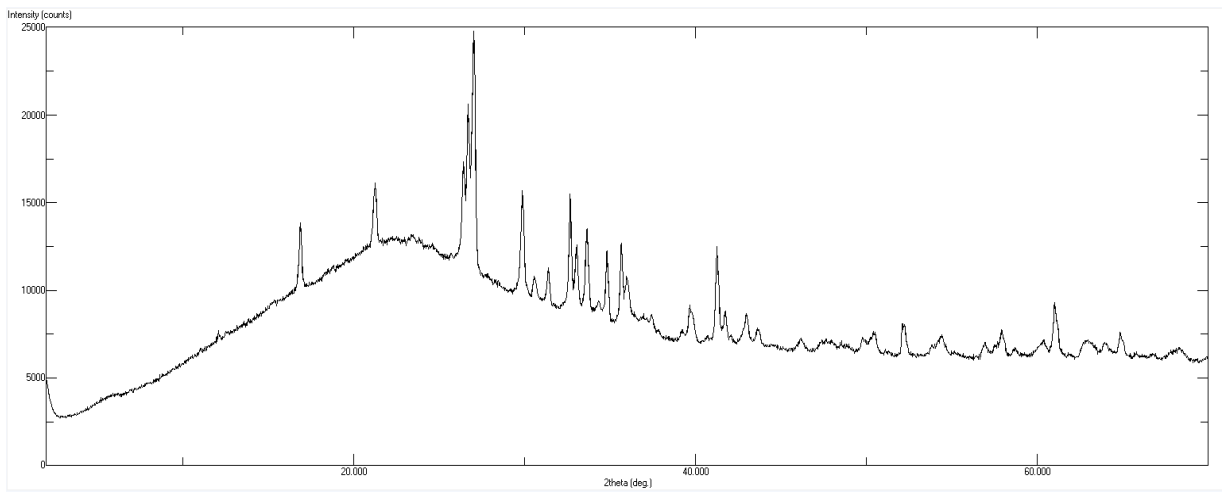


**Figure 4.6:** XRD pattern of fly ash

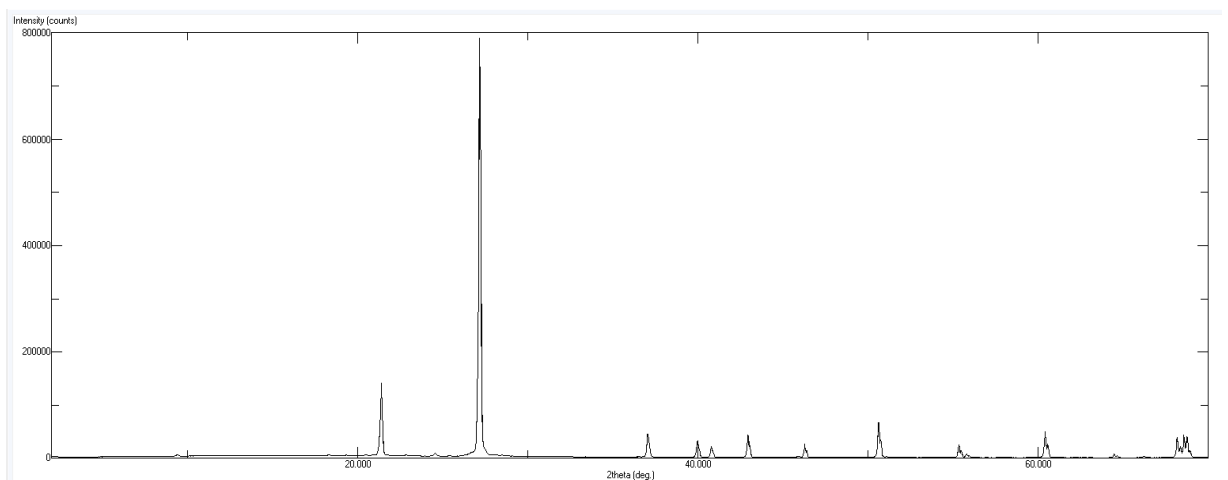


**Figure 4.7:** XRD pattern of fine aggregate

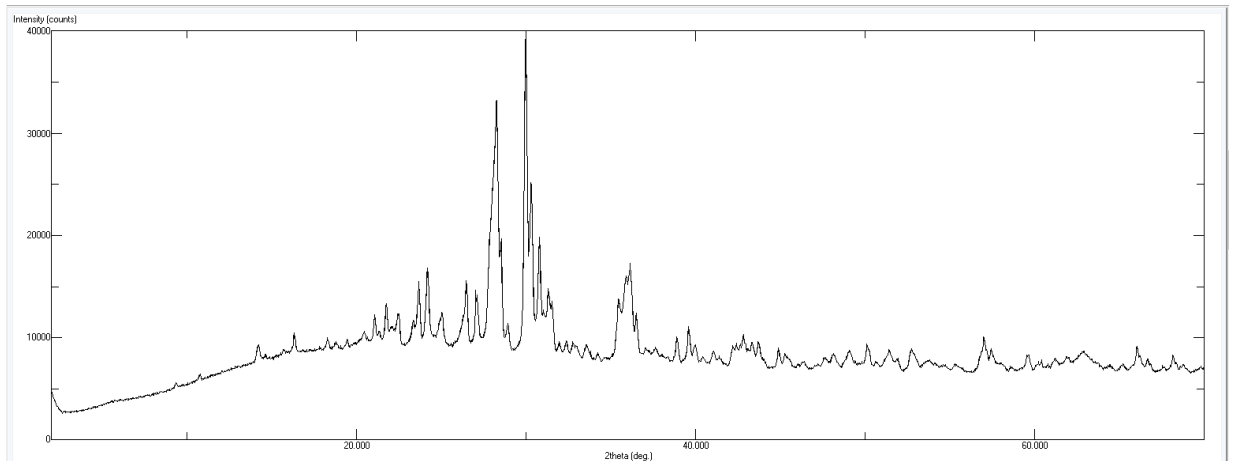


**Figure 4.8:** XRD pattern of course aggregate

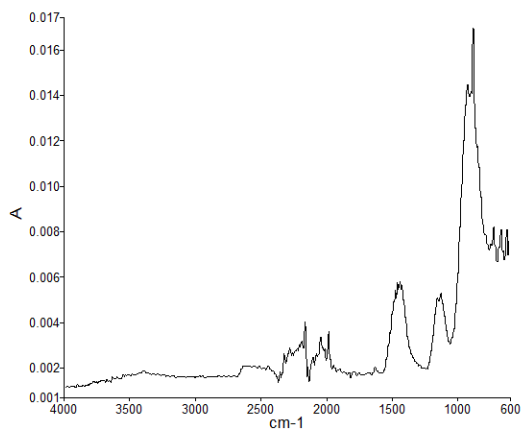


**Figure 4.9:** FT-IR spectrum of cement

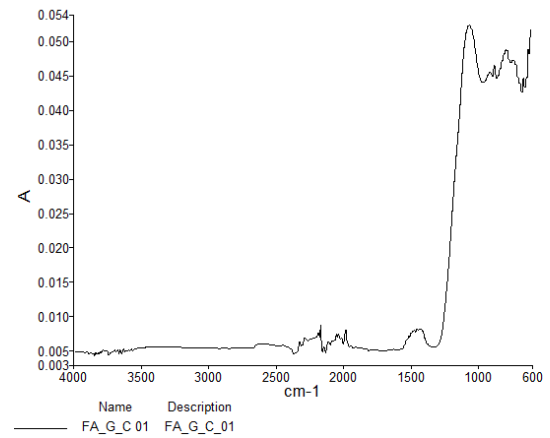


**Figure 4.10:** FT-IR spectrum of fly ash

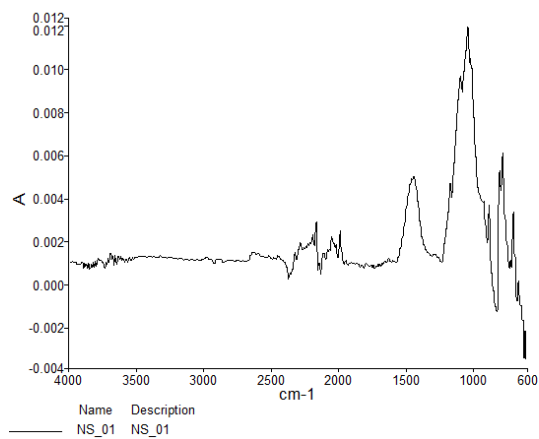


**Figure 4.11:** FT-IR spectrum of fine aggregate

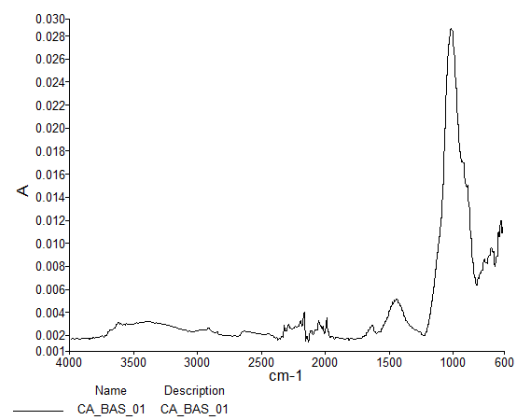


**Figure 4.12:** FT-IR spectrum of coarse aggregate

It is relevant to note here that the empirical data obtained through XRD, and SEM/EDS of the cured/spalled materials are not easy to interpret given the heterogeneity within the matrices of different materials. Furthermore, we chose to rely more on the resonance properties of the nuclei of interest through solid-state NMR techniques (Walkley and Provis, 2019). The major advantage of such an approach is that one could home on to the nuclei of interest (i.e., primarily  $^{27}\text{Al}$  and  $^{29}\text{Si}$ ) more closely without being overly influenced by the heterogeneity arising from the differences in the chemical constitution of the test samples. It is also quite relevant to note here that NMR active nucleus of calcium ( $^{43}\text{Ca}$ ), albeit the nucleus of most importance for elucidating the mechanistic pathway triggering the phenomenon of spalling, is not at all useful given the relatively very low natural abundance and that it is only moderately sensitive to NMR measurements. In addition,  $^{43}\text{Ca}$  is a spin 7/2 nucleus and is therefore quadrupolar. As a result, the signal width increases with asymmetry of the environment.

When considering the four raw materials, i.e., OPC, FA, fine aggregate and coarse aggregate, some of the samples exhibited paramagnetic properties, and hence the solid-state NMR of these could not be recorded (for instance, FA and coarse aggregate, where a relatively higher percentage of iron oxide was present, it can be assumed to act as the paramagnetic centres. There was also corroborative evidence from the SEM/EDS data). For those samples where the spectra were successfully recorded, it generally showed rather weak signals which were inherently less discernible as compared to the corresponding pristine raw materials. In summary, the extent of information obtained through solid-state NMR were also somewhat limited owing to the factors enumerated above. As mentioned before, due to the high paramagnetic magnetic property of FA and the coarse aggregate, the spectra were only recorded for cement and fine aggregate. These spectrums of  $^{27}\text{Al}$  and  $^{29}\text{Si}$  of cement is given in **Figures 4.13 and 4.14** and  $^{27}\text{Al}$  and  $^{29}\text{Si}$  of fine aggregate is given in **Figures 4.15 and 4.16**. Its spectra amply revealed the chemical environments of the nuclei in question.

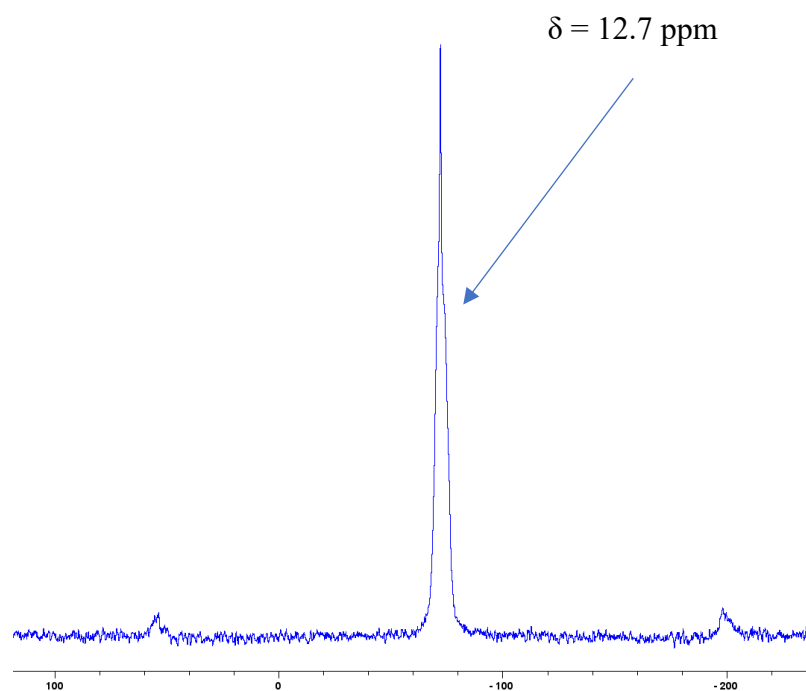


**Figure 4.13:** Solid-state  $^{27}\text{Al}$  spectrum of cement

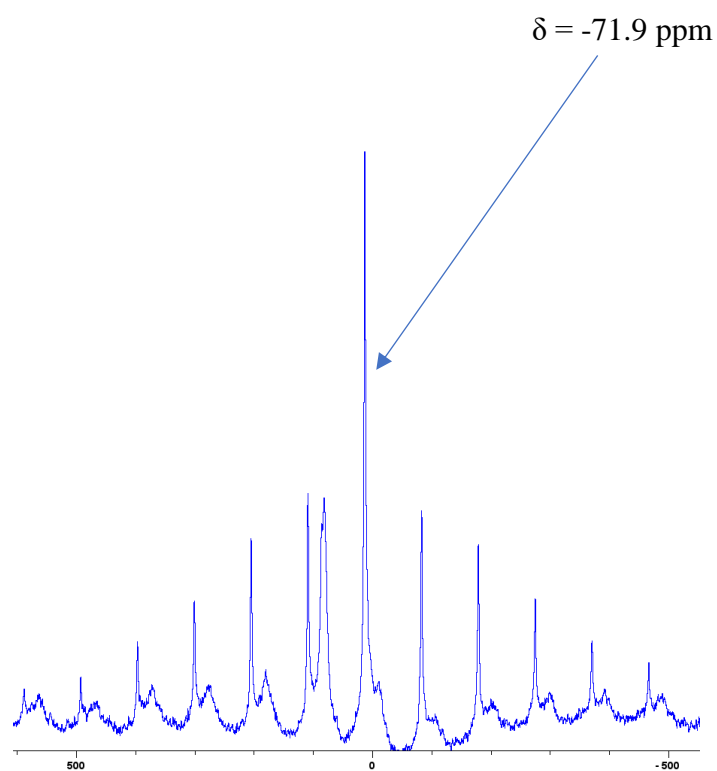


**Figure 4.14:** Solid-state  $^{29}\text{Si}$  spectrum of cement

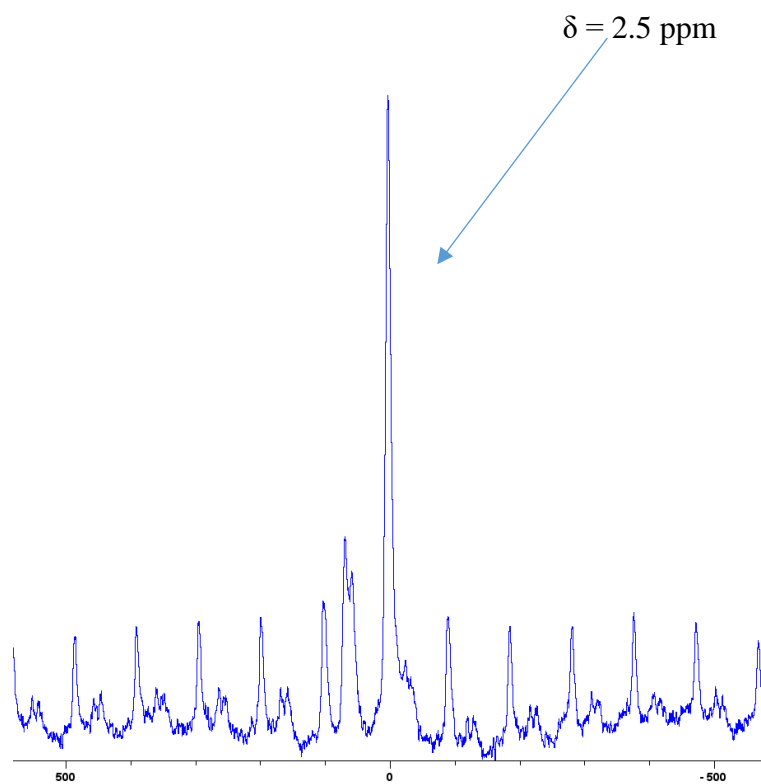


**Figure 4.15:** Solid-state  $^{27}\text{Al}$  spectrum of fine aggregate

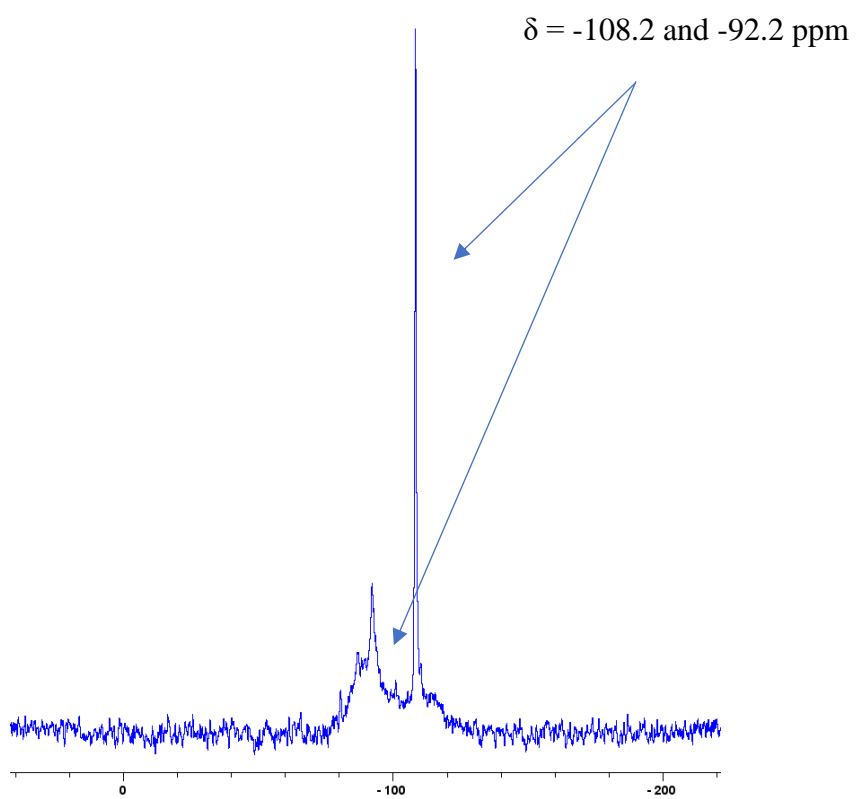


**Figure 4.16:** Solid-state  $^{29}\text{Si}$  spectrum of fine aggregate

The following features can be identified through the spectra; for cement,  $^{27}\text{Al}$  spectrum showed one major peak ( $\delta = 12.7$  ppm);  $^{29}\text{Si}$  exhibited a symmetric multiple peaklet centred around  $\delta = -71.9$  ppm;  $^{27}\text{Al}$  spectrum of fine aggregate showed a major peaklet centred around  $\delta = 2.5$  ppm with minor peaks approximately equidistant from the major peak;  $^{29}\text{Si}$  spectrum of fine aggregate showed a sharp singlet around  $\delta = -108.2$  and a broader peak  $\delta =$  peak centred around  $-92.2$  ppm. It can be inferred from the above spectra, except in the case of  $^{29}\text{Si}$  spectrum of cement (where definite splitting pattern owing to coupling to a vicinal NMR active nucleus was evident), all other spectra showed that the nucleus of interest,  $^{27}\text{Al}$ , or  $^{29}\text{Si}$ , was disposed in a major chemical environment within their oxide, or silicate, as the case may be (Walkley and Provis, 2019). A more detailed discussion pertaining to solid-state NMR spectra, including those obtained from the cubical samples, can be seen in a tabular form in **Table 4.4** (see page 110).

The thermal and calorimetric properties were assessed on the polymeric fibrous, namely PP, cotton and polyester materials, using DSC techniques and a summary of the obtained data is given in **Table 4.1**.

**Table 4.1:** DSC data of the sacrificial agents

Sacrificial agent	Mass (mg)	Melting temperature (°C)	Integral (area under the curve) (mJ)	Area/mass	Degradation temperature (°C)	Integral (area under the second curve) (mJ)	Area/mass
PP 12mm	5.30	167	440.250	83.0	461	2928.05	553
PP 48mm	9.20	167	1102.71	120	458	6919.10	752
Cotton	2.50	n/a	n/a	n/a	356	446.000	178
Polyester	4.40	254	248.290	56.4	431	878.320	200

Samples were degraded in an atmosphere of nitrogen at a heating rate of  $10^\circ\text{C min}^{-1}$  from  $30^\circ\text{C}$  to  $550^\circ\text{C}$ . It was found that the crystalline domains of both the PP fibres (12 mm and 48 mm) melted at a temperature of around  $167^\circ\text{C}$ , whereas those of the polyester fibres melted at a much higher temperature of  $254^\circ\text{C}$ . These samples subsequently underwent pyrolytic decompositions. Cotton sample, being consisted of ligno-cellulosic material, on the other hand underwent degradation (i.e., pyrolytic decomposition) rather than melting.

The degradation process of the PP fibres occurred at about 461°C for the 12 mm fibres and about 458°C for the 48 mm fibres, respectively. Cotton degraded at a much lower temperature of about 356°C, whereas the polyester fibres degraded at a temperature of about 431°C (Majewsky et al., 2016, Joseph et al., 2003, Wong and Lam, 2002, Trask and Beninate, 1986). **Figures 4.17– 4.20** shows the DSC thermograms for the sacrificial agents.

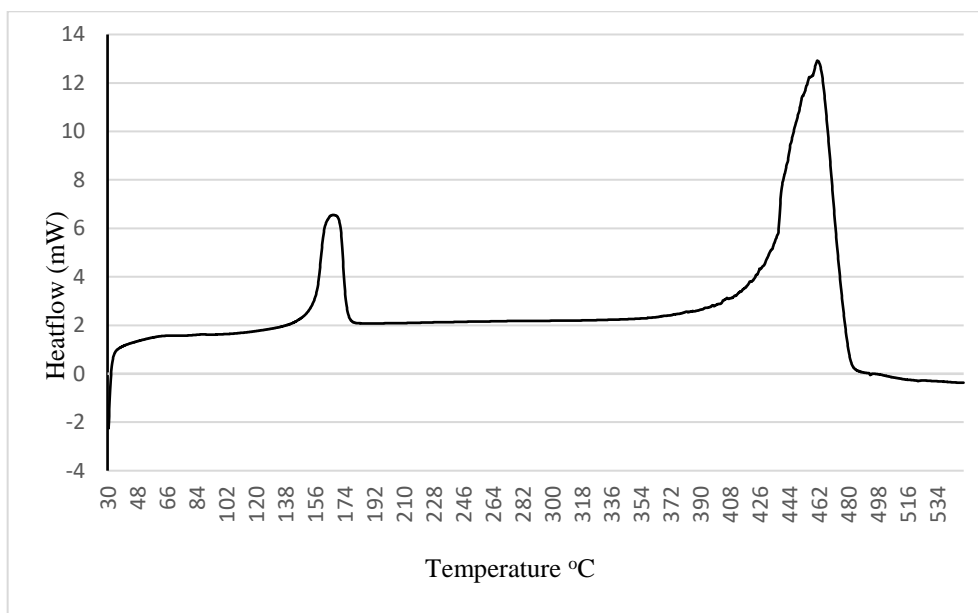


**Figure 4.17:** DSC thermogram of 12mm polypropylene fibres

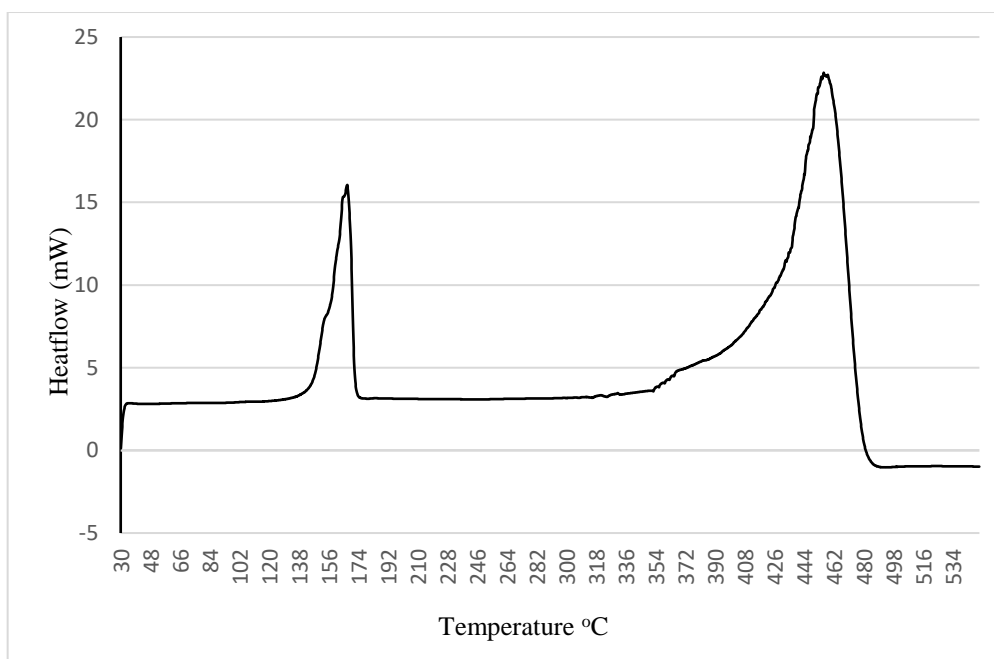


**Figure 4.18:** DSC thermogram of 48mm polypropylene fibres



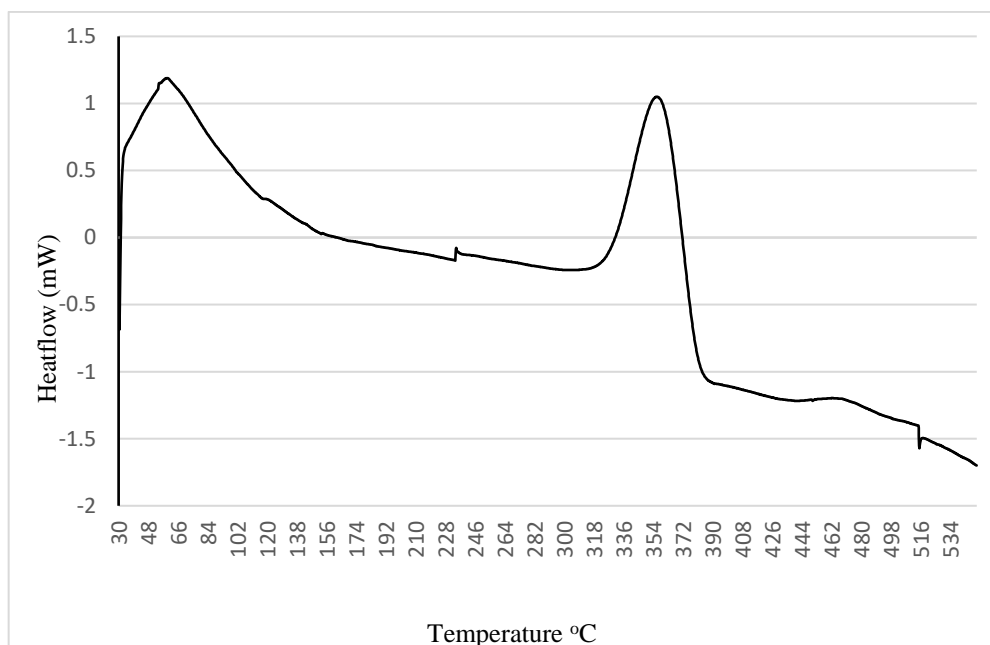


**Figure 4.19:** DSC thermogram of cotton fibres

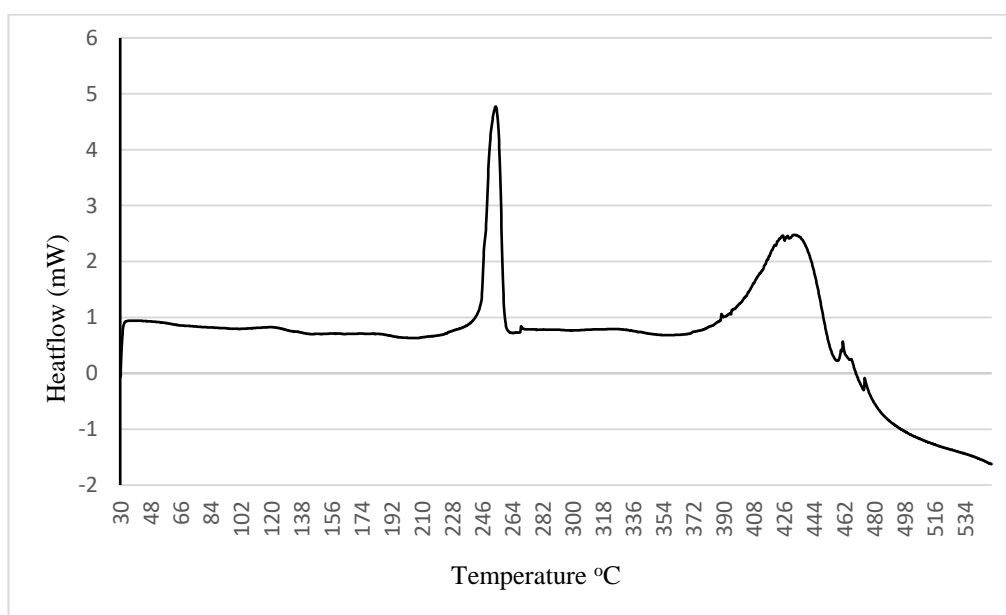


**Figure 4.20:** DSC thermogram of polyester fibres

It can be clearly seen from the above DSC thermograms, all three polymeric components either underwent melting and/or degradation, preferentially, before the onset of severe spalling (see also **Figure 2.1**). Invariably such phase changes, predominantly melting in the case of the synthetic variants, i.e., PP and polyester fibres (refer **Section 2.7**), and

decomposition in the case of cotton (producing porous char residues), can be considered to result in lower pore pressures, thus counteracting the physio-chemical processes leading to spalling. This effect was later validated through heat treatment of MD 03 samples (which are generally prone to the maximum degree of spalling at around 350°C without the addition of any fillers) having incorporated these materials, did not spall even after exposing to 800°C for 1 hour (refer to **Section 4.8**). It is highly relevant to note here the even the large-scale experiments on the concrete slabs incorporating PP fibres showed improved fire resistance (refer to **section 4.12**).

When comparing the phase changes with mass loss (i.e., the pyrolysis) in DSC runs, these are also duly reflected in the corresponding TGA thermograms of the polymeric materials. Overall, the profiles of the thermograms were as expected of PP fibres, polyesters fibres and ligno-cellulosic materials (Joseph et al., 2003, Trask and Beninate, 1986, Zohdy et al., 1999).

**Figures 4.21 – 4.24** show the TGA curves for the sacrificial agents over a temperature range of 30°C – 900°C at a heating rate of 10°C min<sup>-1</sup>. In the case of PP fibres, the predominant degradation pathway involved random chain scissors, producing low molecular weight fragments that could further undergo bond cleavages through radical-mediated processes, thus producing lower molecular weight hydrocarbons that could also include the monomer. In the case of polyesters, the random chain scission involves the backbone ester linkages, and the low molecular weight fragments can in turn undergo further degradations, to form predominantly volatiles and a nominal amount of char residues. Lignocellulosic materials, like cotton on the other hand initially undergoes dehydration reactions, followed by formation levoglucosan and other low molecular fragments owing to main chain degradations. Crosslinking reactions also take a central role in such transformations, leaving carbonaceous char residues (Nurazzi et al., 2021).

It is also evident from the TGA analyses that all the three classes of materials are significantly stable against oxidative degradation (until about 300°C, or even higher). However, in the case of PP and polyester fibres the expected effect of relief of pore pressure can be assumed to start upon the melting of the crystalline domains within the samples (see **in Table 4.1**). In contrast, in the case of cotton, as there are no discernible phase changes, such an effect, need to originate through the formation of a porous char residue (*ca.* 16 wt.% of char residue). On the other hand, generally for polyesters, the scission of mainchain

backbone is affected through the lysis of the ester linkages, resulting in the formation of smaller fragments and other volatiles. These fragments can then undergo further radical-induced transformations producing even smaller fractions. It is also relevant to note that in the case of PPs and polyester, which are not typically char-forming polymers, under a thermo-oxidative degradation, however, can aid in the relief of pore pressure owing to melting well below its pyrolysis temperatures.

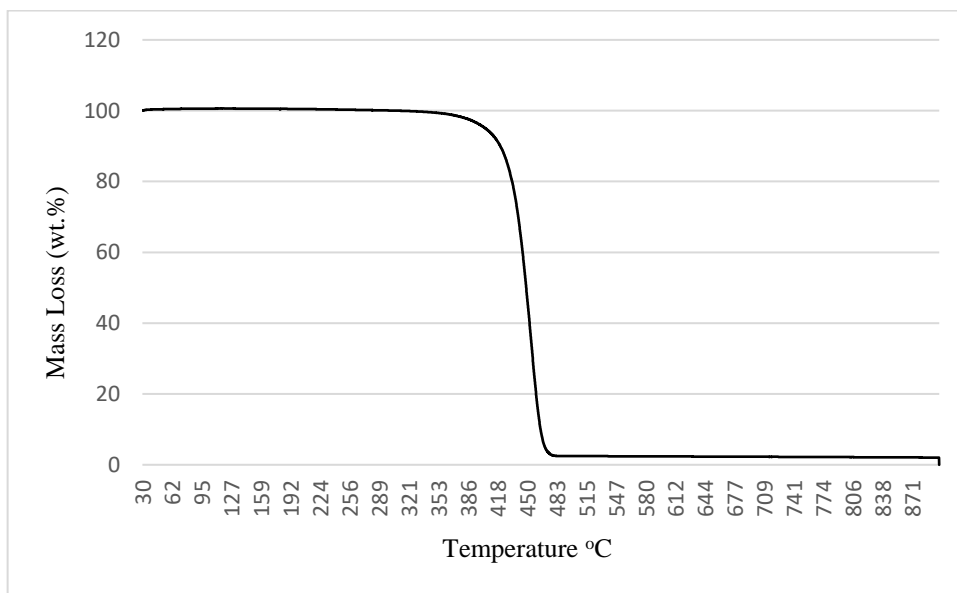


**Figure 4.21:** TGA thermogram of 12 mm PP fibres

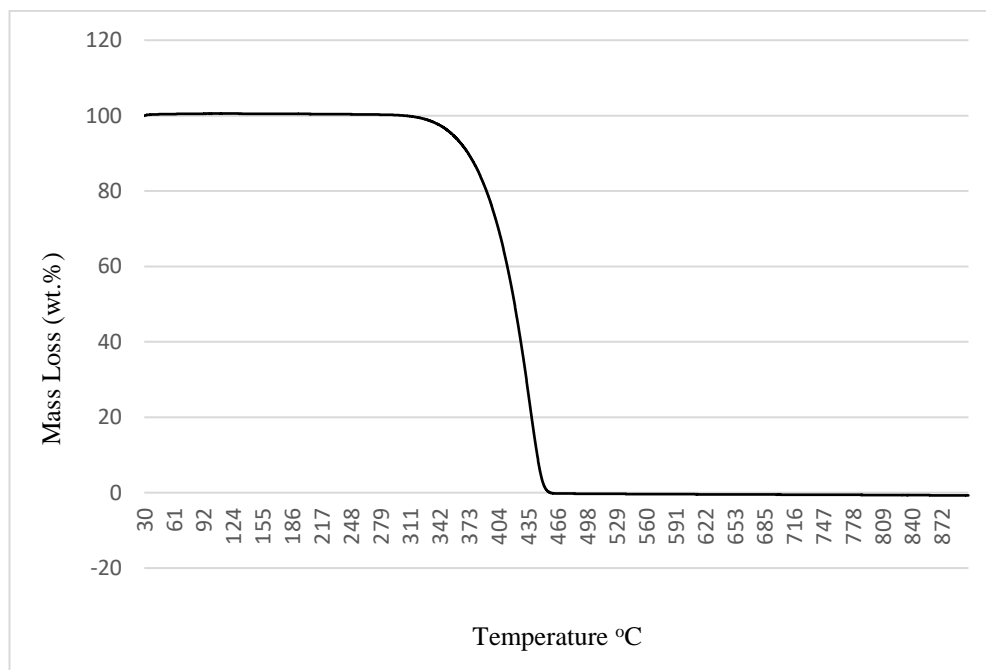


**Figure 4.22:** TGA thermogram of 48 mm PP fibres

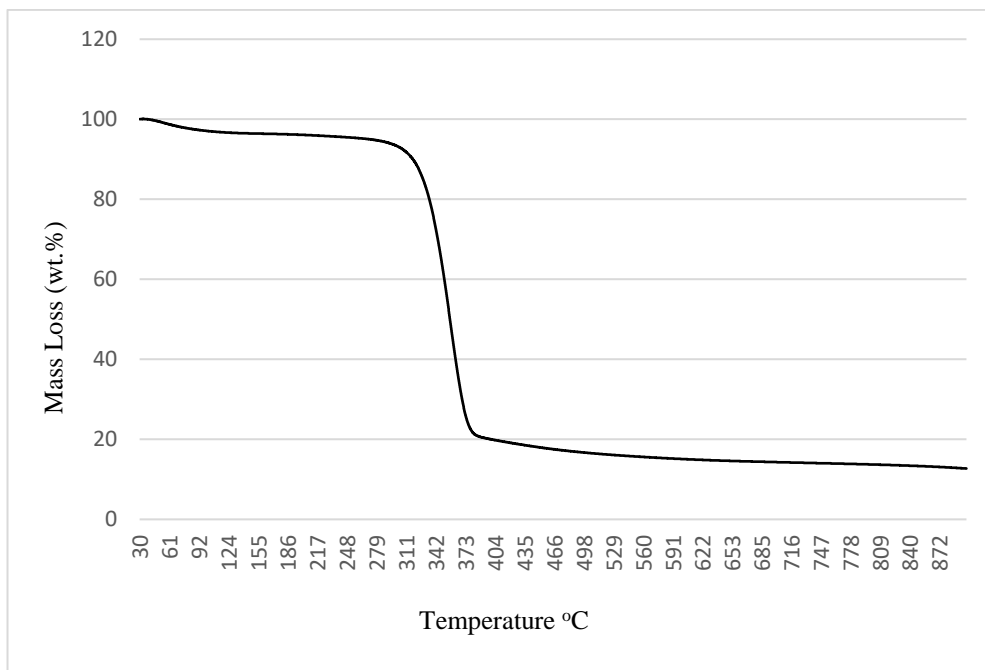


**Figure 4.23:** TGA thermogram of cotton fibres

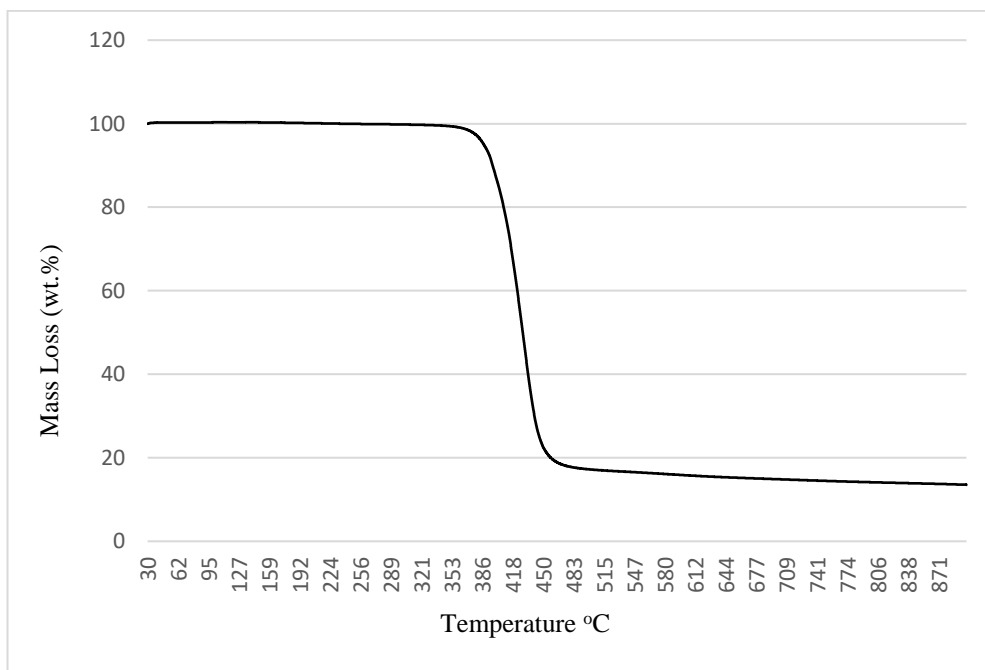


**Figure 4.24:** TGA thermogram of polyester fibres

In addition to the DSC and TGA data, PCFC runs were also conducted on the sacrificial agents (**Table 4.2**) with a view to gauging their combustibility parameters. The general profiles of the heat release rate, and its peak values were found to be truly reflective of their TGA thermograms, as expected, since both tests adopted temperature ramps albeit at different heating rates. The polyester fibres showed a heat release capacity of 387 J/g-K, peak heat release rate of 387 W/g, at a temperature of about 467°C, and 23.38 KJ/g. The corresponding values for PP were: for 12 mm 744 J/g-K; 734 W/g, at a temperature about 473°C; 37.7 KJ/g; and for 48 mm 873 J/g-K; 816 W/g, at a temperature about 474°C; 38.7 KJ/g. In the case of cotton, being a typical lignocellulosic material, is comparatively less flammable as reflected through the reduced values for the relevant PCFC data (192 J/g-K; 192 W/g, at a temperature about 382°C; 12.63 KJ/g), and formation of relatively higher amount of char residue (*ca.* 9 wt.%).

As the relevant PCFC data of all three polymeric components show that they all are relatively combustible, even though they are only present in very low loadings (typically 1 wt.%) within the concrete matrices, they can serve to be advantageous in the overall fire behaviour of the composites. Their beneficial effect is assumed to be from their role as ‘sacrificial agents’, where their melting and degradation properties could help create openings to relieve the pore pressure. This was very evident when incorporated in the MD03 mix which turned out to be quite amenable to spalling otherwise.

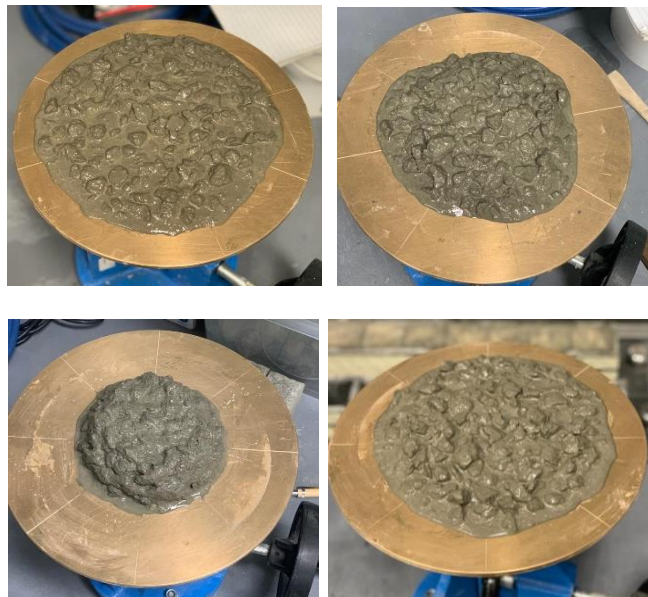
**Table 4.2:** PCFC data for sacrificial agents

Sacrificial agent	Temp to pHRR (°C)	pHRR (W/g)	THR (kJ/g)	HRC (J/g-K)	Char residue (wt.%)	EHC (kJ/g)
<b>PP 12mm</b>	473	734	37.7	744	0.0	37.70
<b>PP 48mm</b>	474	816	38.7	831	0.0	38.70
<b>Cotton</b>	382	192	11.6	192	9.02	12.63
<b>Polyester</b>	467	387	21.1	387	2.56	23.38

### 4.3. Workability

Concrete workability is an importance factor when assessing the performance and behaviour of freshly formed concrete mixtures. **Figure 4.25** shows a comparison of the flow properties amongst the control mix designs and **Table 4.3** gives the average slump flow reading recorded for each of the mixes. As expected, owing to the high w/c ratio, MD01 recorded the highest flow properties with an average slump flow of 193 mm. MD02 recorded an average slump flow of 155 mm, and MD03, in spite of having the lowest water to cement ratio of 0.25, recorded an average slump flow of 118 mm- which can be attributed to the chemical agent (superplasticizer) that was used during mixing of the MD03 samples, which resulted in the enhancement of the flow property of the mix (Faroug et al., 1999, Kannangara, 2018).

It is to be noted here that the GP01 mixes were found to be more cohesive in nature compared to the OPC- based mixes and recorded an average slump flow of 173 mm. This was higher than that of the MD02 mixes, even though the liquid: binder ratio of the GP01 and MD02 mixes were the same. This could be due to the spherical shape and the comparatively finer particle size of the FA compared to OPC which can facilitate in a higher flow during the wet stages of the concrete mix, and combined with the lubricating effect of sodium- based activators, the flowability could be enhanced (Law et al., 2015, Kannangara, 2018).



Top right MD01; top left MD02; bottom right MD03; bottom left GP01

**Figure 4.25:** Images from the flow table tests of control samples

When considering the addition of PP fibres, there was a noticeable drop in the average slump flow readings as the percentages ranged from 0.5 – 1.5, which could be due to the increase in the probability of the fibre overlapping and clustering together, and any fibrous material will reduce the flow properties due to adsorption properties of different fibres (Ibrahim et al., 2019, Dharan and Lal, 2016, Hu et al., 2022, Sasi et al., 2024, Madhavi et al., 2014). In addition to the reduced workability, it was evident that the incorporation of 12 mm PP fibres resulted in a lower slump flow compared to the 48 mm PP fibres, with MD01a, b and c resulting in average slump flow readings of 184, 179 and 166 mm, respectively, and MD01d, e and f resulting in average slump flow readings of 188, 182 and 170 mm, respectively.

**Table 4.3:** Average slump flow readings

Mix	Slump flow (mm)	Mix	Slump flow (mm)	Mix	Slump flow (mm)	Mix	Slump flow (mm)
MD01	193	MD02	155	MD03	118	GP01	173
MD01a	184	MD02a	143	MD03a	107	GP01a	163
MD01b	179	MD02b	137	MD03b	101	GP01b	158
MD01c	166	MD02c	128	MD03c	94.5	GP01c	147
MD01d	188	MD02d	149	MD03d	110	GP01d	164
MD01e	182	MD02e	144	MD03e	103	GP01e	161
MD01f	170	MD02f	135	MD03f	98.5	GP01f	153
MD01g	161	MD02g	121	MD03g	90.5	GP01g	135
MD01h	176	MD02h	132	MD03h	97.5	GP01h	151

Similar trends were observed for the MD02, MD03 and GP01 specimens, where the addition of 12 mm PP fibres resulted in average slump flow readings lower than those for the 48 mm PP fibres. These results could be due to the shorter fibres having a greater distribution when being mixed with the concrete, thus increasing the frictional flow amongst particles, and hindering the flow properties; whereas in the case of the harder fibres (48 mm),

an increase in the entrapped air voids could occur, which can contribute to an increase in the flow properties. Similar results had been reported by Açıkgenç et al. (2012) who stated that compared to the hard fibres, the softer fibres tend to agglomerate during mixing, thus obstructing the flow properties.

When considering the average slump flow of cotton fibre incorporation, the lowest results were recorded from them, i.e., MD01g, MD02g, MD03g and GP01g, with the lowest flow reading from the whole set in all the tests coming from MD03g (90.5 mm). This could be due the adsorption properties of the cotton fibres compared to the PP and polyester counterparts, which tend to hold the water molecules without allowing them to mix and flow with the concrete particles. Mixes consisting of polyester fibres resulted in similar results to those having 1% 12 mm PP fibres, which could be due to the similarities in nature of the two fibres.

It must be noted that the fibres often tend to clump together and separate from the paste, and an even distribution of the fibres is crucial to obtaining a homogenous mix, with better fibre dispersion and improved workability.

#### **4.4 Characterization of cured and heat-treated samples**

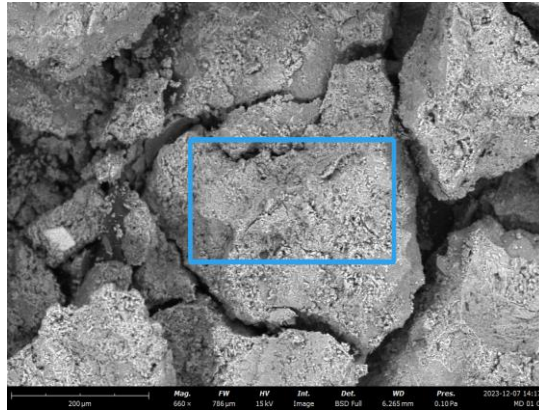
After the different mixes (i.e., MD01, MD02, MD03 and GP01) underwent their relevant curing regimes, they were subjected to microstructural studies using the SEM/EDS, XRD and solid-state NMR. Here, heat-treated specimens at 400°C and 800°C were also tested by using the above-mentioned techniques. It must be noted here that due to the high spalling nature of the MD03 specimens, elevated temperature testing (i.e. at 800°C) could not be carried on for MD03.

**Figures 4.26 – 4.35** (i.e. the outputs from the machine) show the SEM/EDS of MD01, MD02, MD03 and GP01 samples after curing (at ambient temperature), and after heat-treatment at 400°C and 800°C. There were noticeable differences in microstructural features of the cured and heat-treated samples in the cases of MD01, MD02 and GP01. This can be attributed primarily to the thermally induced dehydration reactions, occurring to the hydrated calcium centres, possibly resulting in the formation of micro-cracks within the matrices of the heat-treated samples, in comparison to the cured counterparts. The SEM results also showed that the relative levels of calcium in the MD01 mixes increased from



approximately 32 to 40, and then to 44 weight percentages as the temperature increased from ambient temperature (cured) to 400°C and then to 800°C, respectively. Similar observations were made for the calcium levels in the MD02 samples, with the weight concentrations increasing from approximately 31 to 34, and then to 39 as the temperature increased from ambient temperature (cured) to 400°C and then to 800°C, respectively. This effect cannot be explained with any certainty as the specimens were bound to decrease in masses owing to simultaneous evaporation of water from them. However, the wt.% of calcium in samples in question can also be seen to increase even when normalized to the respective wt.% of oxygen. In addition, there may be a minor component affecting the mass losses of the cubical samples owing to the decomposition of calcium carbonate present in them. This plausible explanation can be also extended to other elements of interest in the tested samples. Cured specimens of MD03 (at ambient temperature) showed a weight concentration of approximately 27 for the calcium level.

As expected, FA-based GP specimen (GP01) displayed different chemical compositions to that of the concrete specimens with the highest weight concentration of oxygen, followed by silicon, which was approximately 20, and then by aluminium, approximately 11. The calcium concentration was relatively low (at approximately 6). It is also relevant to note here that, in the case of GP specimens, increases in temperatures can also aid in further polymerization reactions triggered by the alkaline activator and precursor materials. However, at relative higher temperatures (i.e., 800°C in the present case), the above effect seems to be counteracted by extensive dehydration reactions, thus resulting in the weakening of the base matrix. After being exposed to an elevated temperature of 400°C the weight concentrations for silicon and aluminium were decreased to approximately 19 and 10, respectively. In addition, the calcium concentration was also seen to reduce to about 5.2 at 400°C and 4.5 at 800°C, respectively.



	Element Number	Element Symbol	Element Name	Atomic Conc.	Weight Conc.
	6	C	Carbon	6.185	3.518
	8	O	Oxygen	68.184	51.658
	9	F	Fluorine	0.000	0.000
	13	Al	Aluminum	1.889	2.412
	14	Si	Silicon	5.667	7.538
	16	S	Sulfur	0.463	0.704
	20	Ca	Calcium	16.734	31.759
	25	Mn	Manganese	0.077	0.201
	26	Fe	Iron	0.570	1.508
	29	Cu	Copper	0.134	0.402
	30	Zn	Zinc	0.097	0.302

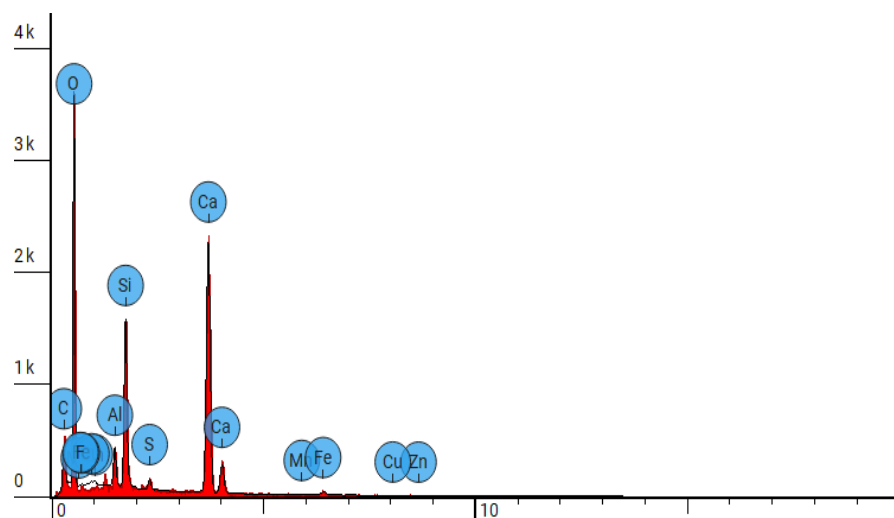
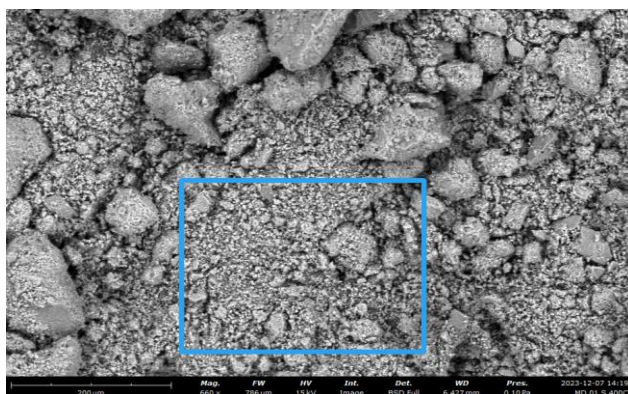


**Figure 4.26:** SEM/EDS of MD01 cured samples



	Element Number	Element Symbol	Element Name	Atomic Conc.	Weight Conc.
	6	C	Carbon	8.138	4.322
	8	O	Oxygen	59.804	42.312
	9	F	Fluorine	0.359	0.302
	13	Al	Aluminum	1.938	2.312
	14	Si	Silicon	5.259	6.533
	16	S	Sulfur	0.638	0.905
	20	Ca	Calcium	22.569	40.000
	25	Mn	Manganese	0.083	0.201
	26	Fe	Iron	0.895	2.211
	29	Cu	Copper	0.143	0.402
	30	Zn	Zinc	0.174	0.503

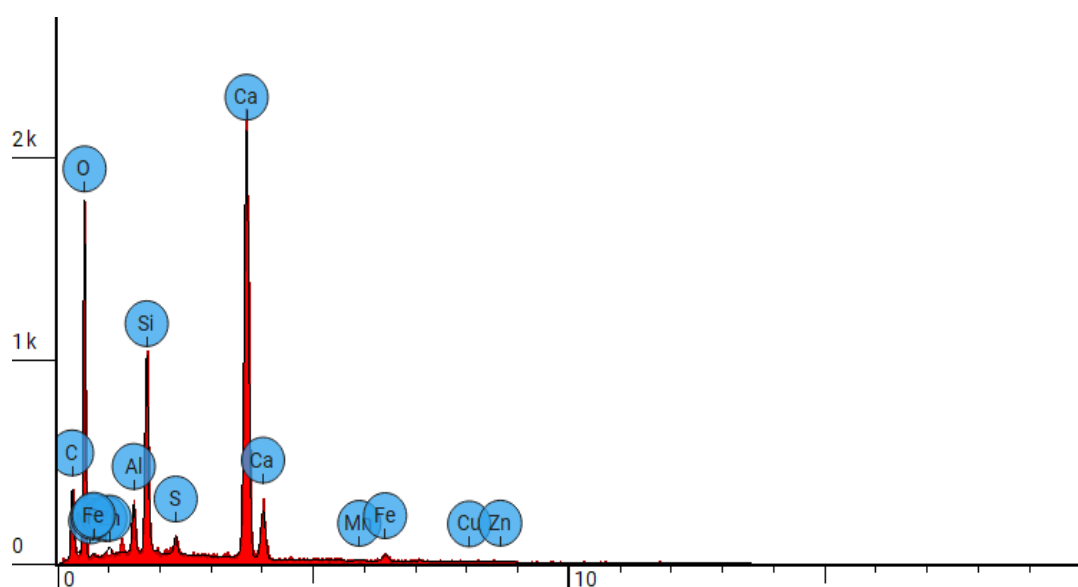
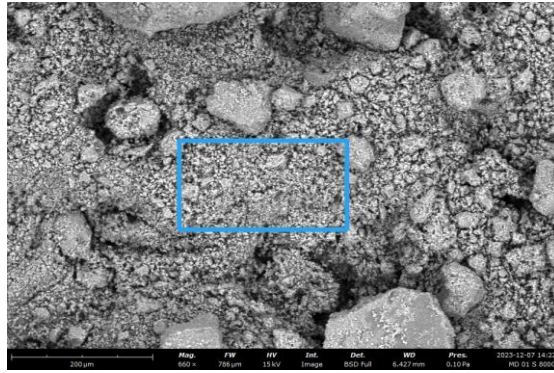
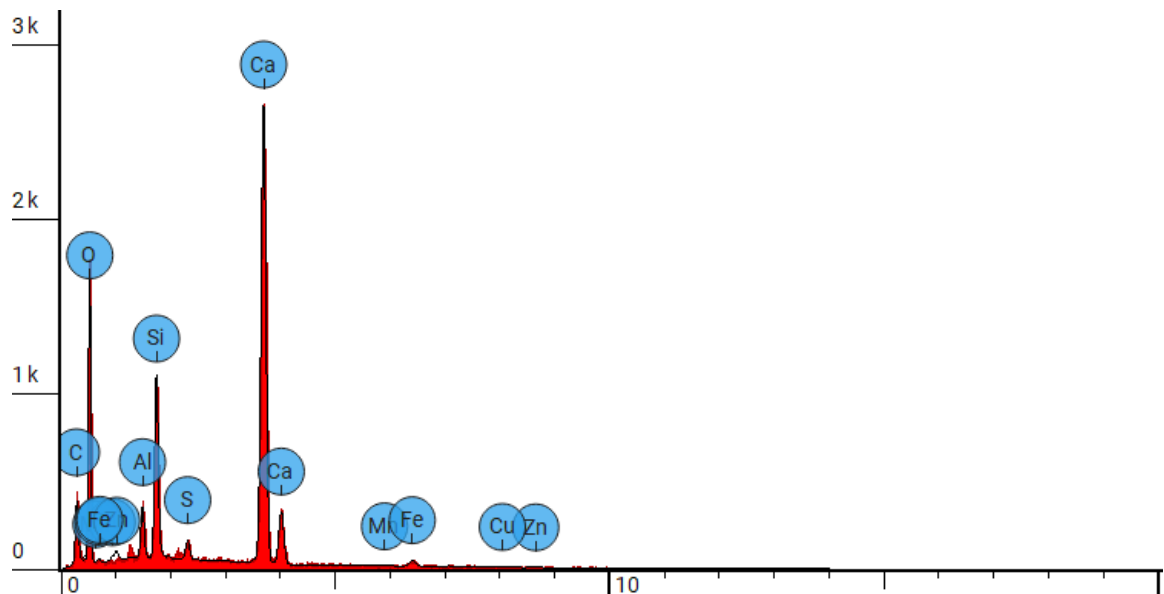


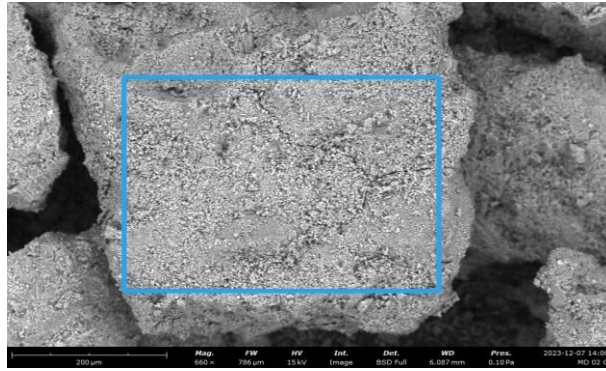
Figure 4.27: SEM/EDS of MD01 samples heat-treated at 400°C



	Element Number	Element Symbol	Element Name	Atomic Conc.	Weight Conc.
	6	C	Carbon	6.322	3.219
	8	O	Oxygen	57.683	39.135
	9	F	Fluorine	0.375	0.302
	13	Al	Aluminum	2.199	2.515
	14	Si	Silicon	5.321	6.338
	16	S	Sulfur	0.740	1.006
	20	Ca	Calcium	26.105	44.366
	25	Mn	Manganese	0.043	0.101
	26	Fe	Iron	0.807	1.911
	29	Cu	Copper	0.187	0.503
	30	Zn	Zinc	0.218	0.604



**Figure 4.28:** SEM/EDS of MD01 samples heat-treated at 800°C



	Element Number	Element Symbol	Element Name	Atomic Conc.	Weight Conc.
	6	C	Carbon	9.991	5.628
	8	O	Oxygen	61.337	46.030
	9	F	Fluorine	0.338	0.302
	12	Mg	Magnesium	0.529	0.603
	13	Al	Aluminum	2.066	2.613
	14	Si	Silicon	7.552	9.950
	16	S	Sulfur	0.668	1.005
	20	Ca	Calcium	16.413	30.854
	25	Mn	Manganese	0.078	0.201
	26	Fe	Iron	0.729	1.910
	29	Cu	Copper	0.169	0.503
	30	Zn	Zinc	0.131	0.402

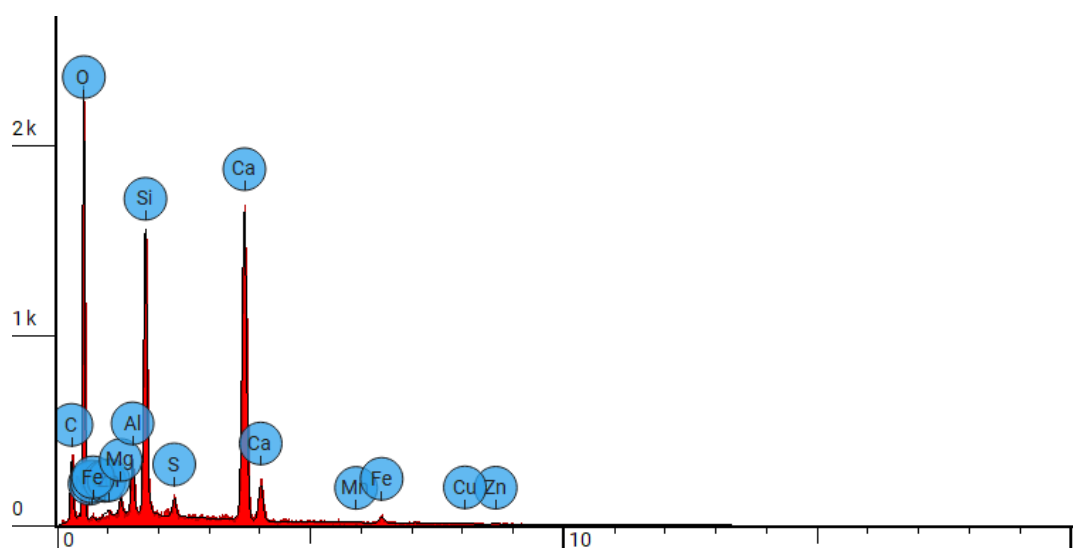
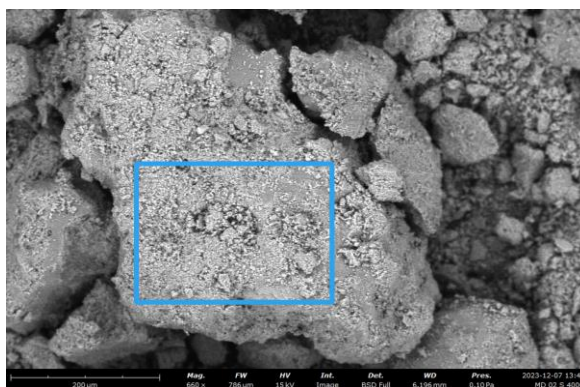


Figure 4.29: SEM/EDS of MD02 cured samples



	Element Number	Element Symbol	Element Name	Atomic Conc.	Weight Conc.
	6	C	Carbon	8.526	4.733
	8	O	Oxygen	63.587	47.029
	9	F	Fluorine	0.344	0.302
	12	Mg	Magnesium	0.448	0.504
	13	Al	Aluminum	1.858	2.316
	14	Si	Silicon	5.894	7.654
	20	Ca	Calcium	18.100	33.535
	25	Mn	Manganese	0.079	0.201
	26	Fe	Iron	0.585	1.511
	29	Cu	Copper	0.103	0.302
	30	Zn	Zinc	0.100	0.302
	41	Nb	Niobium	0.375	1.611

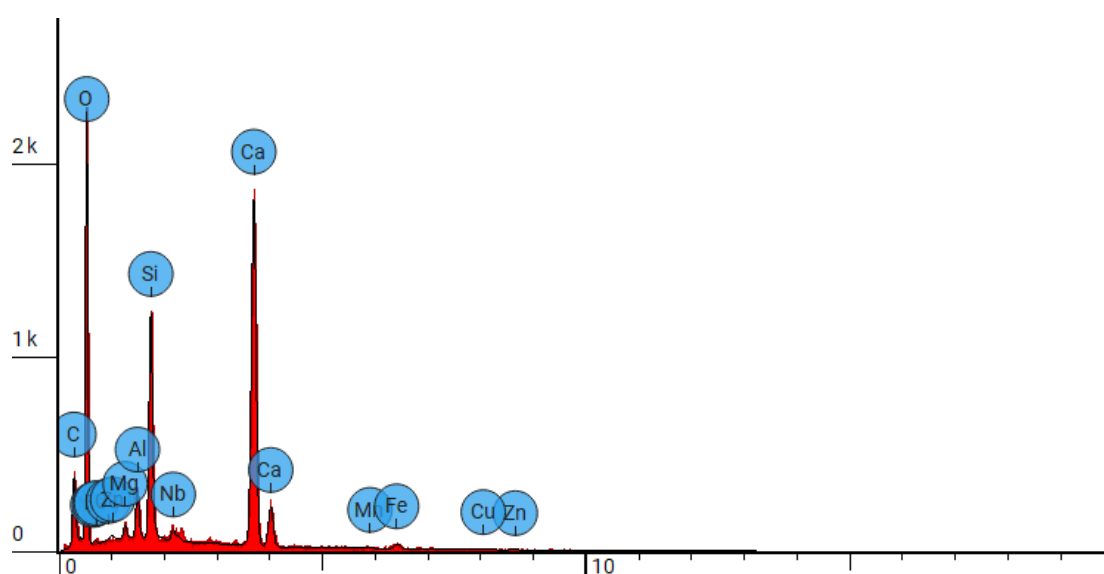
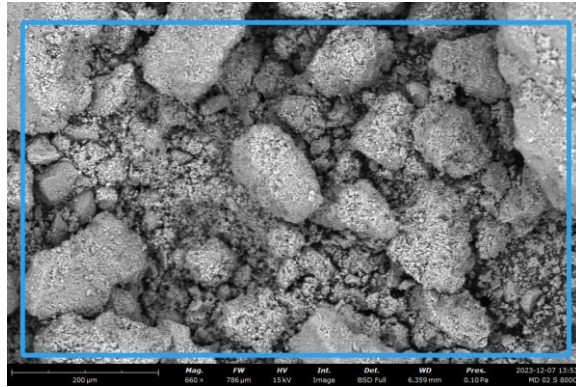


Figure 4.30: SEM/EDS of MD02 samples heat-treated at 400°C



	Element Number	Element Symbol	Element Name	Atomic Conc.	Weight Conc.
	6	C	Carbon	6.836	3.614
	8	O	Oxygen	59.866	42.169
	9	F	Fluorine	0.360	0.301
	13	Al	Aluminum	1.522	1.807
	14	Si	Silicon	7.875	9.739
	16	S	Sulfur	0.427	0.602
	20	Ca	Calcium	21.907	38.655
	25	Mn	Manganese	0.042	0.100
	26	Fe	Iron	0.776	1.908
	29	Cu	Copper	0.179	0.502
	30	Zn	Zinc	0.209	0.602

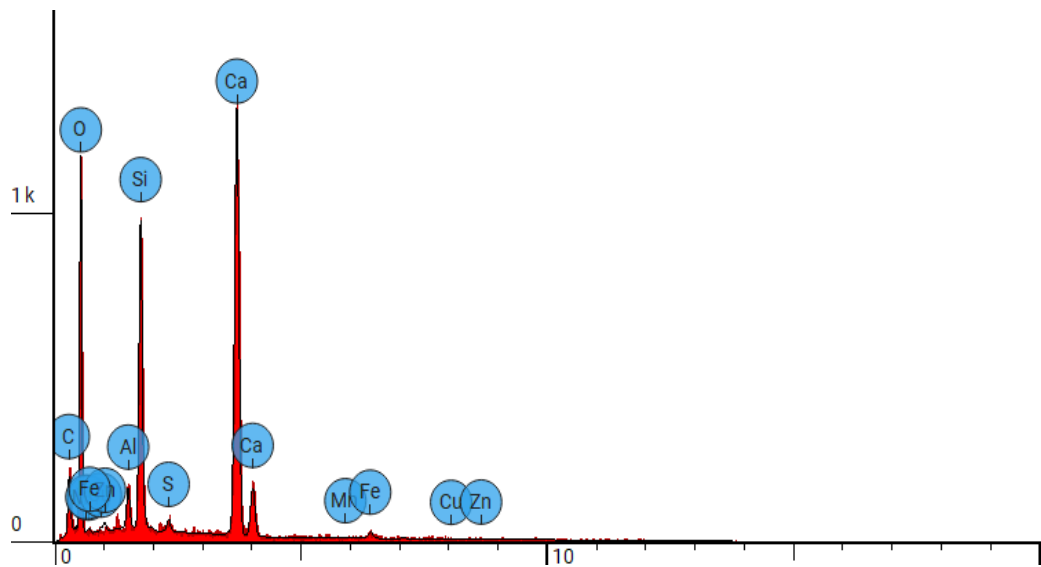
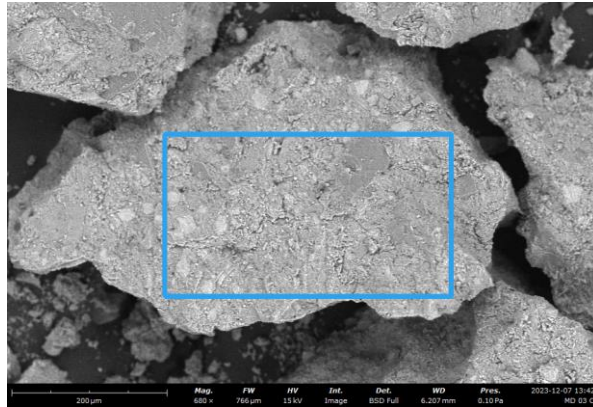


Figure 4.31: SEM/EDS of MD02 samples heat-treated at 800°C



	Element Number	Element Symbol	Element Name	Atomic Conc.	Weight Conc.
	6	C	Carbon	9.712	5.645
	8	O	Oxygen	65.610	50.806
	9	F	Fluorine	0.767	0.706
	13	Al	Aluminum	1.776	2.319
	14	Si	Silicon	6.970	9.476
	20	Ca	Calcium	14.031	27.218
	25	Mn	Manganese	0.038	0.101
	26	Fe	Iron	0.522	1.411
	29	Cu	Copper	0.098	0.302
	30	Zn	Zinc	0.127	0.403
	42	Mo	Molybdenum	0.347	1.613

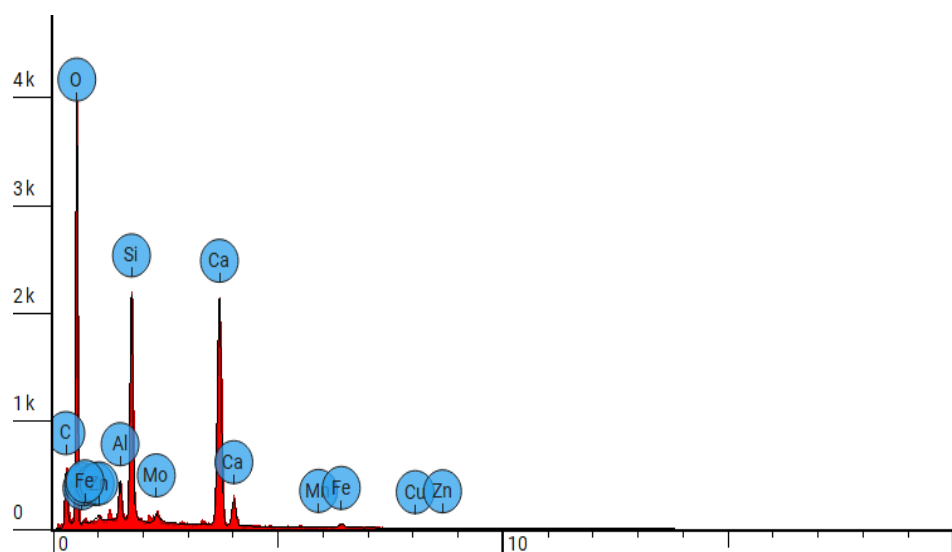
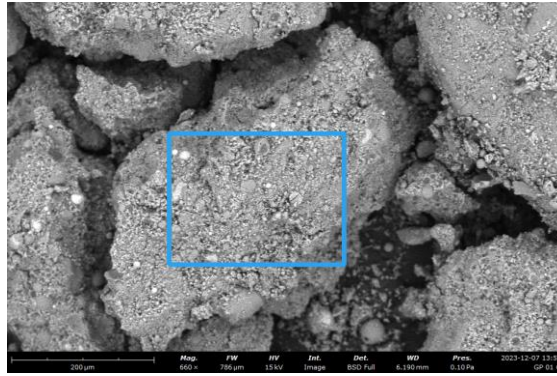


Figure 4.32: SEM/EDS of MD03 cured samples





	Element Number	Element Symbol	Element Name	Atomic Conc.	Weight Conc.
	6	C	Carbon	6.554	3.711
	8	O	Oxygen	56.776	42.828
	9	F	Fluorine	0.560	0.502
	11	Na	Sodium	4.625	5.015
	13	Al	Aluminum	8.914	11.334
	14	Si	Silicon	15.450	20.461
	19	K	Potassium	0.544	1.003
	20	Ca	Calcium	3.397	6.419
	22	Ti	Titanium	0.311	0.702
	25	Mn	Manganese	0.116	0.301
	26	Fe	Iron	2.171	5.717
	29	Cu	Copper	0.268	0.802
	30	Zn	Zinc	0.130	0.401
	41	Nb	Niobium	0.183	0.802

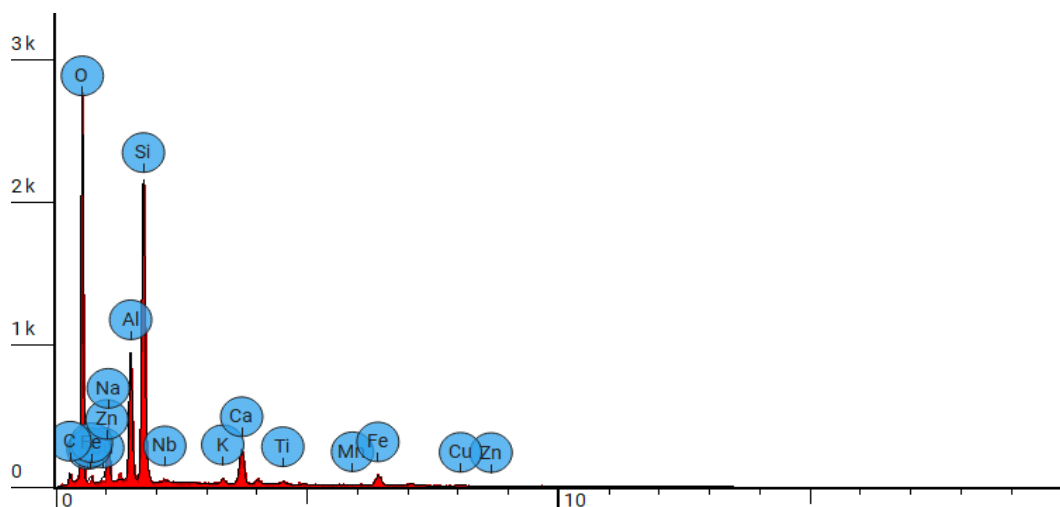
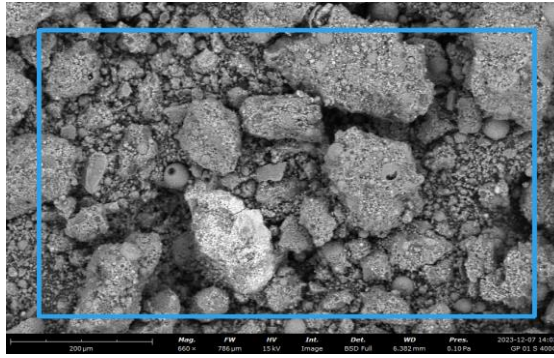


Figure 4.33: SEM/EDS of GP01 cured samples



	Element Number	Element Symbol	Element Name	Atomic Conc.	Weight Conc.
	6	C	Carbon	9.232	5.295
	8	O	Oxygen	55.699	42.557
	9	F	Fluorine	0.771	0.699
	11	Na	Sodium	5.184	5.694
	13	Al	Aluminum	8.067	10.390
	14	Si	Silicon	14.299	19.181
	19	K	Potassium	0.321	0.599
	20	Ca	Calcium	2.714	5.195
	25	Mn	Manganese	0.076	0.200
	26	Fe	Iron	3.109	8.292
	29	Cu	Copper	0.198	0.599
	30	Zn	Zinc	0.128	0.400
	41	Nb	Niobium	0.203	0.899

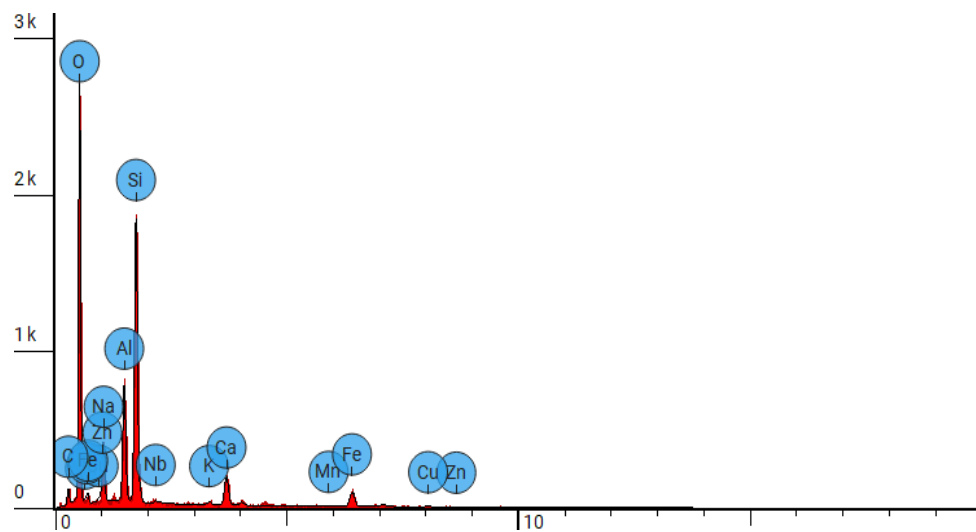
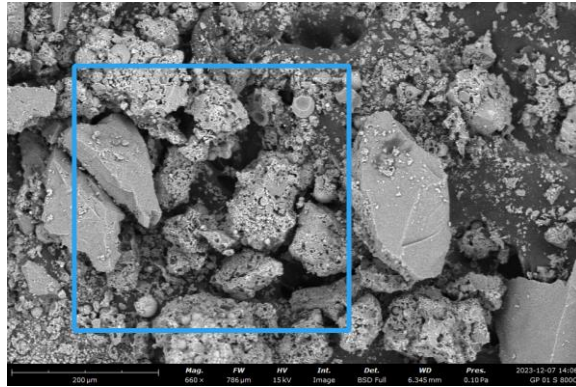
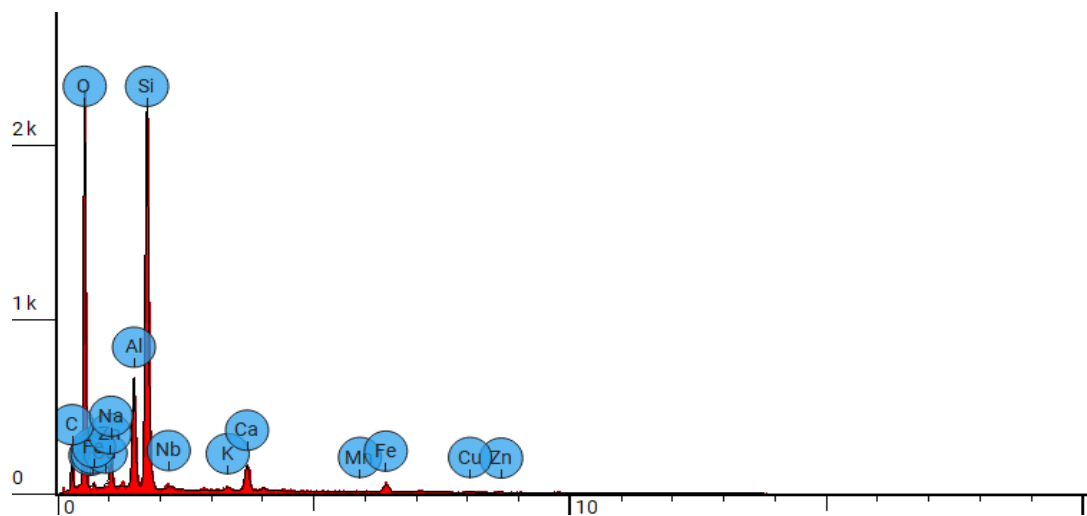


Figure 4.34: SEM/EDS of GP01 samples heat-treated at 400°C



	Element Number	Element Symbol	Element Name	Atomic Conc.	Weight Conc.
	6	C	Carbon	17.874	10.911
	8	O	Oxygen	52.312	42.543
	9	F	Fluorine	0.207	0.200
	11	Na	Sodium	2.312	2.703
	13	Al	Aluminum	6.353	8.709
	14	Si	Silicon	16.336	23.323
	19	K	Potassium	0.302	0.601
	20	Ca	Calcium	2.211	4.505
	25	Mn	Manganese	0.072	0.200
	26	Fe	Iron	1.481	4.204
	29	Cu	Copper	0.186	0.601
	30	Zn	Zinc	0.120	0.400
	41	Nb	Niobium	0.233	1.101



**Figure 4.35:** SEM/EDS of GP01 samples heat-treated at 800°C

The XRD patterns of the concrete mixes and geopolymer specimens (cured and heat treated) are given in **Figures 4.36 – 4.45**. It is to be noted here that for MD03 owing to its explosive spalling behaviour, test samples could not be collected for the heat-treated variants.

In the cases of the XRD diffractograms obtained from the heated samples derived from MD01, it can be clearly seen that the patterns remained essentially very similar to the corresponding ones for the cured samples, apart from some minor features relating to peaks appearing towards the left-hand side of the major peak (below ca.  $2\theta$  value of 25). It can be inferred here that for the three specimens (i.e., cured, and heat-treated ones at 400°C and 800°C), the conspicuous peaks were thought to arise from the fine aggregate component of the mixes (see for example the XRD pattern of fine aggregate: **Figure 4.7**). Furthermore, it can be assumed here that the cement present in these mixes is very likely to lose its crystalline domains upon hydration reactions, whereas the diffraction patterns belonging to the coarse aggregate seem to diminish their intensities beyond threshold levels. Moreover, it is relevant to note that the main phases recognized in the OPC- based samples are the C–S–H gel, CH and calcium carbonate. Furthermore, the XRD-patterns also showed that the presence of CH was affected after the samples were heat treated, where the C–S–H disappeared. This is assumed to be mainly due to the transformation of a new structure to crystalline anhydrous calcium silicate phases i.e., calcite (C) and anorthite (An), as heat treatment can be assumed to occur almost exclusively around the hydration shells of the calcium centres of the cementitious paste (Rashad and Zeedan, 2012, Morsy et al., 2012, Hussin et al., 2015). The observations and inferences can also be extended to the XRD-patterns of samples obtained from the MD02. The XRD pattern obtained from MD03 (cured only) seemed to be crowded and overlapped, thus overall features were ill-resolved.

As expected, the XRD patterns from GP01, cured as well as the heat-treated, appeared to be very similar, as the heat treatment specimens at these temperatures apparently do not have any discernible effects on the structural features of the relatively strong three-dimensional tecto-aluminosilicate network present within them (Goni et al., 2003, Mehta and Siddique, 2017). However, dehydration reactions from hydrated centres in these materials in varying degrees during the heat-treatments cannot be completely ruled out.

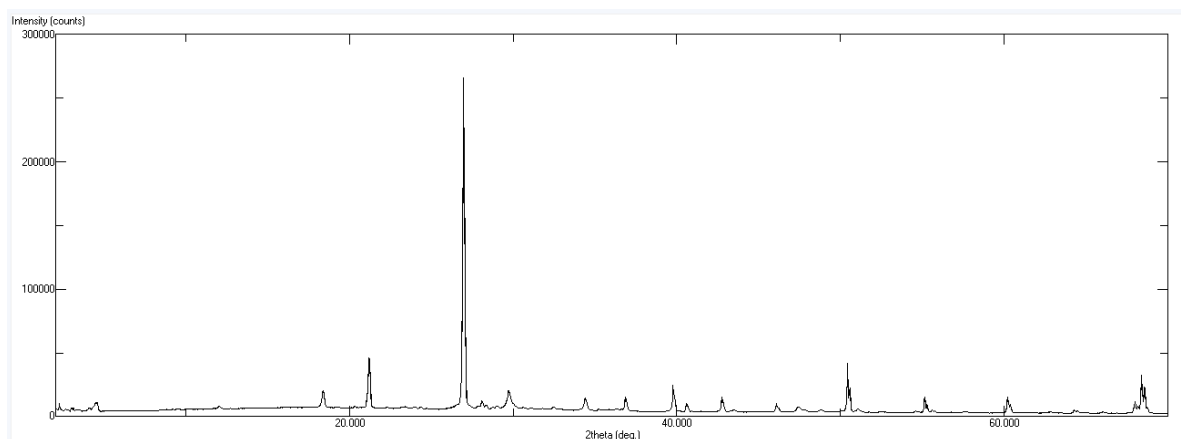


**Figure 4.36:** XRD pattern of MD01 cured

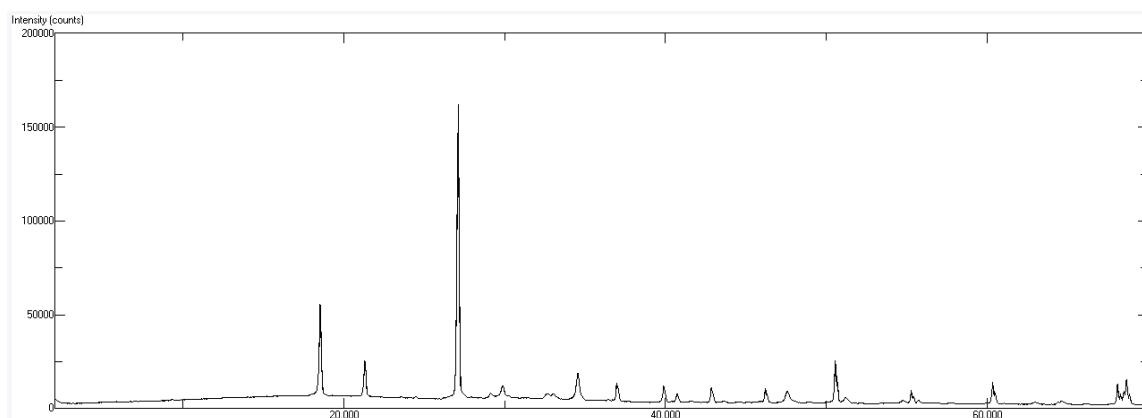


**Figure 4.37:** XRD pattern of MD01 heat-treated at 400°C

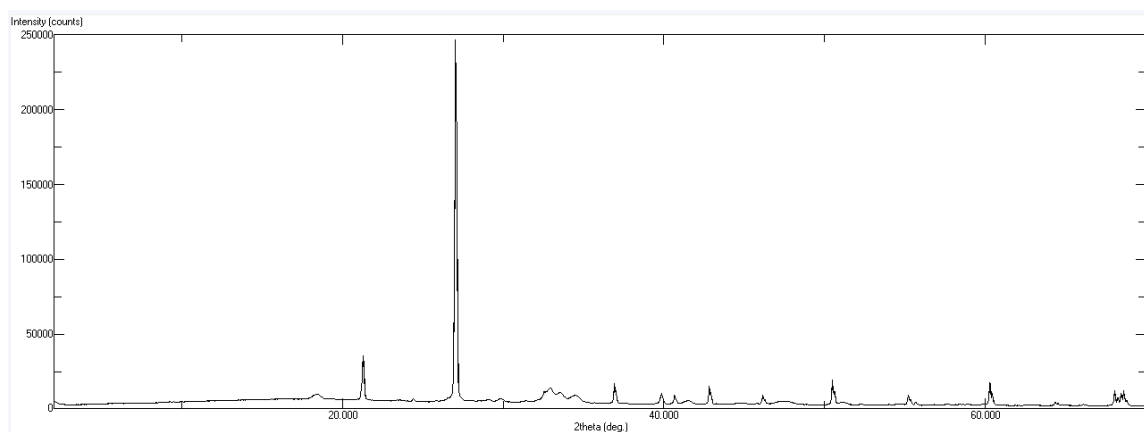


**Figure 4.38:** XRD pattern of MD01 heat-treated at 800°C

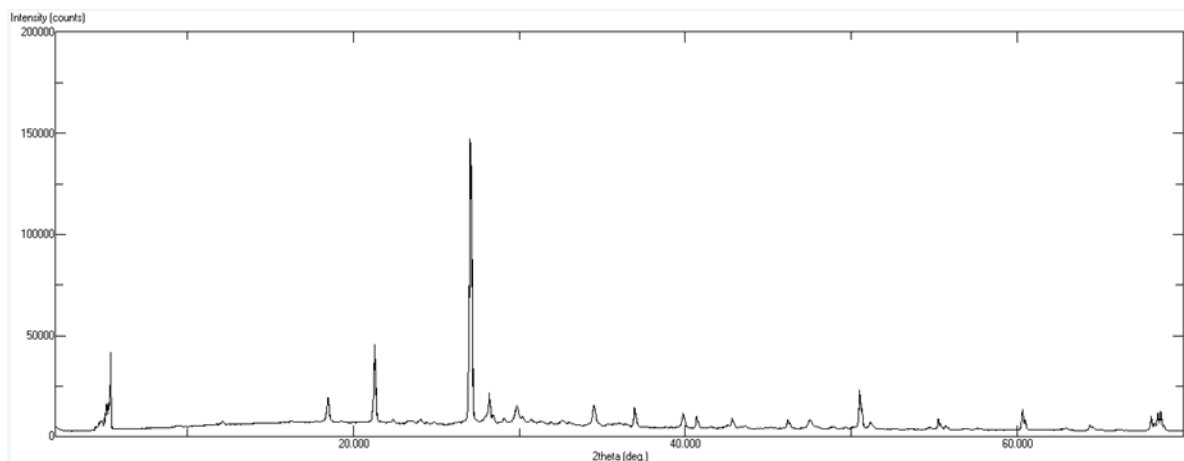


**Figure 4.39:** XRD pattern of MD02 cured

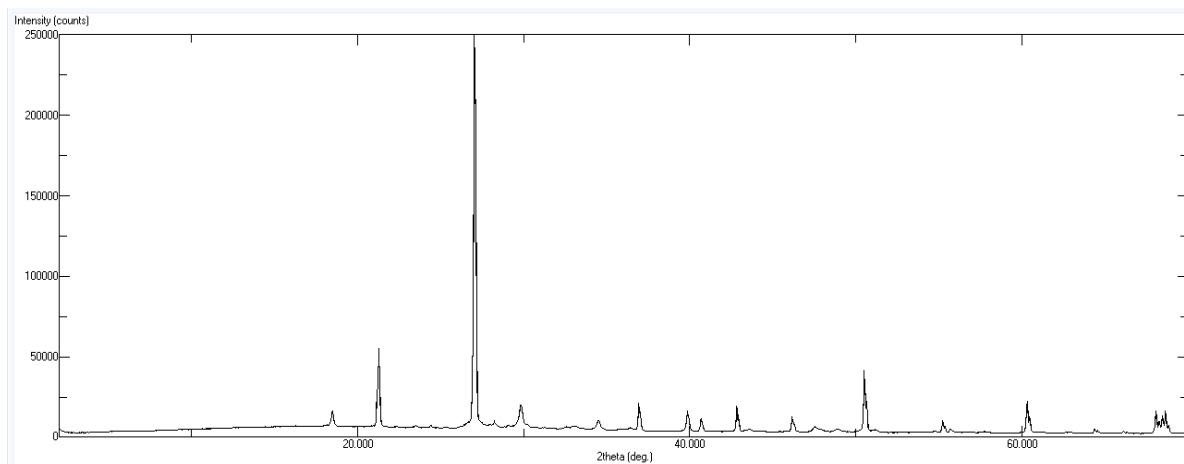


**Figure 4.40:** XRD pattern of MD02 heat-treated at 400°C

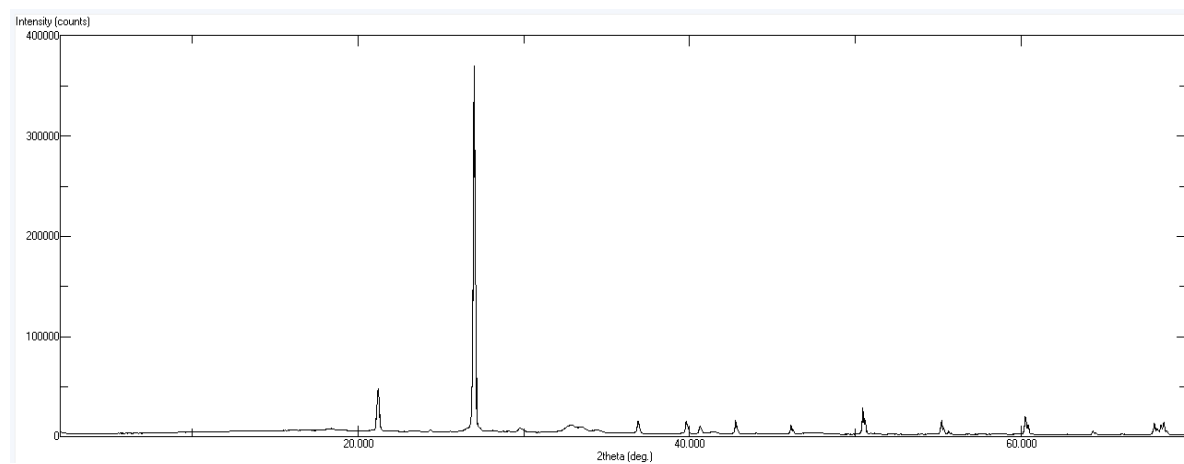


**Figure 4.41:** XRD pattern of MD02 heat-treated at 800°C

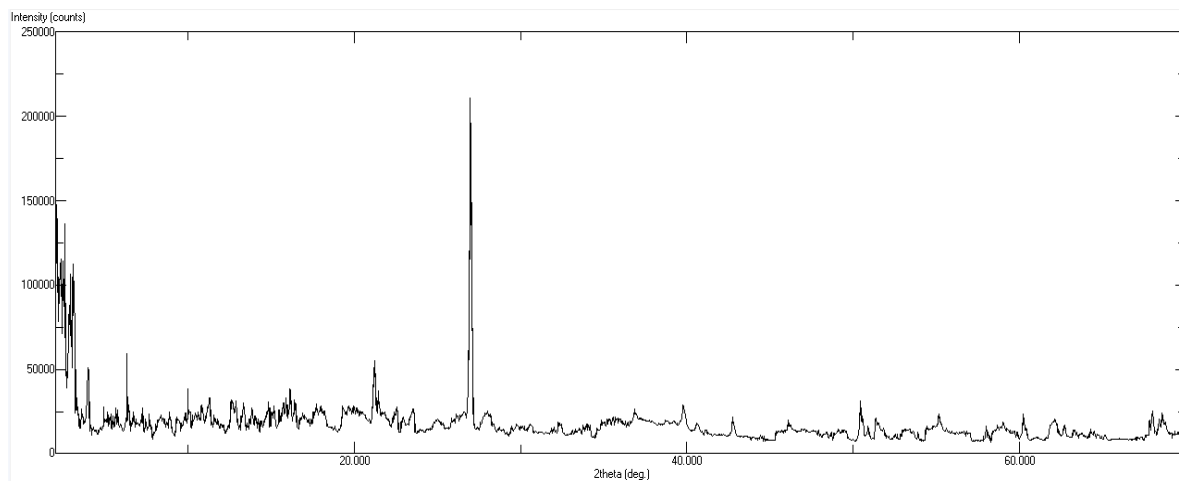


**Figure 4.42:** XRD pattern of GP01 cured

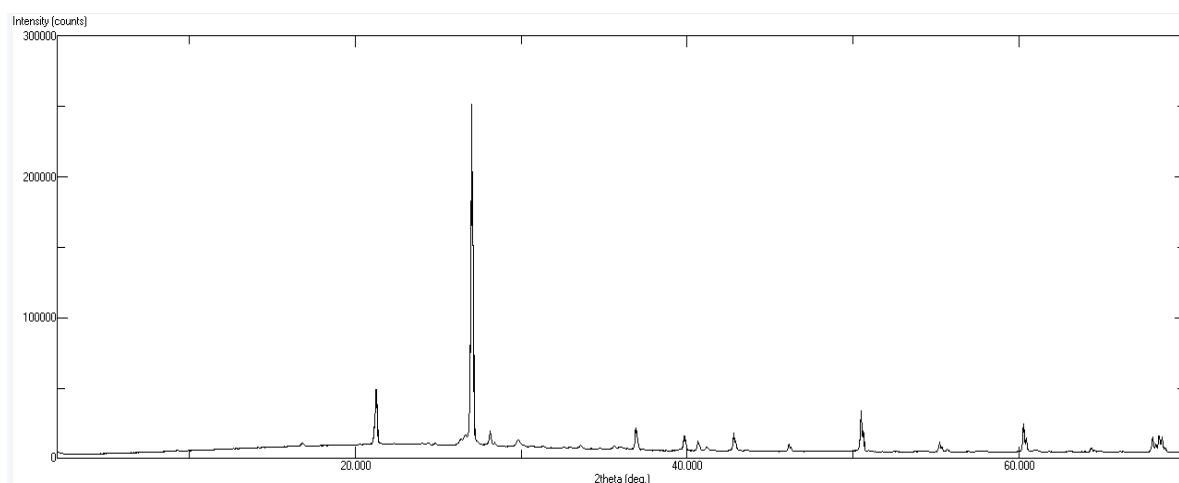


**Figure 4.43:** XRD pattern of GP01 heat-treated at 400°C

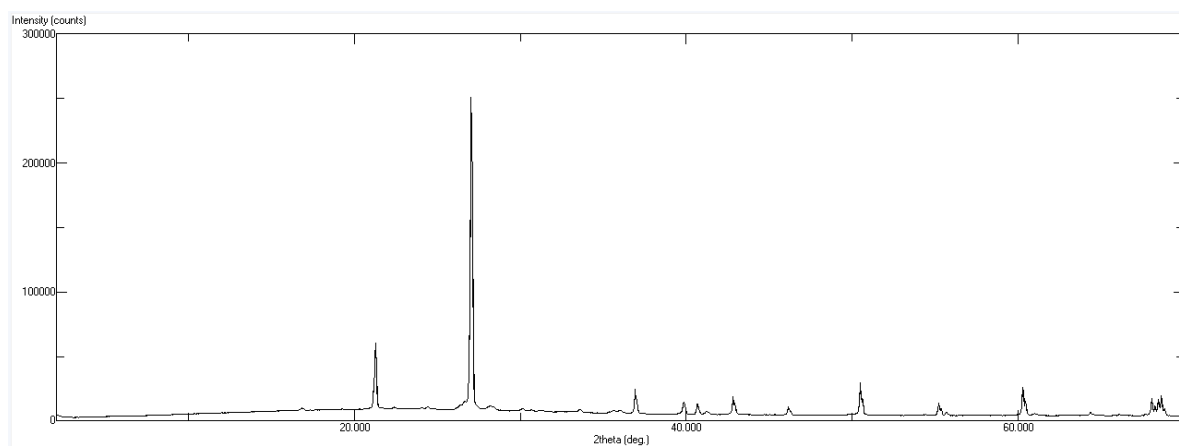


**Figure 4.44:** XRD pattern of GP01 heat-treated at 800°C

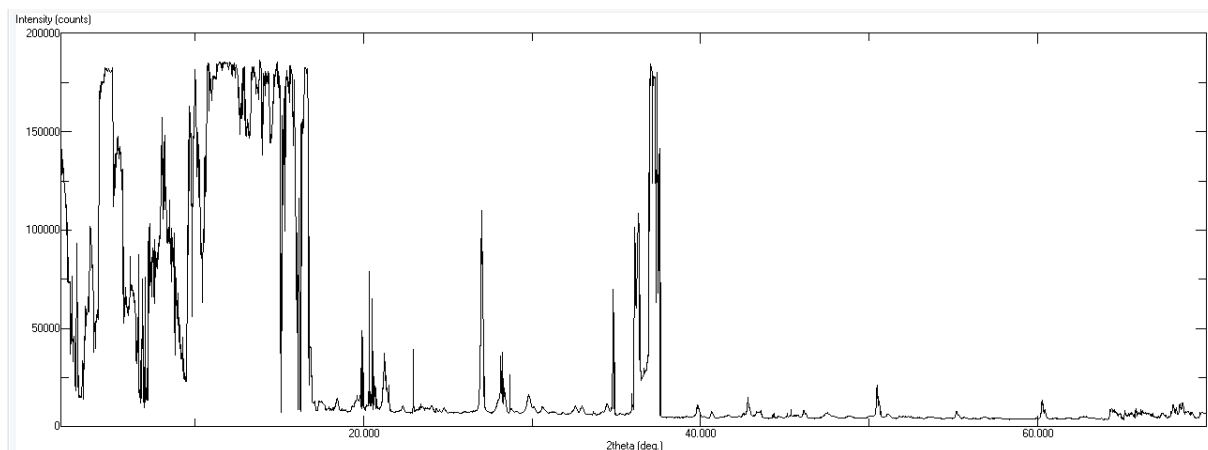


**Figure 4.45:** XRD pattern of MD03 cured

It is relevant to note here that the empirical data obtained through XRD, and SEM/EDS of the cured/spalled materials is challenging to interpret given the heterogeneity within the matrices of different materials, and that the powdered samples obtained from formed cubes from such materials should not be considered as representative.

In the following section the solid-state spectra ( $^{27}\text{Al}$  and  $^{29}\text{Si}$ ) of the powdered samples obtained from the cubical specimens (both cured and heat-treated temperatures of 400°C and 800°C) are given (except that of heat-treated MD 03). Generally, it can be noticed in several of these cases, the signals were rather weak and/or more diffuse in nature than those obtained for the raw materials (i.e., for OPC, FA and fine aggregate). This could be primarily owing to the relatively lower concentrations of species with the active nuclei in question. It is to be noted here that  $^{27}\text{Al}$  and  $^{29}\text{Si}$  of coarse aggregate and FA could not be recorded due to the substantial paramagnetic nature of them.

**Table 4.4** depicts the essential NMR data of the cured samples of concrete and geopolymer before and after exposure to 400°C and 800°C. For comparative purpose the corresponding data of the raw materials (i.e., OPC and fine aggregate) are also given.



**Table 4.4:** Essential NMR data of the cured samples of concrete and geopolymer before and after exposure to 400°C and 800°C

Sl. No.	Sample	$^{27}\text{Al}$ ( $\delta$ )	$^{29}\text{Si}$ ( $\delta$ )	Remarks (as compared to OPC and fine aggregate)
1	OPC	Singlet 12.7 (s)	Symmetric multiple around -71.9 (s)	The symmetric multiple around -71.9 in $^{29}\text{Si}$ can be thought to arise from coupling to vicinal NMR active nucleus, whereas the singlet at 12.7 in the $^{27}\text{Al}$ indicates a preferred chemical environment for the Al centres
2	Fine aggregate	Peaklet centred 2.5 (s) with minor peaks approximately equidistant from the major peak	Singlet at -108.2 (s); broader peak centred--92.2 (s)	No definite conclusions can be drawn from either spectrum, except there are more than one chemical environments of the Al and Si centres (with different predominance) in the fine aggregate
3	MD01 cured	Broad multiplet almost centred around 9.1 (ms)	Very broad signal centred around -84.9 (w)	The chemical environment of Al centres seemed to be shifted and there are indications of cropping up of extra environments; Si centres appeared to be shifted with merging of the different chemical environments to closely clubbed ones (i.e., around -84. 9)
4	MD01 400°C	Basically, two peaks around 3.6 (ms)	Very broad signal centred around -71.3 (w)	Shifting as well as clubbing of various chemical environments into two for the Al centres; Si centres appeared to be shifted with merging of the different chemical environments to closely clubbed ones (i.e., around -71.3)

5	MD01 800°C	Basically, two peaks around 11.7 (ms to w)	A singlet (s) -71.3 (s)	Shifting of various chemical environment into two for the Al centres; Si centres appeared to be shifted with merging of the different chemical environments to a singlet (i.e., around -71.3)
6	MD02 cured	Multiple with no obvious pattern centred around 9.1 (ms)	Very broad signal centred around -80.0 (w)	Shifting as well as clubbing of various chemical environments into two for the Al centres; Si centres appeared to be shifted with merging of the different chemical environments to closely clubbed ones (i.e. around -80.0)
7	MD02 400°C	Two main peaks (ms) centred around 56.8	Very broad (w) peak around -71.0 (w)	Shifting as well as clubbing of various chemical environments into two for the Al centres; Si centres appeared to be shifted with merging of the different chemical environments to closely clubbed ones (i.e. around -71.0)
8	MD02 800°C	Two main peaks (ms) centred around 59.9	A singlet (s) at -70.7 (s)	Shifting as well as clubbing of various chemical environments into two for the Al centres; Si centres appeared to be shifted with merging of the different chemical environments to a singlet (i.e. around -71.7)
9	MD03 cured	Multiple centred around 55.3 (ms)	Very broad peak around -71.0 (w)	Shifting of various chemical environments into two for the Al centres; Si centres appeared to be shifted with merging of the different chemical environments to closely clubbed ones (i.e. around -71.0)

10	GP01 cured	Multiple centred around 57.4 (ms)	Very broad peak centred around -91.7 (w)	For the Al centres the origin of peak around 57.4 ppm cannot be established as the corresponding spectrum of FA could not be run. However, the peak at around -91 can be thought to arise from the fine aggregate component
11	GP01 400°C	Multiple centred around 57.9 (ms)	Very broad peak centred around - 91.1 (w)	The chemical environments of Si and Al centres are more or less retained as compared to the GP01
12	GP01 800°C	Multiple centred around 57.9 (ms)	Very broad peak centred around - 91.1 (w)	The chemical environments of Si and Al centres are more or less retained as compared to the GP01

---

*s = strong; m = medium; ms = medium strong; w = weak*

As expected, the interpretation of the solid-state NMR spectra is not straightforward owing to the following reasons: 1. limitations arising from the relatively lower natural abundance and/or sensitivity of the nuclei of interest ( $^{27}\text{Al}$ , or  $^{29}\text{Si}$ , as the case may); 2. the inherent dipolar broadening effects in recording the NMR spectra in the solid-state even when the sample tubes are spun at relatively high speeds (*ca.* 10,000 Hz); 3. presence of solid paramagnetic impurities in some of the components of the mixes (i.e. FA and coarse aggregate). However, the issues emanating the above were mitigated to a manageable level through running the instrument in CP/MAS (cross polarization/magic angle spinning) mode, so that the spectra acquired in the present study were useful, albeit only limited inferences, as given below, could be deduced:

1. For the FA-based GP samples, the signals from the cured and heat-treated specimens were compared with those of the raw materials (i.e., fine aggregate only), whereas for those made from OPC-based mixes, the cured and heat-treated specimens (except for MD03, as only data for the cured version is available) is compared with that of OPC and fine aggregate.

2. For the GP01, and the heat-treated versions, the Al centres exhibited resonances around 57 ppm, which is only likely to emanate from the fly ash and/or coarse components. Generally, the Si signals of the OPC-based specimens were centred around -90 ppm and the signals were very broad and weak compared to that from the fine aggregate. Here again, there could be interferences from resonance signals from fly ash and/or coarse aggregate.
3. For the OPC-based samples there were noticeable shifts as well as differences in the profiles of the signals from the Al centres in all cases as compared to the raw materials (i.e., OPC and fine aggregates)- these attributes can have influences from resonance of Al centres from the coarse aggregate as well. As for the signals from the Si centres, except for MD01 800°C and MD02 800°C, where sharp signals can be observed, in all other cases very broad and generally weak signals in the region of -70 to -85 ppm were obtained. These were roughly in the region where the signals from Si centres in the raw materials (OPC and fine aggregates) occurred. However, the general profiles of the signals in both cases were different, and any interference from the resonance peaks from the coarse aggregate cannot be ruled out here.

In summary, given that the spectra of the main cementitious component of the mixes of geopolymer (i.e., FA) could not be recorded, no definite inferences relating to significant changes in the chemical environments of Al (as compared to those emanating from the fine aggregate) can be made. However, it can be safely assumed that the changes in the chemical environments of Si, if at all, is minor. Since for the GP samples, Al and Si centres are ‘locked’ into their relatively robust chain structures, changes to these centres, even after heat treatments are less likely. Therefore, the solid-state spectral analyses validate the above assumptions. In addition, heat treatments primarily affect the hydrated Ca centres; however, such effects are not directly observable here as  $^{43}\text{Ca}$  spectra were not recorded in the present study.

For the OPC- based concrete samples, the resonance signals from both Al and Si are noticeably different (especially those corresponding to Al) in terms of the chemical shifts, profiles and intensities. It was also interesting to note that the sharp singlets (ms) for MD01 800°C and MD 02 800°C. Even if these signals are thought to emanate from the fine aggregate component in these mixes, their chemical shift values are noticeably different (i.e.,

-108.2 ppm for fine aggregate, but around -70 ppm for the casted samples) (Ghosh et al., 2022, Walkley and Provis, 2019, Gupta et al., 2020). Generally, for the OPC-based materials, during casting, curing and heating stages solid-state chemical transformations amongst the various active species are quite possible, and therefore these are manifested in the corresponding spectrum. However, the exact mechanistic pathways and or the resultant structures owing such chemistries are not easy to follow, and hence no definite inferences could be drawn using the limited information from the NMR spectra in hand.

#### 4.5. Physical appearance

A comparison between the physical appearances of the mixes of MD01 a-h, MD02 a-h, MD03 a-h and GP01 a-h at room temperature (after curing) and after exposure to 400°C and 800°C are shown in **Figures 4.46 – 4.49**, respectively. In all specimens, no apparent differences could be visually observed amongst the cured specimens (specimens at room temperature) in terms of smoothness or surface finishes. However, due to the length of the longer PP fibres (48 mm), difficulties arose during the removal of these specimens from the mould, with fibres randomly protruding from the surface and in some instances, causing the edges to chip away. In regard to the colour of the specimens, all cured samples, including the GP01 specimens were of a light grey colour (the colour of conventional concretes), with a very slight change in colour being observed in the surface of the cubes having polyester fibres incorporated in them.

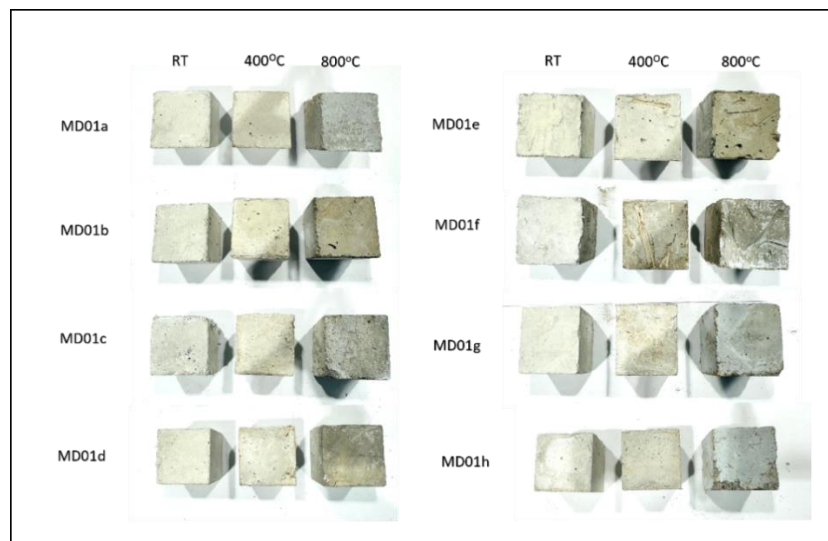


**Figure 4.46:** Physical appearances of MD01 a-h specimens at room temperature, and after exposure to 400°C and 800°C

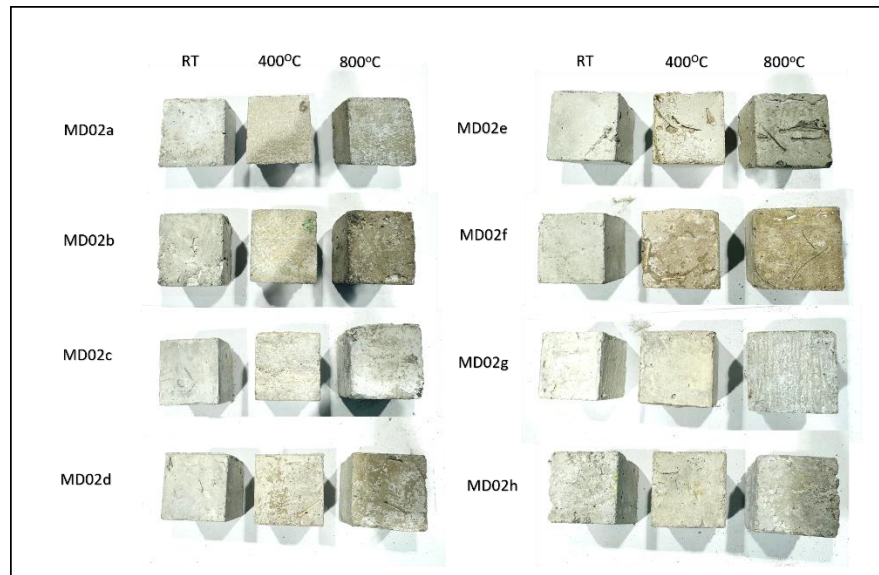


**Figure 4.47:** Physical appearances of MD02 a-h specimens at room temperature, and after exposure to 400°C and 800°C



**Figure 4.48:** Physical appearances of MD03 a-h specimens at room temperature, and after exposure to 400°C and 800°C

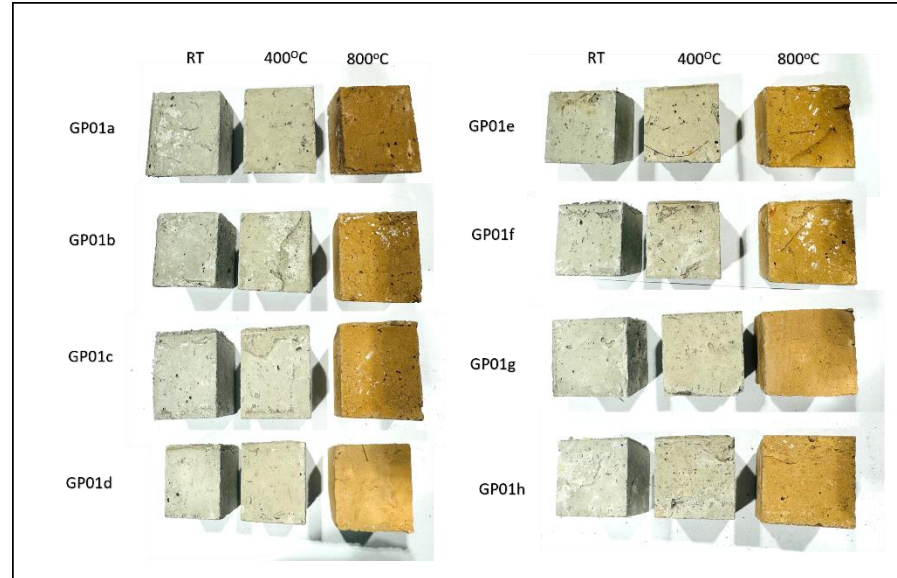


**Figure 4.49:** Physical appearances of GP01 a-h specimens at room temperature, and after exposure to 400°C and 800°C

After exposure to an elevated temperature of 400°C, no apparent changes in colour were witness in the specimens, i.e., MD01, MD02, MD03 and GP01. However, in samples which had 48 mm PP fibres there were empty grooves seen on the surface of the cubes where the fibres had melted under high temperatures.

When comparing the appearance of the OPC- based concrete cubes after exposure to 800°C, some cubes did not display any visual changes; however, others showed a very slight change in colour, i.e., from light grey to dark grey. In contrast, for all the OPC-based specimens, the appearance of a white powdery matter was evident, and in some specimens, flaking away of the top surface was also observed. Some specimens also displayed slight hairline cracks on the surface, while others displayed crack-networks throughout the top face. In some cases, breaking/ chipping away of the edges was also observed. In addition to the flaky surface, void spaces (grooves), caused through the melting of the 48 mm PP fibres, was also quite evident, especially in those having a high fibre content of 1.5%. Such features were not very evident in the cases of test specimens incorporating 12 mm PP fibres. Similarly, such surface modifications were absent in those samples containing cotton and polyester fibres. The observed difference in the case of the 48 mm PP fibres, as against the others, can be attributed to the substantial size difference between 48 mm PP fibres as compared to the other fibrous materials. The melting of the fibres, in the case of the synthetic

variants (i.e., PP and polyester) and dehydration/ degradation/ charring processes in the case of cotton, can be assumed to result in the release of pore pressure within the concrete matrices, thus leading to a reduced degree of spalling. **Table 4.5** gives information of the visual observations made for each of the specimens after exposure to 800°C. As mentioned before, MD03 control samples underwent explosive spalling, hence no images could be obtained from them.

**Figures 4.50** shows a comparison between the MD01, MD02 and GP01 specimens before and after exposure to heat. The most noticeable change was witnessed in the FA-based GP specimens after being exposed to 800°C, where there was a clear difference in colour between the OPC- and FA-based concrete specimens. The colour of the GP01 specimens was observed to change to a reddish-brown colour. This was evident in all the GP specimens. This could be attributed to the high levels of iron oxide in the FA and generally, transition-metal oxides, especially with altered oxidation states, which can result in the formation of coloured compounds. In addition to this, slight formation of white powder matter was clearly witnessed on the surface of the GP specimens. Similar results have been reported by previous researchers (Sarker et al., 2014, Zhang et al., 2014, Ali et al., 2017, Wattimena et al., 2017, Kannangara, 2018). Apart from the prominent change in colour, some specimens displayed cracking on the surface and, similar to the OPC-based specimens, there was definite voids (grooves) formed through the melting of the 48 mm PP fibres.

**Table 4.5:** Visual observations of the physical appearance of cubical specimens after exposure to 800°C

Sample	Surface and spalling observations	Colour
MD01 Control	Prominent crack network on surface	Dark grey
MD01 a	No visible cracking on surface with mild corner spalling	Dark grey
MD01 b	Mild hairline cracking on surface with mild corner spalling	Dark grey
MD01 c	Mild hairline cracking on surface with mild corner spalling	Dark grey
MD01 d	Mild hairline cracking, with empty grooves visible on surface	Dark grey
MD01 e	Mild hairline cracking, with severe corner spalling and visible grooves on surface	Dark grey



MD01 f	Severe corner spalling and visible grooves on surface	Dark grey
MD01 g	Crack network on surface with moderate corner spalling	Dark grey
MD01 h	Prominent crack network on surface with severe corner spalling	Dark grey
MD02 Control	No visible cracking on surface	Dark grey
MD02 a	No visible cracking on surface	Dark grey
MD02 b	No visible cracking but minor corner spalling	Dark grey
MD02 c	No visible cracking on surface, but mild corner spalling	Dark grey
MD02 d	No visible cracking, but mild corner spalling with visible grooves on surface	Dark grey
MD02 e	No visible cracking but severe corner spalling and visible grooves on surface	Dark grey
MD02 f	Slight hairline cracking, with moderate corner spalling and visible grooves on surface	Dark grey
MD02 g	Slight hairline cracking on surface	Dark grey
MD02 h	Prominent crack network on surface with severe corner spalling	Dark grey
MD03 Control	Explosive spalling	-
MD03 a	Prominent crack network on surface with moderate corner spalling	Dark grey
MD03 b	Prominent crack network on surface with moderate corner spalling	Dark grey
MD03 c	Crack network on surface	Dark grey
MD03 d	Crack network on surface with visible grooves on surface	Dark grey
MD03 e	No visible cracking on surface, but mild corner spalling and visible grooves on surface	Dark grey
MD03 f	Crack network on surface with visible grooves on surface	Dark grey
MD03 g	Prominent crack network on surface with severe corner spalling	Dark grey
MD03 h	Prominent crack network on surface with severe corner spalling	Dark grey
GP01 Control	No visible cracking on surface	Reddish brown
GP01 a	Crack network on surface	Reddish brown
GP01 b	Crack network on surface	Reddish brown

GP01 c	Crack network on surface with mild corner spalling	Reddish brown
GP01 d	Mild hairline cracking on surface with visible grooves on surface	Reddish brown
GP01 e	Mild hairline cracking on surface with visible grooves on surface and mild corner spalling	Reddish brown
GP01 f	Mild crack network with visible grooves on surface	Reddish brown
GP01 g	No visible cracking on surface	Reddish brown
GP01 h	Mild crack network on surface	Reddish brown

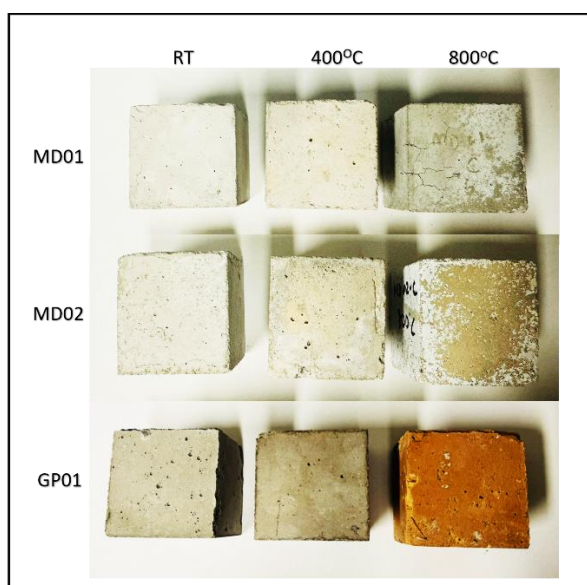


**Figure 4.50:** Comparison of the physical appearance of MD01, MD02 and GP01 specimens

#### 4.6. Density studies

Concrete density can be considered an important factor, especially when assessing the explosive behaviour of concretes during fire-based scenarios. Studies show that the denser the microstructure is, or in other words, as the permeability decreases, the more vulnerable concrete is to spall (Amran et al., 2022, Kannangara et al., 2021b). Hence, density measurements can provide a good insight into the spalling behaviour based on the pore structures. Normal weight concrete generally consist of a density within the range of  $2,200 \text{ kg/m}^3 - 2,600 \text{ kg/m}^3$  (Neville, 1995), with the density of HSC and ultra HSC reaching up to  $4,000 \text{ kg/m}^3$ . In the case of FA- based GP concretes, the density ranges fall similarly to the range of OPC- based concrete, however, GP concretes are reported to be comparatively higher (Bakri et al., 2013). The density values were taken from the mass and volume

measurements of the 50 mm concrete cubes (volume =  $1.25 \times 10^{-4} \text{ m}^3$ ). Test results are presented in **Table 4.6**.

**Table 4.6:** Average density measurements for cubical specimens

Sample	MD01		MD02		MD03		GP01	
	Mass (kg)	Density (kg/m <sup>3</sup> )	Mass (kg)	Density (kg/m <sup>3</sup> )	Mass (kg)	Density (kg/m <sup>3</sup> )	Mass (kg)	Density (kg/m <sup>3</sup> )
<b>Control</b>	0.2970	2376	0.3025	2420	0.3254	2603	0.3075	2460
<b>a</b>	0.2955	2364	0.3006	2405	0.3233	2586	0.3050	2440
<b>b</b>	0.2933	2346	0.2994	2395	0.3216	2573	0.3048	2438
<b>c</b>	0.2913	2330	0.2963	2370	0.3186	2549	0.3003	2402
<b>d</b>	0.2961	2369	0.3014	2411	0.3243	2594	0.3039	2431
<b>e</b>	0.2938	2350	0.3001	2401	0.3231	2585	0.3029	2423
<b>f</b>	0.2926	2341	0.2974	2379	0.3200	2560	0.2985	2388
<b>g</b>	0.2850	2280	0.2930	2344	0.3125	2500	0.2966	2373
<b>h</b>	0.2910	2328	0.2966	2373	0.3158	2526	0.2984	2387

As expected, the MD03 mixes had the highest recorded values of density, which could explain the relatively high explosive property of these types of concretes based on the thermal stress theory (see in **Section 2.4**) (Ali, 2002). In contrast, the least dense specimens were the MD01 specimens. The higher w/c ratio of 0.6% could explain these results, as more of the concrete microstructure would have consisted of water molecules during casting and, upon hardening, some of the water molecules would have evaporated, thus providing a comparatively higher porous internal structure. Results obtained from the porosity measurements in **Section 4.7** seconded this statement. In addition, while the w/c ratio of the MD02 and the GP01 specimens were the same, the densities of the GP01 samples resulted in higher readings compared to the MD02 specimens. This could be due to the higher alkali contents in the GP concretes which produces better reactivity with the FA, hence resulting in denser concretes (Bakri et al., 2013). This also falls in line with the results obtained in **Section 4.3**, where the workability and the cohesiveness of the GP concretes were higher

compared to the MD02 specimens (even though they were made using the same w/c ratio), which could have resulted in better compaction, with reduced air voids, when casted into cubical specimens, thus increasing the density. **Figure 4.51** presents a scatter graph of the density trends for each of the mixes.

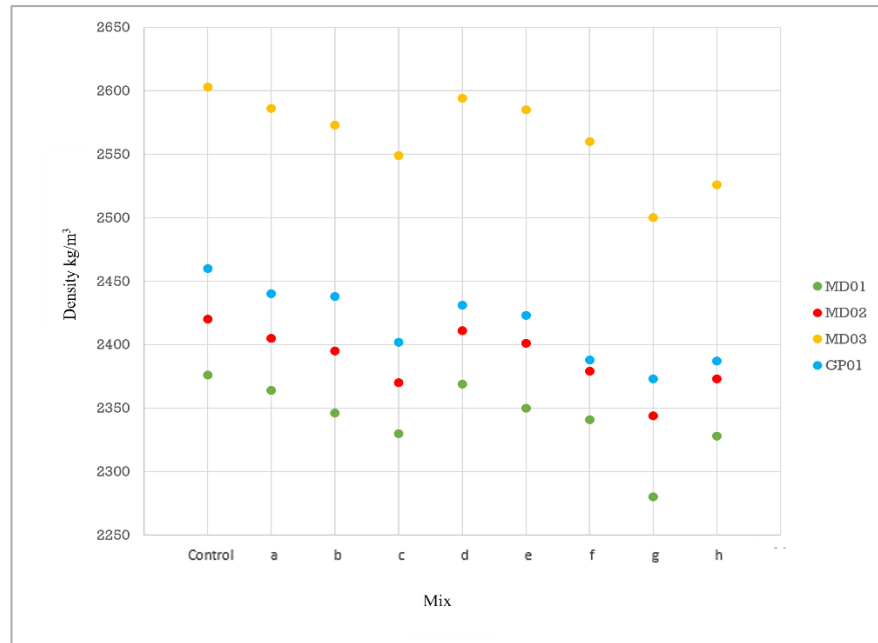


**Figure 4.51:** Density patterns for MD01, MD02, MD03 and GP01 mixes a – h

When considering the addition of the fibrous materials, it was evident that as the PP fibre content increased from 0.5%–1.5%, in both the 12 mm and 48 mm, the density readings reduced. Moreover, when considering all tested specimens, the ones having 1% cotton fibres incorporated in the mix, resulted in the highest drops in density readings. Polyester fibre added specimens (at 1%), on the other hand, resulted in being denser compared to the cotton fibre added specimens, but less dense compared to those with 1% PP fibres (both 12 mm and 48 mm). These trends were common for all mixes, including the GP01 specimens.

The above features could be due to the fibres, that are of lesser weight, taking up the volume of the concrete paste and aggregate materials, which are relatively heavier, within in the concrete mix, thus producing lighter cubes (Richardson, 2006). Moreover, it has been reported that these types of fibres, as a result of the surface treatment they receive during the manufacturing process, can entrain small amounts of air, and when used in concrete mixes, pressure release chambers can arise as a result of the fibres holding small pockets of air

bubbles in their intersections (Gold, 2000). In addition, the comparatively lower workability conditions of the FRC could hinder the compaction of the cubes during casting, thus reducing the overall density of these specimens (Clark, 2006).

#### 4.7. Porosity assessment using rapid chloride penetration test and BET approach

The rapid chloride penetration test (RCPT) was conducted on cylindrical concrete specimens in order to determine the levels of chloride ions passing through the microstructure. Through the course of this test, a quantitative result of the number of charges passing through the specimens in Coulombs (C) were obtained, which can then be correlated to the porosity of the material (using **Table 3.7**). The basic concept here is that the ions are allowed to pass through the specimen *via* the liquid phase in the pores and, based on the level of voids within the concrete, the rate of passing of these ions change, i.e. the more porous the specimen is, the higher the flow rate (Yang and Chiang, 2005, Xu et al., 2021). Hence, if the recorded number is low, the porosity is low, and the specimen is more durable against environmental penetrations. **Table 4.7** shows the charges passing and their relevant classification of porosity for control mixes.

**Table 4.7:** Average charge passed and classification of chloride ion penetration based on (C1202-09)

Mix design	Total charge passed (Coulombs)	Chloride ion penetrability
MD01	5156	High
MD02	4089	High
MD03	1830	Low
GP01	3582	Moderate

**Figure 4.52** provides a graphical representation of the test results, and it is clearly evident here that MD01 control specimens consisted of the highest levels in porosity which was expected due to its high water to cement ratio of 0.6. In contrast, MD03 specimens resulted in much lower porosity levels, thus proving a more durable concrete with a higher bearing capacity. However, it also shows evidence that supports the pore pressure theory, which states that a higher probability of spalling can occur in concretes having a more

compact internal structure which obstruct the release of vapour pressure as the temperature increases (Amran et al., 2022).

Moreover, these results fall in line with the density results obtained in **Section 4.6** where the least dense specimens were from the MD01 crucible specimens. This provides evidence that the size of the specimen (cubical or cylindrical) had not greatly affected the internal structure of the concrete mix.

When considering the GP specimens, the charges recorded resulted in a porosity level of ‘moderate’. This could be directly linked to the chemical nature of the alkaline solution and the pozzolanic properties of the FA material which facilitate a better bond among the constituent materials of concrete. In addition, during the heat curing, the polymerisation process is further enhanced which could result in a reduced porosity compared to MD02 which has a similar liquid: binder ratio (Razak et al., 2020).

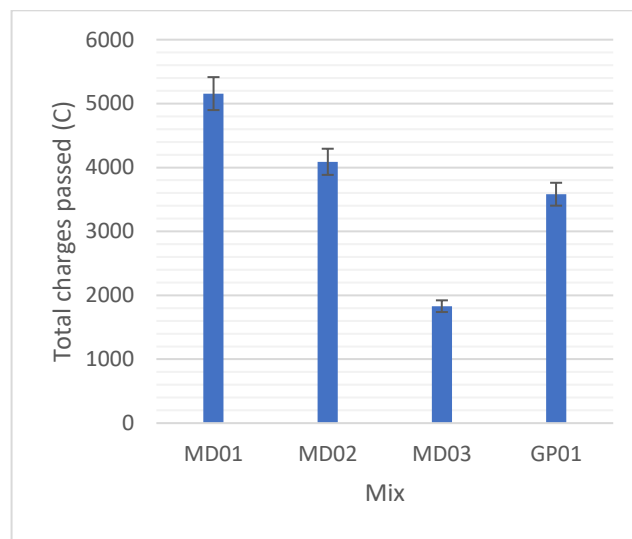


**Figure 4.52:** Graphical representation of the chloride ion penetration test for control mixes

The BET theory was employed to correlate the results obtained with the RCPT results. It must be noted here that while the BET theory was applied to the small chunks of concrete, while full cylindrical specimens were used for the RCPT. Tabulated results obtained from the BET approach is presented in **Tables 4.8 – 4.10**.

**Table 4.8:** Summary of surface area results obtained by the nitrogen adsorption method (output data from the machine)

Surface Area (m <sup>2</sup> /g)	MD01	MD02	MD03	GP01
BET Surface Area:	8.14410	7.2374	5.8683	8.7475
t-Plot Micropore Area:	1.08740	0.4036	5.9084	0.8649
t-Plot External Surface Area:	7.05670	6.8338	5.7020	7.8826
BJH Adsorption cumulative surface area of pores between 17.000 Å and 3,000.000 Å width	7.10000	7.2710	8.4253	8.2400
BJH Desorption cumulative surface area of pores between 17.000 Å and 3,000.000 Å width	11.1325	11.8410	-	11.3207

**Table 4.9:** Summary of pore volume results obtained by the nitrogen adsorption method (output data from the machine)

Pore Volume (cm <sup>3</sup> /g)	MD01	MD02	MD03	GP01
Single point adsorption total pore volume of pores: less than 206.503 Å width at p/p° = 0.900000000:	0.012790	0.012704	0.009738	0.016109
t-Plot micropore volume:	0.000459	0.000146	-0.000073	0.000341
BJH Adsorption cumulative volume of pores between 17.000 Å and 3,000.000 Å width:	0.035835	0.027269	0.026844	0.030620
BJH Desorption cumulative volume of pores between 17.000 Å and 3,000.000 Å width:	0.040725	0.030958	0.030803	0.032808

**Table 4.10:** Summary of pore size results obtained by the nitrogen adsorption method (output data from the machine)

Pore Size	MD01	MD02	MD03	GP01
Adsorption average pore diameter (4V/A by BET):	62.8197 Å	70.2140 Å	66.3748 Å	73.6637 Å
BJH Adsorption average pore width (4V/A):	201.880 Å	150.007 Å	188.306 Å	148.637 Å
BJH Desorption average pore width (4V/A):	146.330 Å	104.580 Å	146.241 Å	115.923 Å

It is evident from the results that the MD03 specimens had the lowest surface area of pores and pore volume, with a lower pore volume for the smallest pores. This falls in line with the results received from the RCPT. In addition to this, the GP01 samples showed a much smaller pore size compared to the other set of samples. However, contradictory to the

RCPT, the GP01 samples resulted in higher overall pore volume compared to the MD02 samples, similar to that of the MD01 samples. It must be taken into consideration that concrete is not a homogenous material and, while specimens may display agreeable results, variations in results can occur from specimen to specimen within the same mix design, or even from one point to another of the same specimen. Moreover, it must be noted that generally, desorption data is more appropriate for pore size distributions, however, the disadvantage is that a false peak around 4nm can occur from the tensile strength effect of the material (Groen et al., 2003, Negahban et al., 2021). **Figure 4.53** graphically represents the pore size distribution of each mix.

The effect of w/c ratio on the surface area of the OPC- based specimens was also evaluated, and it was found that as the ratio increased from 0.26 to 0.6, the surface area increased from 5.9 m<sup>2</sup>/g to 8.1 m<sup>2</sup>/g. In addition to this, the specific surface area of the GP01 specimens were reported to being higher than that of the OPC- based concrete specimens which could be due to the differences in the hydration-based and geopolymerization-based gel pores between the two materials and their connectivity to the aggregate particles (Negahban et al., 2021, Oh et al., 2010, Alehyen et al., 2017).

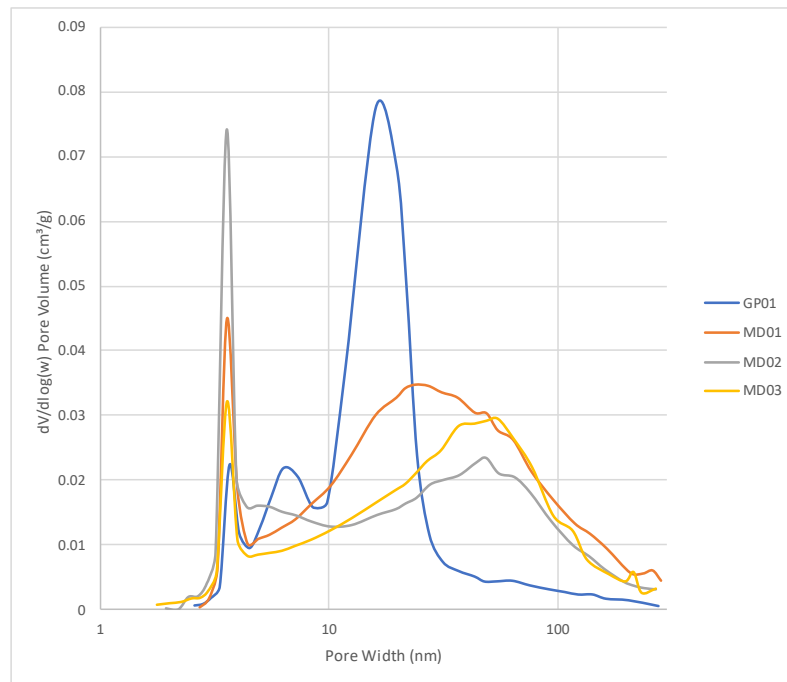


**Figure 4.53:** Pore size distribution of each mix as obtained from the BET approach



It must be noted here that through the set of data obtained from the RCPT and the BET approach extended correlations or trends seem fragmented between the cured samples and spalled samples. As it stands, the spalling behaviour in any of the cases could not be aligned to the test data. Hence, providing pathways for further investigation.

#### **4.8. Compressive and residual performance**

Strength in concrete, mainly the compressive strength, is one of the most important factors which need to be determined when discussing the overall performance of concrete structures. While concrete is comparatively brittle and does not pose good tensile strength or ductile properties, it is a material which possess extremely high compressive strengths, hence the load-bearing capacity is indeed a key parameter to assess. The compressive strength of the different OPC- based and FA- based concrete mixes with and without the incorporation of sacrificial agents at room temperature, and at high temperature levels (400°C and at 800°C) were assessed.

When considering the initial compressive strength readings, as expected, MD03 specimens displayed the highest strength reading of approximately 182.8 MPa. Despite both MD02 and GP01 specimens consisting of the same liquid: binder ratio, the strength of the GP01 specimens were seen to be ever so slightly lower as compared to MD02, with the GP01 specimens displaying a strength of approximately 91.8 MPa and the MD02 specimens displaying an average strength of approximately 93.1 MPa. It must be noted here that while the strength readings of the OPC-based concretes are recorded at 28 days, the strength of the FA- based GP specimens are obtained 24 hours after casting. Therefore, categorising GP concretes as ‘high early strength concrete’ or ‘high early strength cement (HE)’, which is highly valuable and sought out within the scope of quick construction. The reason for this high early strength can be attributed with the alkali-mediated initiation processes, which can lead to insoluble silicate structures and subsequently, an increase in the rate of reaction of geopolymerization. This reaction is a multistage phenomenon, consisting of: dissolution; speciation equilibrium; gelation; reorganization; and polymerization/hardening. During the dissolution process the alkaline solution starts breaking down the FA particles which results in the particles being distributed both inside and outside of the shell of the FA particle making it more reactive. These reactive products can fill in the interior microstructure, thus, forming a denser matrix more quickly (Duxson et al., 2007c, Law et al., 2015). **Table 4.11**

gives tabulate readings of the average initial compressive strength readings of the MD01, MD02, MD03 and GP01 specimens.

**Table 4.11:** Tabulated readings of the average initial compressive of specimens

Mix ID	Average compressive strength (MPa)			
	MD01	MD02	MD03	GP01
<b>Control</b>	63.87	93.18	182.80	91.83
<b>a</b>	61.06	87.28	170.45	79.49
<b>b</b>	59.82	80.72	166.09	77.44
<b>c</b>	59.60	79.97	161.11	77.13
<b>d</b>	58.66	85.12	174.08	77.15
<b>e</b>	57.98	79.13	169.25	73.91
<b>f</b>	56.43	75.89	162.31	73.51
<b>g</b>	51.23	70.63	154.26	70.50
<b>h</b>	58.11	80.21	162.50	74.57

In the MD01 specimens consisting of PP fibre (both 12 mm and 48 mm) the initial compressive strength was seen slightly reduce as compared to the control mix. Similar results have been reported by Ramezaniapour et al. (2013) Richardson (2006). However, an increase in the compressive strength in the specimens having 12 mm PP fibres, was observed as compared to those having longer fibres (48mm). The reason for this may be due to the better distribution of the smaller fibres which may help control any the micro cracking which may occur during the hydration reaction which is an exothermic reaction (i.e., releases a lot of heat) (Latifi et al., 2022, Behera et al., 2020). Similar results were witnessed in the specimens having polyester fibres to that of the specimens having 1% 12 mm PP fibres. This could be due to both fibres been similar in size which helps in a more even distribution within the concrete mix. However, when considering the specimens having cotton fibres, the strength was seen to be the lowest of all other mixes within MD01.

MD02 and GP01 with the addition of fibrous materials displayed similar trends to MD01, with very similar strength readings. However, MD02 specimens recorded slightly higher readings compared to the GP01 specimens. In the MD03 specimens, the incorporation of the longer PP fibres (48mm) resulted in slightly higher results compared to the specimens having 12mm PP fibres. Similar to all others, the incorporation of cotton fibres displayed the

weakest cubes amongst any given mix. This was expected as cotton was incorporated mainly to understand its effects on the spalling behaviour on concretes and not primarily for strength enhancements. In order to achieve strength improvements, further refinement of the cotton fibres are required (Peña-Pichardo et al., 2018). **Figure 4.54** gives a graphical representation of the average initial compressive strength readings of cured specimens with and without the incorporation of fibres.

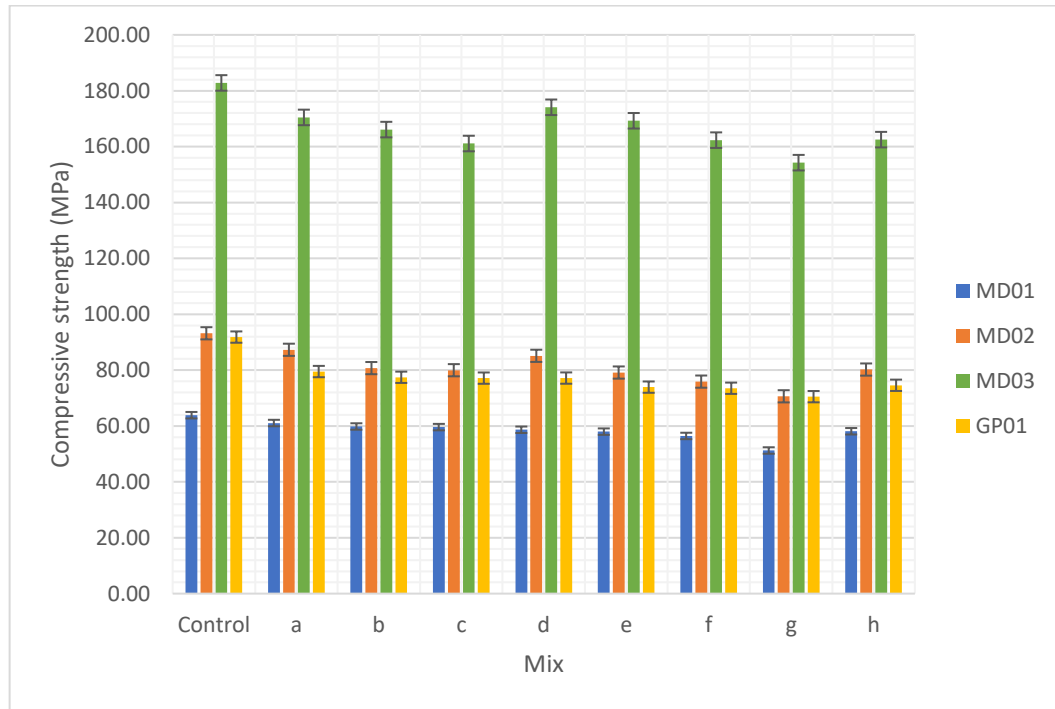


**Figure 4.54:** Graphical representation of the average initial compressive strength readings of specimens

Kodur (2014) categorized the residual compressive strength into 3 groups: from room temperature up to 350°C, from 350°C to 800°C, and over 800°C. In the present study, upon exposure to elevated temperature levels, several changes were observed in the different specimens. Tabulated reading of the average residual strength of specimens is given in **Table 4.12**.

Firstly, MD01 control specimens displayed drops in strength of approximately 18% and 69% at 400°C and 800°C, respectively, compared to MD02 control specimens which displayed lower strength drop of approximately 16% at 400°C and 65% at 800°C, respectively. Both these conditions can be attributed with the physio-chemical changes occurring within the concrete upon heating, which can lead to micro cracking caused by the internal stresses arising from thermal expansion of aggregates. Graphical representations of

the average strength loss (%) of specimens at different temperatures are given in **Figures 4.55** and **4.56**. In addition to this, hydrothermal conditions brought about by the evaporation of the free water molecules, hence breaking up the cement paste and deteriorating the interfacial transition zone (ITZ) at temperatures up to 300°C, can further contribute to the loss in strength (Iqbal et al., 2020, Abid et al., 2017, Zhao et al., 2020, Xiao and König, 2004). Reports also state that beyond 400°C, the decrease in strength can be associated with the dehydration of chemically bound water molecules and disintegration of hydration products of calcium hydroxide (CH), and beyond 600°C the decomposition of calcium carbonate and the instability of aggregate particles can further lead to strength reductions (Varona et al., 2018, Xie et al., 2018, Afroughsabet and Ozbakkaloglu, 2015).

**Table 4.12:** Tabulated readings of the residual strength of specimens

Mix ID	Residual strength (MPa)							
	MD01		MD02		MD03		GP01	
	400°C	800°C	400°C	800°C	400°C	800°C	400°C	800°C
<b>Control</b>	52.43	20.03	78.10	32.87	0.000	0.000	124.3	33.69
<b>a</b>	51.35	20.36	74.40	32.12	144.9	32.09	84.34	28.82
<b>b</b>	51.93	19.93	67.95	30.27	144.2	30.15	83.90	26.31
<b>c</b>	52.21	20.59	67.65	30.25	133.7	34.87	79.82	25.15
<b>d</b>	48.39	20.89	73.24	32.87	144.0	44.13	75.06	30.58
<b>e</b>	48.05	21.12	67.51	29.53	141.8	44.21	76.31	22.10
<b>f</b>	47.26	20.70	64.43	28.17	132.5	43.55	70.47	26.99
<b>g</b>	40.19	13.03	53.99	20.21	114.5	14.46	61.93	13.83
<b>h</b>	47.55	18.20	66.22	26.01	132.1	23.39	67.77	20.99

Moreover, MD03 control specimens experienced explosive spalling condition during heating at a temperature of around 350°C (this temperature is indicated by a cracking and popping sound from inside the muffle furnace), hence no result could be obtained. This is assumed to be associated mainly with the low water content of the MD03 mixes. In the MD01 and MD02 specimen a more permeable microstructure (see **Section 4.7**) can be identified, hence, easy diffusion of pore pressure during increased temperature could be facilitated in such mixes. In contrast, the superior and dense microstructure of the MD03 specimens, while beneficial on the compressive strength at room temperature, provides a highly impermeable and compact environment, which, under high temperatures, can obstruct

the release of build-up pore pressure, thus resulting in the rapid development of microcracks, leading to spalling (Chan et al., 1999, Khaliq and Kodur, 2012, Kannangara, 2018, Poon et al., 2001, Ali, 2002, Amran et al., 2022, Babalola et al., 2021).

In contrast to the thermal behaviour of the OPC- based specimens, an interesting observation was the residual strength readings of the GP01 control specimens at 400°C, which were seen to improve in the residual strength by an average strength gain of approximately 35% at 400°C. Several reports of such an occurrence has been reported in the past (Kannangara et al., 2021a, Zhao and Sanjayan, 2011, Davidovits, 2002b, Nadeem et al., 2014, Akram et al., 2007, Bui et al., 2018), and is said to be associated with the micro filler effect together with the further hydration of the reactive powder in the FA, which can be enhanced as the temperature increases. This warrants an important area of the research given in section 1.3, i.e., in reducing the carbon footprint of concrete materials, through the full replacement of cement with a material (FA) that can produce a similar building material to OPC-based concretes, having enhanced fire resistance properties.

When considering the residual strength of GP01 specimens after exposure to 800°C, an average strength loss of approximately 63% was observed. This can be due to the development of very high internal stresses forming microcracks in the ITZ caused by different thermal expansion coefficients of the materials (Ren et al., 2022, Li et al., 2017, Babalola et al., 2021, Hassan et al., 2020).

In general, the addition of PP fibres was seen to reduce the strength loss at both elevated temperatures compared to the control mixes, with MD01 specimens having PP fibres (from both 12 mm and 48 mm) resulting in the highest average strength loss of 17.5% (from MD01d), compared to 17.9% of the MD01control mix at 400°C, and approximately 66.7% from MD01b compared to the control mix of approximately 68.6% at 800°C. When considering the residual strength of the MD01 specimens after exposure to 400°C, specimens having cotton fibres resulted in higher strength losses, with an average loss of approximately 21.6% as against control samples. Moreover, at 800°C the lowest loss in average strength was recorded from MD01f (*ca.* 63.3%), with total losses falling within the range of about 63 – 75%.

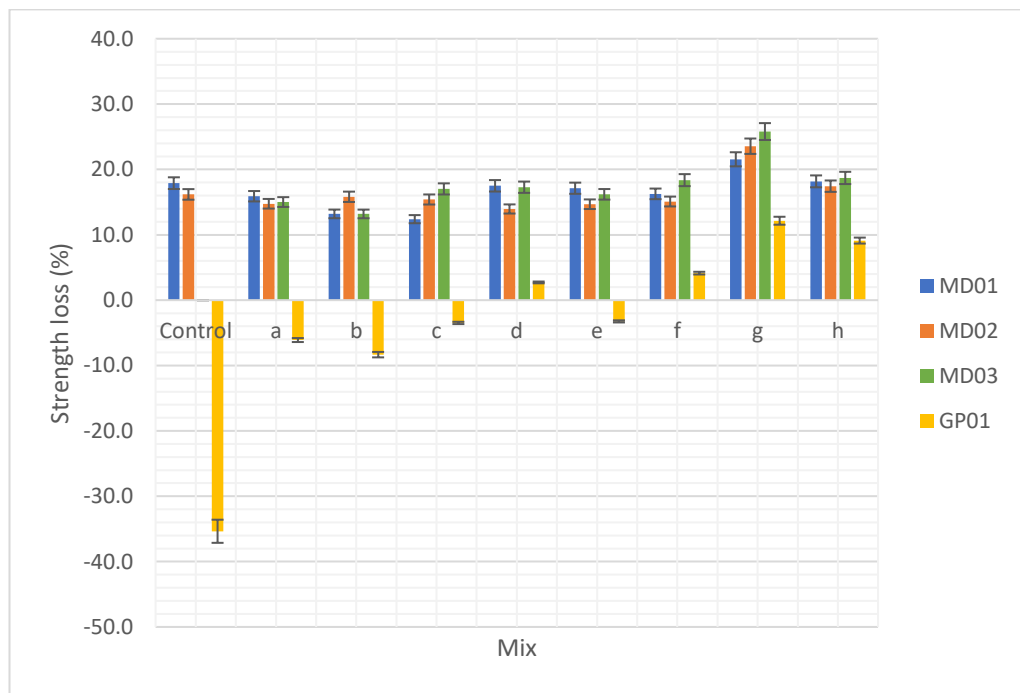
Similarly, at 400°C, the highest average strength loss of the MD02 specimens having PP fibres incorporated was recorded from MD02b (*ca.* 15.8%), which was less compared to

the average strength loss of the control mix (*ca.* 16.2%). Specimens having polyester and cotton fibres showed similar trends to that of the MD01 specimens, with cotton displaying the highest average strength loss of approximately 24%. MD02 specimens displayed similar trends to the MD01 specimens after exposure to 800°C, with average strength losses falling within a range of about 61 – 71%. Similar results have been reported by Lie and Kodur (1996), Lau and Anson (2006), where the addition of fibres was found to reduce the loss in strength after high temperature exposure.

Another very interesting result was the residual strength values of the MD03 specimens with the addition of fibres. As seen above, a residual strength for the MD03 control specimens could not be obtained due to the highly explosive nature of the specimens. However, none of the MD03 specimens which had sacrificial agents incorporated into the mix did not explode under high temperatures of either 400°C or 800°C. This could be due to the sacrificial nature of the polymers, which either melt or char, creating voids/spaces/grooves within the internal structure of the concretes, thus providing pathways for the release of vapor pressure (Noumowe, 2005, Xiao and Falkner, 2006). This provides strong support towards addressing the significance of this research given in section 1.3., where the reduced level of spalling improves the overall structural stability of concrete elements, thus requiring less remedial measures, and hence reducing wastages for reconstruction. In addition to this, knowledge of obtaining reduced spalling levels through the use of polymeric materials, where the waste accumulation is becoming more and more problematic towards the environment (see section 2.7), serves to be highly advantageous in addressing the research gap. While comparisons on the residual strength loss between the control mix cannot be obtained due to the control specimens exploding, on average the strength loss at 400°C for the specimens having PP fibres was within a range of about 13–17%, with specimens having smaller PP fibres resulting in higher strength losses compared to specimens having larger PP fibres. This can be due to a higher distribution of the smaller fibres within the mix matrix, which creates more voids/spaces as the fibres melt at higher temperatures. This in turn provides a less dense microstructure which can cause lower residual strengths, i.e., higher strength losses (Chen and Liu, 2004).

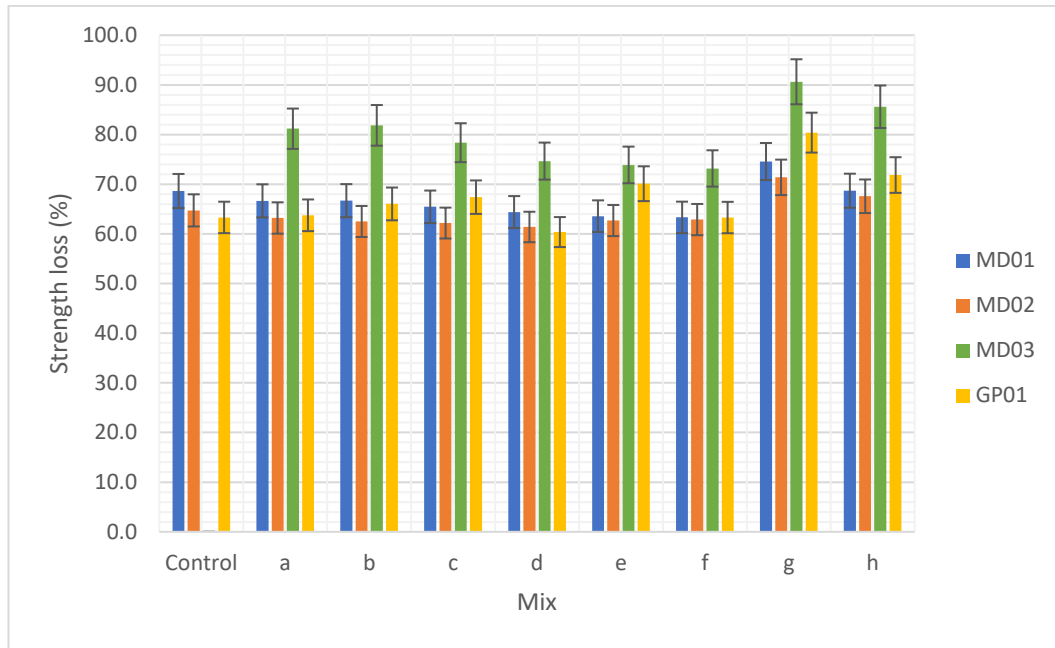
At 400°C, similar to the control GP01 specimens, specimens having PP fibres added showed increments in residual strength as compared to the OPC- based concrete specimens. Past research showed that in plain concrete an increase in the permeable voids would occur

as a result of the polar characteristics of the fibres. These would be filled with water molecules which, during extreme heating, would evaporate, which can cause the formation and progression of cracks in the ITZ between the fibrous material and the cement matrix. Thus, would result in lower residual strength readings in the case of the OPC- based concretes (Yuan et al., 2020, Latifi et al., 2022). However, in the case of GP samples, the further polymerization and the ceramic – like properties of the GP concrete has a tendency to improve residual strength up to temperatures of about 300°C – 400°C (Pliya et al., 2011, Kannangara et al., 2021b). At 800°C, the residual strength of GP01 specimens having fibres added was seen to be much less of those at room temperature. This could be due to the higher thermal stress gradients which can hinder further polymerization and affect the ductility of the material, which can create a drop in bearing capacity beyond 400°C (Aygörmez et al., 2020, Sharma et al., 2024, Kannangara et al., 2021a).



*\*negative readings indicate a strength gain, and the strength loss of control MD03 specimens cannot be presented due to explosive spalling*

**Figure 4.55:** Average strength loss of specimens (%) after exposure to 400°C



*\*the strength loss of control MD03 specimens cannot be presented due to explosive spalling*

**Figure 4.56:** Average strength loss of specimens (%) after exposure to 800°C

In addition to the cubical samples, OPC – based concrete cylindrical samples (100 mm × 200 mm) were tested on for initial compressive strength, to draw up a correlation between cubical strength ( $f_{cu}$ ) and cylindrical strength ( $f_{cy}$ ) readings. Specimens prepared using MD01, MD02 and MD03 mixes were used to compare the compressive strength of cylinders to cubes. **Table 4.13** gives tabulated data of the compressive strength readings of the two types of specimens, and **Table 4.14** provides a correlation between cubical and cylindrical specimens.

**Table 4.13:** Compressive strength readings (MPa) obtained from cubical and cylindrical specimens

Nos.	Compressive strength MPa					
	MD01		MD02		MD03	
	$f_{cu}$	$f_{cy}$	$f_{cu}$	$f_{cy}$	$f_{cu}$	$f_{cy}$
1	65.06	34.94	91.46	45.98	180.06	89.29
2	65.39	29.04	90.26	47.06	185.69	86.16
3	64.89	35.98	96.98	47.35	184.34	85.03
4	64.16	31.49	95.81	49.63	185.22	86.49
5	62.59	30.89	93.66	45.63	180.26	89.5
6	63.09	32.16	92.66	46.72	180.49	89.53
7	64.43	33.06	91.67	47.65	181.73	85.16



<b>8</b>	61.15	31.99	90.65	50.01	186.08	88.29
<b>9</b>	63.11	32.58	95.74	45.87	183.26	91.21
<b>10</b>	64.86	28.16	92.89	46.29	180.87	88.37
<b>Av</b>	<b>63.87</b>	<b>32.03</b>	<b>93.18</b>	<b>47.22</b>	<b>182.80</b>	<b>87.90</b>

**Table 4.14:** Correlation between cubical and cylindrical specimens

	<b>MD01</b>	<b>MD02</b>	<b>MD03</b>
<b><math>f_{cu}/f_{cy}</math></b>	1.9941	1.9733	2.0796
<b>Average Conversion factor</b>			<b>2.0157</b>

Results revealed cubical strength readings to be much higher than those obtained from the cylindrical specimens of the same mix. While the national codes do not provide a standard correlation between cubical and cylindrical strength, it has been suggested for the compressive strength of concretes to be determined using either cubical specimens of 150 mm<sup>3</sup> or cylindrical specimens of 150 mm (d) and 300 mm (l). However, past literature reports cubical samples would achieve higher strength reading, and it is generally assumed to be 1.25 times higher compared to that of cylinder strength based off standard sizes, which are of 150 mm<sup>3</sup> cubical specimens (Gonnerman, 1925). However, in this particular study, 50 mm<sup>3</sup> cubes were used for the measurement of strength, and size comparison studies between these 50 mm<sup>3</sup> cubes and 100 mm × 200 mm cylinders show a factor of approximately 2. Which means that the 50 mm<sup>3</sup> cube strength should be assumed to being about twice that of the 100 mm × 200 mm cylinder strength. It must be highlighted here that studies regarding the strength variations between the 50 mm<sup>3</sup> cubes and cylinders require further investigation.

#### **4.9. Mass loss after thermal exposure**

When considering the mass loss of concrete specimens after completing full curing and obtaining target strength, any loss of in mass could only mean the loss of water from the specimen. Literature presents several studies where the researchers have reported a high rate in the loss of mass upon reaching 100°C–150°C, after which this rate had seen to reduce and level off. It was further reported that any rapid loss in mass during initial heating was due to the evaporation of moisture. In addition to this, studies also show that during the temperature

range of about 600°C – 800°C, chemically bound water in the calcium-silicate-hydrate (C-S-H) bonds would start to break down, and also due to the decomposition of CaCO<sub>3</sub>, there would be a noticeable loss in mass (Kong and Sanjayan, 2010, Abdulkareem et al., 2014, Kannangara, 2018, Su et al., 2016, Nazri et al., 2017). In the present study, the loss in mass of the different mixes was recorded and expressed as a percentage of the initial mass at room temperature to the mass of specimens after exposure to either 400°C or 800°C. Tabulated results are given in **Tables 4.15 – 4.18**.

**Table 4.15:** Average mass loss of MD01 cubical specimens (%)

Sample	Mass loss at 400°C (%)	Mass loss at 800°C (%)
<b>Control</b>	4.7	7.1
<b>a</b>	5.3	7.8
<b>b</b>	5.5	7.9
<b>c</b>	5.6	8.7
<b>d</b>	5.4	7.8
<b>e</b>	5.6	8.0
<b>f</b>	5.6	8.9
<b>g</b>	5.0	7.4
<b>h</b>	5.4	7.9

**Table 4.16:** Average mass loss of MD02 cubical specimens (%)

Sample	Mass loss at 400°C (%)	Mass loss at 800°C (%)
<b>Control</b>	4.1	6.1
<b>a</b>	4.6	6.8
<b>b</b>	4.8	7.0
<b>c</b>	5.4	7.4
<b>d</b>	4.7	6.8
<b>e</b>	4.8	7.2
<b>f</b>	5.6	7.4
<b>g</b>	4.4	6.5
<b>h</b>	4.9	7.1

**Table 4.17:** Average mass loss of MD03 cubical specimens (%)

Sample	Mass loss at 400°C (%)	Mass loss at 800°C (%)
<b>Control</b>	0.0*	0.0*
<b>a</b>	3.1	4.3
<b>b</b>	3.8	4.7
<b>c</b>	4.3	5.0
<b>d</b>	3.1	4.6
<b>e</b>	3.7	4.8
<b>f</b>	4.4	5.3
<b>g</b>	3.0	3.8
<b>h</b>	3.8	4.6

*\*due to the explosive spalling conditions of the MD03 control specimens, no result could be obtained here.*

**Table 4.18:** Average mass loss of GP01 cubical specimens (%)

Sample	Mass loss at 400°C (%)	Mass loss at 800°C (%)
<b>Control</b>	3.1	4.1
<b>a</b>	3.3	4.7
<b>b</b>	4.0	5.0
<b>c</b>	4.7	6.4
<b>d</b>	3.4	4.8
<b>e</b>	4.1	5.1
<b>f</b>	4.6	6.4
<b>g</b>	3.2	4.4
<b>h</b>	4.1	5.2

It is clearly evident from the obtained results that the average mass loss increased as the temperature increased. This was the case in all the specimens. This loss in mass can be attributed to the loss of free water at 100°C, and the total loss of water of hydration, thus, the decomposition of hydration products, at a temperature of about 800°C (refer **Figure 2.1**) (Ma et al., 2015, Düğenci et al., 2015). In addition to this, the spalling, of concrete pieces can also contribute to the loss in mass.

When considering the control samples, it can be seen that the loss in mass is the greatest for MD01, followed by MD02. This can be attributed to the w/c ratio of the mixes where a greater water content in the MD01 specimens can mean a higher percentage of water molecules in the mix matrix, which can cause a greater loss in mass after heating, and *vice versa*. When looking at the percentage mass loss of the GP01 specimens, a lesser percentage in mass loss is observed in the GP01 specimens compared to the MD02 specimens

(regardless of the two having the same liquid: binder ratio). This can be associated with the dehydration of the GP gel and de-hydroxylation of the hydroxyl groups, and the pozzolanic reactions between the highly reactive FA and the alkaline solution, which can create a tighter mix matrix (Hassan et al., 2020, Nadeem et al., 2014, Zhang et al., 2020a).

When using sacrificial agents, the percentage of fibres replace the weight of paste and aggregate materials within the mix. Therefore, in addition to the loss of water and the breaking down of the C–S–H bonds, the melting, in the case of PP and polyester, and charring, in the case of cotton, can further influence the loss in mass after heating (Wu et al., 2020, Deshpande et al., 2019). **Figures 4.57 and 4.58** presents a graphical representation of the average mass loss (%) of the FRC specimens at 400°C and 800°C, respectively. In the present study, this trend was observed, with specimens having fibres, displaying higher percentages in mass loss at both 400°C and 800°C, compared to control samples (Yermak et al., 2017, Pliya et al., 2011), with a greater loss witnesses after exposure to 800°C. Very similar readings, showing the same trends were observed in the mass loss between the specimens having 12 mm PP fibres and 48 mm PP fibres as the percentages increased from 0.5% to 1.5%. In the case of polyester, the loss is mass was very similar to the losses obtained from the PP fibres; however, cotton displayed a slightly higher drop in mass. This was the case on all the OPC-based specimens and the FA- based GP specimens. This could be attributed to the char residue of the cotton fibres, which was found to be highest amongst all fibres (see **Table 4.2**), thus adding to the final mass of the specimens after thermal exposure.

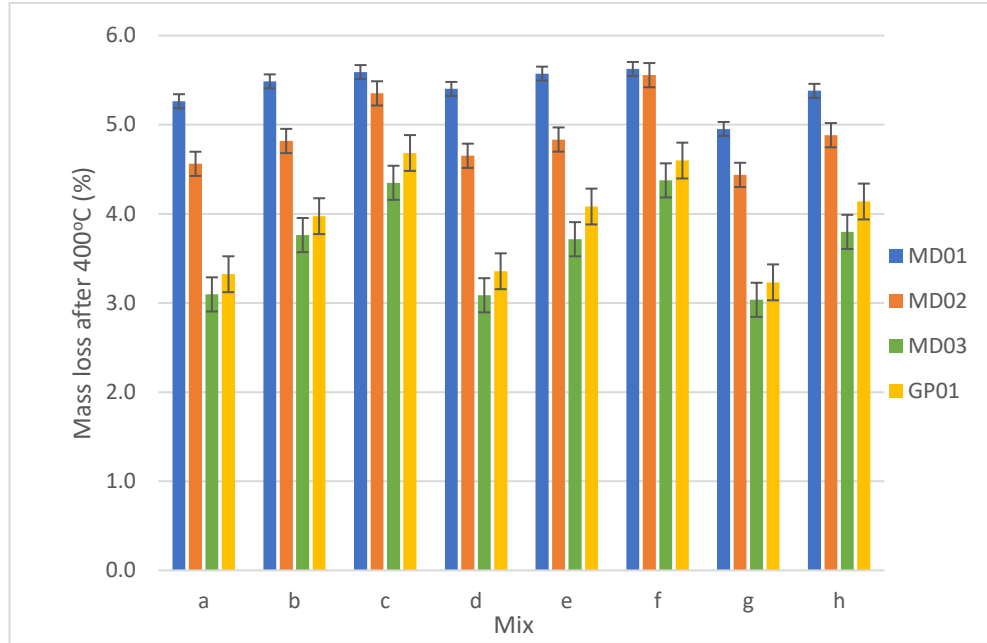


**Figure 4.57:** A comparison of the average mass loss (%) after 400°C

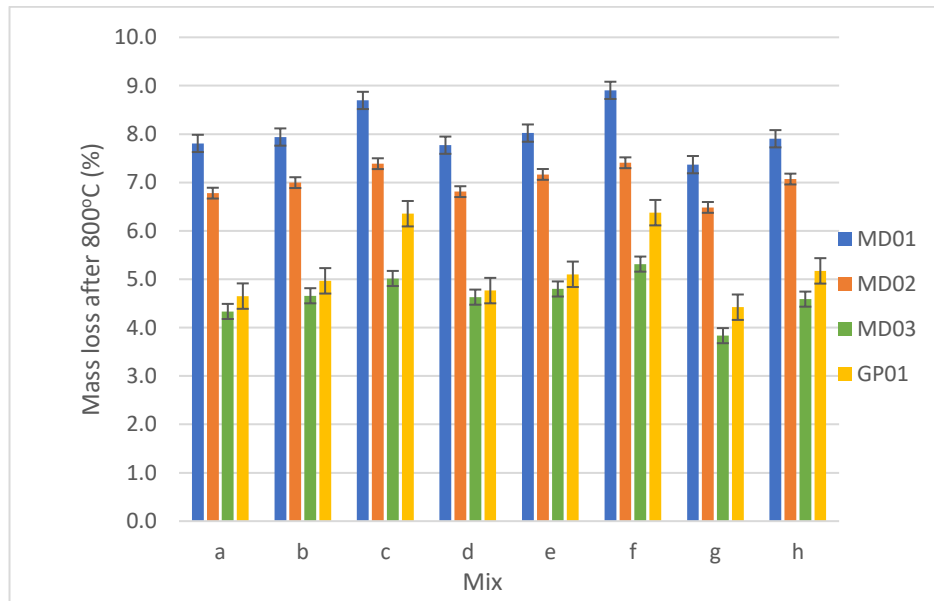


**Figure 4.58:** A comparison of the average mass loss (%) after 800°C

#### 4.10. Carbonation studies on spalled specimens

When considering the fire performance of concretes, the role of moisture has long been assumed to be a key contributing factor to the degree of spalling, where the crucial temperature range for spalling has been reported to be within the range of 400°C and higher.

During this temperature the physically bound water, or the free water molecules have already left the concrete matrix, and the remaining water are the ones found within the C-S-H bonds, or the chemically bound water. Once the internal temperature of the concrete reaches this temperature, the calcium centres are vulnerable to disassociation, hence it is important to understand the chemical environment of these calcium centres using a more quantitative approach (Hong et al., 2022).

In addition to the degradation caused by fire, carbonation of concrete has been reported to cause detrimental effects on the durability of concrete structures. During the carbonation studies, an analysis was conducted between heat treated specimens prepared using both cement (MD01, MD02 and MD03) and FA (GP01) before and after undergoing carbonation. Specimens were subjected to compressive loading to understand the change in compressive strength between the non-carbonated and carbonated samples. In addition, TGA runs were conducted to understand the degradation of the calcium centres from 30°C - 1000°C using the assessment and comparison of the weight loss. **Table 4.19** shows the changes in weight percentage and related strength readings of the non-carbonated and carbonated control samples before and after being exposed to 400°C and 800°C.

**Table 4.19:** Strength and mass loss results of non-carbonated and carbonated specimens

Specimen	Non- carbonated samples		Carbonated samples	
	Change	Strength	Change	Strength
	in wt.	(MPa)	in wt.	(MPa)
	using TGA (%)		using TGA (%)	
MD01 Control	6.14	63.87	10.15	60.28
MD01 400°C	6.03	52.43	11.13	50.31
MD01 800°C	4.68	20.03	8.290	17.99
MD02 Control	6.66	93.18	8.030	90.24
MD02 400°C	7.47	78.10	7.170	74.38
MD02 800°C	6.67	32.87	6.580	28.01
MD03 Control	5.15	182.8	3.670	155.3
GP01 Control	0.93	91.83	1.010	90.64
GP01 400°C	1.35	124.3	1.290	120.3
GP01 800°C	0.73	33.69	0.090	21.85

As can be seen from the above table, carbonation, as expected, resulted in a reduction in compressive strengths, albeit to varying degrees, depending on the mix designs (Li and Wu, 2022). While all specimens displayed drops in the compressive strength after carbonation, MD03 displayed the highest drop in strength. This gives evidence that HSC which undergoes carbonation is more likely to fail as compared to NSC samples which have undergone carbonation. As gauged from their TGA thermograms, in the cases of MD02 specimens heated to 400°C and 800°C, and MD03 specimens, the effect of carbonation on the change in weight was not very evident. In the case of the FA-based GP specimens, the effect of carbonation on the change in weight was relatively minor as compared to those based on the OPC, except for in the case of GP01 heated to 800°C, where the amount of carbonated domains was significantly lower as compared to its non-carbonated counterpart. This feature was also clearly reflected in their measured residual strengths. Given the polymeric structural feature of GP specimens and the relatively low concentrations of hydrated calcium centres, the accelerated carbonation process only has a very minor effect on their matrices (Haq et al., 2014).

#### **4.11. Imaging of the cubical specimens using SANS and high-resolution optical microscopy**

When considering the overall fire performance of concrete structures, the role of moisture has long been identified as a key contributing factor to the degree of spalling, where the crucial temperature range for spalling is reported to be within the range of 400°C. During this temperature the physically bound water, or the free water molecules have already left the concrete matrix, and the remaining water are the ones found within the C-S-H bonds, i.e., the chemically bound water. Once the internal temperature of the concrete reaches this temperature, the calcium centres are vulnerable to disassociation, hence it is important to understand the chemical environment of these calcium centres in a more magnified scale.

In the present study, control mixes that were cured and those subjected to heat treatment were studied using SANS (Häußler et al., 1997, Trapote-Barreira et al., 2015, Allen et al., 1982, Aldridge et al., 1994). The data is supplied as grey-scale stacks with a cubic voxel size of 44.84 microns. For all cases the control (MD01, MD02, MD03 and GP01) samples are darker in the radiographs due to their higher concentration of hydrogen

(moisture), and hence greater neutron attenuation. The datasets for the control samples therefore have a beam-hardening filter applied which increases the inherent noise in the data but flattens out the attenuation effect. The heat-treated samples did not require beam-hardening corrections. **Figures 4.59 – 4.62** presents the processed images through SANS for MD01, MD02, MD03 and GP01 specimens before and after exposure to 300°C. It should be noted here that, due to the explosive nature of MD03 at 350°C, all samples were heat treated to a maximum temperature of 300°C.

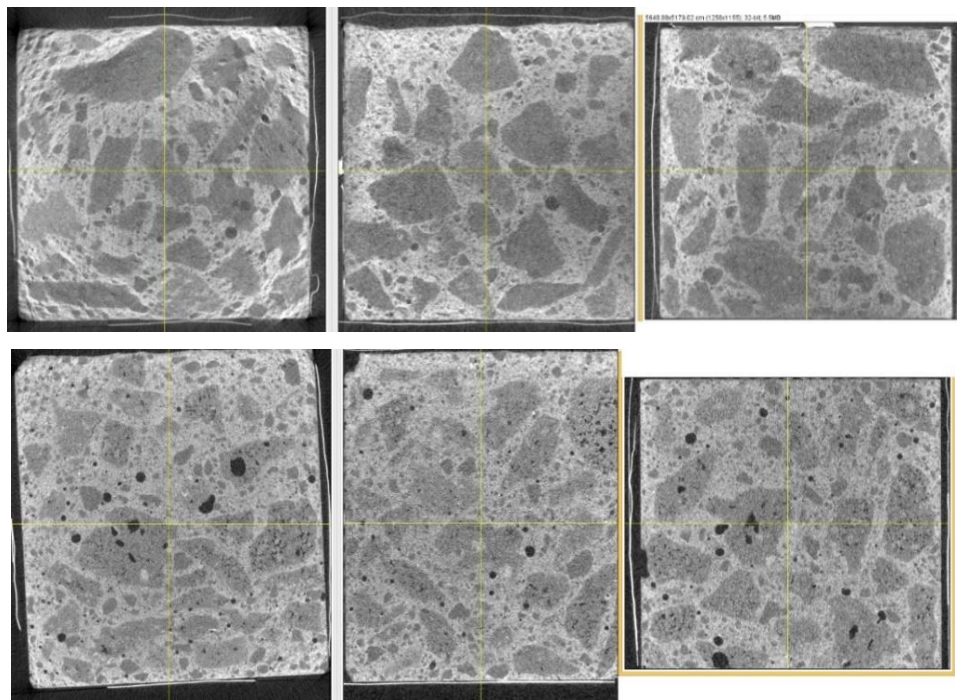


**Figure 4.59:** SANS processed images for MD01 (the three images above are for the cured samples, and the corresponding ones shown below are from the heat-treated ones (300°C))



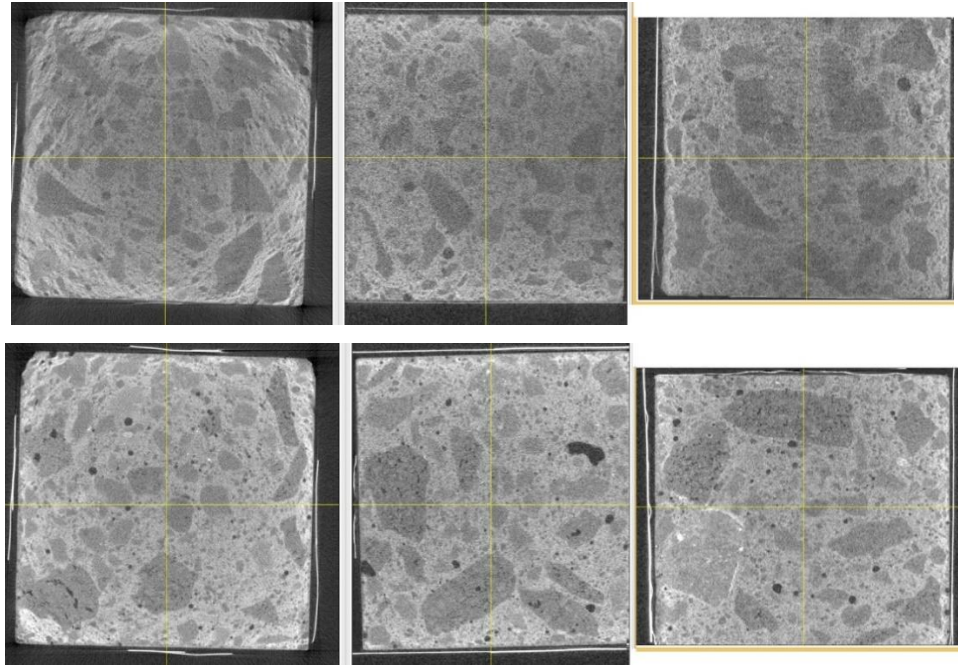


**Figure 4.60:** SANS processed images for MD02 (the three images above are for the cured samples, and the corresponding ones shown below are from the heat-treated ones (300°C))

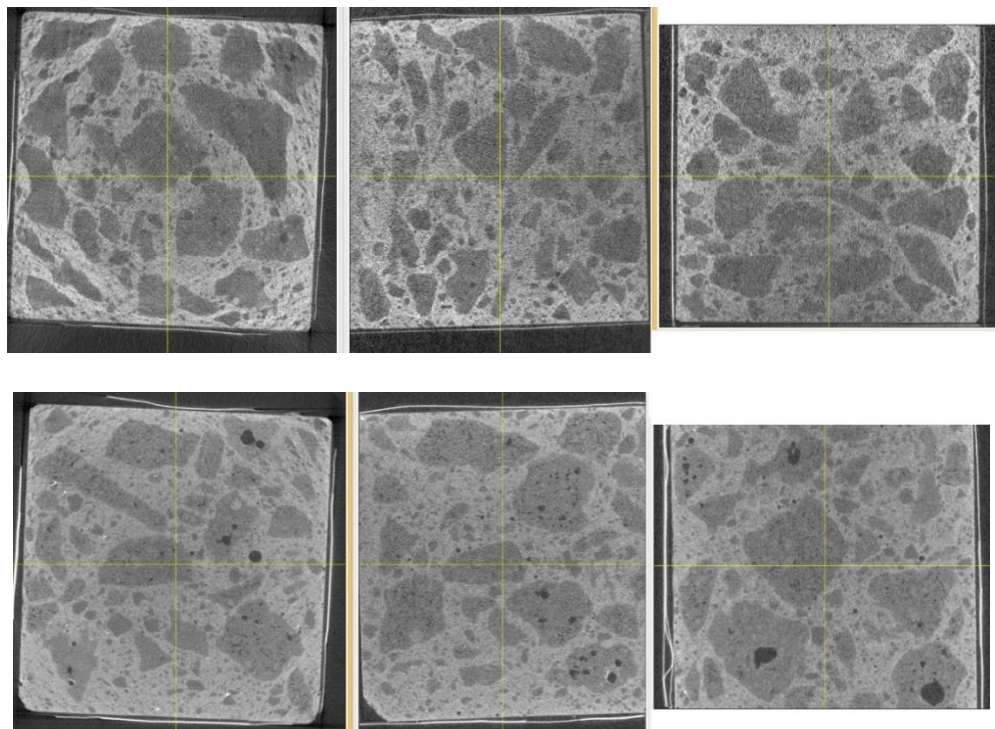


**Figure 4.61:** SANS processed images for MD03 (the three images above are for the cured samples, and the corresponding ones shown below are from the heat-treated ones (300°C))

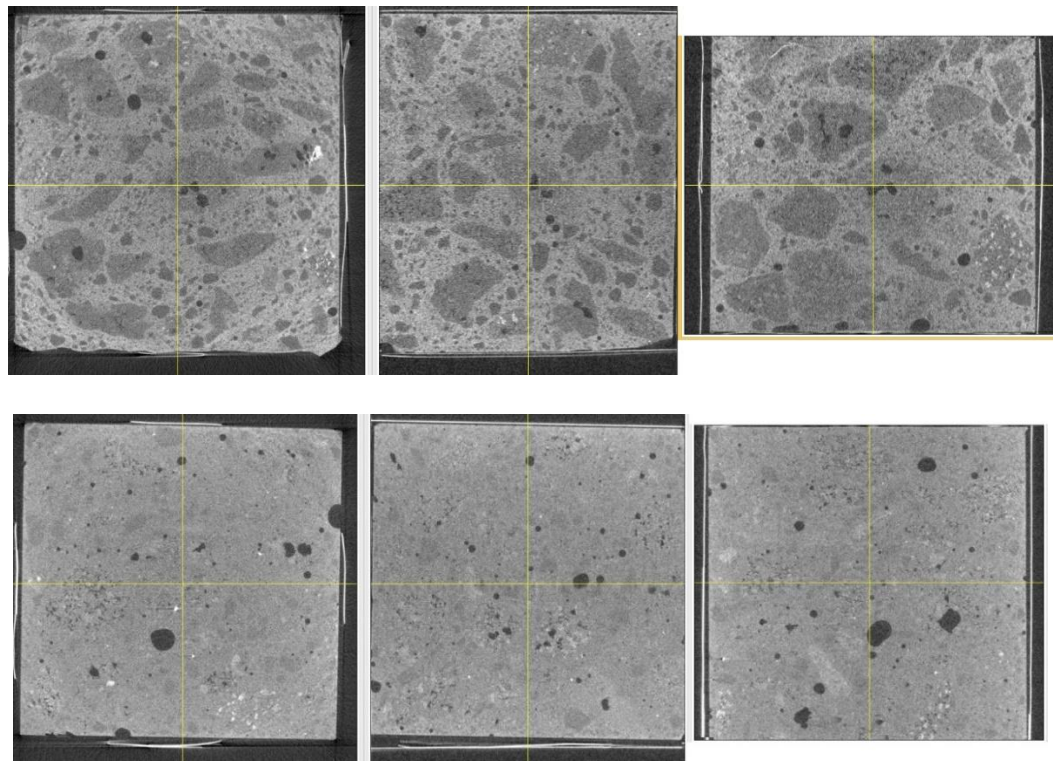
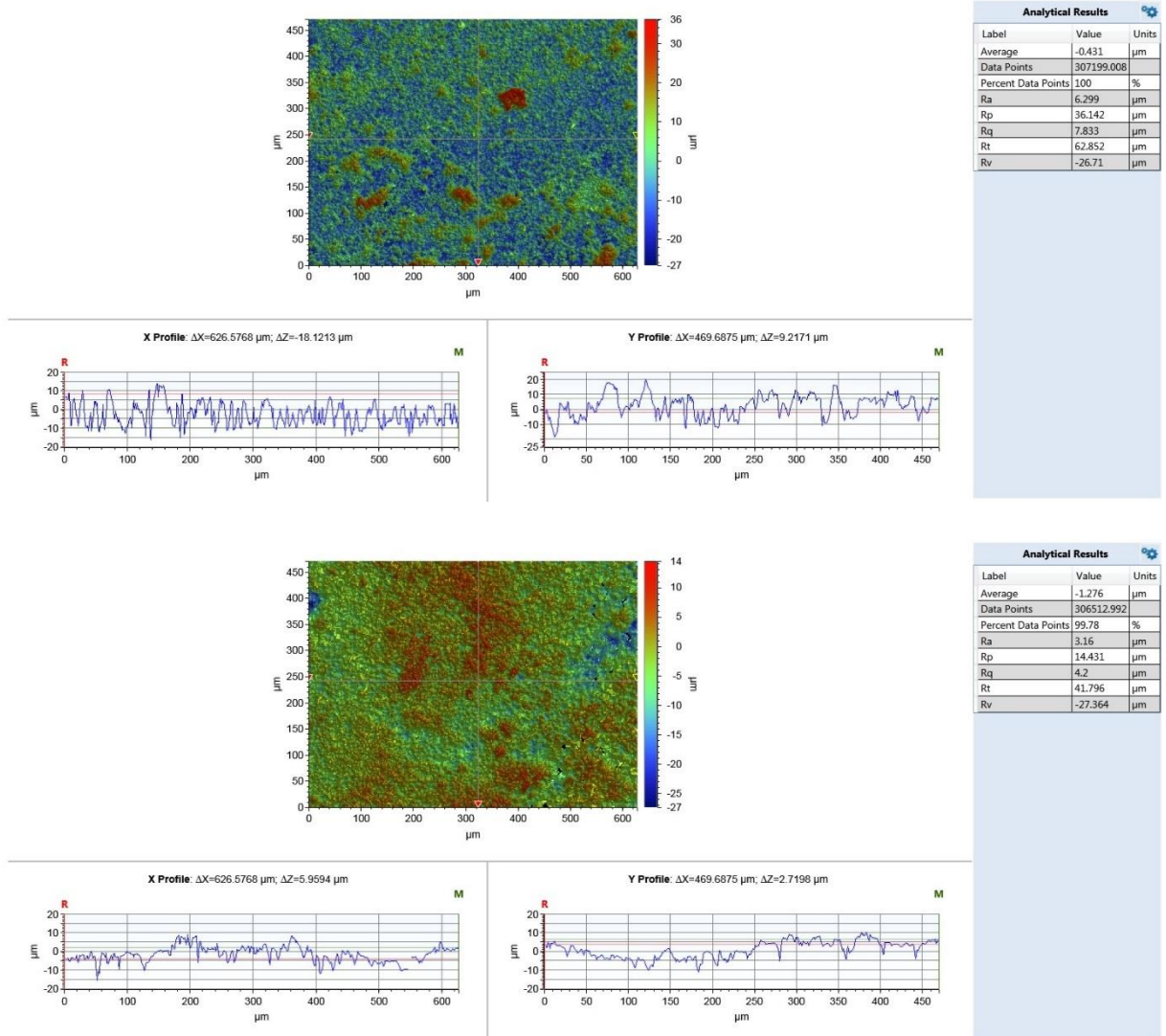


**Figure 4.62:** SANS processed images for GP01 (the three images above are for the cured samples, and the corresponding ones shown below are from the heat-treated ones (300°C))

When comparing the processed images of the OPC-based specimens, it is clearly evident that the more of the hydrated calcium centres (seen as dark voids) turned into dehydrated moieties when the samples underwent heat exposure (i.e., an increase in such an attribute). In addition to this, the degree of porosity was also seen to reduce from MD01 to MD02, and then further reduced in the case MD03, as shown by a more cohesive internal structure of the matrices of these specimens. This also corroborates the previous finding in relation to density and porosity measurements (see **Sections 4.6 and 4.7**). When considering the FA-based GP concrete specimens, the processed images clearly demonstrated further polymerization reactions, upon the heat treatment, thus leading to a more compact structure owing to the amalgamation of the different components within the mix. This could be valuable evidence to support the enhanced behaviour of FA-based concretes under fire exposure.

An investigation using a 3D optical microscopic technique revealed the changes in the surface profiles of the concrete and geopolymer samples before and after exposure to elevated temperature levels of 400°C and 800°C. The contours which were obtained from the study showed the surface morphology between the non-heat treated and heat-treated specimens through the use of colour gradation contour mapping. **Figures 4.63-4.66** (outputs from the machine) presents these colour gradation contour maps for each of the specimens.

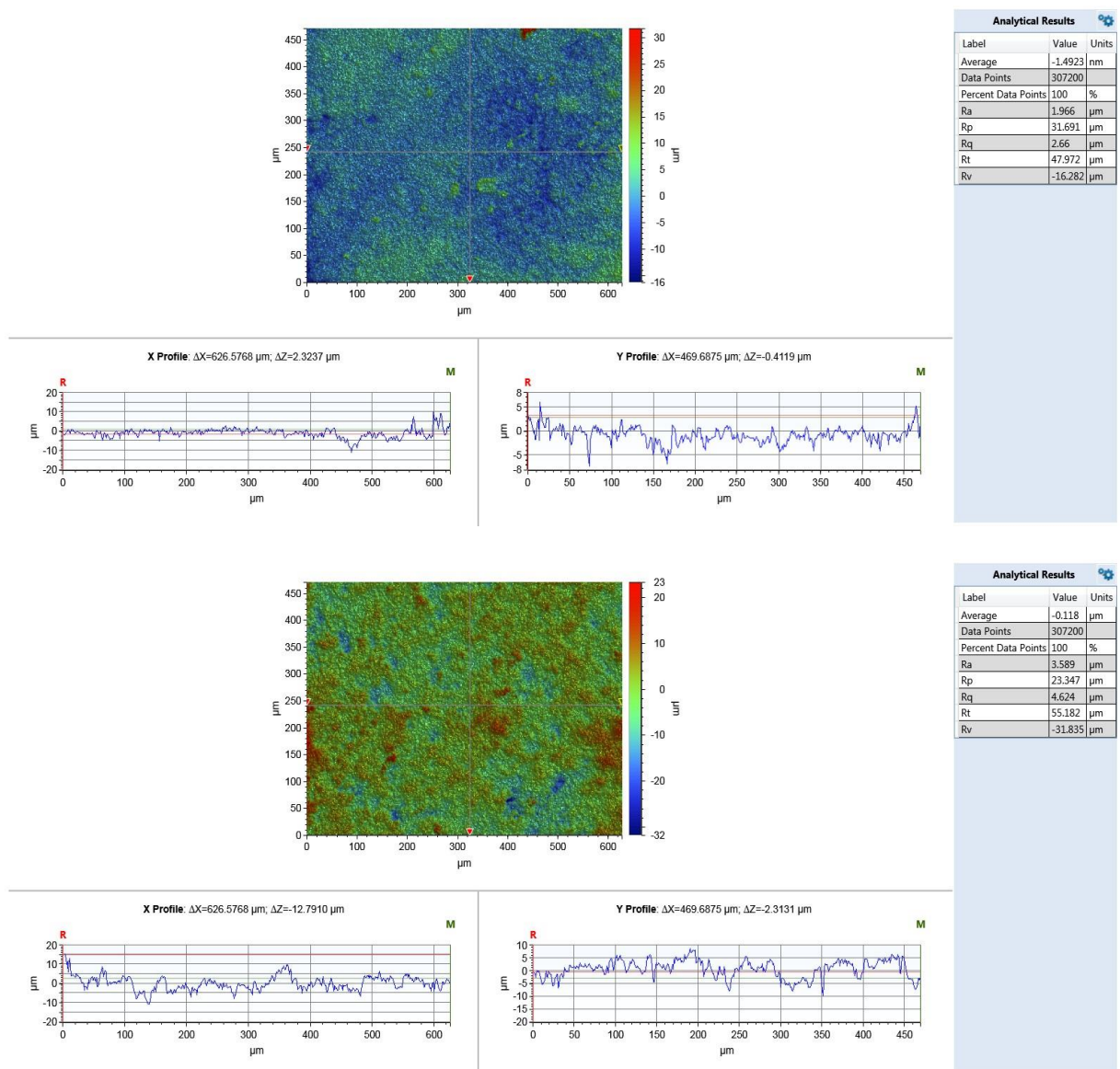
On visual observation, the changes in the surface texture, appearance of micro-cracks, discolouration were evident in the heat-treated samples as compared to the cured counterparts. These changes can be predominantly attributed, with fair degree of confidence, to the loss of water and changes in the textures of the bulk samples in the case of the heat-treated ones. Therefore, and as expected, such changes were exacerbated in the case of samples that were heated to the higher temperature limit (see the contour maps). In addition, the discoloration was most predominant in the heat-treated GP01 specimens, where the exposure to elevated temperatures resulted in the production of coloured compounds. This could be due to the higher oxidation causing a state of transition of the metal oxides present in them (mainly ferric oxides). In summary surface imaging technique, as employed in the present study, has served to illustrate the phenomenological evolution of spalling in the cubical samples in question (Perez et al., 2009).



Top: Before exposure to 300°C Botton: After exposure to 300°C

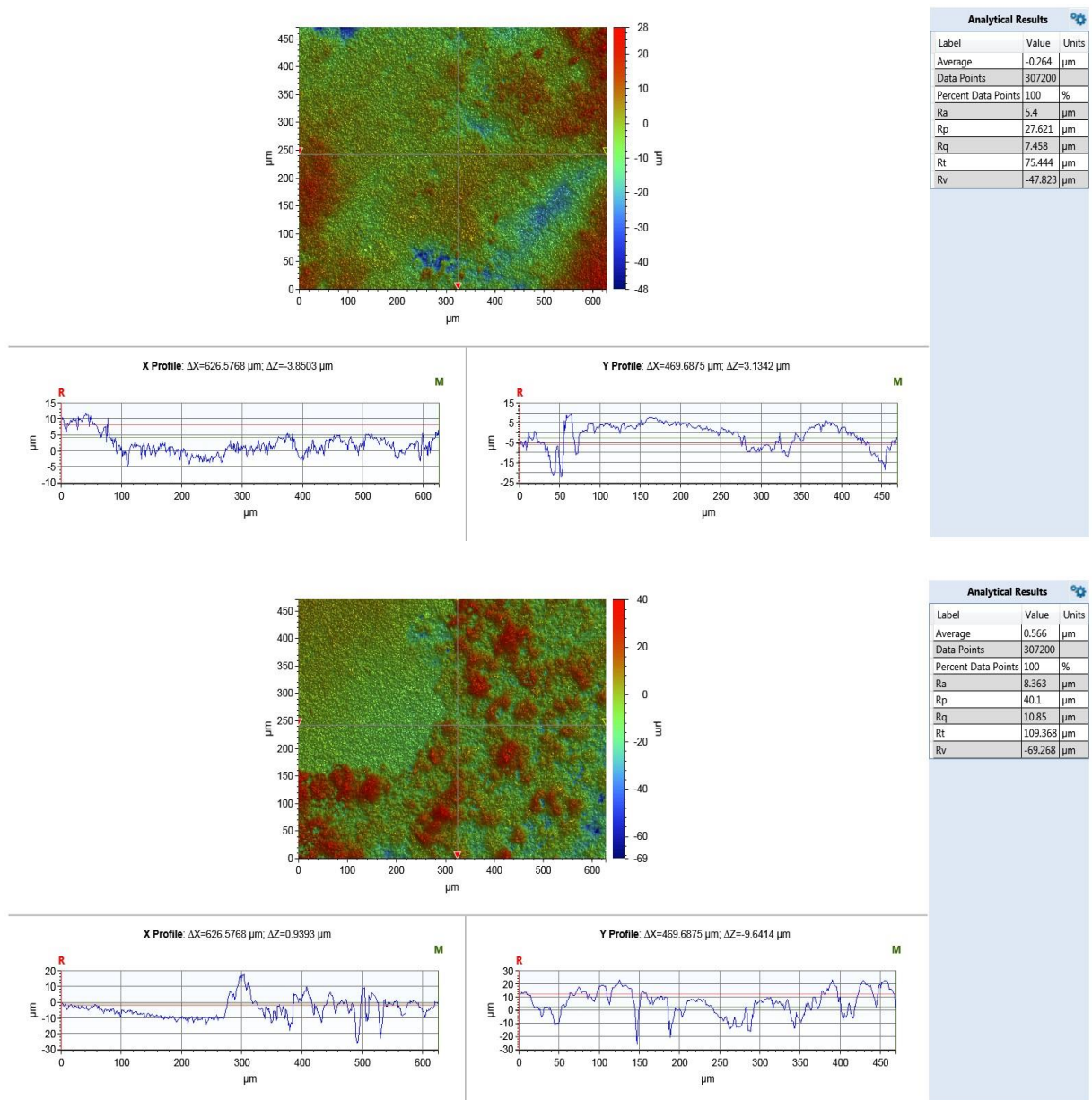
**Figure 4.63:** Colour gradation contour map of MD01 specimens





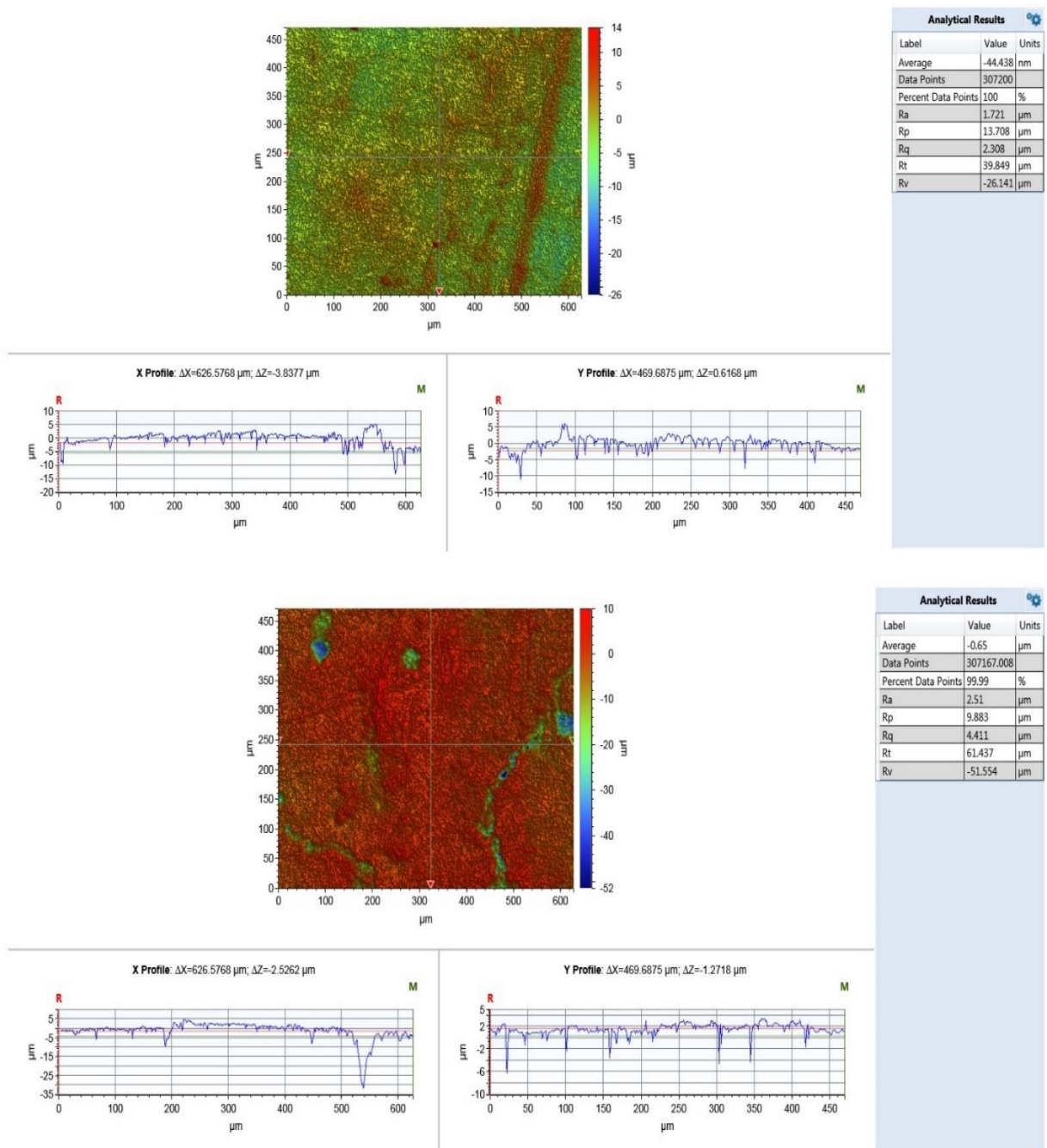
Top: Before exposure to 300°C    Bottom: After exposure to 300°C

**Figure 4.64:** Colour gradation contour map of MD02 specimens



Top: Before exposure to 300°C    Bottom: After exposure to 300°C

**Figure 4.65:** Colour gradation contour map of MD03 specimens



Top: Before exposure to 300°C    Bottom: After exposure to 300°C

**Figure 4.66:** Colour gradation contour map of GP01 specimens

#### 4.12. Spalling behaviour of large-scale specimens

As mentioned before, the physio-chemical properties to understand the spalling behaviours were gathered in this study using 50 mm<sup>3</sup> cubical samples, standard cylindrical samples (100 mm diameter and 200 mm long) and now using larger segments (1800 mm × 1800 mm × 350 mm). The cubical samples were primarily used to follow the morphological, structural and physio-chemical changes of the test specimens upon exposure to heat (at 400°C and 800°C), whereas the cylindrical specimens were employed to obtain information regarding the porosity of the different mixes (including geopolymer-based ones) and to gain an understanding on the effects of cubical and cylindrical specimens on the initial compressive strength. Therefore, the main emphasis of the large-scale tests was to follow the spalling behaviour of real-life size specimens that often form basic structural components of various infrastructures (primarily segments in tunnels in the Australian context), and hence we collated the test results from furnace runs conducted using panels. It is also relevant to note here that these large specimens also incorporate PP fibres as a reinforcing agent. As expected, these reinforcing agents also exhibited mitigation effects on the overall spalling behaviours of the corresponding test specimens at different degrees. In summary, through incorporating the results from the large-scale tests, the scope of the current project was effectively extended to cover spalling behaviour of real-life specimens in more realistic fire scenarios, for instance those emanating from vehicular fires in tunnels.

As previously explained, quantifying the spalling behaviour is not easy to perform, hence, the spalling measurements for the panels were conducted to meet a specific spalling criterion.

Spalling criteria: the central area, which is of 800 × 800 mm, shall not suffer an average concrete loss equal to or greater than 40 mm (depth) for a minimum of 95% of the central area. In addition, this central area shall not suffer a maximum concrete loss of greater than 60 mm (depth) for less than 5% of the central area. Measurements are taken at a 100 mm grid spacing and this data will provide further accuracy and help quantify the maximum and average spalling depths within the central area and entire exposed face.

The spalling depths at every 100 mm within the 800 × 800 mm region are given in **Table 4.20** and a summary of the spalling and mass loss results for each of the panels are



given in **Table 4.21**. Mass loss was calculated by simply deducting the mass of the panel after fire exposure from the mass of the panel before fire exposure

A metrology scanner, with a resolution of 0.1 mm and accuracy of 0.05 mm was used to obtain the measurements. Upon exposure, it was clearly evident that two of the three panels suffered spalling, where one of which suffered high levels of spalling with reinforcing bars exposed on the fire-exposed surface. It must be noted here that negative readings could indicate drip marks of melted steel or aggregate. **Table 4.22** provides the spalling results as per the above-mentioned criteria

**Table 4.20:** Spalling depths (mm) at every 100 mm from the fire exposed surface\*

Panel 1	0	100	200	300	400	500	600	700	800
0	64.02	53.65	50.69	64.42	71.17	69.55	48.93	45.45	51.33
100	70.68	68.90	78.60	67.77	91.79	83.19	61.38	62.38	63.86
200	69.17	78.48	68.75	83.05	88.29	85.44	82.81	81.01	69.46
300	65.27	77.89	74.56	72.29	99.49	90.84	101.47	90.98	85.25
400	69.45	71.89	81.70	88.68	102.77	83.08	99.90	91.51	64.68
500	61.34	91.53	100.09	94.60	106.82	105.44	104.58	99.14	67.47
600	67.65	85.09	94.44	96.83	115.37	119.05	119.28	95.36	75.97
700	91.15	96.21	103.56	99.25	103.87	86.63	96.05	98.16	94.76
800	87.66	90.19	94.43	77.47	78.71	84.82	81.89	90.08	94.30
Av									83.15
Max									119.28
Panel 2	0	100	200	300	400	500	600	700	800
0	45.60	21.92	37.79	43.18	46.48	29.34	28.56	23.74	21.46
100	40.52	42.95	58.96	49.20	48.02	60.36	45.67	35.57	24.81
200	56.89	66.64	70.51	58.71	63.73	67.47	58.06	42.61	29.80
300	54.69	52.63	48.58	64.90	50.89	52.72	33.70	30.19	21.84
400	30.71	34.96	38.52	41.93	37.67	31.18	24.25	18.11	7.76
500	20.76	25.98	25.43	28.93	19.75	-5.62	14.16	-2.04	3.06
600	10.71	9.44	20.39	19.27	11.99	-5.30	3.79	-2.05	9.62
700	3.76	-0.57	4.82	3.18	1.88	-4.83	10.77	24.09	33.60
800	3.19	-9.27	-9.50	-5.66	8.24	10.66	31.48	39.05	41.46
Av									28.25
Max									70.51
Panel 3	0	100	200	300	400	500	600	700	800
0	6.25	8.10	7.35	3.82	4.63	4.01	-1.58	8.64	-18.67
100	1.02	-2.23	-0.23	2.64	-4.01	5.71	-1.81	10.61	0.59

<b>200</b>	-3.79	5.20	-2.87	-2.53	-2.04	4.91	5.04	-0.58	3.81
<b>300</b>	-13.43	0.80	4.08	3.21	1.88	0.11	-1.24	0.85	2.96
<b>400</b>	-1.65	-5.59	5.34	-4.31	3.85	-4.95	-4.90	0.45	4.37
<b>500</b>	-2.19	-0.61	0.18	-5.15	11.78	8.01	-3.28	-16.18	4.13
<b>600</b>	-2.57	-2.22	-2.56	-1.24	-13.64	3.80	5.44	-3.05	6.62
<b>700</b>	-9.63	2.95	-5.54	-0.62	2.27	-12.00	3.89	-0.62	3.35
<b>800</b>	-0.34	-2.59	-3.19	4.05	-6.36	-0.37	2.24	7.61	3.80
								<b>Av</b>	<b>0.12</b>
								<b>Max</b>	<b>11.78</b>

*\*highlighted are the points in the grid which did not pass the spalling criteria*

**Table 4.21** Summary of the spalling and mass loss results

<b>Panel</b>	<b>Max Spalling Depth</b>	<b>Av Depth</b>	<b>Max Depth</b>	<b>Av Depth</b>	<b>Mass Loss</b>	<b>Mass Loss</b>	<b>Spalling Duration</b>
<b>ID</b>	<b>800 x 800 Region (mm)</b>	<b>800 x 800 Region (mm)</b>	<b>(entire region) (mm)</b>	<b>(entire region) (mm)</b>	<b>kg</b>	<b>%</b>	<b>(mins)</b>
<b>1</b>	124.66	84.28	124.66	54.41	369	12.04	18
<b>2</b>	74.68	31.73	74.68	21.26	183	5.940	12
<b>3</b>	15.66	4.280	15.66	3.400	85.0	2.780	0.0

**Table 4.22:** Spalling results as per the above-mentioned criteria

<b>Panel</b>	<b>Spalling criteria</b>
1	Failed
2	Failed
3	Passed

Visual observations on the spalling behaviour and expulsion of water/steam were also recorded through a furnace endoscope, where still frames from a professional camera were recorded. All significant behaviours which were observed from the specimen and details of the occurrence of the various performance criteria are given in **Table 4.23**.

**Table 4.23:** Some qualitative visual observations during the tests

Time		Approximate furnace temperature	Observations
Min	Sec		
00	00	15°C	Start of test
02	10	874°C	Minor surface spalling is occurring in panels 1 and 2
12	10	1168°C	Panel 2 has stopped spalling
19	20	1300°C	Panel 1 has stopped spalling and reinforcement is visible
64	10	1300°C	Water pooling is observed on unexposed surface of panel 1
69	10	1300°C	Water pooling is observed on unexposed surface of panel 2 and 3
75	10	1300°C	Minor surface melting (dripping) observed in all panels
84	00	1300°C	Water vapour can be seen to gush out from the unexposed surface of the panels
120	10	1300°C	Linear cooling at a rate of 12°C/min has begun
232	10	200°C	End of test

#### 4.13. Water analysis test results

Water pooling has been reported in numerous studies as being a prominent factor governing concrete spalling from the early days of research in this subject area (Guerrieri and Fragomeni, 2016, Guerrieri and Fragomeni, 2019, Kannangara et al., 2022, Jansson and Boström, 2010). The main research question in previous investigations was to pinpoint the source of this water, which evidently pooled on the unexposed surface during heat exposure of the test specimens. In the present study, the extraction of water was achieved after the end of the large-scale tests, where water pooling was observed on the top surface of the panels at different intervals (refer **Table 4.23**). The pooled water was analysed using ICP/OES.

Among the panels which underwent heating, different degrees of resistance to fire were found, hence useful correlations can be drawn up between the degree of spalling and water composition. **Figure 4.67** shows an image of water pooling and expulsion of steam during the fire test. The pooled water was collected using sample containers for analyses inductively coupled plasma–optical emission spectrometry (ICP/OES) as explained in **Section 3.6.8**.



Top – Panel 1, middle – Panel 2, bottom – Panel 3

**Figure 4.67:** Water and steam being expelled from the unexposed surface of the panels (time *ca.* 60 mins)

**Tables 4.24 and 4.25** shows the test results obtained through the water analyses. It was evident from the results that the pooled water contained relatively high levels of calcium with averages (over triplicate measurements) of 23.4, 24.9 and 25.2 ppm for panel 1, panel 2 and panel 3, respectively. This result proves that the pooled water is most likely to forced out from the concrete through the breaking down of the calcium-silicate-hydrate bonds, which is responsible for maintaining the cohesive strength of concretes. This also points towards a noticeable leaching out of  $\text{Ca}^{2+}$  species when the test specimens progressively underwent spalling. However, the concentrations of other species of interest, i.e.,  $\text{Al}^{3+}$ ,  $\text{Fe}^{3+}$  and Si were insignificant ( $\text{Fe}^{3+} \sim 0$ ;  $\text{Si} \sim 0$ ;  $\text{Al}^{3+} < 2.0$ ). This could suggest the oxides of aluminium and iron, which do not have a sheath of water molecules around them or are only

very sparingly soluble in the aqueous phase, are thus less likely to leach out, and that most of the silicon is firmly bound as ‘silicate’ structures in the concrete.

**Table 4.24:** Calcium contents, determined through ICP/OES measurement.

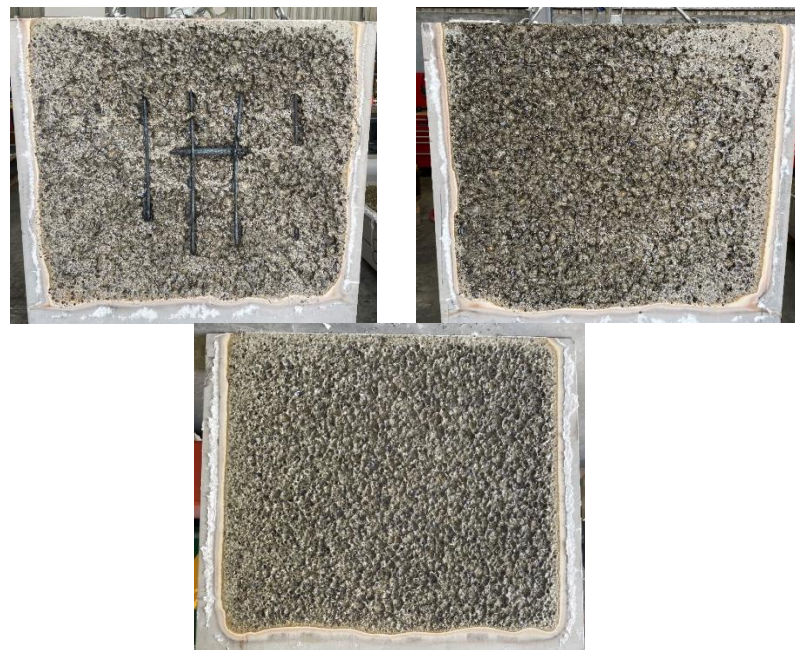
Panel	Ca <sup>2+</sup> ppm	Ca <sup>2+</sup> ppm	Ca <sup>2+</sup> ppm	Ca <sup>2+</sup> (av ppm
1	23.0	23.5	23.7	23.4
2	24.6	25.0	25.1	24.9
3	24.9	25.0	25.7	25.2

**Table 4.25:** Aluminium contents, determined through ICP/OES measurement

Panel	Al <sup>3+</sup> ppm	Al <sup>3+</sup> ppm	Al <sup>3+</sup> ppm	Al <sup>3+</sup> (av) ppm
1	0.908	0.942	0.963	0.938
2	1.590	1.600	1.630	1.610
3	1.550	1.560	1.550	1.550

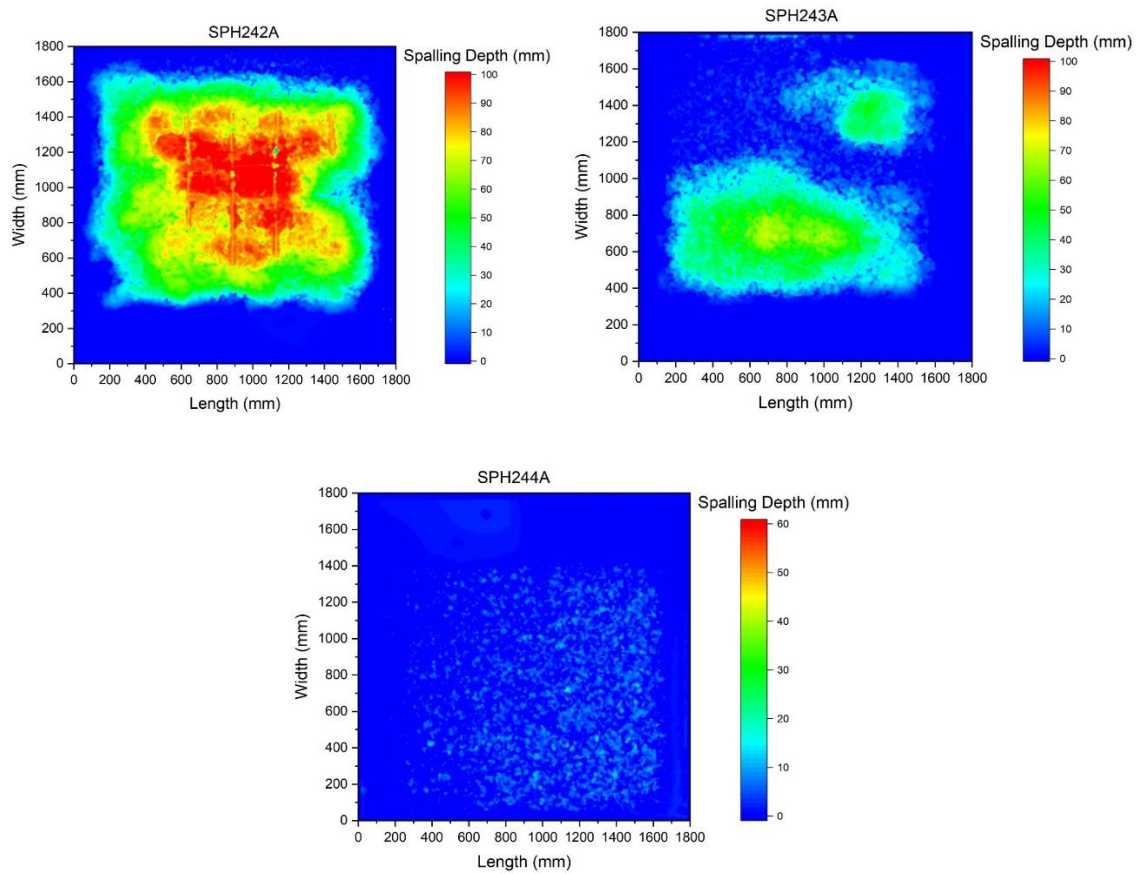
#### 4.14. Post – test spalling assessment of large-scale panels

Upon completion of the fire test, panels were removed from the frame and visually observed for spalling behaviour (**Figure 4.68**). Spalling was also depicted through colour gradation contour map plots (**Figures 4.69**).



Top left – Panel 1, top right – Panel 2, bottom – Panel 3

**Figure 4.68:** Images of the fire exposed surface of the panels after test



Top left – Panel 1, top right – Panel 2, bottom – Panel 3

**Figure 4.69:** A contour plot of Panel 1 after the fire test

It was clearly evident from the results that the panels improved in their fire resistance properties as the loading of PP fibres increased from 1.0 - 2.0 kg/m<sup>3</sup>, with the panel having 1.0 kg/m<sup>3</sup> not only failing under the given spalling criteria but exposing a high area of the reinforcement bars. This can be extremely dangerous in real-life fire scenarios, because steel can start losing its strength at a temperature of around 400°C, and given that the protection provided by the concrete has spalled, the structure is left extremely vulnerable to collapse (Agarwal, 2011, Franssen and Real, 2012). On the other hand, the panel having the highest loading of PP fibres (i.e., panel 3) displayed high resistance to fire with being the only panel which passed the spalling criteria of the test.

#### **4.15. Summary of the main findings**

This chapter depicts the complete results, and subsequent interpretation and discussions obtained through the various test methods which were employed in the study.

Here the morphology, chemical natures, and thermal and calorimetric properties of the raw materials, fibrous fillers, cured powdered samples and heat-treated powdered samples were assessed using appropriate analytical techniques.

In addition, the workability of the wet mixes was assessed. Here, it was clearly evident that all OPC- and FA-based concrete were of a workable state, with the highest slump flow resulting from MD01 which had a w/c ratio of 0.6. MD03, on the other hand, which had the lowest w/c ratio of 0.26, reached workable conditions only with the addition of superplasticizers. Moreover, the FA-based GP concretes were found to be more cohesive in nature compared to the OPC- based mixes. Furthermore, even though the w/c ratios of the MD02 and the GP01 were the same, i.e., 0.45, GP01 mixes recorded higher slump flow readings as compared to the MD02 mixes. The addition of sacrificial agents (PP, cotton and polyester) resulted in drops in the slump flow with the highest drop recorded from mixes having added cotton at 1%.

When considering the density of the mixes, MD03 control specimens proved to be the densest of all specimens with  $2603 \text{ kg/m}^3$  as compared to MD01 control samples of  $2376 \text{ kg/m}^3$ , which was the lowest among the 4 mixes. These results are further verified through the porosity tests conducted using the RCPT and the BET theory, which showed that the MD03 specimens had the lowest recorded porosity and the lowest surface area of pores and pore volume, with a lower pore volume for the smallest pores. The addition of the sacrificial agents was seen to inversely affect the density of the mixes, with increases in the percentage of polymers (from 0.5% – 1.5%), resulting in a decrease in density.

The physical appearance of the cubical samples did not show much change amongst the MD01, MD02, MD03 and GP01 mixes with and without the addition of sacrificial agents. However, a very prominent change in colour was witnessed in the FA-based GP samples after exposure to elevated temperature levels from grey to reddish-brown. Moreover, after exposure to  $400^\circ\text{C}$ , void spaces/ empty grooves were very much visible on the surfaces of the specimens having had 48 mm PP fibres added in during casting.

A majority of the tests were centred around the assessment of the compressive and the residual properties. As expected, MD01 control specimens displayed the lowest average compressive strength reading of approximately 64 MPa, and MD03 controls specimens displayed the highest, of approximately 183 MPa. Both MD02 and GP01 specimens resulted in similar average compressive strength readings. The addition of the sacrificial agents showed a drop in the overall average compressive strength readings in all mixes, with cotton at 1% producing the weakest cubes. However, sacrificial agents were seen to greatly improve the fire resistance properties of the cubes, as seen through the spalling behaviour after exposure to heat. While drops in the initial compressive strengths were witnessed in both the MD01 (18%) and MD02 (16%) specimens after exposure to 400°C, no result could be obtained from the MD03 specimens, due to the explosive condition of the cubes at a temperature of around 350°C. This condition was eliminated with the addition of the sacrificial agents where, in all cases (i.e. addition of PP, cotton and polyester), the cubes remained intact, even after exposing them to a temperature as high as 800°C. Similarly, the testing conducted on the large-scale panels proved that the incorporation of 2 wt.% PP fibres improved the spalling behaviour as per the given spalling criteria in the present work.

Notably, the GP01 specimens showed an improvement in strength after exposure to 400°C, where strength gains of approximately 35% was recorded from the cubical specimens. However, in spite of the above, the strength was seen to drop by about 63% in specimens after exposure to 800°C, i.e. similar to the MD01 and MD02 specimens which resulted in strength drops of about 69% and 65%, respectively.

Compressive strength tests were also conducted on the MD01, MD02 and MD03 cylindrical specimens to gain an understanding of the effect of size on initial strength. Results proved cubical specimen strengths to be approximately twice ( $\times 2.0157$ ) the strength of cylindrical specimens.

Results from the mass loss tests after exposure to high temperature levels showed that the highest average loss in mass originated from the MD01 specimens with approximately 4.7% at 400°C and 7.1% at 800°C, followed by the MD02 specimens. And, while the w/c ratio of the GP01 and MD02 specimens were the same, a lesser loss in mass was witnessed in the GP01 specimens as compared to the MD02 specimens, with approximately 3.1% at 400°C and 4.1% at 800°C for the GP01 specimens, and approximately 4.1% at 400°C and 6.1% at 800°C for the MD02 specimens. Moreover, after the incorporation of sacrificial



agents, an increase in the overall mass loss of the specimens as compared to control cubes, were observed. This was the case for all specimens except for the MD03 specimens which underwent explosive spalling and hence, did not produce a result for control specimens.

It was evident from the carbonation studies that once concrete undergoes carbonation, a reduction in the compressive strengths is witnessed. All specimens resulted in weaker samples after carbonation with the biggest drop in strength of approximately 28 MPa resulting from the MD03 specimens.

Analyses conducted using SANS studies and high-resolution optical microscopy provided strong evidence of the physio-chemical changes within the internal microstructure. The images obtained using SANS studies clearly showed hydrated calcium centres transforming into dehydrated moieties after undergoing heat exposure. This was very much evident in the FA-based GP specimens, where a clear presentation of melting and binding of the mix matrix into a more compact and cohesive structure was shown, as compared with the OPC-based specimens. Moreover, heat-treated GP01 specimens displayed a higher degree of coloured compounds as compared with MD01, MD02 and MD03 specimens as seen on the colour contour maps of the specimens before and after exposure to elevated temperature levels of 300°C.

During the large-scale panel testing, the water which was expelled from the concrete slabs onto the unexposed (top) surface, during heating was analysed using the ICP/OES test apparatus for elemental composition of this pooled water. Results showed high levels of calcium, with average values of 23.4 ppm, 24.9 ppm and 25.2 ppm from panel 1, panel 2 and panel 3, respectively, as compared with aluminium (0.94 ppm, 1.61 ppm and 1.55 ppm from panel 1, panel 2 and panel 3, respectively), and silicon and iron (which resulted in zero composition). This could indicate that the water which is forced out during heating (i.e. pooled water) is indeed from within the broken-down C-S-H strength bonds during heating.

## **CHAPTER 5**

### **CONCLUSIONS AND SUGGESTIONS FOR FUTURE WORK**

## 5.1. Main Conclusions

The various analytical techniques that were employed to evaluate the morphology, chemical natures, and thermal and calorimetric properties of the raw materials, fillers, and samples sourced from both cured and heat-treated products, yielded the relevant and necessary set of empirical data. These included, mainly, high-resolution optical microscopy-SEM/EDS, XRD, Fourier-transform infrared (FT-IR), solid-state NMR, thermogravimetric analysis (TGA), differential scanning calorimetry (DSC) and pyrolysis combustion flow calorimetry (PCFC). A combination of XRD, SEM/EDS, FT-IR and NMR techniques revealed the morphological and structural features of the test samples, whereas the TGA, DSC and PCFC runs measured their thermal and calorimetric attributes.

The basic mix-designs for the FA-based GP concrete samples were obtained through previously published work from our research group, where some preliminary investigations on the spalling behaviours were also carried out. For the OPC-based formulations, i.e. for MD01 and MD02, the standard method of mix design calculations was employed whereas, in the case MD03 the essential mix ratio was adopted in tune with a previously tried version, and subsequently modified through trial and error. All of the chosen mix designs, both in the case of OPC-based and FA-based GP concretes, were found to be quite amenable for the casting of the required test specimens. Samples for the large-scale tests were supplied by commercial firms.

The flow properties of all test specimens were measured using the flow table apparatus in conformance with ASTM 2014 C230/C230M – 14 Standard Specification for Flow Table for Use in Tests of Hydraulic Cement. Here, the flow properties of all mixes were within a workable range with MD01 resulting in the highest flow reading of 193 mm, followed by GP01, MD02 and MD03 readings which were at 173 mm, 155 mm and 118 mm, respectively. This proves that FA- based GP concretes, due to the more spherical and finer structure of the FA compared to OPC, results in better flow properties. The addition of sacrificial agents resulted in a drop in flow properties. This can be attributed with either the agglomerating nature of the fibres which could obstruct the flow properties, or the surface adsorption properties of the fibres which tends to hold water molecules, or both.

The three OPC-based mix designs and the FA-based cubical concrete specimens exhibited varying degrees of spalling behaviours under the set heating regimes. The extents of spalling were primarily gauged through visual observations (i.e. changes in their bulk morphologies). Here FA-based test specimens exhibited the least degree of spalling, if at all, whereas the OPC-based ones, generally were subjected to varying degrees of spalling, which also depending on the maximum temperature of exposure (i.e. 400°C and 800°C). It is to be noted here that MD03 in fact exhibited explosive spalling behaviour even at a temperature around 350°C. The behaviours of the large-scale samples were also evaluated through the in-house built furnace. It is to be noted here that, at a large-scale, the incorporation of commercial-grade PP fibres (at ca. 2 wt.%) effectively prevented spalling as per the specific criteria.

The TGA thermograms of the polymeric components exhibited their overall profiles of thermal degradation, whereas the DSC runs revealed the energetics associated with phase changes, including pyrolysis. The combustion attributes of the polymeric materials were evaluated through PCFC measurements. The relevant combustion parameters favourably compared to those classes of polymers with similar chemical natures/composition. The thermal and calorimetric evaluations of the polymeric components clearly showed that they underwent preferential degradation prior to the onset spalling of the test specimens, thus exhibiting their potential role as ‘sacrificial’ agents. This was particularly true in the case of MD03, which did exhibit explosive spalling even at a higher temperature of 800°C. On the other hand, GP specimens with the incorporation of sacrificial agents displayed only mild cracking and spalling at the corners, as compared to the OPC-based concrete specimens.

Given spalling is mainly manifested through changes in the surface morphology of the test specimens, especially, at the initial stages, the colour/texture of the samples were closely observed. While no significant colour changes were observed among the OPC-based concrete samples even after exposure to 800°C, noticeable colour changes from grey to reddish brown was observed in all the FA-based GP specimens. This could be attributed to the relatively higher levels of iron oxide in the FA and other transition-metal oxides, which can result in the formation of coloured chemical species. The phenomenological evolution of the morphological changes, occurring at the specimens’ surfaces were further followed through high-resolution optical microscopy. Here the necessary optical profilometry studies showed an evolution of surface roughness among the OPC-based concrete samples, where

the susceptibility of the three different mixes to spalling was evident upon heat treatment. FA-based GP specimens on the other hand showed a remarkable discoloration, after the heat treatment, at its surface owing to the formation of iron oxide.

The densities and porosity of selected test specimens were recorded using appropriate methods. These included conventional density measurements, and the porosity of the specimens were gauged through RCPT and BET test methods. The results obtained from the density and porosity measurements did indicate significant variations among the pristine and heat-treated samples, where MD03 specimens recorded the highest density readings. This falls in line with the results regarding the porosity as obtained from the RCPT tests, which also showed that the MD03 specimens had the lowest porosity among all mixes. In addition to this, the BET tests conducted on MD03 specimens indicated the lowest surface area of pores and pore volume compared to other concrete samples. These results clearly indicate that the internal structure of MD03 is very compact, which could restrict the movement of steam during the high heat exposure, thus causing the concrete to undergo excessive spalling. This indeed supports the pore pressure theory being a main underpinning mechanism for spalling of concrete elements.

Given that Ca nucleus is not NMR active, in an attempt to study the chemical environment of calcium-based hydration shells, SANS measurements were conducted on selected samples. Processed images obtained through SANS studies showed that the microstructure of FA-based concrete matrices underwent melting and hardening, thus resulting in the solidification of the internal matrix within the specimen. This provides direct evidence for the higher fire performance of these geopolymer concretes in general. Furthermore, the processed images obtained through SANS studies showed clearly that the MD01 specimens have the highest porosity amongst all the mixes. In addition, upon heat treatment, it was clearly evident that the FA-based GP concrete specimens underwent further polymerization. This has obviously led to a more cohesive internal matrix leading, resulting from an effective amalgamation of the different components within the mix. This also substantiates the enhanced fire resistance properties of the FA-based GP concretes.

Given that carbonation occurs primarily around hydrated Ca-based centres, converting the hydroxide functionalities into carbonates upon the carbonation reaction, it is prudent to study the effect of the extent of carbonation on the spalling behaviours, especially, of OPC-based concrete. The degree of carbonation in the test specimens were primarily gauged

through TGA thermograms obtained from powdered samples. As seen from the TGA thermograms, the effect carbonation on FA- based GP concretes were relatively minor as compared to those based on OPC, with the amount of carbonated domains being significantly lower. This can be due to the polymeric structural feature of GP specimens and the relatively very low concentrations of hydrated calcium centres which allows very minor effects from carbonation.

The results from the large-scale panel tests showed: wide varying degrees of spalling behaviours as indicated through visual inspection of the three-dimensional optical scans, and associated criteria, presumably arising due to the differences in the mix designs and to varying degrees of loadings of PP. Here aliquots of pooled water samples were collected, and these were subjected to elemental analyses using the ICP/OES techniques with view to identifying soluble ions in the leachates. The results showed that the elemental compositional profiles of  $\text{Ca}^{2+}$ ,  $\text{Al}^{3+}$ ,  $\text{Fe}^{3+}$  and Si varied, and in particular, showed relatively large concentrations of  $\text{Ca}^{2+}$  ions, in all cases, presumably originating from the C-S-H domains within the test samples.

With a view to accessing the relevant mechanical properties of the various specimens compressive and residual strength measurements were conducted in accordance with AS 1012.9.2014 - *Methods of testing concrete Method 9: Compressive strength for the determination of the strength tests—Concrete, mortar and grout specimens*. The MD01 cubical specimens were found to exhibit the lowest average compressive strength values, with the MD03 samples achieving ultra-high strengths. Furthermore, generally, the addition of polymeric components was found to result in a drop in values for the initial average compressive strengths of all classes of specimens. When considering the average residual strengths, all OPC-based concrete specimens seem to exhibit a drop in initial strength (for MD03 specimens no measurement could be accomplished as it underwent explosive spalling). However, in the case of the FA-based concrete samples, a residual strength gain was observed after exposure to  $400^{\circ}\text{C}$  as compared to the OPC-based samples. In addition, the effects of specimen size and shape on the compressive strength of control OPC mixes were also studied. The results revealed  $50\text{ mm}^3$  cubical strengths to be higher than that of cylindrical strengths (measuring,  $200\text{ mm} \times 100\text{ mm}$ ) by a factor of approximately 2.

## **5.2. Some suggestions for future work**

Even though some elements the basic physio-chemical process(es) underpinning the phenomenon of spalling were identified, through limited correlations of different test data obtained from the current study, the following points can be identified as suggestions for future work:

1. Conduct extended investigations with a view to obtaining better correlation between compressive strengths of cubical and standard cylindrical samples
2. Gauging the spalling behaviour of cylindrical samples including those with varying amounts the sacrificial agents
3. Assessment of spalling behaviour of the control mixes under large-scale test, and the analyses of the pooled water using ICP/OES
4. Accelerated weathering test (i.e. carbonation assessments) on samples containing the sacrificial agents
5. Completion of porosity tests (BET and RCPT measurements) for heat exposed samples with and without the addition of sacrificial agents
6. Computation of Arrhenius parameters from TGA thermograms
7. Extended analytical correlation(s) of the additional test data with a view to gaining more insights into the underpinning physio-chemical properties of spalling phenomenon at a molecular level in case of the cylindrical and large-scale specimens
8. Improve the compatibility of cotton and polyester fibres, preferably sourced through recycled textile waste, by surface pre-treatment with reactive agents, such as, silica fumes, metakaolin, etc. This is also expected result in materials with improved compressive strength

## **REFERENCES**



- ABD RAZAK, S. N., SHAFIQ, N., NIKBAKHT, E. H., MOHAMMED, B. S., GUILLAUMAT, L. & FARHAN, S. A. 2022. Fire performance of fly-ash-based geopolymer concrete: Effect of burning temperature on mechanical and microstructural properties. *Materials Today: Proceedings*, 66, 2665-2669.
- ABDULKAREEM, O. A., AL BAKRI, A. M., KAMARUDIN, H., NIZAR, I. K. & ALA'EDDIN, A. S. 2014. Effects of elevated temperatures on the thermal behavior and mechanical performance of fly ash geopolymer paste, mortar and lightweight concrete. *Construction and building materials*, 50, 377-387.
- ABID, M., HOU, X., ZHENG, W. & HUSSAIN, R. R. 2017. High temperature and residual properties of reactive powder concrete—A review. *Construction and Building Materials*, 147, 339-351.
- AÇIKGENÇ, M., ARAZSU, U. & ALYAMAÇ, K. 2012. Strength and durability properties of polypropylene fiber-reinforced concrete with different mixture proportions. *SDU International Journal of Technological Sciences*, 4, 41-44.
- AFROUGHSABET, V. & OZBAKKALOGLU, T. 2015. Mechanical and durability properties of high-strength concrete containing steel and polypropylene fibers. *Construction and building materials*, 94, 73-82.
- AGARWAL, A. 2011. Stability behavior of steel building structures in fire conditions. Purdue University.
- AGRA, R. R., SERAFINI, R. & DE FIGUEIREDO, A. D. 2021. Effect of high temperature on the mechanical properties of concrete reinforced with different fiber contents. *Construction and Building Materials*, 301, 124242.
- AKRAM, T., MEMON, S. A. & AKRAM, R. Utilization of Fly Ash as High Volume Replacement of Cement. International conference on advances in cement based materials and applications in civil infrastructure ACBM-ACI, Lahore, Pakistan, 2007.
- ALDRIDGE, L., BERTRAM, W., SABINE, T., BUKOWSKI, J., YOUNG, J. & HEENAN, R. 1994. Small-angle neutron scattering from hydrated cement pastes. *MRS Online Proceedings Library (OPL)*, 376, 471.
- ALEEM, M. A. & ARUMAIRAJ, P. 2012. Geopolymer concrete—a review. *International journal of engineering sciences & emerging technologies*, 1, 118-122.

- ALEHYEN, S., ZERZOURI, M., ELALOUANI, M., EL ACHOURI, M. & TAIBI, M. 2017. Porosity and fire resistance of fly ash based geopolymer. *Journal of Materials and Environmental Sciences*, 9, 3676-3689.
- ALI, A. M., SANJAYAN, J. & GUERRIERI, M. 2017. Performance of geopolymer high strength concrete wall panels and cylinders when exposed to a hydrocarbon fire. *Construction and Building Materials*, 137, 195-207.
- ALI, F. 2002. Is high strength concrete more susceptible to explosive spalling than normal strength concrete in fire? *Fire and Materials*, 26, 127-130.
- ALI, F., O'CONNOR, D. & ABU-TAIR, A. 2001. Explosive spalling of high-strength concrete columns in fire. *Magazine of Concrete Research*, 53, 197-204.
- ALLEN, A., WINDSOR, C., RAINEY, V., PEARSON, D., DOUBLE, D. & ALFORD, N. M. 1982. A small-angle neutron scattering study of cement porosities. *Journal of Physics D: Applied Physics*, 15, 1817.
- AMRAN, M., HUANG, S.-S., ONAIZI, A. M., MURALI, G. & ABDELGADER, H. S. 2022. Fire spalling behavior of high-strength concrete: A critical review. *Construction and Building Materials*, 341, 127902.
- ANAND, S., VRAT, P. & DAHIYA, R. 2006. Application of a system dynamics approach for assessment and mitigation of CO<sub>2</sub> emissions from the cement industry. *Journal of environmental management*, 79, 383-398.
- ASPIRAS, F. & MANALO, J. 1995. Utilization of textile waste cuttings as building material. *Journal of materials processing technology*, 48, 379-384.
- ASTM 2014. C230/C230M – 14 Standard Specification for Flow Table for Use in Tests of Hydraulic Cement. ASTM.
- AYGÖRMEZ, Y., CANPOLAT, O., AL-MASHHADANI, M. M. & UYSAL, M. 2020. Elevated temperature, freezing-thawing and wetting-drying effects on polypropylene fiber reinforced metakaolin based geopolymer composites. *Construction and Building Materials*, 235, 117502.
- BABALOLA, O., AWOYERA, P. O., LE, D.-H. & ROMERO, L. B. 2021. A review of residual strength properties of normal and high strength concrete exposed to elevated temperatures: Impact of materials modification on behaviour of concrete composite. *Construction and Building Materials*, 296, 123448.
- BAE, S., MERAL, C., OH, J.-E., MOON, J., KUNZ, M. & MONTEIRO, P. J. 2014. Characterization of morphology and hydration products of high-volume fly ash paste

- by monochromatic scanning x-ray micro-diffraction ( $\mu$ -SXRD). Cement and concrete research, 59, 155-164.
- BAKHAREV, T. 2006. Thermal behaviour of geopolymers prepared using class F fly ash and elevated temperature curing. Cement and Concrete Research, 36, 1134-1147.
- BAKRI, A., KAMARUDIN, H., BINHUSSAIN, M., NIZAR, I. K., RAFIZA, A. & ZARINA, Y. 2013. Comparison of geopolymer fly ash and ordinary portland cement to the strength of concrete. Advanced Science Letters, 19, 3592-3595.
- BARRET 1854. On the French and other methods of constructing iron floors. Civil Engineering and Architect's Journal, XVII, 94.
- BARTULOVIĆ, B., JURADIN, S., ŽIŽIĆ, D. & MRAKOVČIĆ, S. Possibility of Using Cotton Knitted Fabric Waste in Concrete. IOP Conference Series: Materials Science and Engineering, 2021. IOP Publishing, 022074.
- BAŽANT, Z. & CUSATIS, G. Concrete creep at high temperature and its interaction with fracture: recent progress. Creep, shrinkage and durability of concrete and concrete structures, 2005.
- BEHERA, G. C., PANDA, S. & KANDA, P. Effect of Length of Fibers on Mechanical Properties of Normal Strength Concrete. IOP Conference Series: Materials Science and Engineering, 2020. IOP Publishing, 012020.
- BENTZ, D. P. 2000. Fibers, percolation, and spalling of high-performance concrete. Materials Journal, 97, 351-359.
- BRAHAMMAJI, G. & MUTHYALU, P. V. 2015. A study on performance of Fly Ash Based Geopolymer concrete in Chemical Atmosphere. International Journal of Advances in Engineering & Technology, 8, 574.
- BRUNAUER, S., EMMETT, P. H. & TELLER, E. 1938. Adsorption of gases in multimolecular layers. Journal of the American chemical society, 60, 309-319.
- BUI, N. K., SATOMI, T. & TAKAHASHI, H. 2018. Effect of mineral admixtures on properties of recycled aggregate concrete at high temperature. Construction and Building Materials, 184, 361-373.
- C1202-09, A. Standard Test Method for Electrical Indication of Concrete's Ability to Resist Chloride Ion Penetration. ASTM C1202-09.
- CANBAZ, M. 2014. The effect of high temperature on reactive powder concrete. Construction and Building Materials, 70, 508-513.

- CARRÉ, H., PIMIENTA, P., LA BORDERIE, C., PEREIRA, F. & MINDEGUIA, J.-C. Effect of compressive loading on the risk of spalling. MATEC Web of Conferences, 2013. EDP Sciences, 01007.
- CHAN, Y.-W. & CHU, S.-H. 2004. Effect of silica fume on steel fiber bond characteristics in reactive powder concrete. Cement and Concrete Research, 34, 1167-1172.
- CHAN, Y., PENG, G. & ANSON, M. 1999. Residual strength and pore structure of high-strength concrete and normal strength concrete after exposure to high temperatures. Cement and concrete composites, 21, 23-27.
- CHAPMAN, D. & ENGLAND, G. 1977. Effects of moisture migration on shrinkage, pore pressure and other concrete properties.
- CHAUHAN, A. & CHAUHAN, P. 2015. Usage of powder XRD technique for material characterization and analysis of Portland cement. J. Anal. Bioanal. Tech., 6, 1-3.
- CHEN, B. & LIU, J. 2004. Residual strength of hybrid-fiber-reinforced high-strength concrete after exposure to high temperatures. Cement and Concrete Research, 34, 1065-1069.
- CHEN, X.-T., ROUGELOT, T., DAVY, C. A., CHEN, W., AGOSTINI, F., SKOCZYLAS, F. & BOURBON, X. 2009a. Experimental evidence of a moisture clog effect in cement-based materials under temperature. Cement and Concrete Research, 39, 1139-1148.
- CHEN, Y.-H., CHANG, Y.-F., YAO, G. C. & SHEU, M.-S. 2009b. Experimental research on post-fire behaviour of reinforced concrete columns. Fire safety journal, 44, 741-748.
- CHOE, G., KIM, G., YOON, M., HWANG, E., NAM, J. & GUNCUNSKI, N. 2019. Effect of moisture migration and water vapor pressure build-up with the heating rate on concrete spalling type. Cement and Concrete Research, 116, 1-10.
- CLARK, J. 2006. Concrete Society. UK, regarding reduced density.
- COGEN, J. M., LIN, T. S. & LYON, R. E. 2009. Correlations between pyrolysis combustion flow calorimetry and conventional flammability tests with halogen-free flame retardant polyolefin compounds. Fire and Materials: An International Journal, 33, 33-50.
- CONNOLLY, R. J. 1995. The spalling of concrete in fires. Aston University.
- COOK, G. 2009. Climate Change and the Cement Industry. Climate Strategies, Cambridge, UK [available at [www.climatestrategies.org](http://www.climatestrategies.org)].

- D7309, A. 2021. Standard Test Method for Determining Flammability Characteristics of Plastics and Other Solid Materials Using Microscale Combustion Calorimetry. ASTM D7309.
- DAVIDOVITS, J. Properties of geopolymer cements. First international conference on alkaline cements and concretes, 1994. 131-149.
- DAVIDOVITS, J. Environmentally driven geopolymer cement applications. Proceedings of 2002 Geopolymer Conference. Melbourne. Australia, 2002a.
- DAVIDOVITS, J. years of successes and failures in geopolymer applications. Market trends and potential breakthroughs. Geopolymer 2002 conference, 2002b. Geopolymer Institute Saint-Quentin, France; Melbourne, Australia, 29.
- DAVIDOVITS, J. 2008a. Geopolymer chemistry and applications, Geopolymer Institute.
- DAVIDOVITS, J. 2008b. Geopolymer chemistry and applications. 2008. Saint Quentin: Geopolymer Institute.
- DAVIDOVITS, J. 2013. Geopolymer cement. A review. Geopolymer Institute, Technical papers, 21, 1-11.
- DAVIDOVITS, J. 2015. False values on CO<sub>2</sub> emission for geopolymer cement/concrete published in scientific papers. Technical paper, 24, 1-9.
- DE MATOS, P., NETO, J. A., SAKATA, R., KIRCHHEIM, A., RODRÍGUEZ, E. & CAMPOS, C. 2022. Strategies for XRD quantitative phase analysis of ordinary and blended Portland cements. Cement and Concrete Composites, 131, 104571.
- DEB, P., MORADKHANI, H., ABBASZADEH, P., KIEM, A. S., ENGSTRÖM, J., KEELLINGS, D. & SHARMA, A. 2020. Causes of the widespread 2019–2020 Australian bushfire season. Earth's Future, 8, e2020EF001671.
- DEBICKI, G., HANICHE, R. & DELHOMME, F. 2012. An experimental method for assessing the spalling sensitivity of concrete mixture submitted to high temperature. Cement & Concrete Composites, 34, 958-963.
- DEENY, S., STRATFORD, T., DHAKAL, R., MOSS, P. & BUCHANAN, A. 2008. Spalling of concrete: Implications for structural performance in fire.
- DESHPANDE, A. A., KUMAR, D. & RANADE, R. 2019. Influence of high temperatures on the residual mechanical properties of a hybrid fiber-reinforced strain-hardening cementitious composite. Construction and Building Materials, 208, 283-295.
- DHARAN, D. S. & LAL, A. 2016. Study the effect of polypropylene fiber in concrete. International Research Journal of Engineering and Technology, 3, 616-619.

- DODDS, L. 2013. Microstructure characterisation of ordinary Portland cement composites for the immobilisation of nuclear waste. The University of Manchester (United Kingdom).
- DU, Y., QI, H.-H., HUANG, S.-S. & LIEW, J. R. 2020. Experimental study on the spalling behaviour of ultra-high strength concrete in fire. *Construction and Building Materials*, 258, 120334.
- DÜĞENCI, O., HAKTANIR, T. & ALTUN, F. 2015. Experimental research for the effect of high temperature on the mechanical properties of steel fiber-reinforced concrete. *Construction and Building Materials*, 75, 82-88.
- DUNUWEERA, S. & RAJAPAKSE, R. 2018. Cement types, composition, uses and advantages of nanocement, environmental impact on cement production, and possible solutions. *Advances in Materials Science and Engineering*, 2018, 4158682.
- DURASTANTI, C. & MORETTI, L. 2020. Environmental impacts of cement production: A statistical analysis. *Applied Sciences*, 10, 8212.
- DUXSON, P., FERNÁNDEZ-JIMÉNEZ, A., PROVIS, J. L., LUKEY, G. C., PALOMO, A. & VAN DEVENTER, J. 2007a. Geopolymer technology: the current state of the art. *Journal of Materials Science*, 42, 2917-2933.
- DUXSON, P., FERNÁNDEZ-JIMÉNEZ, A., PROVIS, J. L., LUKEY, G. C., PALOMO, A. & VAN DEVENTER, J. S. 2007b. Geopolymer technology: the current state of the art. *Journal of materials science*, 42, 2917-2933.
- DUXSON, P., LUKEY, G. C. & VAN DEVENTER, J. S. 2007c. Physical evolution of Na-geopolymer derived from metakaolin up to 1000 C. *Journal of Materials Science*, 42, 3044-3054.
- DWAIKAT, M. & KODUR, V. 2010. Fire induced spalling in high strength concrete beams. *Fire technology*, 46, 251.
- EIDAN, J., RASOOLAN, I., REZAEIAN, A. & POORVEIS, D. 2019. Residual mechanical properties of polypropylene fiber-reinforced concrete after heating. *Construction and Building Materials*, 198, 195-206.
- ELFALEH, I., ABBASSI, F., HABIBI, M., AHMAD, F., GUEDRI, M., NASRI, M. & GARNIER, C. 2023. A comprehensive review of natural fibers and their composites: an eco-friendly alternative to conventional materials. *Results in Engineering*, 101271.

- ENGLAND, G. & KHOYLOU, N. 1995. Moisture flow in concrete under steady state non-uniform temperature states: experimental observations and theoretical modelling. *Nuclear Engineering and Design*, 156, 83-107.
- EXCHANGE, T. 2018. Preferred Fiber and Materials Market Report [Online]. 2019.
- FAIYADH, F. & AL-AUSI, M. 1989. Effect of elevated temperature on splitting tensile strength of fibre concrete. *International Journal of Cement Composites and Lightweight Concrete*, 11, 175-178.
- FARAGE, M., SERCOMBE, J. & GALLE, C. 2003. Rehydration and microstructure of cement paste after heating at temperatures up to 300 C. *Cement and Concrete Research*, 33, 1047-1056.
- FAROUG, F., SZWABOWSKI, J. & WILD, S. 1999. Influence of superplasticizers on workability of concrete. *Journal of materials in civil engineering*, 11, 151-157.
- FLOWER, D. J. & SANJAYAN, J. G. 2007. Green house gas emissions due to concrete manufacture. *The international Journal of life cycle assessment*, 12, 282-288.
- FRANSSEN, J.-M. & REAL, P. V. 2012. *Fire Design of Steel Structures: Eurocode 1: Actions on structures; Part 1-2: General actions--Actions on structures exposed to fire; Eurocode 3: Design of steel structures; Part 1-2: General rules--Structural fire design*, John Wiley & Sons.
- FU, Y. & LI, L. 2011. Study on mechanism of thermal spalling in concrete exposed to elevated temperatures. *Materials and structures*, 44, 361-376.
- GAN, M. 1997. *Cement and concrete*, CRC Press.
- GARBE, U., RANDALL, T., HUGHES, C., DAVIDSON, G., PANGELIS, S. & KENNEDY, S. 2015. A new neutron radiography/tomography/imaging station DINGO at OPAL. *Physics Procedia*, 69, 27-32.
- GEE, B. M., BEVITT, J. J., GARBE, U. & REISZ, R. R. 2019. New material of the 'microsaur' *Llistrofus* from the cave deposits of Richards Spur, Oklahoma and the paleoecology of the Hapsidopareiidae. *PeerJ*, 7, e6327.
- GERASIMIDIS, S., CIVJAN, S. & MENZ, N. 2021. *Post-Fire Damage Assessment of Concrete Structures - Final Report*. University of Massachusetts Amherst.
- GHOSH, R., LAHOTI, M. & SHAH, B. 2022. A succinct review on the use of NMR spectroscopy in monitoring hydration, strength development, and inspection of concrete. *Materials Today: Proceedings*, 61, 167-173.

- GOLD, S. 2000. An investigation into the effects of polypropylene fibres on certain properties of reinforced concrete", Ready Mixed Concrete, p. 2.
- GONG, F., JIANG, X., GAMIL, Y., IFTIKHAR, B. & THOMAS, B. S. 2023. An overview on spalling behavior, mechanism, residual strength and microstructure of fiber reinforced concrete under high temperatures. *Frontiers in Materials*, 10, 1258195.
- GONI, S., GUERRERO, A., LUXÁN, M. & MACÍAS, A. 2003. Activation of the fly ash pozzolanic reaction by hydrothermal conditions. *Cement and Concrete Research*, 33, 1399-1405.
- GONNERMAN, H. F. 1925. Effect of size and shape of test specimen on compressive strength of concrete, Structural materials research laboratory.
- GOURLEY, J. & JOHNSON, G. Developments in geopolymer precast concrete. World Congress Geopolymer, 2005. 139-143.
- GREY, H. & CANTER, L. 2011. Plants environmental impact assessments for cement plants,(May).
- GRIFFIN, R. 1987. CO<sub>2</sub> Release from Cement Production 1950-1985. Institute for Energy Analysis, Oak Ridge Associated Universities, Oak Ridge, Tenn., USA In G. Marland et al.(1989), Estimates of CO<sub>2</sub>, 2.
- GROEN, J. C., PEFFER, L. A. & PÉREZ-RAMÍREZ, J. 2003. Pore size determination in modified micro-and mesoporous materials. Pitfalls and limitations in gas adsorption data analysis. *Microporous and mesoporous materials*, 60, 1-17.
- GUERRIERI, M. 2008. Fire Performance of Alkali Activated Slag and Geopolymers. PhD, Monash University.
- GUERRIERI, M. 2009. Fire Performance of Alkali Activated Slag and Geopolymers. Monash University.
- GUERRIERI, M. & FRAGOMENI, S. 2010. Spalling of normal strength concrete walls in fire. *Structures in Fire - Proceedings of the Sixth International Conference, SiF'10*, 301-311.
- GUERRIERI, M. & FRAGOMENI, S. 2016. Mechanisms of spalling of concrete panels of different geometry in hydrocarbon fire. *Journal of Materials in Civil Engineering*, 28, 04016164.
- GUERRIERI, M. & FRAGOMENI, S. 2019. Spalling of large-scale walls exposed to a hydrocarbon fire. *Journal of Materials in Civil Engineering*, 31, 04019249.



- GUERRIERI, M., SANABRIA, C., LEE, W. M., PAZMINO, E. & PATEL, R. 2020. Design of the metro tunnel project tunnel linings for fire testing. *Structural Concrete*, 21, 2452-2480.
- GUERRIERI, M. & SANJAYAN, J. G. 2010. Behavior of combined fly ash/slag-based geopolymers when exposed to high temperatures. *Fire and Materials: An International Journal*, 34, 163-175.
- GUPTA, R., TOMAR, A. S., MISHRA, D. & SANGHI, S. K. 2020. Multinuclear MAS NMR Characterization of Fly-Ash-Based Advanced Sodium Aluminosilicate Geopolymer: Exploring Solid-State Reactions. *ChemistrySelect*, 5, 4920-4927.
- HAGEN, B. C., FRETTE, V., KLEPPE, G. & ARNTZEN, B. J. 2011. Onset of smoldering in cotton: Effects of density. *Fire Safety Journal*, 46, 73-80.
- HAMADA, H. M., SHI, J., AL JAWAHERY, M. S., MAJDI, A., YOUSIF, S. T. & KAPLAN, G. 2023. Application of natural fibres in cement concrete: A critical review. *Materials Today Communications*, 35, 105833.
- HAN, C. G., HAN, M. C. & HEO, Y. S. 2009. Improvement of residual compressive strength and spalling resistance of high-strength RC columns subjected to fire. *Construction and Building Materials*, 23, 107-116.
- HAQ, E. U., PADMANABHAN, S. K. & LICCIULLI, A. 2014. In-situ carbonation of alkali activated fly ash geopolymer. *Construction and Building Materials*, 66, 781-786.
- HARDJITO, D. 2005. Studies on Fly Ash-Based Geopolymer Concrete
- HARDJITO, D. & RANGAN, B. V. 2005. Development and properties of low-calcium fly ash-based geopolymer concrete.
- HARDJITO, D., WALLAH, S., SUMAJOUW, D. & RANGAN, B. Introducing fly ash-based geopolymer concrete: manufacture and engineering properties. 30th Conference on our World in Concrete and Structures, 2005. 23-4.
- HARDJITO, D., WALLAH, S. E., SUMAJOUW, D. M. & RANGAN, B. V. 2004a. On the development of fly ash-based geopolymer concrete. *Materials Journal*, 101, 467-472.
- HARDJITO, D., WALLAH, S. E., SUMAJOUW, D. M. & RANGAN, B. V. 2004b. On the development of fly ash-based geopolymer concrete. *ACI Materials Journal-American Concrete Institute*, 101, 467-472.
- HARMATHY, T. 1965. Effect of moisture on the fire endurance of building elements. Moisture in materials in relation to fire tests. ASTM International.

- HASENJÄGER, S. 1935. Ueber das Verhalten des Betons und Eisenbetons im Feuer und die Ausbildung von Dehnungsfugen im Eisenbetonbau.
- HASSAN, A., ARIF, M. & SHARIQ, M. 2020. Mechanical behaviour and microstructural investigation of geopolymer concrete after exposure to elevated temperatures. *Arabian Journal for Science and Engineering*, 45, 3843-3861.
- HÄUBLER, F., HEMPEL, M. & BAUMBACH, H. 1997. Long-time monitoring of the microstructural change in hardening cement paste by SANS. *Advances in cement research*, 9, 139-147.
- HEDAYATI, M., SOFI, M., MENDIS, P. & NGO, T. 2015. A comprehensive review of spalling and fire performance of concrete members. *Electronic journal of structural engineering*, 15, 8-34.
- HERTZ, K. 1984. Heat induced explosion of dense concretes. Report 166. CIB W14/84/33 (DK). Institute of Building Design (now Department of Civil ....
- HERTZ, K. D. 2003. Limits of spalling of fire-exposed concrete. *Fire Safety Journal*, 38, 103-116.
- HERTZ, K. D. & SORENSEN, L. S. 2005. Test method for spalling of fire exposed concrete. *Fire Safety Journal*, 40, 466-476.
- HONG, S., JIANG, R., ZHENG, F., FAN, S. & DONG, B. 2022. Quantitative characterization of carbonation of cement-based materials using X-ray imaging. *Cement and Concrete Composites*, 134, 104794.
- HORGNIES, M., CHEN, J. & BOUILLON, C. 2013. Overview about the use of Fourier transform infrared spectroscopy to study cementitious materials. *WIT Trans. Eng. Sci*, 77, 251-262.
- HU, C.-F., LI, L. & LI, Z. 2022. Effect of fiber factor on the workability and mechanical properties of polyethylene fiber-reinforced high toughness geopolymers. *Ceramics International*, 48, 10458-10471.
- HUISMANN, S., KORZEN, M., WEISE, F. & MENG, B. Concrete spalling due to fire exposure and the influence of polypropylene fibres on microcracking. 2nd International RILEM Workshop on Concrete Spalling due to Fire Exposure, 2011. RILEM Publications SARL, 327-336.
- HUN, S., LEE, S. & SUGAHARA, S. 2005. Spalling prevention measures of high performance concrete. *Magazine of the Korea Concrete Institute*, 17, 33-39.

- HUSSIN, M., BHUTTA, M., AZREEN, M., RAMADHANSYAH, P. & MIRZA, J. 2015. Performance of blended ash geopolymer concrete at elevated temperatures. *Materials and Structures*, 48, 709-720.
- IBRAHIM, Y. A., HASAN, A. H. & MAROOF, N. R. 2019. Effects of polypropylene fiber content on strength and workability properties of concrete. *Polytechnic Journal*, 9, 3.
- ICHIKAWA, Y. 2000. Predictions of pressures, heat and moisture transfer leading to spalling of concrete in fire. PhD Thesis, Imperial Collage, London, Great Britain.
- INITIATIVE, C. 2009. Buildings and climate change.
- IQBAL, H. W., KHUSHNOOD, R. A., BALOCH, W. L., NAWAZ, A. & TUFAIL, R. F. 2020. Influence of graphite nano/micro platelets on the residual performance of high strength concrete exposed to elevated temperature. *Construction and Building Materials*, 253, 119029.
- ISMAIL, M. H., MEGAT JOHARI, M. A., ARIFFIN, K. S., JAYA, R. P., WAN IBRAHIM, M. H. & YUGASHINI, Y. 2022. [Retracted] Performance of High Strength Concrete Containing Palm Oil Fuel Ash and Metakaolin as Cement Replacement Material. *Advances in Civil Engineering*, 2022, 6454789.
- JANSSENS, M. 2024. Material Flammability Measurements and Test Methods. Fire Retardancy of Polymeric Materials. CRC Press.
- JANSSON, R. 2008. Material properties related to fire spalling of concrete, Division of Building Materials, Lund Institute of Technology, Lund University.
- JANSSON, R. 2013a. Fire spalling of concrete – A historical overview. *MATEC Web of Conferences*, 6, 01001.
- JANSSON, R. 2013b. Fire Spalling of Concrete: Theoretical and Experimental Studies. PhD PhD, KTH.
- JANSSON, R. & BOSTRÖM, L. Fire spalling—the moisture effect. 1st International workshop on concrete fire spalling due to fire exposure, 2009.
- JANSSON, R. & BOSTRÖM, L. 2010. The influence of pressure in the pore system on fire spalling of concrete. *Fire technology*, 46, 217-230.
- JANSSON, R. & BOSTRÖM, L. Fire spalling of concrete—A re-assessment of test data. *Proceedings of the 8th international conference on structures in fire—SiF*, 2014. 297-304.

- JANSSON, R. B., L 2015. Three experiments to validate basic functions in fire spalling models. The 4th International RILEM Workshop on Concrete Spalling due to Fire Exposure. Leipzig, Germany.
- JOLLY, W. M., COCHRANE, M. A., FREEBORN, P. H., HOLDEN, Z. A., BROWN, T. J., WILLIAMSON, G. J. & BOWMAN, D. M. 2015. Climate-induced variations in global wildfire danger from 1979 to 2013. *Nature communications*, 6, 1-11.
- JOSEPH, P., JOSEPH, K., THOMAS, S., PILLAI, C., PRASAD, V., GROENINCKX, G. & SARKISSOVA, M. 2003. The thermal and crystallisation studies of short sisal fibre reinforced polypropylene composites. *Composites Part A: Applied Science and Manufacturing*, 34, 253-266.
- KALIFA, P., CHENE, G. & GALLE, C. 2001. High-temperature behaviour of HPC with polypropylene fibres: From spalling to microstructure. *Cement and concrete research*, 31, 1487-1499.
- KALIFA, P., MENNETEAU, F.-D. & QUENARD, D. 2000. Spalling and pore pressure in HPC at high temperatures. *Cement and concrete research*, 30, 1915-1927.
- KANAN, A. H., MARINE, S. S., RAIHAN, F., REDOWAN, M. & MIAH, M. 2014. Textile effluents changes physiochemical parameters of water and soil: Threat for agriculture. *African Journal of Agronomy*, 2, 219-223.
- KANG, J., YOON, H., KIM, W., KODUR, V., SHIN, Y. & KIM, H. 2016. Effect of Wall Thickness on Thermal Behaviors of RC Walls Under Fire Conditions. *International Journal of Concrete Structures and Materials*, 10, 19-31.
- KANNANGARA, A. 2018. The Behaviour of Reactive Powder Geopolymer Concrete at Elevated Temperature. Victoria University.
- KANNANGARA, T., GUERRIERI, M., FRAGOMENI, S. & JOSEPH, P. 2021a. Effects of Initial Surface Evaporation on the Performance of Fly Ash-Based Geopolymer Paste at Elevated Temperatures. *Applied Sciences*, 12, 364.
- KANNANGARA, T., GUERRIERI, M., FRAGOMENI, S. & JOSEPH, P. 2021b. A Study of the Residual Strength of Reactive Powder-Based Geopolymer Concrete under Elevated Temperatures. *Applied Sciences*, 11, 11834.
- KANNANGARA, T., JOSEPH, P., FRAGOMENI, S. & GUERRIERI, M. 2022. Existing theories of concrete spalling and test methods relating to moisture migration patterns upon exposure to elevated temperatures—A review. *Case Studies in Construction Materials*, 16, e01111.

- KANT, R. 2011. Textile dyeing industry an environmental hazard.
- KAUR, P. & TALWAR, M. 2017. Different types of Fibres used in FRC. *International Journal of Advanced Research in Computer Science*, 8.
- KHALIQ, W. & KODUR, V. 2012. High Temperature Mechanical Properties of High-Strength Fly Ash Concrete with and without Fibers. *ACI Materials Journal*, 109.
- KHONGPROM, P., CHAMPANOI, S. & SUWANMANEE, U. 2020. An Input-Output Approach for Environmental Life Cycle Assessment of Cement Production. *CET Journal-Chemical Engineering Transactions*, 81.
- KHOURY, G. 2008. Polypropylene fibres in heated concrete. Part 2: Pressure relief mechanisms and modelling criteria. *Magazine of concrete research*, 60, 189-204.
- KHOURY, G. A. 2000. Effect of fire on concrete and concrete structures. *Progress in structural engineering and materials*, 2, 429-447.
- KHOYLOU, N. 1997. Modelling of moisture migration and spalling behaviour in non-uniformly heated concrete.
- KODUR, V. 2000. Spalling in high strength concrete exposed to fire: concerns, causes, critical parameters and cures. *Advanced Technology in Structural Engineering*.
- KODUR, V. 2014. Properties of concrete at elevated temperatures. *International Scholarly Research Notices*, 2014, 468510.
- KODUR, V. & PHAN, L. 2007. Critical factors governing the fire performance of high strength concrete systems. *Fire safety journal*, 42, 482-488.
- KODUR, V. K. R. & SULTAN, M. A. 1998. Structural behaviour of high strength concrete columns exposed to fire.
- KONG, D. L. & SANJAYAN, J. G. 2010. Effect of elevated temperatures on geopolymer paste, mortar and concrete. *Cement and concrete research*, 40, 334-339.
- KRZEMIENÍ, K. & HAGER, I. 2015. Assessment of concrete susceptibility to fire spalling: A report on the state-of-the-art in testing procedures. *Procedia Engineering*, 108, 285-292.
- KUSHNIR, A. R., HEAP, M. J., GRIFFITHS, L., WADSWORTH, F. B., LANGELLA, A., BAUD, P., REUSCHLÉ, T., KENDRICK, J. E. & UTLEY, J. E. 2021. The fire resistance of high-strength concrete containing natural zeolites. *Cement and Concrete Composites*, 116, 103897.
- KUTCHKO, B. G. & KIM, A. G. 2006. Fly ash characterization by SEM–EDS. *Fuel*, 85, 2537-2544.

- LALU, O., DARMON, R. & LENNON, T. Spalling of high strength concrete in fire. IOP conference series: Materials science and engineering, 2021. IOP Publishing, 012027.
- LATIFI, M. R., BIRICIK, Ö. & MARDANI AGHABAGLOU, A. 2022. Effect of the addition of polypropylene fiber on concrete properties. *Journal of Adhesion Science and Technology*, 36, 345-369.
- LAU, A. & ANSON, M. 2006. Effect of high temperatures on high performance steel fibre reinforced concrete. *Cement and concrete research*, 36, 1698-1707.
- LAW, D. W., ADAM, A. A., MOLYNEAUX, T. K., PATNAIKUNI, I. & WARDHONO, A. 2015. Long term durability properties of class F fly ash geopolymer concrete. *Materials and Structures*, 48, 721-731.
- LEE, W. M., FRAGOMENI, S., MONCKTON, H. & GUERRIERI, M. 2023. A review of test Methods, issues and challenges of Large-Scale fire testing of concrete tunnel linings. *Construction and Building Materials*, 392, 131901.
- LI, G. & WU, X. 2005. Influence of fly ash and its mean particle size on certain engineering properties of cement composite mortars. *Cement and Concrete Research*, 35, 1128-1134.
- LI, L. & WU, M. 2022. An overview of utilizing CO<sub>2</sub> for accelerated carbonation treatment in the concrete industry. *Journal of CO<sub>2</sub> Utilization*, 60, 102000.
- LI, M., QIAN, C. & SUN, W. 2004a. Mechanical properties of high-strength concrete after fire. *Cement and concrete research*, 34, 1001-1005.
- LI, P., CHU, Y., WANG, L., WENSLOW, R. M., YU, K., ZHANG, H. & DENG, Z. 2014. Structure determination of the theophylline–nicotinamide cocrystal: a combined powder XRD, 1D solid-state NMR, and theoretical calculation study. *CrystEngComm*, 16, 3141-3147.
- LI, W., LUO, Z., TAO, Z., DUAN, W. H. & SHAH, S. P. 2017. Mechanical behavior of recycled aggregate concrete-filled steel tube stub columns after exposure to elevated temperatures. *Construction and Building Materials*, 146, 571-581.
- LI, Y., JI, H., FAN, J. & SU, H. 2023. Microstructure changes and reaction process of cotton at low-temperature oxidation stage. *Fuel Processing Technology*, 242, 107660.
- LI, Y., PIMIENTA, P., PINOTEAU, N. & TAN, K. H. 2019. Effect of aggregate size and inclusion of polypropylene and steel fibers on explosive spalling and pore pressure in ultra-high-performance concrete (UHPC) at elevated temperature. *Cement and Concrete Composites*, 99, 62-71.

- LI, Y., YANG, E.-H., ZHOU, A. & LIU, T. 2021. Pore pressure build-up and explosive spalling in concrete at elevated temperature: A review. *Construction and Building Materials*, 284, 122818.
- LI, Z., DING, Z. & ZHANG, Y. Development of sustainable cementitious materials. *Proceedings of international workshop on sustainable development and concrete technology*, Beijing, China, 2004b. 55-76.
- LIE, T. & KODUR, V. 1996. Thermal and mechanical properties of steel-fibre-reinforced concrete at elevated temperatures. *Canadian Journal of Civil Engineering*, 23, 511-517.
- LISS, K.-D., BARTELS, A., SCHREYER, A. & CLEMENS, H. 2003. High-energy X-rays: a tool for advanced bulk investigations in materials science and physics. *Textures and Microstructures*, 35, 219-252.
- LIU, J.-C., TAN, K. H. & YAO, Y. 2018. A new perspective on nature of fire-induced spalling in concrete. *Construction and Building Materials*, 184, 581-590.
- LLOYD, N. & RANGAN, V. Geopolymer concrete with fly ash. *Proceedings of the Second International Conference on sustainable construction Materials and Technologies*, 2010. UWM Center for By-Products Utilization, 1493-1504.
- LÖFGREN, I. 2005. Fibre-reinforced concrete for industrial construction. Department of civil and environment engineering. Chalmers university of technology, Göteborg, Sweden.
- LYON, R. E. & WALTERS, R. N. 2004. Pyrolysis combustion flow calorimetry. *Journal of Analytical and Applied Pyrolysis*, 71, 27-46.
- MA, Q., GUO, R., ZHAO, Z., LIN, Z. & HE, K. 2015. Mechanical properties of concrete at high temperature—A review. *Construction and Building Materials*, 93, 371-383.
- MADHAVI, T. C., RAJU, L. S. & MATHUR, D. 2014. Polypropylene fiber reinforced concrete-a review. *International journal of emerging technology and advanced engineering*, 4, 114-118.
- MAJEWSKY, M., BITTER, H., EICHE, E. & HORN, H. 2016. Determination of microplastic polyethylene (PE) and polypropylene (PP) in environmental samples using thermal analysis (TGA-DSC). *Science of the Total Environment*, 568, 507-511.
- MANE, S. & JADHAV, H. 2012a. Investigation of geopolymer mortar and concrete under high temperature. *Magnesium*, 1, 384-390.

- MANE, S. & JADHAV, H. 2012b. Investigation of geopolymer mortar and concrete under high temperature. *Magnesium*, 1, 5.
- MAYS, C., BEVITT, J. & STILWELL, J. 2017. Pushing the limits of neutron tomography in palaeontology: three-dimensional modelling of in situ resin within fossil plants. *Palaeontologia Electronica*, 20, 1-12.
- MCCORMACK, J. & POSTMA, A. 1977. Experimental and theoretical studies on water and gas release from heated concrete. *Proceedings of the Third Post-Accident Heat Removal" Information Exchange*, ANL-78-10, 205.
- MCLELLAN, B. C., WILLIAMS, R. P., LAY, J., VAN RIESSEN, A. & CORDER, G. D. 2011. Costs and carbon emissions for geopolymer pastes in comparison to ordinary portland cement. *Journal of cleaner production*, 19, 1080-1090.
- MCLENNAN, J., PATON, D. & WRIGHT, L. 2015. At-risk householders' responses to potential and actual bushfire threat: an analysis of findings from seven Australian post-bushfire interview studies 2009–2014. *International Journal of Disaster Risk Reduction*, 12, 319-327.
- MCNAMEE, R. 2019. Fire Spalling Theories - Realistic and More Exotic Ones. *Proceedings of the 6th International Workshop on Concrete Spalling due to Fire Exposure*. Sheffield, United Kingdom.
- MEHTA, A. & SIDDIQUE, R. 2017. Properties of low-calcium fly ash based geopolymer concrete incorporating OPC as partial replacement of fly ash. *Construction and Building Materials*, 150, 792-807.
- MEHTA, K. P. 2001. Reducing the environmental impact of concrete. *Concrete international*, 23, 61-66.
- MENCZEL, J. D., JUDOVITS, L., PRIME, R. B., BAIR, H. E., READING, M. & SWIER, S. 2009. Differential scanning calorimetry (DSC). *Thermal analysis of polymers: Fundamentals and applications*, 7-239.
- MENEFY, L. 2007. Investigation of reactive powder concrete and its damping characteristics when utilised in beam elements. Griffith University, Gold Coast.
- MEYER-OTTENS, C. 1975. Zur Frage der Abplatzungen an bauteilen aus Beton bei Brandbeanspruchungen. *Deutscher Ausschuss für Stahlbeton*, 248.
- MINDEGUIA, J.-C., PIMIENTA, P., HAGER, I. & CARRÉ, H. Influence of water content on gas pore pressure in concretes at high temperature. *2nd International RILEM Workshop on Concrete spalling due to fire exposure*, 2011. 113-121.



- MOHAMAD, N., MUTHUSAMY, K., EMBONG, R., KUSBIANTORO, A. & HASHIM, M. H. 2022. Environmental impact of cement production and Solutions: A review. *Materials Today: Proceedings*, 48, 741-746.
- MOHD ALI, A., SANJAYAN, J. & GUERRIERI, M. 2018. Specimens size, aggregate size, and aggregate type effect on spalling of concrete in fire. *Fire and Materials*, 42, 59-68.
- MOLLAH, M. Y. A., LU, F. & COCKE, D. L. 1998. An X-ray diffraction (XRD) and Fourier transform infrared spectroscopic (FT-IR) characterization of the speciation of arsenic (V) in Portland cement type-V. *Science of the total environment*, 224, 57-68.
- MONTE, F. L., LOMBARDI, F., FELICETTI, R. & LUALDI, M. 2017. Ground-penetrating radar monitoring of concrete at high temperature. *Construction and Building Materials*, 151, 881-888.
- MORSY, M., AL-SALLOUM, Y., ABBAS, H. & ALSAYED, S. 2012. Behavior of blended cement mortars containing nano-metakaolin at elevated temperatures. *Construction and Building materials*, 35, 900-905.
- NADEEM, A., MEMON, S. A. & LO, T. Y. 2014. The performance of fly ash and metakaolin concrete at elevated temperatures. *Construction and Building Materials*, 62, 67-76.
- NAZRI, F. M., SHAHIDAN, S., BAHARUDDIN, N. K., BEDDU, S. & BAKAR, B. H. A. Effects of heating durations on normal concrete residual properties: compressive strength and mass loss. *IOP conference series: materials science and engineering*, 2017. IOP Publishing, 012013.
- NEGAHBAN, E., BAGHERI, A. & SANJAYAN, J. 2021. Pore gradation effect on Portland cement and geopolymer concretes. *Cement and Concrete Composites*, 122, 104141.
- NEVILLE, A. M. 1995. *Properties of concrete*. Longman.
- NILI, M., AZARIOON, A., DANESH, A. & DEIHIMI, A. 2018. Experimental study and modeling of fiber volume effects on frost resistance of fiber reinforced concrete. *International Journal of Civil Engineering*, 16, 263-272.
- NILSSON, L.-O., NILSSON, L.-O. & JACOBS 2018. *Methods of measuring moisture in building materials and structures*, Springer.

- NISTORAC, A. & LOGHIN, M. C. The Future of Textile Waste Materials in Construction. The 18th Romanian Textiles and Leather Conference, 2023 Romania. Sciendo, 157-164.
- NOUMOWE, A. 2005. Mechanical properties and microstructure of high strength concrete containing polypropylene fibres exposed to temperatures up to 200 C. Cement and concrete research, 35, 2192-2198.
- NURAZZI, N., ASYRAF, M., RAYUNG, M., NORRRAHIM, M., SHAZLEEN, S., RANI, M., SHAFI, A., AISYAH, H., RADZI, M. & SABARUDDIN, F. 2021. Thermogravimetric analysis properties of cellulosic natural fiber polymer composites: A review on influence of chemical treatments. Polymers, 13, 2710.
- ODLER, I. 2003. The BET-specific surface area of hydrated Portland cement and related materials. Cement and Concrete Research, 33, 2049-2056.
- OH, J. E., MONTEIRO, P. J., JUN, S. S., CHOI, S. & CLARK, S. M. 2010. The evolution of strength and crystalline phases for alkali-activated ground blast furnace slag and fly ash-based geopolymers. Cement and Concrete Research, 40, 189-196.
- PALOMO, A., BLANCO-VARELA, M. T., GRANIZO, M., PUERTAS, F., VAZQUEZ, T. & GRUTZECK, M. 1999. Chemical stability of cementitious materials based on metakaolin. Cement and Concrete research, 29, 997-1004.
- PAN, Z., SANJAYAN, J. G. & RANGAN, B. V. 2009. An investigation of the mechanisms for strength gain or loss of geopolymer mortar after exposure to elevated temperature. Journal of Materials Science, 44, 1873-1880.
- PAPALOU, A. & BAROS, D. K. 2019. Assessing Structural Damage after a Severe Wildfire: A Case Study. Buildings, 9, 171.
- PEL, L., VAN DER HEIJDEN, G. & KOPINGA, K. Moisture transport in concrete during fire as studied by NMR. Second international conference on microstructural-related durability of cementitious composites, 2012. 11-13.
- PEÑA-PICHARDO, P., MARTÍNEZ-BARRERA, G., MARTÍNEZ-LÓPEZ, M., UREÑA-NÚÑEZ, F. & DOS REIS, J. M. L. 2018. Recovery of cotton fibers from waste Blue-Jeans and its use in polyester concrete. Construction and Building Materials, 177, 409-416.
- PENG, G.-F., KANG, Y.-R., HUANG, Y.-Z., LIU, X.-P. & CHEN, Q. 2012. Experimental research on fire resistance of reactive powder concrete. Advances in Materials Science and Engineering, 2012.

- PEREZ, F., BISSONNETTE, B. & COURARD, L. 2009. Combination of mechanical and optical profilometry techniques for concrete surface roughness characterisation. *Magazine of Concrete Research*, 61, 389-400.
- PHAN, L. T. 2008. Pore pressure and explosive spalling in concrete. *Materials and structures*, 41, 1623-1632.
- PHAN, L. T. & PEACOCK, R. D. 1999. Experimental Plan for Testing the Mechanical Properties of High-Strength Concrete at Elevated Temperatures (NISTIR 6210).
- PISTOL, K., WEISE, F., MENG, B. & DIEDERICHS, U. Polypropylene fibres and micro cracking in fire exposed concrete. *Advanced materials research*, 2014. Trans Tech Publ, 284-289.
- PLIYA, P., BEAUCOUR, A. & NOUMOWÉ, A. 2011. Contribution of cocktail of polypropylene and steel fibres in improving the behaviour of high strength concrete subjected to high temperature. *Construction and building materials*, 25, 1926-1934.
- POON, C.-S., AZHAR, S., ANSON, M. & WONG, Y.-L. 2001. Comparison of the strength and durability performance of normal-and high-strength pozzolanic concretes at elevated temperatures. *Cement and concrete research*, 31, 1291-1300.
- POON, C. S., SHUI, Z. & LAM, L. 2004. Compressive behavior of fiber reinforced high-performance concrete subjected to elevated temperatures. *Cement and concrete Research*, 34, 2215-2222.
- POWIERZA, B., STELZNER, L., OESCH, T., GOLLWITZER, C., WEISE, F. & BRUNO, G. 2018. Water Migration in One-Side Heated Concrete: 4D In-Situ CT Monitoring of the Moisture-Clog-Effect. *Journal of Nondestructive Evaluation*, 38.
- PURKISS, J. 1984. Steel fibre reinforced concrete at elevated temperatures. *International Journal of Cement Composites and Lightweight Concrete*, 6, 179-184.
- RAI, A. & JOSHI, Y. 2014. Applications and properties of fibre reinforced concrete. *Journal of Engineering Research and Applications*, 4, 123-131.
- RAJAMANE, N. & JEYALAKSHMI, R. 2014. Quantities of sodium hydroxide solids and water to prepare sodium hydroxide solution of given molarity for geopolymer concrete mixes. *Indian Concrete Institute Technical Paper*, SRM University, India.
- RAMEZANIANPOUR, A., ESMAEILI, M., GHAHARI, S.-A. & NAJAFI, M. 2013. Laboratory study on the effect of polypropylene fiber on durability, and physical and mechanical characteristic of concrete for application in sleepers. *Construction and Building Materials*, 44, 411-418.

- RAMEZANIANPOUR, A. A. 2014. Cement replacement materials. Springer geochemistry/mineralogy, DOI, 10, 978-3.
- RANGAN, B. V., WALLAH, S., SUMAJOUW, D. & HARDJITO, D. 2006. Heat-cured, low-calcium, fly ash-based geopolymer concrete. *Indian Concrete Journal*, 80, 47.
- RASHAD, A. M. & ZEEDAN, S. R. 2012. A preliminary study of blended pastes of cement and quartz powder under the effect of elevated temperature. *Construction and building materials*, 29, 672-681.
- RAZAK, S., ZAINAL, F. F. & SHAMSUDIN, S. R. Effect of porosity and water absorption on compressive strength of fly ash based geopolymer and OPC Paste. IOP conference series: materials science and engineering, 2020. IOP Publishing, 012035.
- REIS, J. M. L. D. 2009. Effect of textile waste on the mechanical properties of polymer concrete. *Materials Research*, 12, 63-67.
- REIS, M. D. L. B., NEVES, I. C., TADEU, A. & RODRIGUES, J. P. C. 2001. High-temperature compressive strength of steel fiber high-strength concrete. *Journal of Materials in Civil Engineering*, 13, 230-234.
- REN, Q., WU, Y., ZHANG, X. & WANG, Y. 2022. Effects of fly ash on the mechanical and impact properties of recycled aggregate concrete after exposure to high temperature. *European Journal of Environmental and Civil Engineering*, 26, 683-699.
- RICHARDSON, A. E. 2006. Compressive strength of concrete with polypropylene fibre additions. *Structural survey*, 24, 138-153.
- ROMUALDI, J. P. & BATSON, G. B. 1963. Mechanics of crack arrest in concrete. *Journal of the Engineering Mechanics Division*, 89, 147-168.
- ROMUALDI, J. P. & MANDEL, J. A. Tensile strength of concrete affected by uniformly distributed and closely spaced short lengths of wire reinforcement. *Journal Proceedings*, 1964. 657-672.
- ROSSINO, C., LO MONTE, F., CANGIANO, S., FELICETTI, R. & GAMBAROVA, P. G. HPC subjected to high temperature: a study on intrinsic and mechanical damage. *Key Engineering Materials*, 2015. Trans Tech Publ, 239-244.
- ROVNANÍK, P. 2010. Effect of curing temperature on the development of hard structure of metakaolin-based geopolymer. *Construction and building materials*, 24, 1176-1183.

- RYU, G. S., LEE, Y. B., KOH, K. T. & CHUNG, Y. S. 2013. The mechanical properties of fly ash-based geopolymer concrete with alkaline activators. *Construction and building materials*, 47, 409-418.
- SAKKAS, K., NOMIKOS, P., SOFIANOS, A. & PANIAS, D. 2015. Sodium-based fire resistant geopolymer for passive fire protection. *Fire and Materials*, 39, 258-270.
- SANCHAYAN, S. & FOSTER, S. J. 2016. High temperature behaviour of hybrid steel–PVA fibre reinforced reactive powder concrete. *Materials and Structures*, 49, 769-782.
- SANDIN, G. & PETERS, G. M. 2018. Environmental impact of textile reuse and recycling–A review. *Journal of cleaner production*, 184, 353-365.
- SANJAYAN, G. & STOCKS, L. J. 1993. Spalling of High-Strength Silica Fume Concrete in Fire. *Aci Materials Journal*, 90, 170-173.
- SARKER, P. & MCBEATH, S. Reinforced Geopolymer Concrete after Exposure to Fire. *Proceedings of the 2011 PCI Convention and National Bridge Conference*, 2011. Precast/Prestressed Concrete Institute.
- SARKER, P. K., KELLY, S. & YAO, Z. 2014. Effect of fire exposure on cracking, spalling and residual strength of fly ash geopolymer concrete. *Materials & Design*, 63, 584-592.
- SASI, S., JOSEPH, P., HAIGH, R., SANDANAYAKE, M., VRCELJ, Z. & YAGHOUBI, E. 2024. A Review on the Effects of Waste Textile Polymer Fiber on Concrete Strength: Exploring the Key Parameters. *Buildings*, 14, 1486.
- SCHULZE, S. S., FISCHER, E. C., HAMIDEH, S. & MAHMOUD, H. 2020. Wildfire impacts on schools and hospitals following the 2018 California Camp Fire. *Natural Hazards*, 104, 901-925.
- ŠELIH, J., SOUSA, A. C. & BREMNER, T. W. 1994. Moisture and heat flow in concrete walls exposed to fire. *Journal of engineering mechanics*, 120, 2028-2043.
- SHAH, A. H. & SHARMA, U. 2017. Fire resistance and spalling performance of confined concrete columns. *Construction and Building Materials*, 156, 161-174.
- SHAH, S., AKASHAH, F. & SHAFIGH, P. 2019. Performance of high strength concrete subjected to elevated temperatures: a review. *Fire Technology*, 55, 1571-1597.
- SHARMA, U., GUPTA, N., BAHRAMI, A., ÖZKİLİÇ, Y. O., VERMA, M., BERWAL, P., ALTHAQAFI, E., KHAN, M. A. & ISLAM, S. 2024. Behavior of fibers in geopolymer concrete: A comprehensive review. *Buildings*, 14, 136.

- SHORTER, G. & HARMATHY, T. 1961. Discussion on the article “The fire resistance of concrete beams” by Ashton and Bate. *Proceedings, Institute of Civil Engineers*, 20, 313.
- SHUAIBU, R. 1950. Compressive Strength of Low Calcium Fly Ash Geopolymer Concrete- A Review.
- SIDDIQUE, R. 2008. *Cement Kiln Dust. Waste Materials and By-Products in Concrete*. Springer.
- SINDHUNATA, G. C. L., SJ, X. J., WEISS, J., KOVLER, K., MARCHAND, J. & MINDESS, S. The effect of curing conditions on the properties of geopolymeric materials derived from fly ash. *International RILEM Symposium on Concrete Science and Engineering: A Tribute to Arnon Bentur*, 2004. RILEM Publications SARL.
- SINGH, A. K., SINGH, P., SHARMA, P. & SHARMA, N. Environmental effects of cement production: A review. *AIP Conference Proceedings*, 2023. AIP Publishing.
- SLATER, K. 2008. Environmental impact of polyester and polyamide textiles. *Polyesters and polyamides*. Elsevier.
- SO, H.-S. 2016. Spalling prevention of high performance concrete at high temperatures. *High Performance Concrete Technology and Applications*. IntechOpen.
- SONNIER, R., VAHABI, H., FERRY, L. & LOPEZ-CUESTA, J.-M. 2012. Pyrolysis-combustion flow calorimetry: A powerful tool to evaluate the flame retardancy of polymers. *Fire and polymers VI: new advances in flame retardant chemistry and science*, 361-390.
- STANDARD, A. 2010. General purpose and blended cements. Standard, Standard Australia.
- STANDARD, A. 2014. Methods of testing concrete. Method 9: Compressive strength tests: Concrete, mortar and grout specimens. Sydney, NSW, Australia: Standards Australia Limited.
- STANDARD, A. 2016. Supplementary cementitious materials. Part 1: Fly ash.
- STELZNER, L., POWIERZA, B., OESCH, T., DLUGOSCH, R. & WEISE, F. 2019a. Thermally-induced moisture transport in high-performance concrete studied by X-ray-CT and <sup>1</sup>H-NMR. *Construction and Building Materials*, 224, 600-609.
- STELZNER, L., WEISE, F., OESCH, T., DLUGOSCH, R. & POWIERZA, B. Transport and reconfiguration of moisture in HPC due to unilateral heating. *Proceedings of the*

- 6th International Workshop on Concrete Spalling due to Fire Exposure, 2019b. 181-190.
- STEWART, S. I., RADELOFF, V. C., HAMMER, R. B. & HAWBAKER, T. J. 2007. Defining the wildland–urban interface. *Journal of Forestry*, 105, 201-207.
- SU, H., XU, J. & REN, W. 2016. Mechanical properties of geopolymer concrete exposed to dynamic compression under elevated temperatures. *Ceramics International*, 42, 3888-3898.
- SULTANGALIYEVA, F., FERNANDES, B., CARRÉ, H., PIMIENTA, P., BORDERIE, C. & ROUSSEL, N. Experimental contribution to the optimization of the choice of polypropylene fibers in concrete for its thermal stability. 6th International Workshop on Concrete Spalling due to Fire Exposure, 2019.
- SWAMY, R. N. 1986. Cement replacement materials.
- SWANEPOEL, J. & STRYDOM, C. 2002. Utilisation of fly ash in a geopolymeric material. *Applied geochemistry*, 17, 1143-1148.
- TAI, Y.-S., PAN, H.-H. & KUNG, Y.-N. 2011. Mechanical properties of steel fiber reinforced reactive powder concrete following exposure to high temperature reaching 800 C. *Nuclear Engineering and Design*, 241, 2416-2424.
- THOMAS, J., THAICKAVIL, N. N. & SYAMALA, T. Supplementary cement replacement materials for sustainable concrete. *Green Buildings and Sustainable Engineering: Proceedings of GBSE 2018, 2019*. Springer, 387-403.
- TOPÇU, İ. B. & UYGUNOĞLU, T. 2010. Influence of mineral additive type on slump-flow and yield stress of self-consolidating mortar. *Scientific Research and Essays*, 5, 1492-1500.
- TRAPOTE-BARREIRA, A., PORCAR, L., CAMA, J., SOLER, J. M. & ALLEN, A. J. 2015. Structural changes in C–S–H gel during dissolution: Small-angle neutron scattering and Si-NMR characterization. *Cement and Concrete Research*, 72, 76-89.
- TRASK, B. J. & BENINATE, J. V. 1986. Thermal analyses of flame-retardant twills containing cotton, polyester and wool. *Journal of applied polymer science*, 32, 4945-4957.
- UCAR, M. & WANG, Y. 2011. Utilization of recycled post consumer carpet waste fibers as reinforcement in lightweight cementitious composites. *International Journal of Clothing Science and Technology*, 23, 242-248.

- VAN DER HEIJDEN, G., HUININK, H., PEL, L. & KOPINGA, K. 2011. One-dimensional scanning of moisture in heated porous building materials with NMR. *Journal of Magnetic Resonance*, 208, 235-242.
- VAN DER HEIJDEN, G., PEL, L. & ADAN, O. 2012. Fire spalling of concrete, as studied by NMR. *Cement and concrete research*, 42, 265-271.
- VAN DER HEIJDEN, G. H. A., VAN BIJNEN, R. M. W., PEL, L. & HUININK, H. P. 2007. Moisture transport in heated concrete, as studied by NMR, and its consequences for fire spalling. *Cement and Concrete Research*, 37, 894-901.
- VARGHESE, A., N, A., ANDRUSHIA, D. & ARULRAJ, P. 2021. Investigation on the performance of fiber reinforced concrete subjected to standard fire exposure. *World Journal of Engineering*, 18, 442-451.
- VARONA, F., BAEZA, F. J., BRU, D. & IVORRA, S. 2018. Influence of high temperature on the mechanical properties of hybrid fibre reinforced normal and high strength concrete. *Construction and Building Materials*, 159, 73-82.
- VERMA, M. & DEV, N. 2021. Sodium hydroxide effect on the mechanical properties of flyash-slag based geopolymer concrete. *Structural Concrete*, 22, E368-E379.
- WALKLEY, B. & PROVIS, J. 2019. Solid-state nuclear magnetic resonance spectroscopy of cements. *Materials Today Advances*, 1, 100007.
- WALLAH, S. & RANGAN, B. V. 2006. Low-calcium fly ash-based geopolymer concrete: long-term properties.
- WATTIMENA, O. K., ANTONI, A. & HARDJITO, D. A review on the effect of fly ash characteristics and their variations on the synthesis of fly ash based geopolymer. *AIP Conference Proceedings*, 2017. AIP Publishing.
- WEBER, B. A critical review of the moisture clog theory. *7th International Workshop*, 2022. 97.
- WEI, J. & MEYER, C. 2014. Degradation rate of natural fiber in cement composites exposed to various accelerated aging environment conditions. *Corrosion science*, 88, 118-132.
- WONG, A.-Y. & LAM, F. 2002. Study of selected thermal characteristics of polypropylene/polyethylene binary blends using DSC and TGA. *Polymer testing*, 21, 691-696.
- WOOLSON, I. H. 1905. Investigation of the effect of heat upon the crushing strength and elastic properties of concrete.



- WU, H., LIN, X. & ZHOU, A. 2020. A review of mechanical properties of fibre reinforced concrete at elevated temperatures. *Cement and Concrete Research*, 135, 106117.
- XIAO, J. & FALKNER, H. 2006. On residual strength of high-performance concrete with and without polypropylene fibres at elevated temperatures. *Fire safety journal*, 41, 115-121.
- XIAO, J. & KÖNIG, G. 2004. Study on concrete at high temperature in China—an overview. *Fire safety journal*, 39, 89-103.
- XIAO, Q., JU, G., YE, F., WANG, Y., JIN, L. & FU, W. 2024. An innovative approach for assessing the tensile strength of concrete: Experimental and numerical investigations. *Construction and Building Materials*, 417, 135249.
- XIE, J., ZHANG, Z., LU, Z. & SUN, M. 2018. Coupling effects of silica fume and steel-fiber on the compressive behaviour of recycled aggregate concrete after exposure to elevated temperature. *Construction and Building Materials*, 184, 752-764.
- XING, Y.-F., XU, Y.-H., SHI, M.-H. & LIAN, Y.-X. 2016. The impact of PM2. 5 on the human respiratory system. *Journal of thoracic disease*, 8, E69.
- XU, H., WANG, Z., SHAO, Z., CAI, L., JIN, H., ZHANG, Z., QIU, Z., RUI, X. & CHEN, T. 2021. Experimental study on durability of fiber reinforced concrete: Effect of cellulose fiber, polyvinyl alcohol fiber and polyolefin fiber. *Construction and Building Materials*, 306, 124867.
- YAN, X., LI, H. & WONG, Y. L. 2007. Effect of aggregate on high-strength concrete in fire. *Magazine of Concrete Research*, 59, 323-328.
- YANG, C.-C. & CHIANG, C. 2005. On the relationship between pore structure and charge passed from RCPT in mineral-free cement-based materials. *Materials chemistry and physics*, 93, 202-207.
- YAZI, Y. 1956. On the Burning Speed and the Ignition Temperature of Cotton (1). *Bulletin of Japan Association for Fire Science and Engineering*, 6, 23-26.
- YE, L., ZHANG, D. & TAN, K. H. 2020. On measuring techniques of pore pressure in concrete at elevated temperature. *Cement and Concrete Composites*, 114, 103737.
- YERMAK, N., PLIYA, P., BEAUCOUR, A.-L., SIMON, A. & NOUMOWÉ, A. 2017. Influence of steel and/or polypropylene fibres on the behaviour of concrete at high temperature: Spalling, transfer and mechanical properties. *Construction and Building Materials*, 132, 240-250.

- YUAN, Y., ZHAO, R., LI, R., WANG, Y., CHENG, Z., LI, F. & MA, Z. J. 2020. Frost resistance of fiber-reinforced blended slag and Class F fly ash-based geopolymer concrete under the coupling effect of freeze-thaw cycling and axial compressive loading. *Construction and Building Materials*, 250, 118831.
- ZEIML, M., LEITHNER, D., LACKNER, R. & MANG, H. A. 2006. How do polypropylene fibers improve the spalling behavior of in-situ concrete? *Cement and concrete research*, 36, 929-942.
- ZHANG, D., LIU, Y. & TAN, K. H. 2021. Spalling resistance and mechanical properties of strain-hardening ultra-high performance concrete at elevated temperature. *Construction and Building Materials*, 266, 120961.
- ZHANG, H., LI, L., YUAN, C., WANG, Q., SARKER, P. K. & SHI, X. 2020a. Deterioration of ambient-cured and heat-cured fly ash geopolymer concrete by high temperature exposure and prediction of its residual compressive strength. *Construction and Building Materials*, 262, 120924.
- ZHANG, H. Y., KODUR, V., QI, S. L., CAO, L. & WU, B. 2014. Development of metakaolin–fly ash based geopolymers for fire resistance applications. *Construction and Building Materials*, 55, 38-45.
- ZHANG, P., KANG, L., WANG, J., GUO, J., HU, S. & LING, Y. 2020b. Mechanical properties and explosive spalling behavior of steel-fiber-reinforced concrete exposed to high temperature—a review. *Applied Sciences*, 10, 2324.
- ZHAO, H., LIU, F. & YANG, H. 2020. Residual compressive response of concrete produced with both coarse and fine recycled concrete aggregates after thermal exposure. *Construction and Building Materials*, 244, 118397.
- ZHAO, R. & SANJAYAN, J. G. 2011. Geopolymer and Portland cement concretes in simulated fire. *Magazine of Concrete research*, 63, 163-173.
- ZOHDY, M., SAHAR, S., HASSAN, M., KHALIL, E., EL-HOSSAMY, M. & EL-NAGGAR, A. 1999. Thermal behaviour stability of polyester and cotton/polyester graft copolymers obtained by direct radiation grafting of individual and mixed vinyl monomers. *Polymer degradation and stability*, 63, 187-193.
- ZOLLO, R. F. 1997. Fiber-reinforced concrete: an overview after 30 years of development. *Cement and concrete composites*, 19, 107-122.

ZUO, C., LI, Y., CHEN, Y., JIANG, J., QIU, W. & CHEN, Q. 2024. Leaching of heavy metals from polyester microplastic fibers and the potential risks in simulated real-world scenarios. *Journal of Hazardous Materials*, 461, 132639.